TRANSPORTATION RESEARCH
RECORD

No. 1473

Pavement Design, Management, and Performance

Strength and Deformation Characteristics of Pavement Sections and Pavement Rehabilitation

A peer-reviewed publication of the Transportation Research Board

TRANSPORTATION RESEARCH BOARD
NATIONAL RESEARCH COUNCIL

NATIONAL ACADEMY PRESS
WASHINGTON, D.C. 1995

Transportation Research Record 1473
ISSN 0361-1981
ISBN 0-309-06112-1
Price: $35.00

Subscriber Category
IIB pavement design, management, and performance

Printed in the United States of America

Sponsorship of Transportation Research Record 1473

GROUP 2—DESIGN AND CONSTRUCTION OF TRANSPORTATION FACILITIES
Chairman: Michael G. Katona, U.S. Air Force Armstrong Laboratory

Pavement Management Section
Chairman: Albert J. Bush III, U.S. Army Corps of Engineers Waterways Experiment Station

Committee on Pavement Rehabilitation
Chairman: David E. Newcomb, University of Minnesota
Secretary: Roger C. Olson, Minnesota Department of Transportation
Janice L. Arellano, Fouad M. Bayomy, Thomas L. Boswell, James L. Brown, Alfred B. Crawley, Denis E. Donnelly, Kathleen T. Hall, Joseph B. Hannon, Don M. Harriott, Thomas M. Hearne, Jr., Mustaque Hossain, Ira J. Huddleston, Tom J. Kazmierowski, Walter P. Kilareski, Aramis Lopez, Jr., Joe P. Mahoney, Emmanuel B. Owusu-Antwi, Elias H. Rmeili, Gary Wayne Sharpe, Eugene L. Skok, Jr., Shiraz D. Tayabji, Gerald F. Voigt

Committee on Strength and Deformation Characteristics of Pavement Sections
Chairman: Tom Scullion, Texas A&M University
Albert J. Bush III, George R. Cochran, Judith B. Corley-Lay, Mark P. Gardner, Max G. Grogg, Dennis R. Hiltunen, Mario S. Hoffman, Anastasios M. Ioannides, Lynne H. Irwin, Starr D. Kohn, Robert L. Lytton, Michael S. Mamlouk, Richard W. May, Soheil Nazarian, Rasmus S. Nordal, Gonzalo R. Rada, Cheryl Allen Richter, Glenn J. Rix, Byron E. Ruth, Larry A. Scofield, Peter Sebaaly, Stephen B. Seeds, Marshall R. Thompson, Per Ullidtz, Jacob Uzan, Thomas D. White, Wei-Shih Yang

Transportation Research Board Staff
Robert E. Spicher, Director, Technical Activities
D. W. Dearasaugh, Engineer of Design
Nancy A. Ackerman, Director, Reports and Editorial Services
Marianna Rigamer, Oversight Editor

Sponsorship is indicated by a footnote at the end of each paper. The organizational units, officers, and members are as of December 31, 1994.

Transportation Research Record 1473

Contents

Foreword

Of the 17 papers in this volume, the first 12 were peer reviewed by the TRB Committee on Strength and Deformation Characteristics of Pavement Sections. The final five papers were reviewed by the TRB Committee on Pavement Rehabilitation. Most of the papers were presented at three sessions sponsored by those committees during the 1995 TRB Annual Meeting.

Livneh et al. report a research effort to evaluate how the strength values of granular pavement layers and subgrade layers measured with a dynamic core penetrometer may vary because of vertical confinement effects. Simpson et al. use transverse profiles instead of typical rutting measurements to predict additional rutting and hypothesize on its cause. Miller et al. developed regression models to predict field rutting on the basis of results from the Georgia loaded-wheel testing device. The next two papers deal with rutting of asphalt pavements in extremely hot, dry environments. Vallerga et al. present a case study of a pavement in the United Arab Emirates, and Wahhab et al. discuss a national study of pavements in Saudi Arabia. Bay et al. report on a new device that is used to evaluate the properties of pavement layers, the rolling dynamic deflectometer. Kim et al. present a temperature correction procedure for deflections and backcalculated moduli based on the middepth temperature of the asphalt layer. Newcomb et al. show that when pavement layer moduli are backcalculated, there is a need to determine the depth to the water table and the modulus of the material below the water table. Meier and Rix use artificial neural networks trained to backcalculate pavement layer moduli for three-layer flexible pavement systems from synthetic dynamic deflection basins. Wu and Todres study the behaviors of roller-compacted concrete pavements by nondestructive deflectometer tests. Inge and Kim present a new method for predicting asphalt middepth temperature based on a data base approach. Hsu et al. compare measured data on vehicle response to dynamic wheel loads with data predicted by computer simulation.

Ksaibati et al. compute asphalt overlay thicknesses based on subgrade resilient modulus values obtained by three different methods. Hall and Watkins describe enhancements to Arkansas's ROADHOG overlay design procedure that allows it to be used for any flexible pavement. Kazmierowski and Bradbury present an alternative strategy for the rehabilitation of surface distress through the use of microsurfacing. Arudi et al. show that the performances of asphalt overlays on broken and seated concrete pavements more closely resemble those of composite pavements rather than flexible pavements. McAuliffe et al. summarize the performances of bituminous overlays of faulted rigid pavements in New York State.

Effect of Vertical Confinement on Dynamic Cone Penetrometer Strength Values in Pavement and Subgrade Evaluations

MOSHE LIVNEH, ILAN ISHAI, AND NOAM A. LIVNEH

The Dynamic Cone Penetrometer (DCP) has become one of the most useful testing devices in pavement evaluation in Israel and other parts of the world. Consequently, a reliable true meaning and interpretation of the results are needed. Research work dedicated to studying the effects of vertical confinement on the DCP strength values of the granular pavement layers and subgrade is summarized. Specifically, four major effects were studied: vertical confinement of granular layers, vertical confinement of cohesive layers, vertical confinement of rigid structural layers, and the effect of vertical confinement of upper asphalt layers on the DCP strength values of the granular layers below them. Based on engineering analysis and experimental testing in the laboratory and in the field, the following conclusions were made. (a) No vertical confinement effect by rigid pavement structure, the upper granular layers, or the upper cohesive layers on the DCP strength values of lower cohesive subgrade layers was found. Any differences in the results between the confined and unconfined DCP values can be explained by the friction that developed in the rod during tilted penetration. (b) However, vertical confinement effects by upper asphalt layers on the DCP values of the granular pavement layers exist. Since this is the true effect of the pavement structure, any DCP measurement for pavement evaluation purposes should be performed through a narrow boring in the asphalt layers and not after removal of a wide strip of asphalt. Generally, these confinement effects decrease the DCP values, and thus increase the structural strength measured. These confinement and friction effects, which can be evaluated quantitatively, should be taken into consideration when using the DCP method to evaluate existing pavements.

During the last decade, the Dynamic Cone Penetrometer (DCP) test has been increasingly used in many parts of the world for pavement and subgrade evaluation through its relationship with the in situ California Bearing Ratio (CBR). This is because of its economy, simplicity, and capability of providing rapid measurements of the in situ strengths of subgrades and pavement layers without excavation of the existing pavement, as in the in situ CBR test (*1–9*).

Extensive work with DCP testing and the experience gained in Israel have shown that, in addition to the CBR-DCP correlation, some other factors that have an influence, such as vertical confinements, should be taken into consideration (*10*). For example, a question occasionally arises, that is, whether DCP results, obtained from the subgrade by means of the rod's penetration through the structural layers, are identical to the results obtained from the same subgrade after removal of the pavement structural layers. In other words, are the subgrade DCP results affected by the presence of the flexible structure? Similarly, the question can be applied to an all–asphalt pavement whose subgrade was examined following drilling of a small-diameter hole in the asphalt structure. These issues are considered to be related to vertical confinement.

Since the DCP has become one of the most useful testing devices in pavement evaluation in Israel, a reliable true meaning of the results and an interpretation of the results were required. Consequently, research work was dedicated to studying the effects of vertical confinement on the DCP values. Specifically, the following effects were studied:

1. Effect of vertical confinement of granular structural layers on clay and silt subgrade DCP values;
2. Effect of vertical confinement of cohesive layers on clay subgrade DCP values;
3. Effect of vertical confinement of rigid structural layers (an all-asphaltic structure) on clay subgrade DCP values; and
4. Effect of the vertical confinement of upper asphaltic layers on the DCP values of the granular layers below them.

The study of these effects is important for use of the DCP in the reliable evaluation of existing pavements. This paper presents the theoretical background for vertical confinement, as well as an analysis of the results obtained from both laboratory and field tests designed to study the effects mentioned earlier.

DCP TEST IN PAVEMENT EVALUATION

The DCP, as developed in South Africa (*11*), consists of a steel rod with a cone at one end. It is driven into the pavement or the subgrade with a sliding hammer, and the material resistance to penetration is measured in terms of millimeters per blow. The cone is angled at 30 degrees, with the larger diameter of the cone being 20 mm. The hammer weighs 8 kg, and the dropping sliding height is 575 mm (Figure 1).

The DCP was originally designed and used to determine the strength profile of the flexible pavement structure and subgrade (*12–14*). Usually, pavement testing at a given point involves the extrusion of a 4-in. circular core from the top asphalt layers only and penetrating the DCP from the top of the base course layer down to the required pavement or subgrade layer. The properties of the asphalt layers are directly evaluated in the laboratory by a proper mechanical test (resilient modulus, diametrical test, splitting test, Marshall test, or others). The pavement parameters are continuously measured and recorded with depth by the DCP. Immediately at the test's conclusion, the shallow 4-in. hole is easily filled with either portland cement concrete (regular or fast curing) or a proper cold asphaltic mixture. In case of only subgrade evaluation for pavement

Transportation Research Institute, Technion, Haifa 32000, Israel.

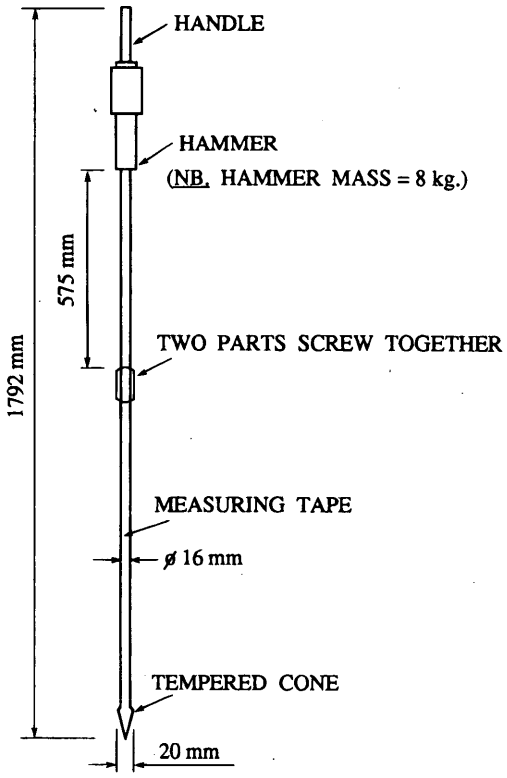

FIGURE 1 General details of South African DCP.

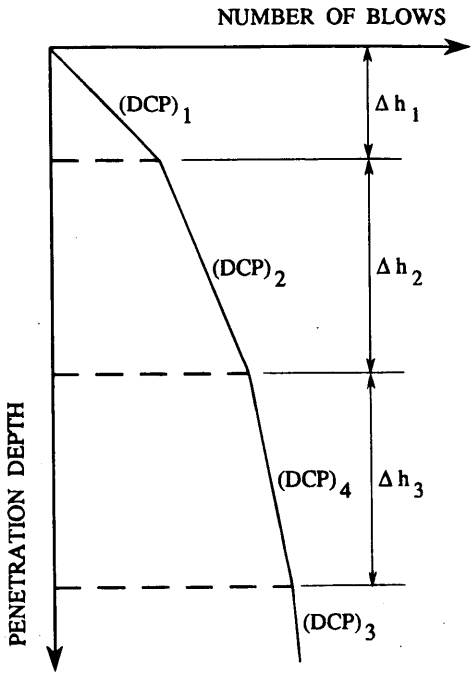

FIGURE 2 DCP test output.

design purposes, the DCP is penetrated down from the top of the natural soil or compacted subgrade.

During testing the number of blows versus depth is recorded. The DCP value is defined as the slope of the blows-versus-depth curve (in millimeters per blow) at a given linear depth segment (Figure 2).

CORRELATION BETWEEN DCP AND CBR

To be able to relate DCP values to the structural parameter of the pavement under the local pavement design and evaluation technology, an extensive controlled laboratory and field test was carried out to correlate DCP to CBR (*10,15*). In the laboratory conventional and DCP tests were performed on a wide range of undisturbed and compacted fine-grained soil samples with and without saturation. Compacted granular soils were tested in flexible molds with variable controlled lateral pressures. Field tests were made on natural and compacted layers representing a wide range of potential pavement and subgrade materials. Pavement evaluation tests were also performed for pavement and material evaluation and for correlation with pavement condition.

The correlative laboratory and field testing program resulted in a quantitative relationship between the CBR of the material and its DCP value as follows (Figure 3):

$$\log \text{CBR} = 2.20 - 0.71 (\log \text{DCP})^{1.5} \quad (R^2 > 0.95) \qquad (1)$$

where the DCP is the penetration ratio in millimeters per blow.

This relationship, which was initially formulated in 1985, was based on 56 comparative test results. Later, this correlation was checked as data accumulated over several years (10). Finally, on the basis of 135 tests the total equation, which was based on old and new data, is formulated as follows (Figure 3):

$$\log \text{CBR} = 2.14 - 0.69 (\log \text{DCP})^{1.5} \quad (R^2 = 0.876, N = 135) \qquad (2)$$

From a practical standpoint, both Equations 1 and 2 yield almost identical results (*10*).

Several other agencies and researchers around the world have also tried to develop correlations between DCP and CBR values (*3,8,11,16*). Webster et al. (*8*) compared some of these correlations (Figure 4). It is evident that general agreement was reached between

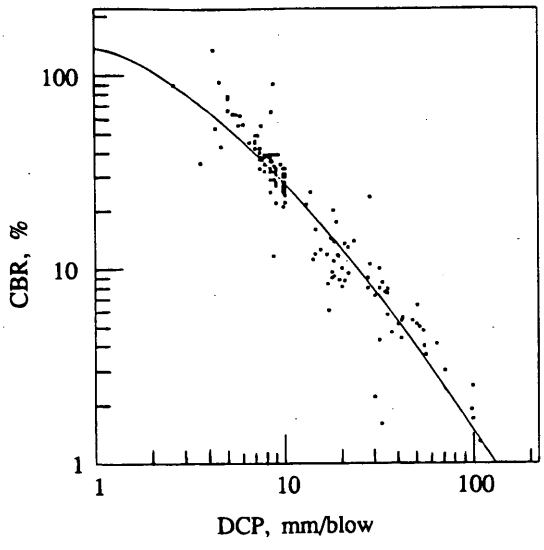

FIGURE 3 Relationship between CBR values and DCP values (*10,15*).

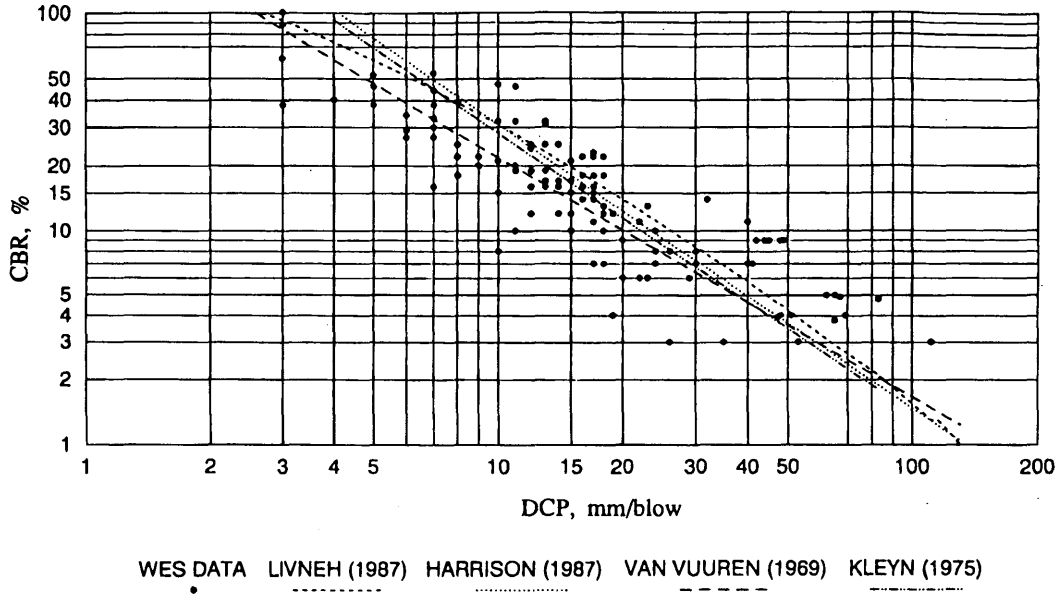

FIGURE 4 Universal data for relationship between DCP and CBR (*8*).

the various sources of information. On the basis of these results the following equation was selected as the best correlation:

$$\log \text{CBR} = 2.46 - 1.12 (\log \text{DCP}) \quad (3)$$

It can be seen that a universal correlation exists between the DCP and CBR for a wide range of pavement and subgrade materials, testing conditions, and technologies.

ENGINEERING BACKGROUND OF VERTICAL CONFINEMENT EFFECT

In the context of the basic bearing capacity approach, a plastic failure mechanism can be adopted to describe soil behavior under cone-shaped penetrometers. This approach was adopted by Livneh (*17*) and Livneh and Greenstein (*18*) to find the effects of lateral pressure on CBR values in granular materials. Similarly, few analytical or numerical solutions for wedge and cone-shaped penetrometers, which account for both cone apex-angle and roughness, are given in the literature (*19–21*).

Durgunoglu and Mitchell (*20*) proposed three types of failure mechanisms relevant to deep foundations that can also be adopted for penetration tests (Figure 5). On the basis of actual test results with variable apex-angles and cone roughness, they concluded that the failure mechanisms described in Figure 5(*b*) and 5(*c*) are inappropriate, whereas the failure mechanism represented in Figure 5(*a*) closely represents the actual failure surface associated with wedge penetration.

On the other hand, Meyerhof (*19*) provided solutions for both cohesive and cohesionless soils for certain conditions assuming the failure mechanism shown in Figure 5(*b*), whereas Nowatzki and Karafiath (*21*) used a finite-difference technique for limited conditions and obtained some penetration resistance values for cohesionless soils assuming the failure mechanism shown in Figure 5(*c*). It should be noted that this mechanism is only possible in the situation in which the ratio D/B is larger than 4 to 10. For the DCP device this ratio means depths of more than about 10 cm.

In this context it is important to show that the state of deep foundation is defined by Meyerhof (*19*) as follows:

$$D = 4\sqrt{N_\phi} B \quad (4)$$

where

$$N_\phi = \tan^2 (1/4\pi + 1/2\phi) \quad (5)$$

and

D = the foundation depth,
B = the width or diameter of the foundation, and
ϕ = the material's internal angle of friction.

Here, for cohesive soils (where ϕ is equal to 0), Equations 4 and 5 lead to the ratio of D/B equal to 4, whereas for cohesionless soils (where ϕ is > 0) a deep foundation is defined at a depth of D greater than $4B$.

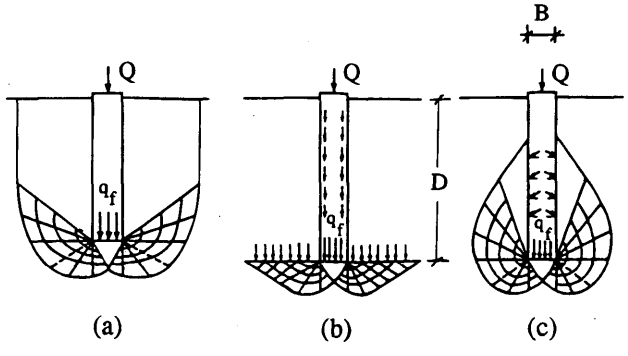

FIGURE 5 Different failure mechanisms proposed for penetration test (*20*).

To investigate the vertical confinement effect one should look at the Terzaghi's basic bearing capacity formula. Under this concept the penetration resistance q_u can be defined as follows:

$$q_u = K_c C N_c + K_\gamma \gamma B^{1/2} N_\gamma + \gamma D N_q \quad (6)$$

where

q_u = the unit tip resistance,
C = the unit cohesion,
γ = the material density,
D = the depth of the penetrometer tip,
N_c, N_γ, N_q = Terzaghi's bearing capacity coefficients (Figure 6), and
K_c, K_γ = the shape factors.

The question then asked is whether DCP test results obtained at a depth of 10 cm and more below the clay subgrade, when the test is conducted in the clay subgrade after drilling into the pavement, are different from the results obtained from a similar subgrade at a depth of 10 cm and more below the surface, when the test is conducted following the removal of a wide strip of pavement. In other words are DCP test results obtained at a depth of 10 cm and more still subject to the possible effects of vertical confinement?

The answer according to Meyerhof (*19*) is negative when cohesive subgrade is concerned. If one looks at Figure 6 (which presents the bearing capacity coefficients as a function of the angle of internal friction), it can be seen that for ϕ equal to 0, the value of N_c remains constant, commencing from a depth equal or greater than that expressed in Equation 4. Brinch-Hansen (*22*) also provide a negative answer since, commencing from a certain value of D, the increase in N_c as a consequence of the continued increase in D is negligible. This is reflected in the following equation:

$$d_c = 1.0 + \frac{0.35}{\frac{B}{D} + \frac{0.6}{(1 + 7tg^4\phi)}} \quad (7)$$

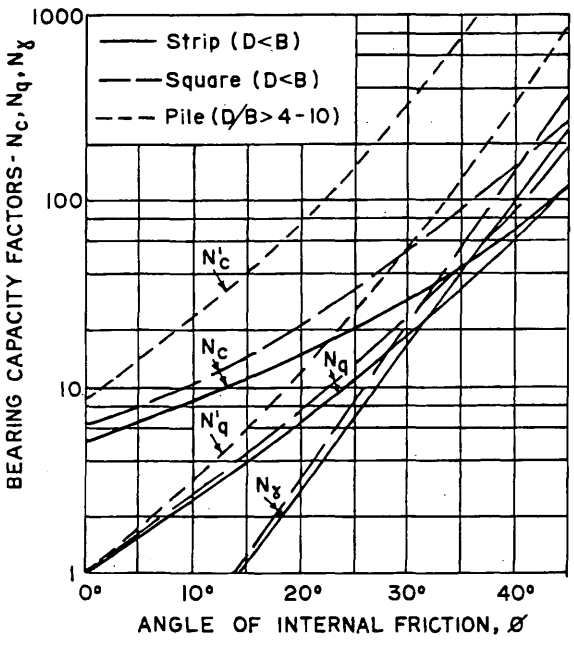

FIGURE 6 Bearing capacity factors for spread and pile foundations (*16*).

where d_c is the increase factor of N_c depending on the foundation depth.

Theoretically, vertical confinement is mainly possible because of the bearing capacity component $\gamma D N_q$ (Equation 6). In cohesive soils, when ϕ is equal to 0, N_q is equal to 1.0, and thus, this component is quite negligible. Hence, it can be seen that for clay subgrades the values of both N_c and N_q in Equation 6 eliminate the effect of vertical confinement in deep penetration measurements of the DCP.

On the other hand, for granular materials (where ϕ is > 0), both N_q and N_c possess significant values that increase with depth. Therefore, the vertical confinement of the upper layers will be significant and will increase with the depth of the DCP tip.

This situation of a very deep foundation is similar to a position in which the foundation is not as deep but the soil surface is bound by a rigid structure (as, for example, in an all-asphalt structure). On the basis of the preceding discussion, it can be concluded that the DCP results obtained from a penetration depth of 10 cm or more from the surface of the clay subgrade will be only negligibly affected by the presence of a rigid structure on the subgrade's surface or will be totally unaffected.

These conclusions are derived from the engineering analysis, and they are compared with the empirical testing described later in this paper.

EFFECT OF CONFINEMENT BY GRANULAR STRUCTURE

The effect of confinement by the granular structure on the subgrade's DCP values was studied on the basis of an analysis of actual DCP test data (*10*). The analysis presented in this section is based on 11 DCP test locations. The DCP test was conducted following the drilling of asphalt cores at these points. The subgrade DCP values obtained by this method are referred to as the confined values, that is, DCP_{con}. These values are compared with the DCP values derived from the subgrade values described earlier following removal of all structural layers (i.e., after the digging of test pits). The DCP values obtained from the exposed subgrade are referred to as the unconfined values, that is, DCP_{unc}.

The test results obtained are presented in Figure 7. It can immediately be seen from Figure 7 that the two test populations are not identical, as also verified statistically. Thus, for example, a statistical t-test of the results showed that the mean unconfined DCP ($\bar{x}$) is larger than the mean confined DCP ($\bar{y}$) at a confidence level of 95 percent.

Moreover, a linear $y = a + bx$ type of regression analysis leads to the following results:

$a = 21.03$ ($S_a = 6.42$), $b = 0.103$ ($S_b = 0.158$), $R^2 = 0.45$, and $\sigma^2 = 46.21$

where

S_a and S_b = standard deviations for a and b, respectively;
σ^2 = mean square error (MSE); and
R = correlation coefficient.

A statistical F-test of this regression leads to the conclusion that at a confidence level of 95 percent, the regression is not significant or, in other words, that there is no correlation between x values and y values. The analysis according to Grubbs (*23*) leads to the conclusion that the systematic error related to measuring x values is sig-

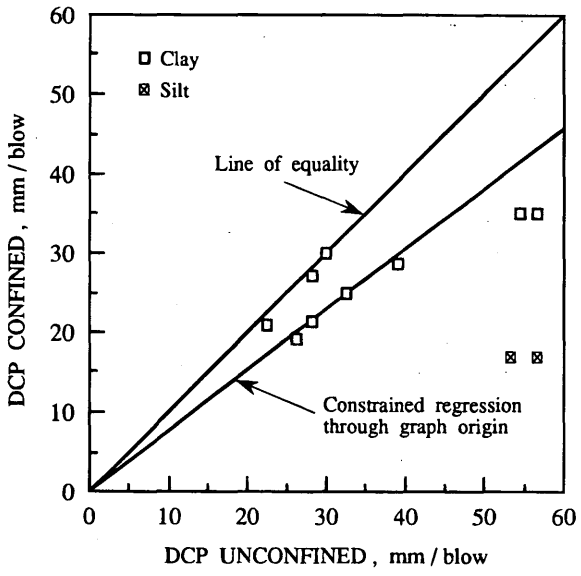

FIGURE 7 DCP test results for subgrade beneath granular structure.

nificantly different from the systematic error related to measuring y values. At the same time, the precisions of the readings in both tests (as expressed by the standard deviation of the random error) can be considered identical. This analysis proves once again that the two test populations are not identical, and thus indicates the possible existence of vertical confinement.

Now, attention should be given to the two silt points in Figure 7. Since in the silt ϕ is > 0 on the basis of the discussion in the engineering background, it is conceivable that the two test points in the silt are indeed related to the phenomenon of vertical confinement, whereas there is no reason for the confinement effect to take place in the rest of the test points, which are in clay. For this reason the character of the two populations should be reexamined following exclusion of the two silt test points (marked separately in Figure 7).

The hypothesis that the two silt points do not belong to the population was examined by similar linear regression without the two points described earlier. The regression led to the following parameters:

$a = 12.10$ ($S_a = 3.199$), $b = 0.418$ ($S_b = 0.086$), $R^2 = 0.771$, and $\sigma^2 = 9.005$

An F-test of this regression leads to the conclusion that at a confidence level of 95 percent the model is significant and a linear correlation between x and y does exist.

The conclusion is that the two points do not belong to the same population, because without them there is a significant linear correlation. Finally, it can be assumed that the difference between the two populations (x,y) is a result of the friction created in the rod during tilted penetration of the DCP rod through the granular material (as will be discussed later or of the friction created in the rod during a collapse of the granular material on the rod surface during penetration. A constrained regression through the graph origin was conducted to obtain the extent of the friction's effect on the results, and the following correlation was obtained: $y = 0.73x$. This leads to the following relationship:

$$DCP_{unc} = 1.34\ DCP_{con} \quad (8)$$

In other words when the DCP test is conducted through granular layers, an error of 34 percent magnitude may occur. In this specific case the DCP values of the clay subgrade should be increased by about 34 percent to obtain the true reduced strength of the material beneath the granular structure.

Finally, it should be mentioned that the effect of friction created in the rod (either by tilted penetration or by material collapse) can be quantitatively evaluated by torque measurement in the DCP device during penetration intervals. This work is being done and will be reported in the near future.

EFFECT OF CONFINEMENT BY CLAY LAYERS

It is also important to examine whether conducting the DCP test on the surface of the clay subgrade and conducting the DCP test through this subgrade (commencing from a certain depth) lead to identical results. The results of the 27 tests are presented in Figure 8. The method was to conduct a DCP test on the surface and then dig a 0.5-m-deep test pit and conduct the DCP test again, commencing from the pit bottom downward.

The DCP value in the first test, which corresponds to a depth of 0.5 to 0.7 from the soil surface, is compared with a DCP value in the second test, which corresponds to a depth of 0.0 to 0.2 from the pit bottom. The first test provides the value of the confined DCP (the x values), and the second test provides the value of the unconfined DCP (the y value).

To test whether the two test populations are identical, a statistical analysis similar to that described earlier was performed. According to the statistical t-test results, both populations are identical. However, this result should be accepted with caution because there is no assurance that in the test population (derived from various sites with a wide range of strengths) the condition requiring that the standard deviation from the mean does not change with the change in the number of sites is indeed obtained.

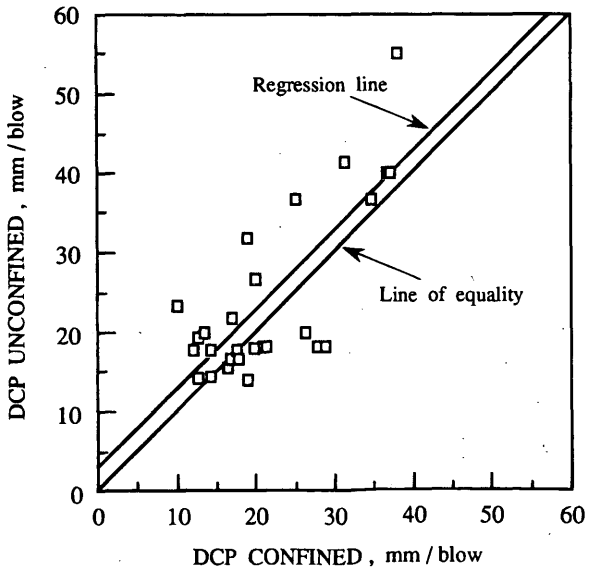

FIGURE 8 Correlation between confined and unconfined DCP within clay subgrades.

A regression analysis of the linear $y = ax + b$ type leads to the following results:

$a = 2.86$ ($S_a = 3.75$), $b = 0.98$ ($S_b = 0.16$), $R^2 = 0.59$, and $\sigma^2 = 48.23$

Examination of the confidence interval for the parameters a and b at a confidence level of 95 percent leads to the acceptance of the hypothesis that a equals zero and b equals *1*, that is, that there is no additive or multiplicative bias. Hence, the calculated values for a and b, 2.86 and 0.98, respectively, are not significant.

An analysis by the method of Grubbs (*23*) also indicates that both the systematic error and the standard deviation of the one population's random error are identical to those of the other population.

The final conclusion is that despite the variations shown in Figure 8, it seems that the two populations are identical. In other words the effects of the penetrating rod's surface friction are not felt in this case. This is logical, since in clay material (in contrast to granular material) the chances of preserving the gap between the sides of the hole created with the cone's penetration and the penetrating rod's surface, whose radius is smaller, are better.

EFFECT OF CONFINEMENT BY RIGID STRUCTURE

An examination of the DCP values of a clay subgrade confined beneath a 50-cm-thick all-asphaltic pavement has yielded deviant strength results compared with the CBR values obtained by direct testing. The DCP test was conducted in the subgrade following drilling of the core for the entire depth of the all-asphalt structure. The results are presented in Figure 9.

When the regression is restrained through the graph zero of Figure 9, the equation is:

$$CBR_D = 1.75\ CBR_s \quad (9)$$

or

$$DCP_s = 1.55\ DCP_D \quad (10)$$

where CBR_D is the CBR value calculated from the DCP test conducted through the all-asphalt structure, and CBR_s is the direct CBR value.

To test whether the increase in strength presented in Equations 9 and 10 is the result of vertical confinement caused by the rigid all-asphalt structure, a special series of tests was conducted in the laboratory as described in the next paragraph.

In the test series clay samples (liquid limit, 66 percent; plasticity index, 43 percent) were compacted by 12 blows (4 samples) and 26 blows (18 samples) in the standard CBR mold. The moisture contents were higher than the plasticity limit. These clay samples were not saturated with water. Each pair of samples was tested with the DCP instrument both without vertical pressure (free top surface) and with the surface restrained by means of a thick metal plate with a 3-cm-diameter hole. At the end of the test it was clearly observed that when the sample was unrestrained there were vertical movements and cracking around the area of penetration, whereas in the case of the restrained samples, the upper soil surface remained smooth and uncracked and without any vertical movement.

All of the various statistical tests indicate that restraining the samples does not affect the DCP results. This can also be seen from the plotted results presented in Figure 10. The regression model leads to the following parameters:

$a = 1.26$ ($S_a = 3.51$), $b = 1.01$ ($S_b = 0.114$), $R^2 = 0.90$, and $\sigma^2 = 8.73$

For a confidence level of 95 percent, a equals zero and b equals 1. This analysis does not follow the trend of results presented in Figure 9. The explanation for this can be given by assuming that friction forces do develop along the penetrating rod as a result of nonvertical penetration rather than because of the artificial restraining of the clay in the laboratory or its restraint by the all-asphalt pavement at the site. To test this assumption a series of tests was conducted in which the rod was inserted both vertically and at an angle of 15 degrees.

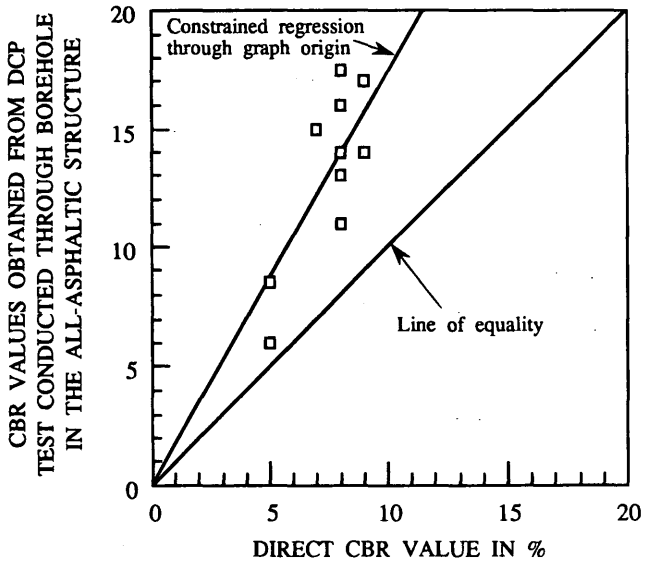

FIGURE 9 CBR results from clay subgrade beneath 50-cm-thick all-asphalt structure.

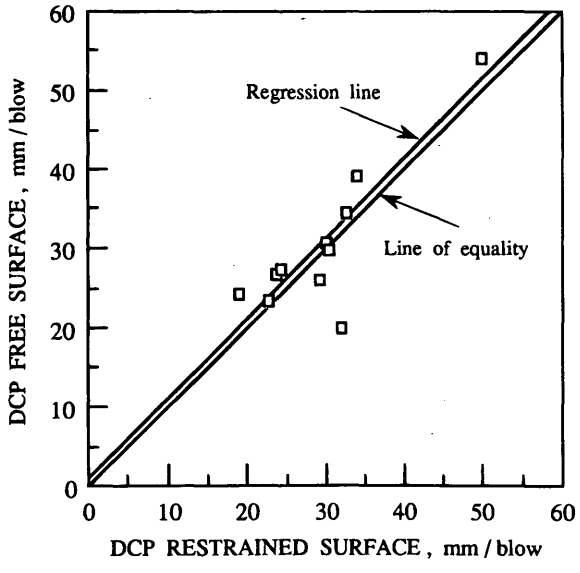

FIGURE 10 Effects of restrained sample surface on DCP values.

The statistical analysis indicates that there is a difference between the two tests. The mean CBR_v value for the vertical penetration is 6.6 percent, whereas the CBR_t value for penetration at a 15-degree angle is 8.9 percent. A constrained regression through the origin produces the following correlation (Figure 11):

$$CBR_v = 0.78\ CBR_t \quad (11)$$

The meaning of this above regression is that the DCP value decreases (the strength increases) when the penetrating rod is inserted at an angle. This fact can be used to explain the results presented in Figure 9, since in many cases under actual deep DCP penetration, the rod tends to tilt at an angle of up to 15 degrees. It should be noted that the tilted penetration can be avoided by penetrating the DCP rod through a vertical supporting frame. This is accomplished by the regular DCP device or by an automated DCP device (*24*).

EFFECT OF CONFINEMENT BY ASPHALT LAYERS

The effect of confinement by the asphalt layers on the granular pavement layers was examined by conducting DCP tests on the base course materials after drilling an asphalt core and comparing the results with those obtained from performance of the DCP test on these materials following the removal of a wide asphalt strip from the same spot tested previously. In contrast to the case described in the preceding section, one can expect here an increase in the normal DCP value compared with the confined DCP values in granular materials, since the bearing capacity factor, $N_{\gamma q}$, is far greater than 1. Indeed, the results obtained indicate the following correlation, as can also be seen in Figure 12:

$$DCP_{unc} = 1.84\ DCP_{con} \quad (12)$$

The difference between the DCP values is statistically significant, and thus, the asphalt does indeed have a confining effect on the state

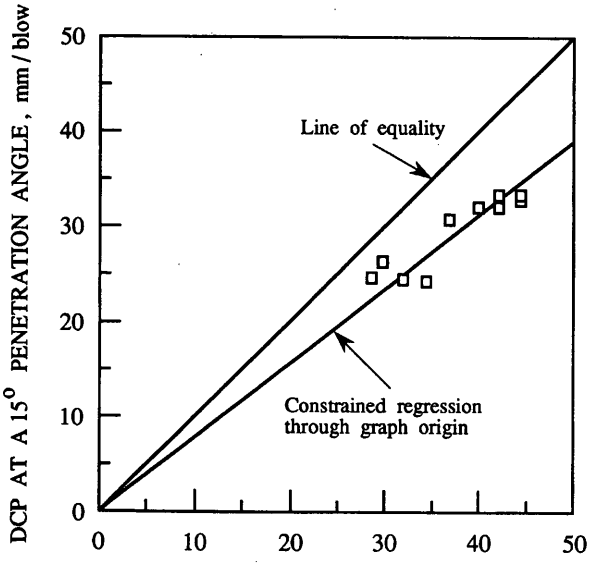

FIGURE 11 DCP values from vertical penetration and penetration at a 15-degree angle.

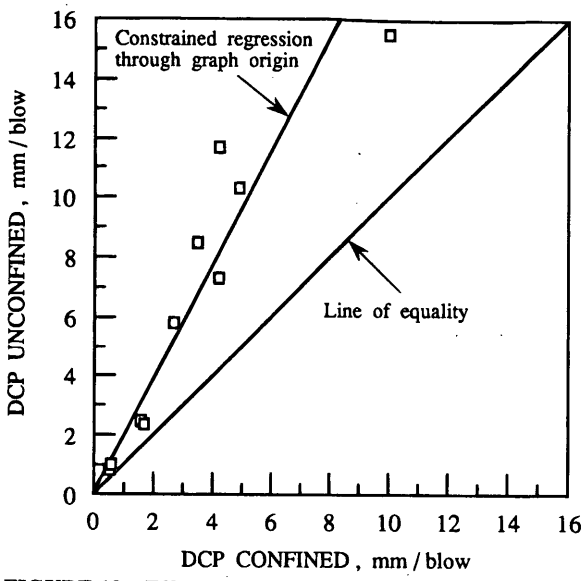

FIGURE 12 Effects of asphalt confinement on DCP values in granular material.

of the granular material. Since this effect has been shown to exist, it is now appropriate that the strength values of the granular material in the CBR or DCP field tests should be determined only after the drilling of asphalt cores and not after the removal of a wide strip of asphalt.

SUMMARY

The DCP has become one of the most useful testing devices in pavement evaluation in Israel and other parts of the world. Consequently, a reliable true meaning of the results and an interpretation of the results were needed. This paper summarized research work that was dedicated to studying the effects of vertical confinement on the DCP values of the subgrade and the granular pavement layers. Specifically, four major effects were studied: vertical confinement of granular layers, vertical confinement of cohesive layers, vertical confinement of rigid structural layers, and the effect of vertical confinement of upper asphalt layers on the DCP values of the granular layers beneath them.

On the basis of the theoretical analysis, experimental testing in the laboratory and in the field, and statistical analysis, the following conclusions were made.

1. No vertical confinement effect by rigid pavement structure or by upper cohesive layers on the DCP values (or strength) of lower cohesive subgrade layers exists. Also, no vertical confinement effect by the upper granular layers on the DCP values of the cohesive subgrade beneath them exists. Any difference in the results between the confined and unconfined DCP values in the rigid structure case or in the case of the granular layers can be explained by the friction that developed in the DCP rod by tilted penetration or by a collapse of the granular material on the rod surface during regular penetration. This friction effect, which is also a function of the ratio between the cone tip and the rod diameters, can be quantitatively evaluated by torque measurements in the DCP device during penetration intervals.

2. A vertical confinement effect by the upper asphaltic layers on the DCP values of the granular pavement layers does exist. Generally, these confinement effects cause a decrease in the DCP values, thus increasing the structural strength measured. Since this is the true effect of the pavement structure, any DCP measurements for pavement evaluation purposes should be performed through a narrow boring in the asphalt layers and not after removal of a wide strip of asphalt.

3. The vertical confinement effects and the friction effects described earlier, which can be quantitatively evaluated, should be taken into consideration when using the DCP method in pavement and subgrade evaluation.

ACKNOWLEDGMENTS

This work was conducted as part of a comprehensive project on the carrying capacity of unsurfaced runways financed by the U.S. Air Force Engineering & Services Center, Tyndall Air Force Base, Florida. The authors thank that organization for the sponsorship and aid. Thanks are also due to the Israel Air Force, the Technion Soils & Roads Testing Laboratory, and also to A. Aines and F. Hirosh for their technical and administrative assistance.

REFERENCES

1. Kleyn, E. G., J. H. Maree, and P. F. Savage. The Application of a Portable Pavement Dynamic Cone Penetrometer to Determine In-Situ Bearing Properties of Road Pavement Layers & Subgrades in South Africa. *Proc., 2nd European Symposium on Penetration Testing*, Amsterdam, May 1982.
2. Smith, R. B., and D. N. Pratt. *Field Study of In-Situ California Bearing Ratio and Dynamic Penetrometer Testing for Road Subgrade Investigation.* Australian Road Subgrade Investigation. Australian Road Subgrade Investigation, Australian Road Research Board, Vol. 13, No. 4, p. 198.
3. Harrison, J. A. Correlation Between the California Bearing Ratio and the Dynamic Cone Penetrometer Strength Measurements of Soils. *Proc., Institute of Civil Engineers*, Part 2.83, Technical Note 463. Institute of Civil Engineers, 1987.
4. *Operating Instrumentation for the TRRL Dynamic Cone Penetrometer.* Information Note. Transport and Road Research Laboratory, Crowthorne, Berkshire, United Kingdom, 1986.
5. Livneh, M., and I. Ishai. Pavement and Material Evaluation by a Dynamic Cone Penetrometer. *Proc., 6th International Conference on the Structural Design of Asphalt Pavements*, Ann Arbor, Mich. July 1987, pp. 665–676.
6. Chu, K. M. Determination of CBR and Elastic Modulus of Soils Using a Portable Pavement Dynamic Cone Penetrometer. *Proc., 1st International Symposium on Penetration Testing—ISOPT-1*, Orlando, Fla., March 1988.
7. Buncher, M. S., and D. J. Christiansen. *USAF New Contingency Soils/Pavement Testing Van.* ASCE Special Publication on Road and Airport Pavement Response Monitoring Systems. ASCE, 1991, pp. 27–40.
8. Webster, S. L., R. H. Grau, and T. P. Williams. *Description and Application of Dual Mass Dynamic Cone Penetrometer.* Instruction Report GL-92-3. U.S. Army Engineers Waterways Experimental Station, May 1992.
9. de Beer, M. Developments in the Failure Criteria of South African Mechanistic Design Procedure for Asphalt Pavements. *Proc., 7th International Conference on Asphalt Pavements*, Vol. 3, 1992, pp. 54–75.
10. Livneh, M., I. Ishai, and N. A. Livneh. Carrying Capacity of Unsurfaced Runways for Low Volume Aircraft Traffic. Phase III. Application of the Dynamic Cone Penetrometer. Preliminary Report. Transportation Research Institute, Technion, Haifa, Israel, April 1990.
11. Kleyn, E. G. *The Use of the Dynamic Cone Penetrometer (DCP).* Report 2/74. Transvaal Roads Department, 1975.
12. Kleyn, E. G., and M. J. J. Van Neerden. Using DCP Soundings to Optimize Pavement Rehabilitation. Presented at Annual Transportation Convention, South Africa, 1983.
13. Kleyn, E. G., and P. F. Savage. *The Application of the Pavement DCP to Determine the Bearing Properties and Performance of Road Pavements.* Report L7/82. Transvaal Roads Department, South Africa, 1982.
14. Kleyn, E. G., and P. F. Savage. The Application of the Pavement DCP to Determine the Bearing Properties and Performance of Road Pavements. *Proc., International Symposium on Bearing Capacity of Roads & Airfields*, Trondheim, Norway, 1982.
15. Livneh, M. *Correlation Between the DCP and CBR Values.* Publication 87-065. Transportation Research Institute, Technion, Haifa, Israel, 1987.
16. Van Vuuren, D. J. Rapid Determination of CBR with the Portable Dynamic Cone Penetrometer. *The Rhodesian Engineer*, Vol. 7, No. 5, 1969, pp. 852–854.
17. Livneh, M. The CBR Test with Lateral Pressures. *Proc., 3rd Asian Regional Conference on Soil Mechanics and Foundation Engineering*, Vol. 1, 1967, pp. 293–297.
18. Livneh, M., and J. Greenstein. A Modified CBR Test for Granular Materials. *Geotechnical Testing Journal, ASTM*, Vol. 1, No. 3, 1978, pp. 141–147.
19. Meyerhof, G. G. The Ultimate Bearing Capacity of Wedge-Shaped Foundations. *Proc., 5th International Conference on Soils Mechanics & Foundation Engineering*, Vol. 2, 1961.
20. Durnunoglu, H. T., and J. K. Mitchell. Influence of Penetrometer Characteristics on Static Penetration Resistance. *Proc., European Symposium on Penetration Testing*, Stockholm, Sweden, 1974.
21. Nowatzki, E. A., and L. L. Karafiath. The Effect of Cone Angle on Penetration Resistance. In *Highway Research Record 405*, HRB, National Research Council, Washington, D.C., 1972.
22. Brinch-Hansen, J. *A General Formula for Bearing Capacity.* Bulletin 11. Danish Geotechnical Institute, Copenhagen, Denmark, 1961.
23. Grubbs, F. E. Errors of Measurements, Precision, Accuracy and the Statistical Comparison of Measurement Instruments. *Technometrics*, Vol. 15, No. 1, Feb. 1973, pp. 53–66.
24. Livneh, M., I. Ishai, and N. A. Livneh. *Automated DCP vs. Manual DCP in Carrying Capacity of Unsurfaced Runways.* Project 115-101. Transportation Research Institute, Technion, Haifa, Israel, 1992, 42 p.

Publication of this paper sponsored by Committee on Strength and Deformation Characteristics of Pavement Sections.

Rutting Analysis From a Different Perspective

AMY L. SIMPSON, JEROME F. DALEIDEN, AND WILLIAM O. HADLEY

Rutting is a common distress in pavements with asphalt concrete surfaces. For many agencies the magnitude of rutting plays a significant role in their rehabilitation decision process. As a result many different approaches have been taken to address the prediction of rutting and its causes. As more agencies shift to the collection of transverse profiles instead of rutting to provide greater repeatability of the measurements and to avoid debates regarding the appropriate straightedge length, additional analytical possibilities are being identified. One such analytical opportunity explored in the present investigation suggests that the area under the transverse profile can be used to hypothesize the origin of the rutting from within the pavement structure. This in turn allows for greater prediction capabilities when the cause of the distress can be further isolated in this fashion. With the benefit of the numerous transverse profiles collected as part of Long-Term Pavement Performance Program monitoring, investigations have been conducted to sort the test sections into data subsets based on the areas described above. Neural networks were developed to model these data subsets. The models are in turn compared with other previously developed models to evaluate the impact of sorting by areal magnitude on the prediction of rutting.

Rutting in pavements with asphalt concrete surfaces is commonly used as an indicator of needed rehabilitation. As such many studies have been conducted to analyze the causes of rutting and to predict its development. Many of these studies, however, have been impeded by one or more of the following deficiencies associated with this important performance indicator. First, and probably foremost, rut depths in and of themselves provide very little, if any, indication of the origin of the rutting. That is, it is difficult to establish which layer within the pavement structure contributed the most to the deformations that are measured at the pavement surface. The second drawback of this particular performance indicator revolves around the lack of standardization in the collection of rut depth data. The common use of a 4-ft straightedge in the past (as at the AASHO Road Test) to obtain these measurements and the resulting limitations with repeatability have made it relatively unreliable for satisfactory pavement performance modeling needs. In addition, wider wheel bases are being used in trucks. These two events introduced large amounts of variation in 4-ft rut depth measurements.

With continuing advances in pavement monitoring technology, such deficiencies no longer need to be tolerated. Most automated units that collect pavement data are now capable of recording transverse profile measurements that minimize or eliminate most (if not all) of the past limitations associated with the collection of rut depth data. Automated collection of transverse profile data has now become one of the more standardized and repeatable operations for the collection of pavement data. Standards under development by ASTM will improve the level of data quality achievable.

A. L. Simpson and J. F. Daleiden, Brent Rauhut Engineering, Inc., 8240 Mopac, Suite 220, Austin, Tex. 78759. W. O. Hadley, Hadley & Associates, 12402 Mercury Lane, Austin, Tex. 78759.

The point yet to be investigated fully is the insight into the origination of rutting within a pavement structure than can be provided by a transverse profile. Boussinesq (*1*) and Burmister Theory (*2–4*) indicate that an analyst should be able to establish weaknesses within a given pavement structure on the basis of the shape and dimensions of deformations at the pavement surface. Although these theories apply to elastic deformation, it is the continued application of the load that causes both the elastic deformation and the plastic deformation. It is assumed that the plastic deformation follows a trend similar to that of the elastic deformation. Although several studies have been conducted in an attempt to pursue this theory further, sufficient data were never available to thoroughly investigate and support studies of this type until the recent efforts of the Long-Term Pavement Performance (LTPP) Program.

With the data available from LTPP test sections this paper evaluates the use of transverse profile data for distinguishing rutting modes to facilitate performance predictions and model development. In addition, the capabilities of neural networks in data analysis are demonstrated.

Neural networks are a form of artificial intelligence that has been quite useful in many areas of robotics and other applications and that has come to the attention of other engineering disciplines in recent years. They provide a very confident means of identifying patterns. In the past they have often been used for handwriting recognition, hand–eye coordination in robots, and many other areas of robotics technology. More recently, these networks are being used by financial analysts to predict the stock market or the winner of Saturday's ball game.

ANALYSIS

The first step in conducting these analyses was to assemble and process all of the transverse profiles. For the LTPP Program transverse profiles were reduced from projections of a hairline at an angle onto the pavement and were photographed from above. The presence of rutting is recorded on the film as departures from a straight line, and the magnitudes of the ruts are directly proportional to the magnitudes of the departures from a straight line. A PASCO Road Recon Unit projects the hairline onto the pavement surface and records the projections on film at 15.24-m (50-ft) intervals. These film projections were later processed to identify the distance between the string line projection and the string line itself. Measurements were taken every 0.30 m (12 in.) across the monitored lane [typically 3.7 m (12 ft) in width]. This series of measurements then makes up the transverse profile.

As noted earlier the shape of the transverse profile is theoretically indicative of where the rutting originated within the pavement structure. As noted in Figure 1 the transverse profiles generally fit into one of four categories representing (a) subgrade rutting, (b) base

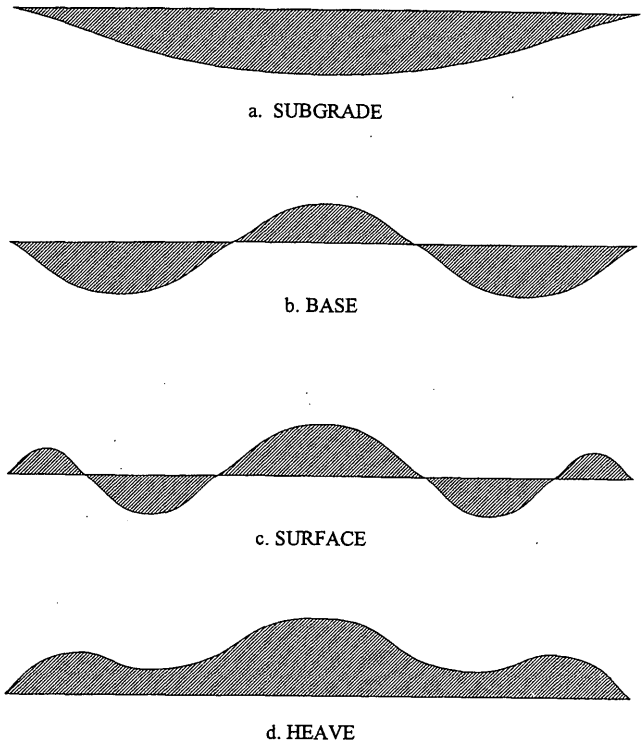

FIGURE 1 Rutting properties.

rutting, (c) surface rutting, or (d) heave (from increases in soil volume because of environmental conditions).

To identify into which of these four categories the various transverse profiles fit, the algebraic area between the transverse profile and the straight line connecting its end points was calculated (Figure 1). The diagrams in Figure 1 indicate that sections from within the deep rutting category will be entirely negative and sections from within the heave category will be entirely positive. Sorting out the distinctions between base rutting and surface rutting are somewhat more involved. In this process it is generally perceived that the marginally positive areas would be considered surface rutting and that the marginally negative areas would be perceived as base rutting.

The area or distortion term was used to determine where in the pavement structure the rutting occurred. If the total distortion was less than -4500 mm^2 and the ratio of the positive area to the negative area was less than 0.4, the rutting was hypothesized to have occurred in the subgrade. If the total distortion was between -4500 and 700 mm^2 and the ratio of the positive area to the negative area was between 0.4 and 1.25, the rutting was hypothesized to have occurred in the base layers. If the total distortion was between 700 and 5000 mm^2 and the ratio of the positive area to the negative area was between 1.25 and 3.0, the rutting was hypothesized to be primarily due to the lateral migration of the asphalt concrete surface layer. If the total distortion was greater than 5000 mm^2 and the ratio of the positive area to the negative area was greater than 3.0, the rutting was hypothesized to be primarily due to frost heave. Table 1 demonstrates the criteria used and the actual number of sections in each group. The dual classification method did not agree for six sections. These sections were left out of the analysis. Cross-profile data were not available for 18 test sections.

The data used in this effort were the same as those used in the early analysis of the LTPP data base (*5*) for analysis of hot-mix asphalt concrete (HMAC) pavements with granular bases. This data set includes 152 sections from the LTPP General Pavement Studies 1 and 2 experiments. Two datum points in time were available for each section: the first was the 0 boundary condition (0 rutting after 0 traffic) and the second was the first measured cross-profile. The cross-profile measurements were analyzed by using RUT (*6*), a program created by the Texas Research and Development Foundation. This program determines the rut depth by using a 4-ft straightedge, a 6-ft straightedge, and the areal distortion of the roadway from the string line described previously. After the data set was sorted by rutting origin (as described above) modeling was initiated by using the 6-ft straightedge values as the dependent variable. Because the 4-ft straightedge has limitations in repeatability, only the 6-ft straightedge was used for the purposes of modeling. Each of the four data sets described was modeled by using neural network technology.

NEURAL NETWORKS

The data were then analyzed by using neural networks. Neural networks are a computational form that loosely models the human brain. The following definition provides some explanation:

> Neural networks are rough models of the mental processes their name implies. Because of their massive parallelism, they can process information and carry out solutions almost simultaneously. They learn by being shown examples and the expected results. Or, they form their own associations without being prompted and rewarded. They are good at pattern-matching types of problems. Because the kinds of things neural nets can do address many of today's problems, a new industry is emerging. This is happening on several continents and involves a wide variety of disciplines (*7*).

They learn by example and are very good at recognizing patterns and modeling data that had been quite difficult to emulate by standard regression techniques.

Each neural network was made up of at least three layers. Figure 2 illustrates a pictorial representation of neural networks. Each layer is made up of one or more nodes. These nodes, or processing ele-

TABLE 1 Rut Origin Sorting Criteria

Type	Total Distortion	Ratio of Distortion (Positive/Negative)	Number of Sections
Subgrade	< -4500	< 0.4	61
Base	-4500 < x < 700	0.4 < x < 1.25	24
Surface	700 < x < 5000	1.25 < x < 3.0	15
Heave	> 5000	> 3.0	28

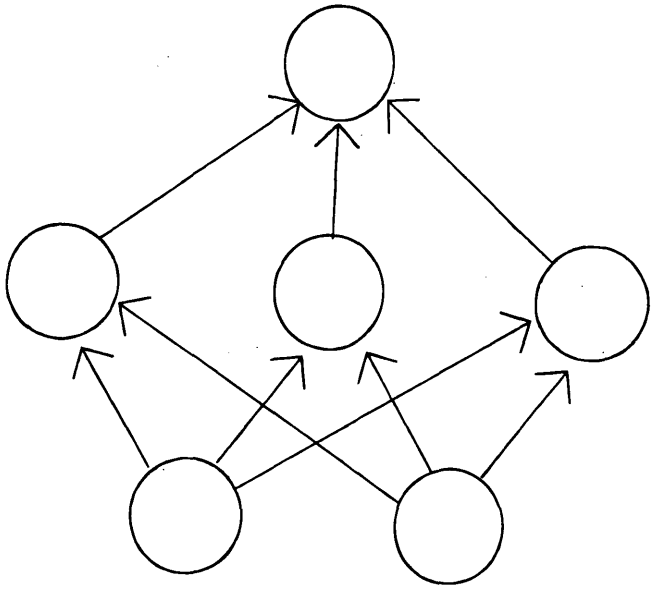

FIGURE 2 Pictorial representation of neural networks.

ments, take in information and sum it, and if it passes a certain threshold value it will be passed to the next layer. The first layer of the network is the input layer. Each node of this layer is an input value. These values are automatically passed to each of the nodes in the next layer via a weighted connection. This second layer is a hidden layer, which is analogous to the interactions of independent variables in conventional statistical analyses. It is hidden because one normally does not see what comes directly out of this layer. It is possible to have more than one hidden layer, but usually, only the most complicated of networks have more than one hidden layer. The values in the nodes of the hidden layer are passed to the output layer, or the third layer, on the basis of whether or not those values meet some acceptance criterion. Again, the connections between the hidden layer and the output layer are weighted. The output layer is, for example, the result that one would see from an equation. The network learns in an iterative process whereby it makes changes to the weights of the connections on the basis of how close the value is to the required output.

To apply neural network analyses it is necessary to obtain software that is called a shell. When data are provided to the shell for as many observations as possible, the shell creates a neural network by using the hidden layers described earlier to model interactions between the variables. The analyst has some control over the result through selection of independent variables to be included and their format [e.g., equivalent single axle loads (ESALs) or log ESALs], selection of the rate of learning, specification of the percentage of test sections to be used only for testing, specification of tolerances between predicted and measured values, and ordering of input data. For this analysis, the shell used was BrainMaker (*8*).

The result after hundreds or thousands of iterations of learning (or study of the available data) is not an equation, such as that which is normally produced from statistical regressions. Instead, it is a small computer program that can receive input and provide predictions. This program can then be used in design procedures or for pavement management systems instead of an equation that one might get by standard regression techniques. Although this may appear to be strange because most analysts are accustomed to having equations to look at and think about, it makes little difference as long as the network has been thoroughly checked out and its capabilities have been thoroughly evaluated.

One of the difficult things about standard regression techniques is finding the right forms of the equation that provide a quality fit to the data. It would be much easier if the operation were in three dimensions, in which everything could be plotted and the functions could be determined visually. However, analysts are virtually always operating in n-space when they are developing predictive distress models, so the resultant models are often more approximate than one would wish. One advantage of neural networks is that the analyst does not have to experiment with equation forms until a suitable one is found. The neural network generally sorts that out with its iterative studies of the data and continuing modifications of the network.

RESULTS

For comparative purposes a neural network was developed by using the entire data set to assess distinctions in the dependent variables needed for modeling the various data sets and to compare summary statistics with the other models that have been developed. Comparing the neural network for the entire data set against the linear model developed from the early analyses of the LTPP data base (Strategic Highway Research Program Contract P-020), it is fairly apparent that the neural network concept is capable of computing models with considerably less residual error than the residual error from the standard linear models. The neural network had a coefficient of determination (R^2) of 82 percent and a root mean square error (RMSE) of 0.05, versus values of 49 percent and 0.12, respectively, for the P-020 model. It should be noted here that the P-020 equation was formed with log rut depth as the dependent variable; therefore, RMSE is a multiplicative error term rather than an additive term like the other RMSEs presented in this paper. As can be seen from Table 2 both models were a function of essentially the same independent variables.

TABLE 2 Independent Variables Included in P-020 Model and "All" Network

Model	Independent Variables
P-020	log(HMAC Aggregate < #4), log(Air Voids), log(Base Thickness), Subgrade < #200, Freeze Index, log(HMAC Thickness), Cumulative KESALs
"All" Network	Asphalt Thickness, Air Voids, Asphalt Viscosity @ 140°F, Annual Precipitation, Average No. of Days > 90°F, Average Freeze Thaw Cycles, PI, Subgrade Moisture, Subgrade < #200, Base Thickness, log(Cumulative KESALs)

Note: KESALs=1000 80kN (18 kip) equivalent single axle loads

TABLE 3 Summary Statistics for All Models

Data Set	R^2	RMSE
P-020 (Entire Data Set)	45%	0.18
Network (Entire Data Set)	82%	0.07
Subgrade Rutting Data Set	94%	0.05
Base Rutting Data Set	90%	0.04
Surface Rutting Data Set	98%	0.02
Heave Data Set	96%	0.02

By using the guidance described earlier, sections were then redistributed into one of the four data sets on the basis of the anticipated source of rutting associated with that section. For the most part these distinctions were fairly clear-cut and straightforward.

By using the data sets distinguished by anticipated rutting origin, separate neural networks were created for each data set. As can be seen from Table 3, the summary statistics for these neural network models are again considerably better than those for previously developed linear models. These networks also show a considerable improvement over the network formulated for the entire data set. Each has an R^2 in the 90th percentile range, with RMSEs of 0.04 on average versus the R^2 of 82 percent and RMSE of 0.07 for the network formulated from the entire data set. The predictive capabilities of the networks are illustrated in Figures 3 to 7. Figure 3 illustrates the predicted versus the actual rut depths for the neural network created for the entire data set. The lines in the graphs are the 45 degrees that would describe a perfect prediction. Figures 4 to 7 show the same graphs for each of the data subsets. These graphs show that much better networks can be obtained when the data are separated into the four categories of rutting. One could argue that these improvements could be the result of the relatively smaller data sets used in the analyses; however, considering the levels of improvement shown, it is difficult to accept that this is the entire explanation for the difference.

One result that is particularly unique is the limited number of independent variables required to formulate rutting origin-specific networks. As can be seen from Table 4 the independent variable sets for each of these models are considerably more refined and are oriented toward the form or origin noted. Figures 8 to 11 graphically compare the various models developed for each of the rutting origin data sets. Note that the network (entire data set) and P-020 model graphs are plots of those models obtained with the entire data set applied to these data subsets. All of the parameters in each model except traffic were held at their means for Figures 8 to 11. Figure 8 also includes the results from a linear regression on this data set (Equation). This equation had an R^2 of 32 percent and an RMSE of

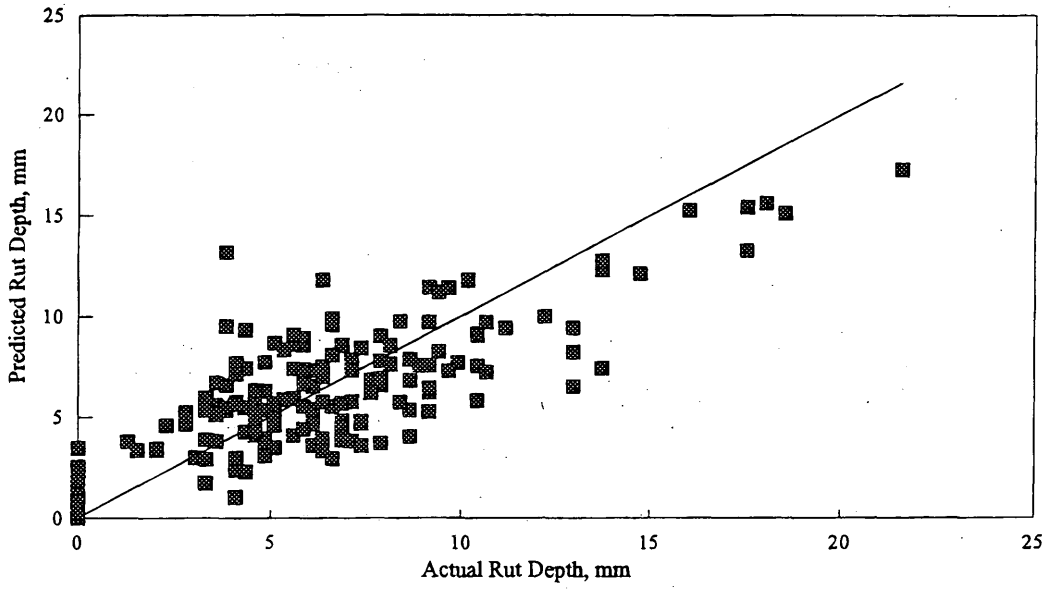

FIGURE 3 Predicted versus actual rut depths for the neural network created with entire data set.

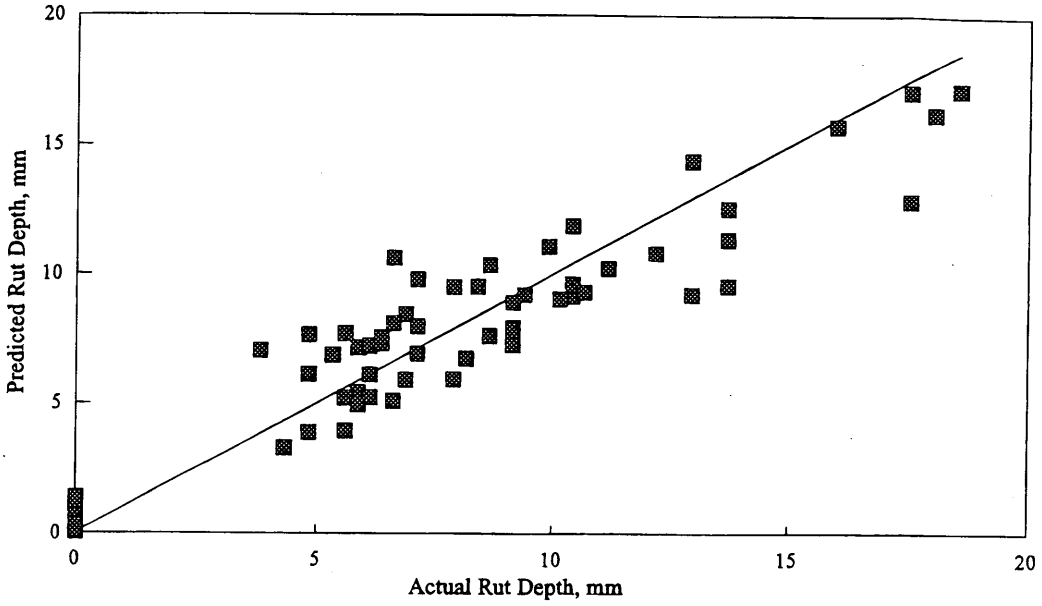

FIGURE 4 Predicted versus actual rut depths for subgrade rutting data set.

0.35 in the log of rut depth. This RMSE is a multiplicative error term, just as the error terms for the P-020 model analysis are also multiplicative. The regression analysis was limited and did not extend to nonlinear regression, but it will give the reader a chance to examine the kinds of improvements that can be made when using the neural network for analysis purposes.

CONCLUSIONS

From the analyses described here two conclusions can be made. Although application of neural networks for pavement performance modeling is still a fairly new concept, it does appear that they are capable of predicting pavement performance considerably better

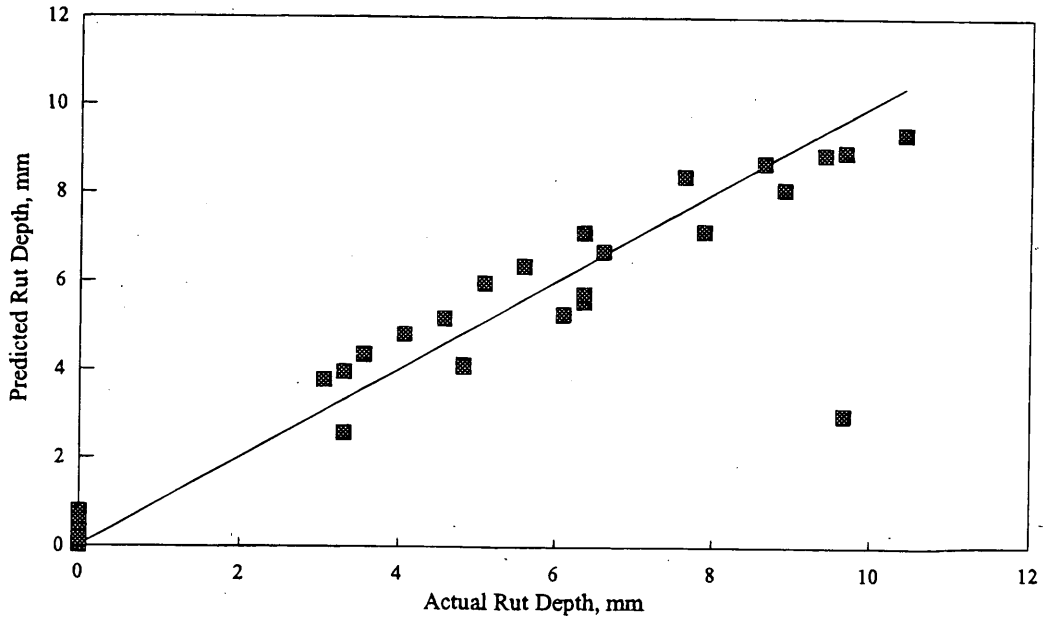

FIGURE 5 Predicted versus actual rut depths for base rutting data set.

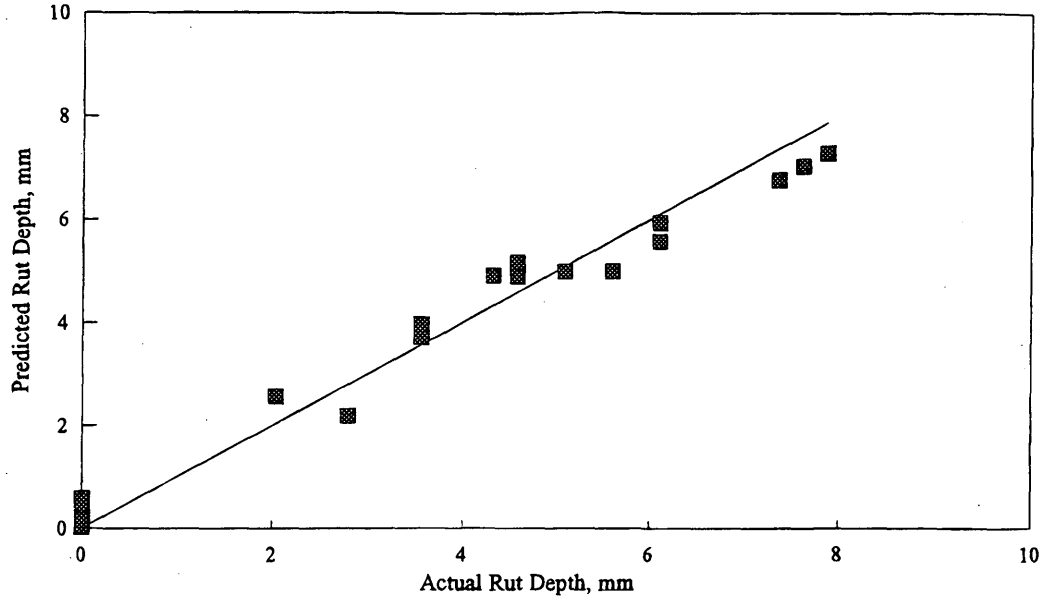

FIGURE 6 Predicted versus actual rut depths for surface rutting data set.

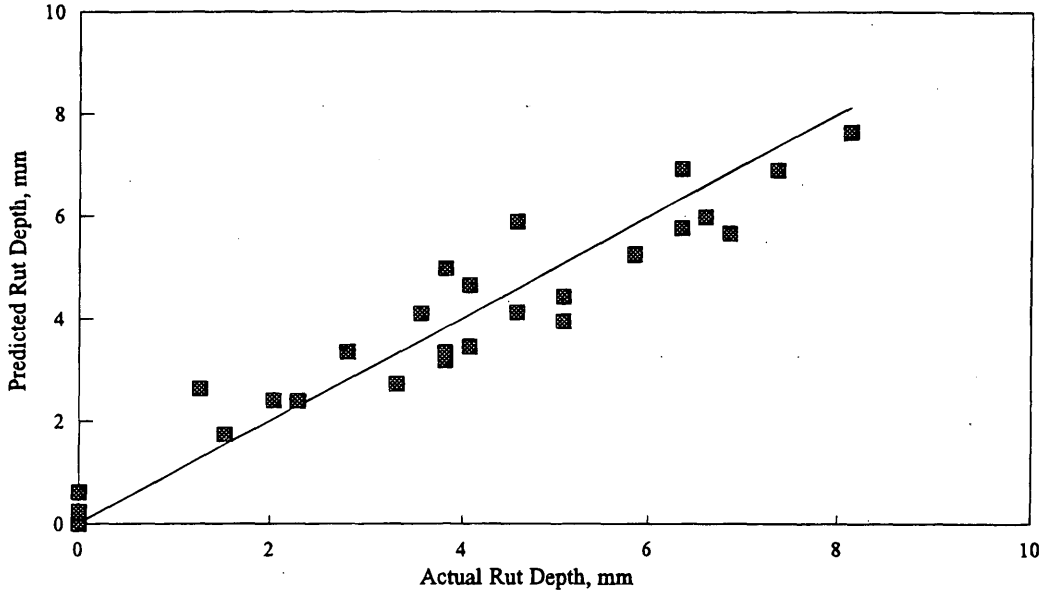

FIGURE 7 Predicted versus actual rut depths for heave data set.

TABLE 4 Independent Variables Included in Each Model

Model	Independent Variables
Entire Data Set	HMAC Thickness, Air Voids, Asphalt Viscosity @ 140°F, Annual Precipitation, Avg. No. of Days > 90°F, Avg. Freeze Thaw Cycles, PI, Subgrade Moisture, Subgrade < #200, Base Thickness, log(Cumulative KESALs)
Subgrade Rutting Data Set	Annual Precipitation, Avg. No. of Days > 90°F, Avg. Freeze Thaw Cycles, PI, Subgrade Moisture, Subgrade < #200, log(Cumulative KESALs)
Base Rutting Data Set	Annual Precipitation, Avg. No. of Days > 90°F, Base Thickness, Base Compaction, log(Cumulative KESALs)
Surface Rutting Data Set	HMAC Thickness, Asphalt Content, Air Voids, HMAC Aggregate < #4, Viscosity @ 140°F, Avg. No. of Days > 90°F, log(Cumulative KESALs)
Heave Data Set	Annual Precipitation, Avg. No. of Freeze Thaw Cycles, PI, Subgrade Moisture, Subgrade < #200, log(Cumulative KESALs)

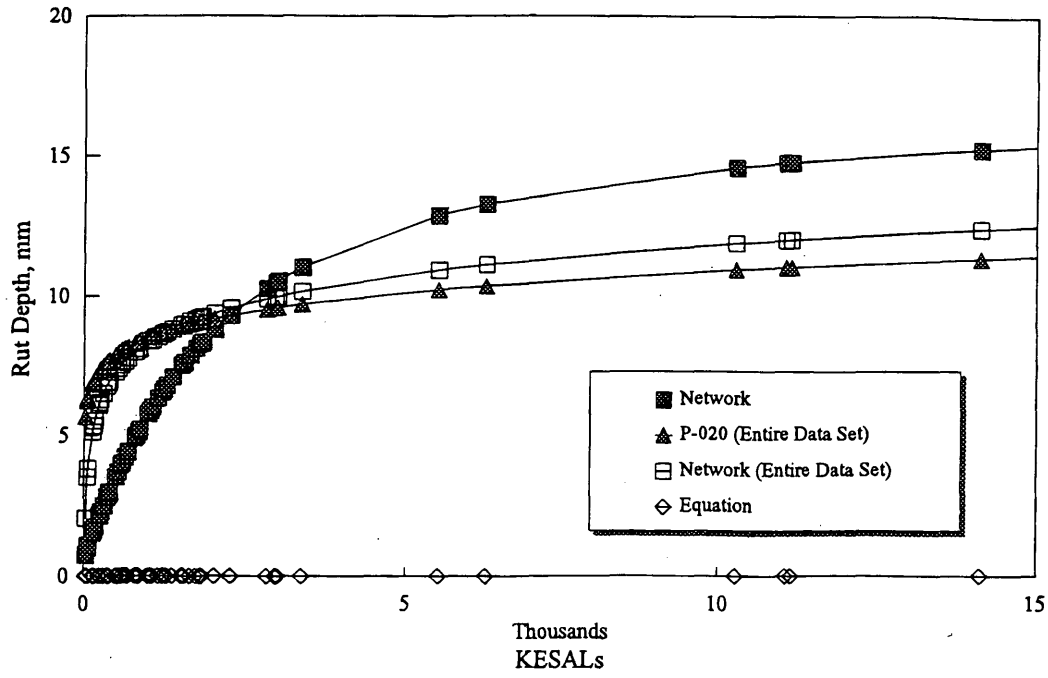

FIGURE 8 Predicted rut depths using various models on subgrade rutting data set.

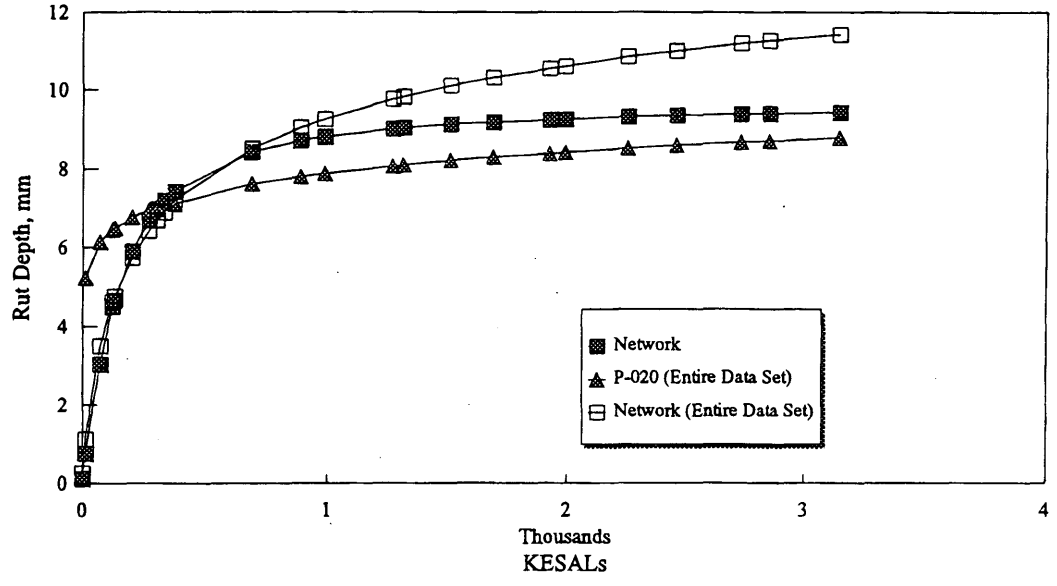

FIGURE 9 Predicted rut depths using various models on base rutting data set.

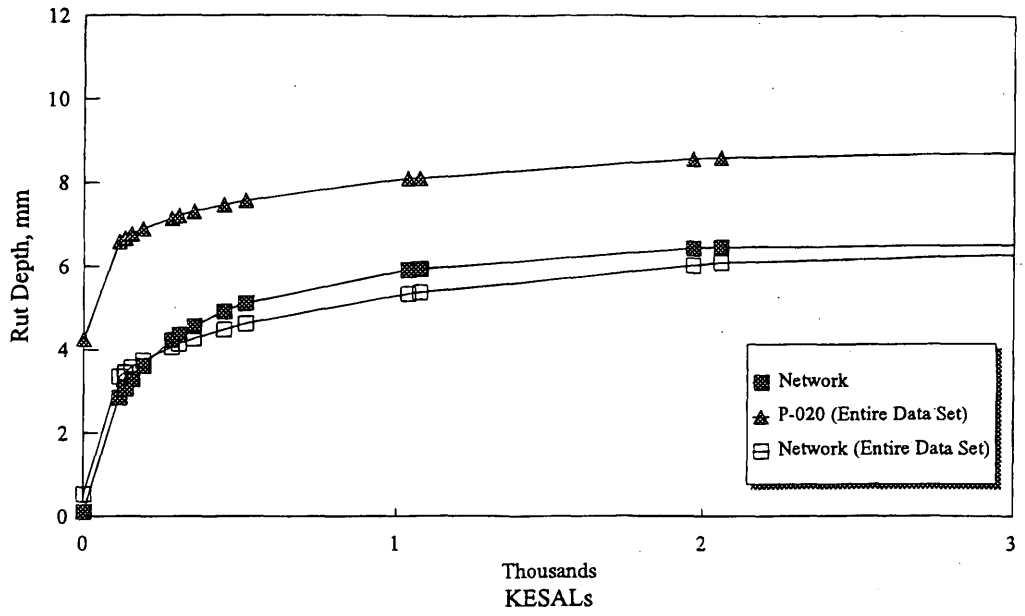

FIGURE 10 Predicted rut depths using various models on surface rutting data set.

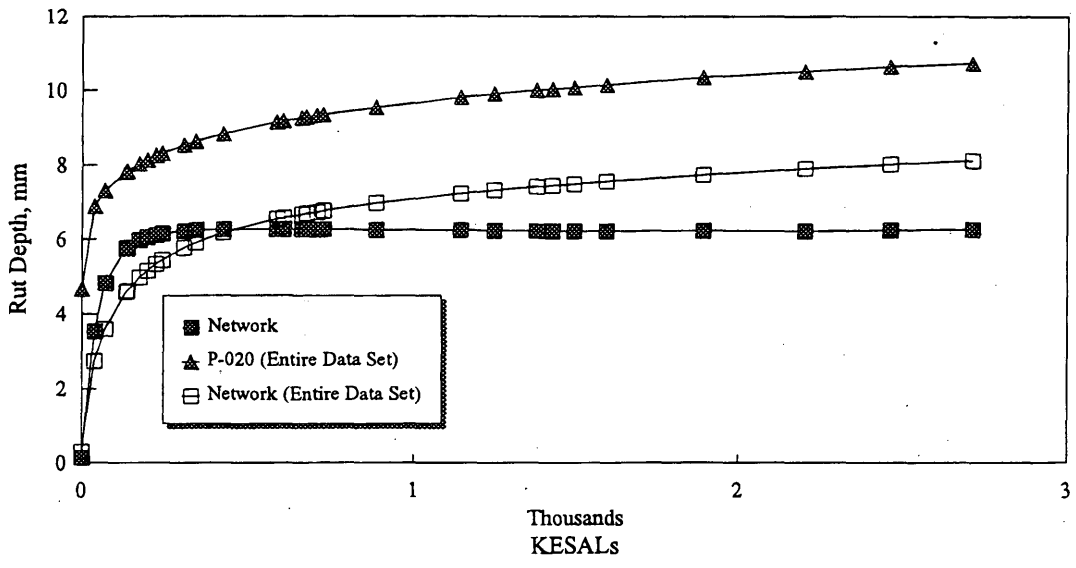

FIGURE 11 Predicted rut depths using various models on heave data set.

than the linear models of the past. It will be necessary to experiment with those networks and check the models to ensure that all of the trends are logical.

The second conclusion is that the division of sections by rutting origin does allow for the development of more refined and specific models, which also appear to be more accurate as a result.

REFERENCES

1. Yoder, E. J., and M. W. Witczak. *Principles of Pavement Design,* 2nd ed. John Wiley and Sons, Inc., New York, 1975.
2. Burmister, D. M. The Theory of Stresses and Displacements in Layered Systems and Application to the Design of Airport Runways. HRB *Proc.,* 1943.
3. Burmister, D. M. The General Theory of Stresses and Displacements in Layered Soil Systems. *Journal of Applied Physics*, Vol. 16, 1945.
4. Burmister, D. M. Evaluation of Pavement Systems of the WASHO Road Test by Layered Systems Methods. *Bulletin 177*, HRB, National Research council, Washington, D.C., 1958.
5. Simpson, A. L., J. B. Rauhut, P. R. Jordahl, E. Owusu-Antwi, M. I. Darter, R. Ahmad, O. J. Pendleton, and Y. H. Lee. *Early Analyses of LTPP General Pavement Studies Data—Sensitivity Analyses for Selected Pavement Distresses*. Report SHRP-P-394. Strategic Highway Research Program, National Research Council, Washington, D.C., 1994.
6. Copeland, C., and W. O. Hadley. RUT. Texas Research and Development Foundation, June 25, 1991.
7. Nelson, M. M., and W. T. Illingsworth. *A Practical Guide to Neural Nets*. Addison-Wesley Publishing Company, Inc., Reading, Mass. 1991.
8. BrainMaker. California Scientific Software, Nevada City, Calif. Aug. 1993.

Publication of this paper sponsored by Committee on Strength and Deformation Characteristics of Pavement Sections.

Using Georgia Loaded-Wheel Tester To Predict Rutting

TYLER MILLER, KHALED KSAIBATI, AND MIKE FARRAR

The feasibility of using the Georgia Loaded-Wheel Tester (GLWT) to predict rutting in the laboratory was analyzed. The study consisted of modifying the GLWT to handle 15.2-cm (6-in.) cores, obtaining asphalt pavement cores from several test sites throughout Wyoming, collecting rut depth data, compiling the data in a computerized data base, and conducting statistical analyses. The analyses resulted in regression models that can be used to predict field rutting on the basis of rut depth measurements from the GLWT.

In the last decade pavement rutting has become a major problem for many state highway agencies. Increased truck tire pressure and heavier axle loads are the two leading causes of this problem. Rutting stems from the permanent deformation in any of the pavement layers or the subgrade, usually caused by the consolidation or lateral movement of the materials caused by traffic loads. Significant rutting can lead to major structural failures and hydroplane potentials (*1*).

Most mix design procedures currently used by state highway agencies are reliable in eliminating extremely poor asphalt mixes. However, they offer little assistance in distinguishing among mixes with high, moderate, or even low rut resistances. With this dilemma many state agencies are looking for reliable alternative methods for predicting the rut resistance of asphalt mixes. Construction of test sections is one method of determining whether an asphalt mix has adequate rut resistance, but this procedure is expensive and requires years of field measurements and analysis. On the other hand, by using accelerated rut testing devices in the laboratory, the rutting characteristics of an asphalt mix can be determined in a matter of days.

Accelerated rut testers have been used by several countries for quite some time. The Europeans have taken the leading role in developing accelerated pavement testing devices. The French Rutting Tester evaluates the resistance to permanent deformation on slabs 50 by 18 cm (19.7 by 7.1 in.) and 2 to 10 cm (0.8 to 3.9 in.) thick (*2*). Two slabs can be tested simultaneously. Slabs are prepared with the Laboratoire Central des Pons et Chaussees (LCPC) plate compactor. During testing the slabs are loaded with 5000 N (1,124 lb) by a pneumatic tire inflated to 0.6 MPa (87 lb/in.^{2}). The environmental chamber enclosing the specimen can be set to any temperature between 35 and 60°C. Tests are typically conducted at 60°C (140°F). Rut depth measurements are taken from 100 up to 100,000 cycles. A successful test will have a rut depth that is less than 10 percent of the slab thickness after 30,000 cycles. A pair of slabs can be tested in approximately 9 hr. The cost of the French rutting tester and LCPC plate compactor is $185,000 (*2*).

The Hamburg Wheel Tracking Device was developed in Germany to measure the resistance to moisture damage. The slab size is 25 by 28 cm (9.8 by 11 in.) and is 6 to 9 cm (2.4 to 3.5 in.) thick. Two slabs can be tested simultaneously. This device is similar to the French rutting tester except that the slabs are immersed in a 50°C (122°F) water bath and loaded with a steel wheel. The temperature can be varied from 30°C to 65°C (86°F to 149°F). The wheel is loaded with 705 N (158 lb). The machine is automated and records the deformation after each cycle. A successful test will have less than 4 mm (0.16 in.) of rut depth after 20,000 cycles. A pair of slabs can be tested in approximately 6 hr. The cost of the Hamburg Wheel Tracking Device is $45,000 (*2*).

The Simple Shear Testing Device was developed at the University of California at Berkeley. Several prototypes are being tested. The cost of this accelerated tester is $150,000. This device is being considered for use by the Strategic Highway Research Program (SHRP) to predict the permanent deformation characteristics of asphalt pavements (*2*).

A device being developed at Oregon State University is the Environmental Conditioning System (ECS). The cost for this device is $45,000. ECS is being considered for use by SHRP to predict moisture sensitivity characteristics (*2*).

The Accelerated Loading Facility (ALF) used by FHWA is a duplicate of an Australian model. ALF is a full-scale pavement testing facility with programmable transverse distribution-of-load passes to simulate the random nonuniformity of actual traffic patterns. ALF is capable of loading the pavement with 4 to 10 tons in a unidirectional motion to provide the most realistic testing possible (*3*). The cost of an ALF is in excess of $1,000,000.

The Georgia Loaded-Wheel Tester (GLWT) was originally developed to test asphalt slurry seals (*4*). It has since been modified and shown by Lai and Lee (*5*) to potentially distinguish between the levels of rut resistance in asphalt mixes. The Georgia Institute of Technology developed a testing system similar to the GLWT. The primary difference with the Georgia Tech device is that the loaded wheel is stationary and the beam moves back and forth on a steel plate and bearing apparatus. The general concept for the Georgia Institute of Technology's accelerated rut tester came from one developed at the University of Nottingham, Nottingham, England (*6*).

The state of Wyoming, like other states, has its share of pavement rutting. Predicting pavement rutting before construction is at the top of the Wyoming Department of Transportation's (DOT's) priority list. As a first step, the University of Wyoming investigated the feasibility of using the GLWT to predict field rutting in the laboratory. The major findings of that investigation are described.

DESIGN OF EXPERIMENT

Figure 1 shows the overall testing and analysis strategies used in the research project described here. First, the GLWT was modified to test 15.2-cm (6-in.) cores instead of beams. Several cores with identical

T. Miller and K. Ksaibati, University of Wyoming, P.O. Box 3295, University Station, Laramie, Wyo. 82071. M. Farrar, Wyoming Department of Transportation, Cheyenne, Wyo. 82002-9019.

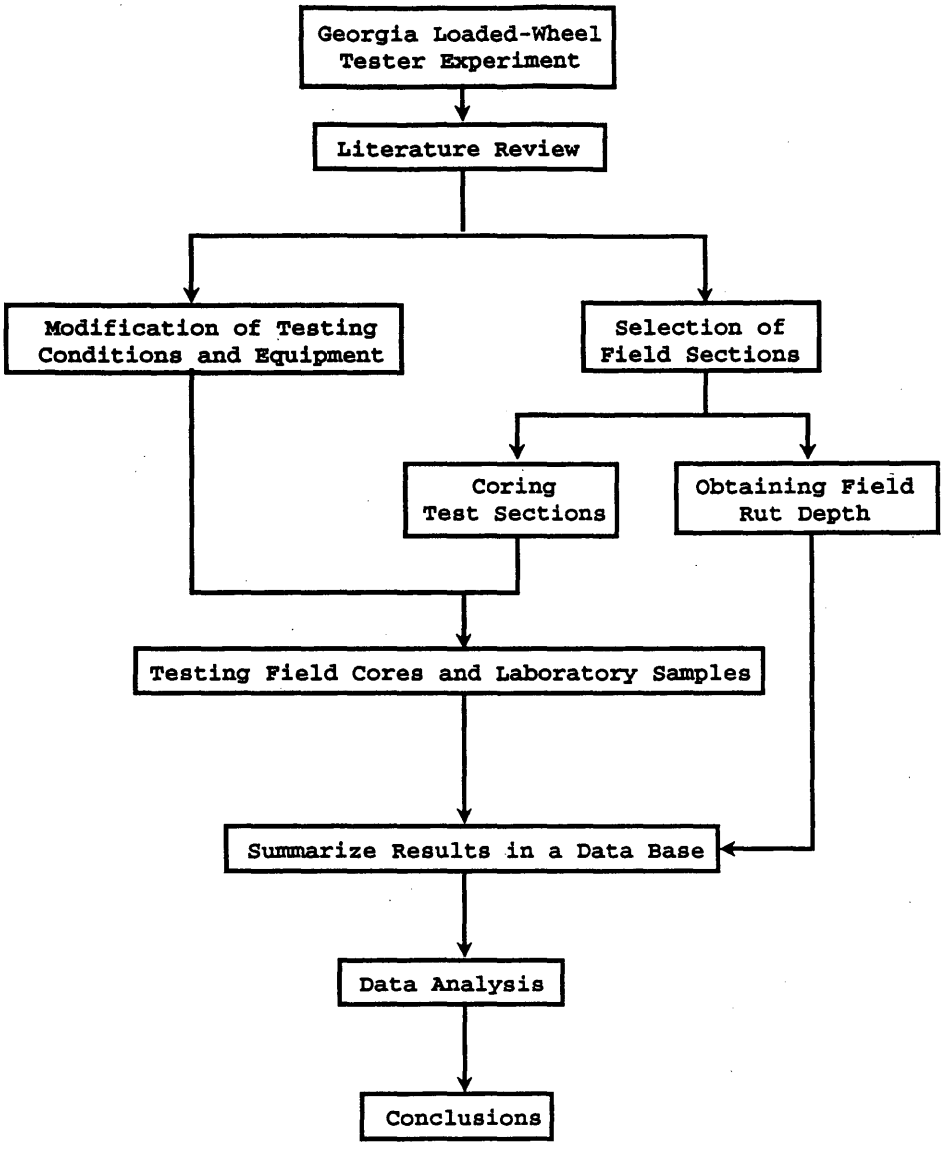

FIGURE 1 Evaluation of asphalt mixes with GLWT.

characteristics were later prepared in the laboratory and were tested with the GLWT to verify the repeatability of the results. Thirteen pavement test sections were selected for inclusion in this experiment. All of these sections were primary roads in the state of Wyoming. Three cores were obtained from each site for testing with the GLWT. After the testing was completed, the field and laboratory rut depth values were summarized in a computerized data base. Statistical analyses were later conducted on the data to correlate laboratory and field rut depth measurements and to verify the repeatability of the GLWT.

MODIFICATIONS TO GLWT

The GLWT was developed by Benedict Slurry Inc. for the Georgia DOT Materials Testing Laboratory to test asphalt slurry seals (*4*). The original version of the GLWT included a loaded wheel driven by an electric motor, a weight-holding box, and a mounting plate for the asphalt specimen. The original GLWT device was modified by replacing the rubber tire assembly with an inflated, stationary rubber hose on which a loaded metal wheel traverses. This eliminated most of the excess rutting on the ends of the test specimens caused by the skidding and shoving actions of the tire. Another modification to the GLWT was the addition of a temperature-controlled environmental chamber that could maintain temperatures up to 51.7°C (125°F) for testing. This made the GLWT portable and capable of testing elevated pavement temperatures corresponding to summer conditions.

The dimensions of a typical GLWT test specimen are 7.5 by 7.5 by 38.1 cm (3 by 3 by 15 in.). These beams are normally prepared in the laboratory by using a press, a kneading compactor, or a combination of the two. This research project concentrated on modifying the GLWT to test 15.2-cm (6-in.) cores as opposed to beams. The use of 15.2-cm cores is beneficial for several reasons. First, cores can be extracted from recently constructed projects. These cores would have characteristics identical to those achieved in the field. Second, cores could be extracted from between the wheelpaths of existing pavements with known levels of performance in the field. With aging in consideration these cores could be tested in

the GLWT. From the standpoint of feasibility of collection cores are much easier to obtain from the field than beams. The final advantage that 15.2-cm cores have over beams is that they are easier to compact in the laboratory and require less time and material to prepare.

Modifications had to be made to the GLWT apparatus before testing the cores. New holes were drilled in the base plate so that the sample-holding mold could handle 15.2-cm (6-in.) cores.

The initial attempt to test cores was performed by placing three samples simultaneously in the GLWT. This endeavor was quickly abandoned because of excessive rocking of the cores during testing. To overcome the rocking problem, fresh concrete was placed around individual cores and was allowed to set before testing. This procedure was time-consuming. Single cores were finally tested by placing precast concrete spacers on both sides of the cores to accommodate the 30.5-cm (12-in.) travel path of the loaded wheel. Several spacers were made in advance to accommodate slight fluctuations in core heights. Figure 2 demonstrates how cores are arranged in the GLWT. This has become the standard procedure for testing cores in the GLWT at the University of Wyoming.

A measuring device was developed in the laboratory to provide standardized rut depth measurements. The measuring device is a 63.5-cm (25-in.)-long aluminum dowel, 3.175 cm (1.25 in.) in diameter, that is machined on the ends to slide into the hose clamping brackets. Three dial indicators were permanently attached to the dowel with set screws to take a center measurement and measurements 5.08 cm (2 in.) off center in both directions. Figure 3 shows this rut depth measuring device being used.

RESULTS FROM REPEATABILITY STUDY

After modifying the GLWT, 22 identical laboratory cores were prepared. A standard technique was followed in compacting the cores with a combination of kneading and static compaction efforts. Cores were first compacted with 100 blows at 2413 kPa (350 lb/in.^{2}) for a 0.5-sec duration from a kneading compactor. A static leveling load of 4536 kg (10,000 lb) for 1 min was later applied to achieve actual field densities for similar mixes. After the compacted specimen cooled it was extracted. The time required to prepare a sample is approximately 4 hr.

Most of the cores were then tested at either 40.6°C (105°F) or 46.1°C (115°F). In studies described in nearly all of the literature reviewed, testing was conducted at 40.6°C (105°F) but testing at higher temperatures was also recommended. In the present research it was believed that the 40.6°C (105°F) testing temperature may not be severe enough to predict pavement rutting. This was determined after comparing laboratory rut depth measurements with field rut depth measurements. Tests were then conducted at 51.7°C (125°F), which was the highest temperature that could be sustained by the GLWT without possibly overheating the mechanical apparatus. After testing only a few cores it was determined that this temperature was too high. All of the samples either failed or approached failure. Therefore, 46.1°C (115°F) was selected for the remainder of the testing.

Table 1 provides the average rut depth measurements after 1,000, 4,000, and 8,000 cycles for the cores tested at 46.1°C (115°F). The coefficients of variance for the measurements were 0.243, 0.215, and 0.213 after 1,000, 4,000, and 8,000 cycles, respectively. These levels of variance were expected since the cores were hand mixed and individually prepared in the laboratory. The average rut depth increased from 0.230 cm (0.091 in.) after 1,000 cycles to 0.381 cm (0.15 in.) after 8,000 cycles. The standard deviation also increased from 0.056 cm (0.022 in.) to 0.081 cm (.032 in.).

SELECTION OF FIELD TEST SECTIONS

After verifying the repeatability of testing cores with the GLWT, 13 actual pavement test sections were selected for inclusion in this experiment. These sections were selected according to their geographic locations and rut depth severity levels. Field rut depth measurements, ages, elevations, equivalent daily 18-kip axle loads (EDLAs), highest monthly mean temperature, and type of surface treatment were obtained for all test sections. Three cores from each site were extracted between the wheelpaths. Initially, the cores were used to determine actual pavement thicknesses and later for testing in the GLWT. Table 2 provides the thicknesses of all of the pavement test sections.

Average field rut depth data were obtained for all sections from the Wyoming Rut Depth Report (*7*) and are summarized in Table 2. The rut depth data consisted of an average of 2,640 measurements

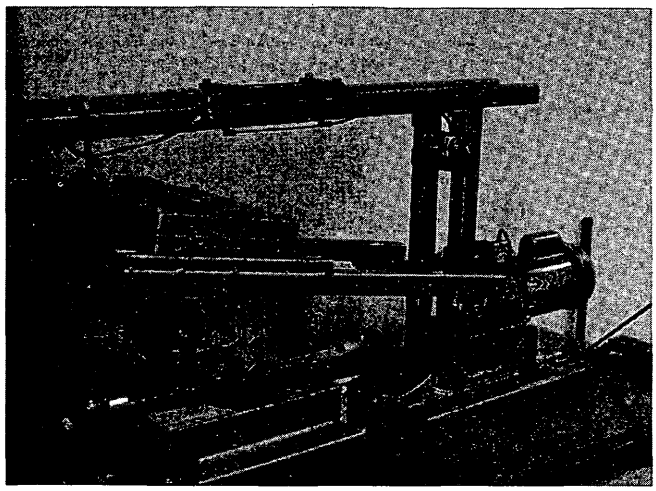

FIGURE 2 Modified GLWT: (1) weights, (2) electric motor, (3) sample-holding mold, (4) rut depth measuring device, and (5) machined aluminum wheel.

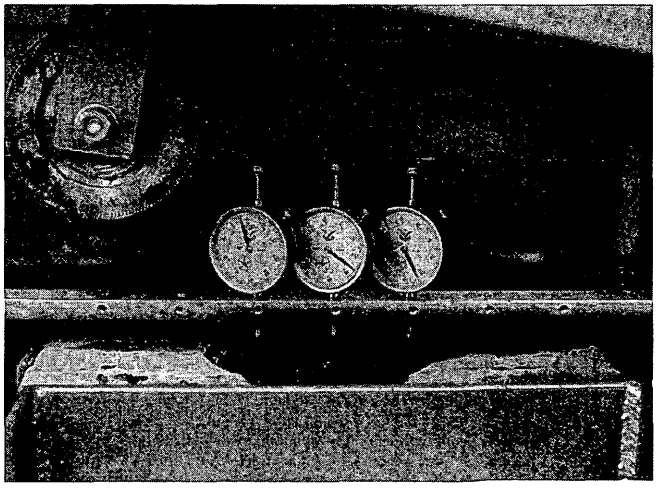

FIGURE 3 Demonstration of rut depth measuring device for GLWT.

TABLE 1 Average Rut Depth Measurements from Repeatability Study at 46.1°C (115°F)

	AVERAGE RUT DEPTH AFTER 1000 CYCLES (cm)	AVERAGE RUT DEPTH AFTER 4000 CYCLES (cm)	AVERAGE RUT DEPTH AFTER 8000 CYCLES (cm)
	.211	.312	.373
	.180	.264	.305
	.264	.401	.450
	.168	.198	.221
	.363	.432	.483
	.152	.224	.251
	.221	.323	.401
	.249	.353	.429
	.224	.312	.409
	.234	.335	.419
	.274	.386	.445
	.216	.315	.386
Mean	.230	.321	.381
Coefficient of Variance	.243	.215	.213
Standard Deviation	.056	.069	.081

taken per mile with a Wyoming version of the South Dakota Road Profiler. Average annual daily truck traffic volumes were converted to EDLAs to analyze the differences between traffic volumes on the test sections. Traffic volumes are summarized in Table 3. Since all of the test sections were more than 5 years old, it was believed that the majority of rutting had already occurred. For this reason cumulative equivalent single axle loads were not included in the analysis.

LABORATORY TESTING OF FIELD CORES

All field cores were cut to an approximate height of 8 cm (3.1 in.). The bulk specific gravities were determined for all cores by the standard method of testing for bulk specific gravity of compacted bituminous mixtures (AASHTO standard T 166-88). The densities and heights of the cores were determined and are summarized in Table 4. At least 12 hr before testing each core was placed in the preheating box of the GLWT.

To begin testing a preheated core is secured in the temperature-controlled GLWT. The measuring device is placed in the hose mounting brackets, and initial dial indicator readings are recorded. The measuring device is removed, and the rubber hose is placed in the mounting brackets. The hose is inflated and maintained at 690 kPa (100 lb/in.^{2}) with a compressor and regulator. With the hose tightened to the mounting brackets, the loaded wheel is lowered on top of the hose. When the door is closed the testing can proceed. Cycles are recorded with an internal electronic counter. At a preset number of cycles the loaded wheel automatically stops. The hose is removed, and the dial indicator readings are recorded. Rut depths are recorded at 1,000, 4,000, and 8,000 cycles. Single cores can be tested in approximately 3.5 hr.

RESULTS AND ANALYSIS

Cores from the test sections included in the experiment described here were tested at 40.6°C and 46.1°C (105°F and 115°F). All rut depth measurements obtained after 8,000 cycles are summarized in Table 5. Figure 4 shows the relationship between rut depth and number of cycles for the field cores tested at 46.1°C. The mean rut depths for all samples after 8,000 cycles were 0.26 cm (0.10 in.) and 0.41 cm (0.16 in.) at 40.6°C (105°F) and 46.1°C (115°F), respectively.

TABLE 2 Field Conditions for Test Sections

PROJECT	AVERAGE PAVEMENT THICKNESS (cm)	AVERAGE FIELD RUT DEPTH (cm)
P 23-03	17.1	0.18
P-25-04	10.8	0.84
P-34-09	12.1	0.33
P-34-10	14	0.28
P-40-13	19.1	0.53
P-20-15	15.2	0.13
P-20-17	18.4	0.46
P-30-18	15.9	0.84
P-12-20	13.3	0.41
P-12-21	15.2	0.53
P-12-26	12.1	0.51
P-12-27	11.4	0.61
P-12-28	17.1	0.46

TABLE 3 Traffic Volumes for Projects

PROJECT	AVERAGE ANNUAL DAILY TRAFFIC	AVERAGE ANNUAL DAILY TRUCK TRAFFIC	EDLAs
P-23-03	4555	1045	199
P-25-04	6475	635	121
P-34-09	1720	240	46
P-34-10	3360	370	70
P-40-13	2110	360	68
P-20-15	3310	620	118
P-20-17	2730	440	84
P-30-18	1265	145	28
P-12-20	3005	995	189
P-12-21	3120	1050	200
P-12-26	2400	830	158
P-12-27	2400	830	158
P-12-28	2550	860	163

An attempt was made to correlate all field and laboratory rut depth data at 46.1°C (115°F). Several regression models incorporating linear, quadratic, and cubic relationships were used. However, regression models with appropriate R^2 values could not be obtained. Therefore, the data set was split into two categories, first on the basis of the elevations of the sections and second on the basis of the pavement surface types. Statistical analyses were then performed separately on each data set. The ages of the test sections were not included in the models because all of the sections were more than 5 years old and had achieved most of their permanent deformation. The effects of traffic volumes and temperature were found to be insignificant in the models because all of the test sites had similar traffic levels and average ambient air temperatures.

All test sections at elevations of between 1158 and 1676 m (3800 and 5500 ft) were grouped together. Six projects were in this elevation range. The following regression model was obtained for this category:

$$\text{rut depth} = -3.71 + 1.50 \cdot A + 0.461 \cdot H \quad (1)$$

TABLE 4 Heights and Densities of Field Cores

PROJECT	CORES TESTED AT 40.6°C (105°F)		CORES TESTED AT 46.1°C (115°F)	
	HEIGHT (cm)	DENSITY (kg/m^3)	HEIGHT (cm)	DENSITY (kg/m^3)
P-23-03	7.6	2265.0	7.6	2263.4
P-25-04	8.1	2353.1	8.3	2332.3
P-34-09	8.4	2319.5	8.1	2324.3
P-34-10	7.6	2338.7	7.0	2329.1
P-40-13	7.0	2357.9	7.6	2337.1
P-20-15	8.3	2330.7	7.0	2338.7
P-20-17	7.5	2329.1	7.3	2327.5
P-30-18	7.5	2271.4	8.3	2295.4
P-12-20	8.1	2287.4	8.9	2269.8
P-12-21	7.8	2277.8	7.6	2277.8
P-12-26	7.6	2284.2	7.3	2293.8
P-12-27	7.6	2289.0	8.3	2289.0
P-12-28	7.1	2319.5	6.4	2327.5

TABLE 5 Average Laboratory Rut Depths for Field Cores After 8,000 Cycles

PROJECT	AVERAGE LABORATORY RUT DEPTH AT 40.6°C (105°F) (cm)	AVERAGE LABORATORY RUT DEPTH AT 46.1°C (115°F) (cm)
P-23-03	0.191	0.452
P-25-04	0.193	0.466
P-34-09	0.213	0.218
P-34-10	0.592	0.445
P-40-13	0.262	0.526
P-20-15	0.406	0.462
P-20-17	++	0.528
P-30-18	0.277	0.762+
P-12-20	0.191	0.297
P-12-21	0.130	0.201
P-12-26	0.284	0.328
P-12-27	0.086	0.175
P-12-28	0.310	++

\+ Test was stopped after rutting exceeded 0.762 cm (0.3 in)
++ Cores failed during testing

where

rut depth = predicted field rut depth (cm),
A = average laboratory rut depth after 8,000 cycles at 46.1°C (115°F) (cm), and
H = height of the field core tested in the GLWT (cm).

The R^2 for this regression model was 92.6 percent. Figure 5 illustrates the relationship between field rut depths and the rut depths predicted by this model. The heights of the cores tested were found to be significant in this relationship. A similar regression model was developed for elevations between 1676 and 2316 m (5500 and 7600 ft). The model equation for these higher elevations is

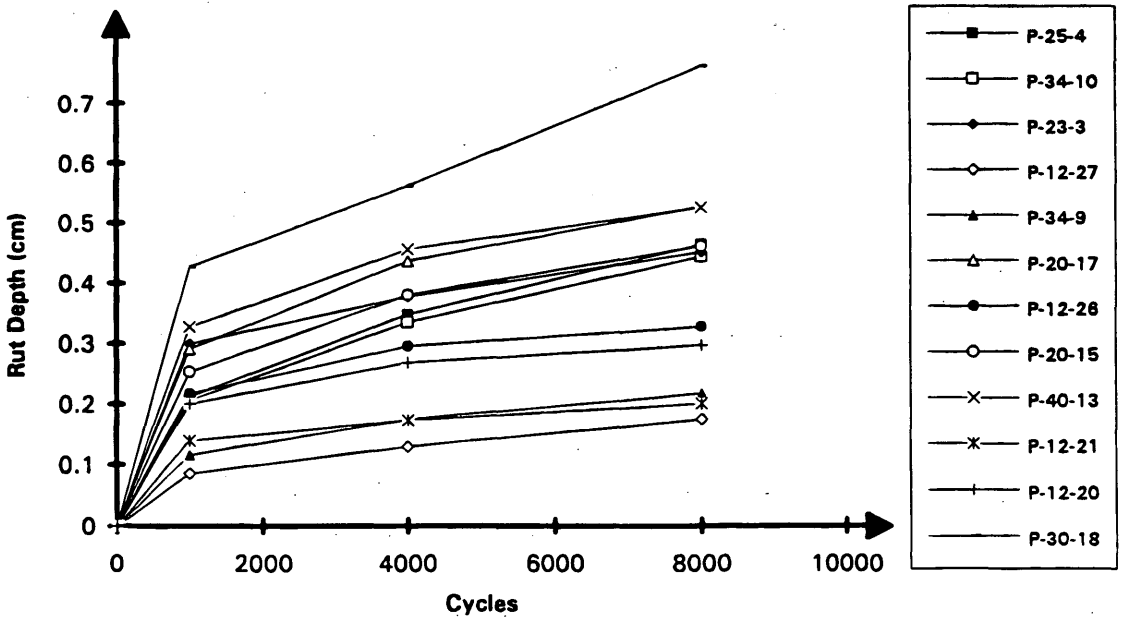

FIGURE 4 Rut depth plot for field cores tested at 46.1°C (115°F).

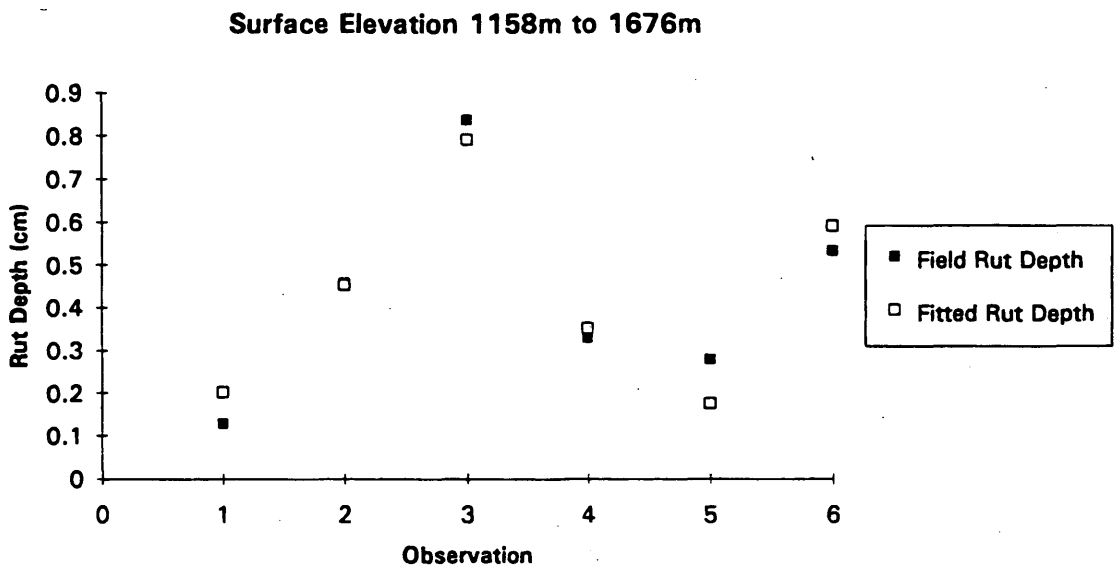

FIGURE 5 Fitted versus actual rut depth measurements for Regression Model 1.

$$\text{rut depth} = 0.776 + 0.39 \cdot A - 1.39 \cdot B \quad (2)$$

where

rut depth = predicted field rut depth (cm),
A = average laboratory rut depth after 8,000 cycles at 46.1°C (115°F) (cm), and
B = center laboratory rut depth after 8,000 cycles at 46.1°C (115°F) (cm).

The R^2 coefficient for this model was 91.9 percent. Five projects were used in the determination of this regression model.

Next the field test sections were divided into two categories according to their surface types. The cores were classified as either having a surface treatment (wearing course or chip seal) or not having a separate surface treatment (single layer of dense graded asphalt). An analysis was first performed on the data from cores with no surface treatments. The following regression equation resulted from that analysis:

$$\text{rut depth} = -4.32 + 1.63 \cdot A + 0.53 \cdot H \quad (3)$$

where

rut depth = predicted field rut depth (cm),
A = average laboratory rut depth after 8,000 cycles at 46.1°C (115°F) (cm), and
H = height of the field core tested in the GLWT (cm).

The R^2 coefficient for this model was 97.3 percent. Four cores were used in the determination of this regression model.

Finally, a similar analysis was performed on test sections with surface treatments. The following linear model was found:

$$\text{rut depth} = 0.784 + 0.59 \cdot A - 1.60 \cdot B \quad (4)$$

where

rut depth = predicted field rut depth (cm),
A = average laboratory rut depth after 8,000 cycles at 46.1°C (115°F) (cm), and
B = center laboratory rut depth after 8,000 cycles at 46.1°C (115°F) (cm).

The R^2 coefficient for this model was 93.4 percent. Seven cores were used in the determination of this regression model. All of the cores in the upper elevation category (Regression Model 2) had a surface treatment.

Problems developed while testing a few of the surface-treated cores in the GLWT. Some of the more rigid surface treatments fractured. This effect became apparent when cracking developed on the core adjacent to the hose. In these cases rutting was a function of structural failure instead of plastic flow. Another problem was noticed with cores that had extremely rough surfaces. When repeated cycles are applied to the samples some of the larger surface aggregates tilt or shift. The rut depth-measuring device takes measurements at identical locations each time. The movements inflate the initial dial indicator readings, which causes all successive rut depth measurements to be inflated. The rut depth measurements in these samples are masked by the shifting surface aggregate. Since Regression Models 2 and 4 contain the cores with surface treatments their validities are questioned. Further laboratory analysis will determine the effects of the shifting aggregates.

When statistical analyses were performed at 40.6°C (105°F), the GLWT rut depth values did not correlate well with the field rut depth data.

CONCLUSIONS

In the present research project the GLWT was modified to test 15.2-cm (6-in.) cores instead of beams. The feasibility of using the modified GLWT to predict field rutting in the laboratory was later examined. The following conclusions can be drawn from the study:

1. The GLWT can be used to test pavement cores instead of beams. The repeatability of the GLWT measurements is acceptable.
2. Rut depth measurements from the GLWT at 40.6°C (105°F) did not correlate well with actual field measurements.
3. Rut depth measurements from the GLWT at 46.1°C (115°F)

correlated with actual field rut depths after considering factors such as elevation and pavement surface type.

4. Surface-treated cores are sensitive to rut depth measurements because the aggregates on the surface tend to shift during testing. Future analyses should study removing surface treatments before testing in the GLWT.

5. The GLWT may not be the most accurate device for predicting rutting, but it is an inexpensive device that can produce quick results and an idea about the rut resistance of new asphalt mixes.

Although the data set used in this research project was limited, the GLWT showed some promising results. More test sections will be added to the data base in the future to verify the results that were obtained.

ACKNOWLEDGMENTS

This cooperative study was funded by U.S. DOT's University Transportation Program through the Mountain-Plains Consortium, the Wyoming DOT, and the University of Wyoming. The authors express their appreciation to the engineers of the materials branch at the Wyoming DOT.

REFERENCES

1. Huang, Y. H. *Pavement Analysis and Design*. Prentice-Hall, Englewood Cliffs, N.J., 1993.
2. Aschenbrener, T. B., and K. Stuart. *Description of the Demonstration of European Testing Equipment for Hot Mix Asphalt Pavement.* Report CDOT-DTD-R-92-10. Colorado Department of Transportation, Denver, 1992.
3. *Biennial Report*. Office of Research, Development, and Technology, FHWA, U.S. Department of Transportation, 1988–1989.
4. Lai, J. S. Development of a Laboratory Rutting Resistance Testing Method for Asphalt Mixes. Project 8717. Georgia Institute of Technology, Atlanta, Aug. 1989.
5. Lai, J. S., and T.-M. Lee. Use of a Loaded Wheel Testing Machine to Evaluate Rutting of Asphalt Mixes. In *Transportation Research Record 1269*, TRB, National Research Council, Washington, D.C., 1990, pp. 116–124.
6. Barksdale, R. D., et al. A Test Device for Evaluating Rutting of A.C. Mixes. Presented at 72nd Annual Meeting of the Transportation Research Board, Washington, D.C., 1993.
7. *Wyoming Rut Depth Report (1992 Programming)*. Programming Division, Wyoming Department of Transportation, Cheyenne, 1992.

Publication of this paper sponsored by Committee on Strength and Deformation Characteristics of Pavement Sections.

Early Rutting of Asphalt Concrete Pavement Under Heavy Axle Loads in Hot Desert Environment: Case History

BERNARD A. VALLERGA, AKHTARHUSEIN A. TAYEBALI, AND CARL L. MONISMITH

A case study of early rutting of an asphalt concrete pavement under heavy axle loads in a hot desert environment is presented. A section of four-lane divided Dubai–Hatta Highway in the Dubai Municipality of the United Arab Emirates experienced a 13-mm (0.51-in.) rutting in a mere 10-month period. Review of the project documents indicated that the pavement section under consideration was properly designed and constructed by a mix design procedure that used the Marshall test equipment applicable to heavy-duty asphalt pavements. By this procedure a design asphalt content of 4.3 percent by the weight of mix was selected. During the course of the investigation the design asphalt content was confirmed by the Hveem mix design procedure. However, neither of these conventional mix design methods indicated any potential for rutting; moreover, the method of laboratory test specimen fabrication did not produce compaction levels representative of those obtained in situ under the actual traffic loading. On the basis of the results of this investigation the most probable cause for premature rutting was attributed to axle loadings that exceeded the loading conditions for which the Marshall and Hveem mix design criteria have empirically been developed. Creep testing appeared to better characterize asphalt concrete in a more fundamental manner with a potential use in mechanistic analysis to estimate the propensity of the mix for rutting. Its limited use in the study confirmed that the rutting that did occur was to be expected for the existing unconventional loading conditions for the environment in which the pavement was located. Although not performed in the present study, an improved analysis method developed by Strategic Highway Research Program Project A-003A researchers to evaluate rutting is briefly described.

In February 1987 a 29-km (18.1-mi) asphalt concrete pavement was constructed on a section of the four-lane, divided Dubai–Hatta Highway by the Municipality of Dubai in the United Arab Emirates. The asphalt concrete pavement was designed and constructed by accepted conventional methods generally applicable to heavy-duty asphalt pavements. Within several months it became evident that veining and rutting were beginning to develop within the asphalt concrete itself and in the wheelpaths of the outer lanes in both directions, although they were more pronounced in the eastbound direction (i.e., toward Dubai). By December 1987, after about 10 months of truck traffic, the early rutting was quite pronounced, ranging up to 13 mm (0.51 in.) in the asphalt concrete surfacing layer.

Consequently, a study was immediately initiated to determine the most probable cause of this early rutting of the asphalt concrete. Cores were obtained from the pavement for analysis, and samples of the original asphalt and the aggregate used to produce the asphalt concrete were supplied by the contractor for a program of laboratory testing, evaluation, and analysis. Tests included Hveem stabilometer and creep tests on field cores and Hveem stabilometer tests on laboratory-fabricated specimens of the same materials in similar proportions at a range of compactive effort by using the Triaxial Institute Kneading compactor.

The results of the study were quite revealing with respect to the shortcomings of present conventional methods of asphalt concrete mix design, which are empirically related to rutting resistance. It also demonstrates, quite dramatically, the need for a method and procedure for fabricating more realistic test specimens in the laboratory if engineers are to rely on laboratory-generated mix designs and their associated job-mix formulas to produce rut-resistant asphalt concretes.

It was therefore considered highly desirable to record the results of this particular study as a case history to underscore for the engineering practitioner the limitations of present mix design methods, which are based on empirical analysis, while simultaneously pointing out to the research community the extent of the problem and suggesting a direction that could be taken for its ultimate solution.

DESIGN AND CONSTRUCTION ASPECTS

A review of the project documents and an inspection of the laboratory facilities indicated that the laboratory equipment was in good order and was operated by qualified laboratory technicians. In all respects everything was in line with present standards for the design of conventional heavy-duty highways.

The design criteria included in the project specifications for the asphalt concrete wearing course were those associated with the so-called 75-blow Marshall procedure for heavy-duty asphalt concrete. Figure 1 presents the results of the mix design developed in the field laboratory with a well-graded, fully-crushed granite aggregate with a maximum size of 19 mm (0.75 in.) and a 60–70 penetration-grade asphalt. The granite aggregate had a bulk specific gravity of 2.93 and a water absorption value of less than 0.5 percent. In addition, it appeared to have the requisite particle surface microtexture to produce a highly rut-resistant asphalt concrete in a properly formulated mix. The selection of the 4.3 percent asphalt content was predicated on meeting the voids-filled-with-asphalt criterion of 70 percent minimum; otherwise, a 4.1 percent asphalt content would most likely have been used. The job-mix formula used on this project was based on the Marshall method of mix design, as depicted in Figure 1.

B. A. Vallerga, B. A. Vallerga, Inc., 1330 Broadway, Suite 1044, Oakland, Calif. 94612. A. A. Tayebali, Department of Civil Engineering, North Carolina State University, P.O. Box 7908, Raleigh, N.C. 27695-7908. C. L. Monismith, Richmond Field Station, University of California, Berkeley, 1301 South 46th Street, Building 452, Richmond, Calif. 94804.

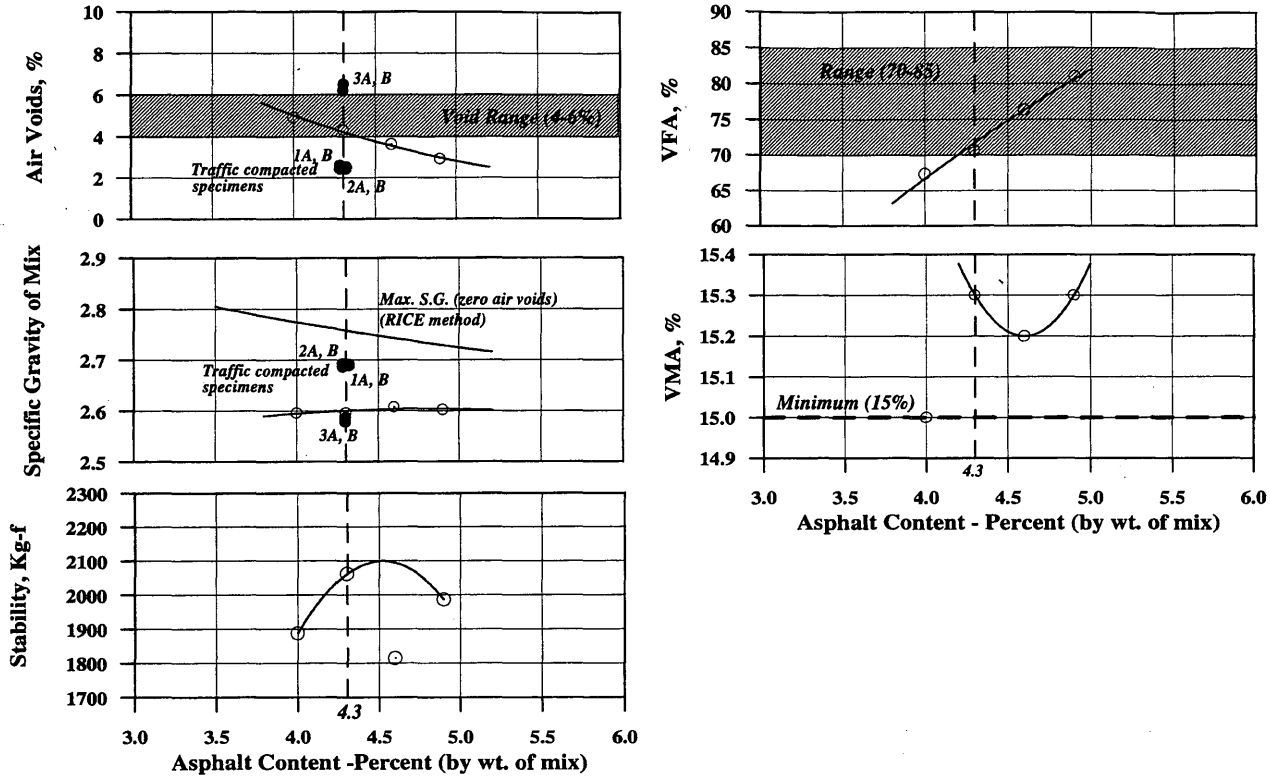

FIGURE 1 Asphalt concrete mix design by Marshall method for wearing course on Dubai-Hatta Highway with specific gravities and air voids from added field cores.

The asphalt concrete paving was placed in February 1987 in dry warm weather, with no difficulties encountered. A review of the records of the quality control program showed that the asphalt concrete readily conformed with the project specification and the job-mix formula requirements. No factors in the design and construction aspects of this project would lead one to expect any rutting problem, let alone an early expression of wheel-track rutting in a mere 10 months after opening to traffic.

FIELD PERFORMANCE OBSERVATIONS

The following observations were made during a visual examination of the condition of the asphalt concrete surface course in December 1987, which was approximately 10 months after construction:

1. The asphalt concrete wearing course definitely exhibited early rutting in the wheelpaths of heavy truck traffic, particularly in the Dubai-bound outer traffic lane (Figure 2). Although the depths of the most noticeable ruts were generally less than 13 mm (0.51 in.), the manifestation of a permanent deformation of this magnitude occurring in the relatively short time span of 10 months was indicative of the potential development of sufficiently deep ruts under additional wheel-load repetitions to affect adversely the rideability of the pavement surface.
2. Where rutting had already occurred and in many areas where rutting was not yet visible, migration of the asphalt binder to the pavement surface between aggregate particles (often referred to as *veining*) was evident. This veining was more extensive in the wheelpaths of the Dubai-bound outer lane, but it was also incipient in the Hatta-bound outer lane in several areas.
3. The trucks, of which there is a continual stream, that use the Dubai-bound outer lane were observed to be heavily loaded (Figure 2 inset), whereas the same types of three-axle trucks and five-axle tractor trailers that use the Hatta-bound outer lane were, in general, moderately loaded or empty.
4. All other aspects of the asphalt concrete wearing course other than the veining and early rutting appeared to be in good order. The pavement surface appeared to be smooth and free of defects, with good texture and no segregation. The workmanship was good, with well-formed longitudinal and transverse joints.

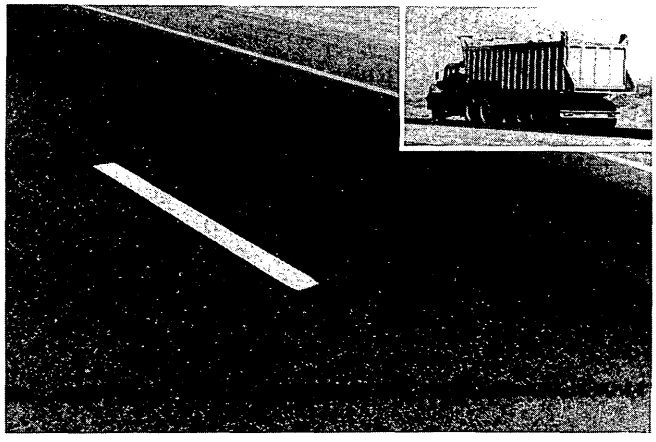

FIGURE 2 Early rutting in channelized wheel tracks of heavy truck traffic in the Dubai-bound outer traffic lane at station 73 + 335 (inset is typical truck loaded with rock).

Examination of a trench excavated across the Dubai-bound outer lane indicated that rutting was confined to the top 60-mm (2.4-in.) lift of the 120-mm (4.8-in.) asphalt surfacing itself, with no apparent contribution to the rutting by other structural layers or by the subgrade soil. Consequently, the early rutting appeared to be a deficiency in the asphalt concrete strength characteristics (i.e., resistance to rutting) or to be the result of the application of loading intensities (i.e., contact pressures) far beyond those for which the Marshall mix design criteria had been established. The Figure 2 inset shows an example of an excessively loaded five-axle tractor trailer carrying rocks, estimated to weigh approximately 68 metric tons (150,000 lbs), using the Dubai-bound outer traffic lane.

LABORATORY TEST PROGRAM

A limited laboratory program of research was initiated with the objective of determining whether the cause of the rutting could readily be discovered on the basis of deficiencies either in the development of the job-mix formula or in the proportioning of the materials by the contractor to meet the mix design requirements.

To ascertain the reason(s) for the development of premature rutting in the Dubai–Hatta Highway, six cores of 101.6 mm (4 in.) in diameter, along with the original samples of asphalt and aggregate, were obtained from the construction site for laboratory testing and evaluation. Figure 3 shows the locations of the six cores obtained from the wheel tracks of the Dubai-bound lanes (seen visually in Figure 2) at station 73 + 335.

Tests on Cores

The following series of tests were carried out on the cores in the indicated order:

1. Unconfined axial creep tests on the cores, as received, under a static compressive stress of 138 to 207 kPa (20 to 30 lb/in.^{2}) at a temperature of 37.8°C (100°F).
2. Hveem stabilometer tests at 60°C (140°F) on specimens of the wearing course layer sawn from the top of the core [approximately 60 mm (2.4 in.) high].

It should be noted that this order of testing and the single temperature of 37.8°C (100°F) in axial creep were selected to preserve intact the specimens of 101.6 mm (4 in.) in diameter for subsequent testing in the Hveem stabilometer.

Analysis and Evaluation of Results

Table 1 contains a summary of the heights and bulk specific gravities of the cores of 101.6 mm (4 in.) in diameter as received and of the top wearing course layer sawn off the cores, as well as the air void content and Hveem stability values of the wearing course layer. Figure 4 shows the axial creep modulus-versus-time relationship for the cores tested as received.

From Table 1 it can be seen that the bulk specific gravities of the full thicknesses of cores 1A, 1B, 2A, and 2B, as received, are quite similar to those of the wearing course layers, with a maximum difference of 0.009 for Core 2B, which is quite close to the reproducibility of the test method. This is most likely because these cores

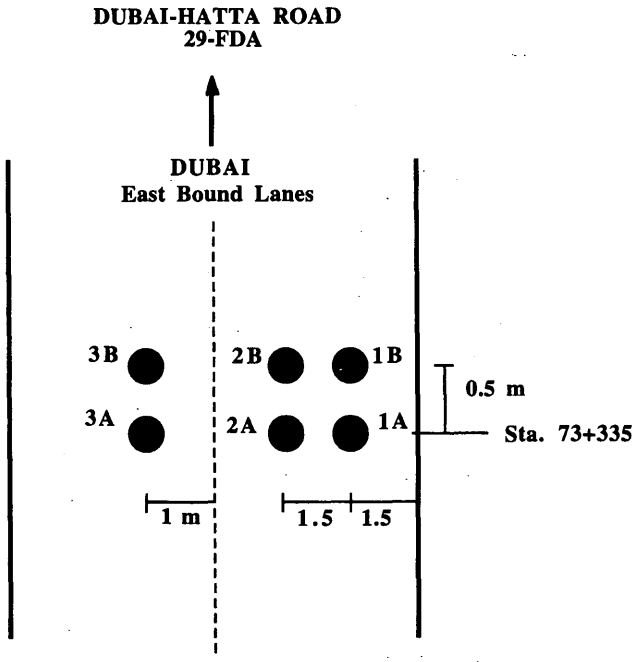

FIGURE 3 Locations of field cores taken for laboratory testing.

were taken from the wheel tracks of the outer lane and have been thoroughly compacted. Cores 3A and 3B show differences of 0.013 and 0.032 in specific gravity, respectively, most likely because they are from the outer wheel track of the inner lane and have not been subjected to the repeated loading of heavy truck traffic.

From these laboratory test results in Figure 4 it is evident that although the axial creep curves show no sharp break up to a 3,600-sec (1-hr) loading time at 37.8°C (100°F), they do show a significant difference in modulus values (i.e., 103 versus 345 MPa) between Cores 1A-1B, which were taken from the outer wheel track of the outer lane, where substantial rutting has occurred, and Cores 2A-2B, where rutting is less pronounced, and Cores 3A and 3B, where rutting is not yet visible, even though the creep stress applied was higher for Cores 2A, 2B, 3A, and 3B, namely, 207 versus 138 kPa (Figure 4).

Following testing asphalt extraction and recovery tests were performed on the top portions of the cores. The extraction was necessary to ensure that the asphalt contents were reasonably close to the target design asphalt content of 4.3 percent. The recovery of the asphalt component was considered highly desirable to ascertain the viscosities of the recovered asphalt at the service temperature of 60°C (140°F).

The results of the extraction and recovery tests are tabulated in Table 2. From Table 2 it can be seen that the asphalt contents vary from 3.93 to 4.52 percent, which results in an average of 4.29 percent with a standard deviation of ±0.28 percent. This compares quite favorably with the target design asphalt of 4.3 ± 0.2 percent tolerance of the job-mix formula. It should be noted that in asphalt concrete production the usual tolerance range for asphalt content is ±0.3 percent, which, if applied here, would show excellent control of the work by the contractor.

From Table 2 it is also seen that at 60°C (140°F) the viscosities of the asphalt range from 4,560 to 13,250 poises. This range is within what is normally expected of asphalts after about a year of service in the road. The noticeable variation here is that the vis-

TABLE 1 Specific Gravity, Height, and Hveem Stability Values of Asphalt Concrete Test Specimens Sawn from Field Cores Taken at Station 73 + 335, Dubai–Hatta Highway

Core No.	Bulk Specific Gravity			Height of Test Specimens		**Air Voids in Top Layer	Hveem Stability Top Layer
	All Layers	Top Layer	Difference	All Layers mm.	*Top Layer mm.		
1A	2.686	2.686	0.000	115.9	60.0	2.6	24
1B	2.692	2.689	0.003	114.3	60.7	2.5	32
Average							28
2A	2.684	2.692	0.008	119.0	59.5	2.4	36
2B	2.682	2.691	0.009	119.9	59.9	2.4	42
Average							39
3A	2.610	2.587	0.013	124.6	64.3	6.2	40
3B	2.610	2.578	0.032	123.8	62.7	6.5	30
Average							35

* Top layer is essentially the wearing course
** Based on theoretical maximum density (TMD) of 2.757

cosities in the heavily loaded wheelpaths of the outer lane (i.e., Cores 1A, 1B, 2A, and 2B) are substantially less than those in the lightly loaded wheelpaths of the inner lane. Such differences are normally encountered in service. Moreover, the viscosities measured in this case are still sufficiently low to permit deformations to occur under repeated loads of truck tires at high pavement contact pressures and high pavement temperatures.

Tests on Laboratory-Prepared Specimens

A series of tests were performed on laboratory-compacted specimens. The Triaxial Institute Kneading Compactor (ASTM D1561; Standard Method for Preparation of Bituminous Mixture Test Specimens by Means of California Kneading Compactor) was used to prepare the majority of the specimens, although a few were compacted by the impact compaction procedure (ASTM 1559; Standard Test Method for Resistance to Plastic Flow of Bituminous Mixtures Using Marshall Apparatus). This test program included

1. Tests on specimens compacted at asphalt contents ranging in 0.5 percent increments from 3.5 to 5.0 percent (by weight of mix) for stabilometer tests at 60°C (140°F), using the standard Hveem method of 150 tamps in the kneading compactor.
2. Tests on specimens prepared at asphalt contents of 4.1 and 4.3 percent for stabilometer tests at 60°C (140°F), using higher levels of kneading compaction, namely, 300, 600, 1,200, and 2,400 tamps.

Hveem Stabilometer Tests Results

The samples of aggregate and asphalt received were used to perform an asphalt concrete mix design based on the standard Hveem stabilometer method (i.e., 150 tamps) to see how it compared with the Marshall method (i.e., 75 blows) performed for this project in

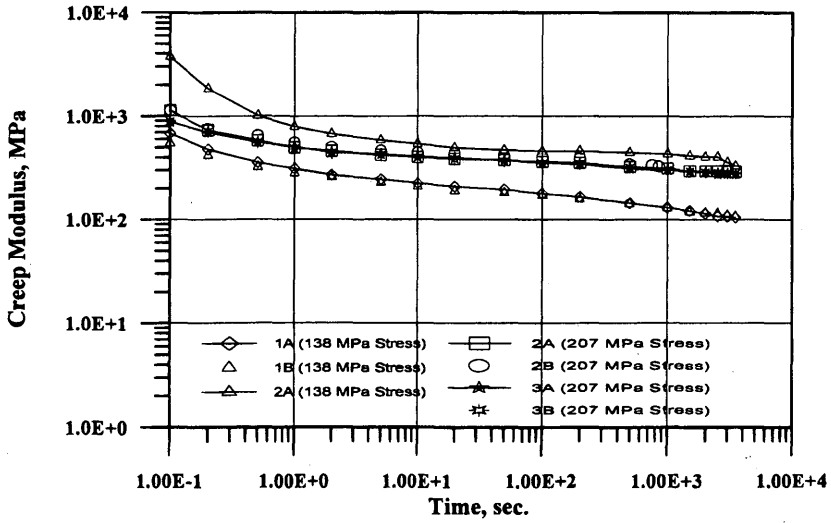

FIGURE 4 Axial creep test results for field cores, creep modulus versus time (37.8°C).

TABLE 2 Extraction and Recovery of Asphalt from Asphalt Concrete Cores, Dubai–Hatta Highway

Test	Method	Measured					
		Core 1A	Core 1B	Core 2A	Core 2B	Core 3A	Core 3B
Quantitative extraction of bitumen Recovery of asphalt from solution	ASTM D2172 ASTM D1856						
Asphalt Content, percent of total per 100 aggregate		4.52 4.73	4.31 4.51	3.96 4.13	3.93 4.10	4.49 4.71	4.52 4.74
Silt correction, %		0.72	0.71	0.47	0.41	0.30	0.32
Unaccounted loss, %		0.18	0.15	0.15	0.13	0.17	0.13
Tests on recovered asphalt: Absolute viscosity at 140°F, P	ASTM D2171	4560	4770	6260	6850	11,980	13,250

Dubai. The results of the Hveem test procedure on mixes containing 3.5, 4.0, 4.5, and 5.0 percent asphalt content (by weight of mix) are plotted in Figure 5, which shows the stabilometer values, bulk specific gravities, and percent voids as functions of asphalt content. On the basis of the results presented in Figure 5, the most appropriate target design asphalt content by the Hveem method is shown to be 4.3 percent for conventional truck traffic (i.e., meeting legal axle load limit requirements in the United States). Hence, it is evident that the Hveem method of mix design produced for this project the same target asphalt content selected by the Dubai's engineering consultant by the Marshall method of mix design and used by the contractor on this project.

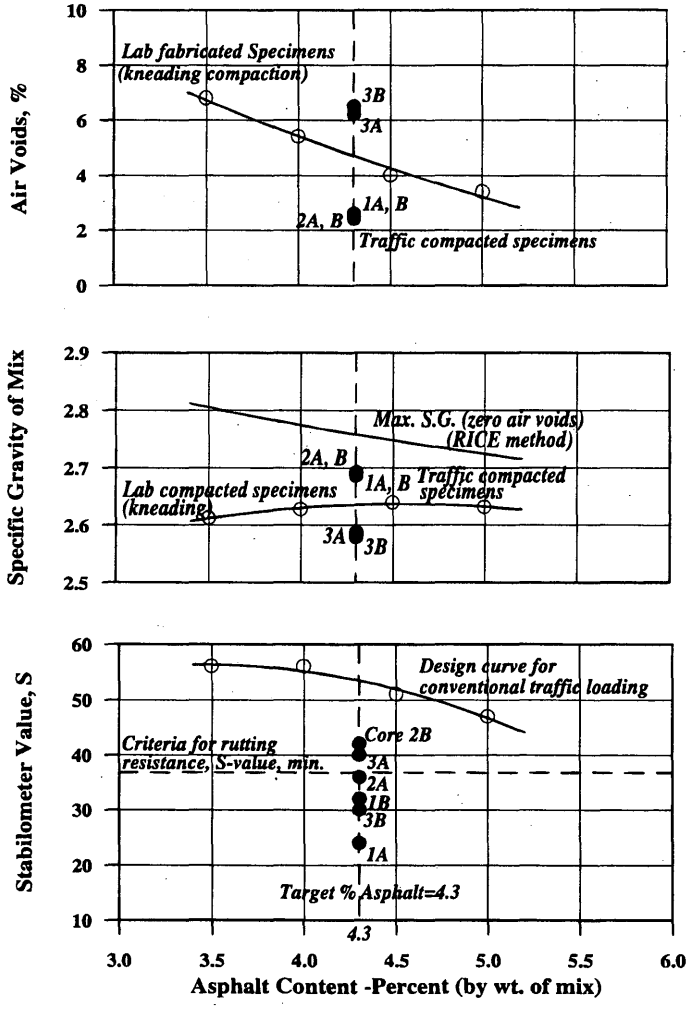

FIGURE 5 Comparison of Hveem stabilometer test results between field cores and laboratory-compacted specimens.

Comparison of Test Results for Laboratory-Compacted Specimens and Field Cores

Figures 1 and 5 also show the available results of Marshall and stabilometer tests on the field cores, respectively. In Figure 1 it is observed that the specific gravities of the field cores from the wheelpaths (Cores 1A, 1B, 2A, and 2B) are substantially higher than those of corresponding specimens produced by the 75-blow impact compaction effort. Similarly, the void contents of the specimens are below 3 percent, a value that is generally considered a desirable lower limit to ensure that instability in the mix will not develop. The specific gravities and air void contents of the cores from the inner lane (Cores 3A and 3B) indicate that they have not been subjected to the same amount of trafficking as the cores in the outer lane.

Relative to the stabilometer data (Figure 5) it is seen that the bulk specific gravities of the cores from the outer lane are higher than those produced by the recommended compaction procedure of the Hveem method (California Test 304; Method of Preparation of Bituminous Mixtures for Testing), namely, 150 tamps at 3.5 MPa (500 lb/in.^{2}) of compaction pressure. Similarly, the air void contents are lower. The cores from the less trafficked inner lane have lower specific gravities and higher air void contents, indicating that this portion of the roadway had not yet attained conditions corresponding to those from the compactive effort in the laboratory.

Relative to the Hveem stabilometer test results, Table 1 and Figure 5 show that the Hveem stabilometer values of the traffic-compacted wearing course layer range from a low of 24 to a high of 42, with an overall average value of 34, which is below the criterion of 37 (minimum) generally specified for heavy-duty pavements on major highways with high volumes of truck traffic. Hence, the asphalt concrete on this project was found to be inadequate with respect to its resistance to deformation (i.e., rutting) when it was compacted to the degree indicated by the low air voids that have resulted from the 10 months of heavily loaded truck traffic in the Dubai-bound direction. In other words, had the laboratory compaction duplicated that of the Dubai-bound traffic, the Hveem stabilometer would have predicted the high potential for rutting that did occur. This will be illustrated in the next section with the results of tests on specimens subjected to additional compactive effort.

Since the densities obtained in the field were higher than those obtained in both the 75-blow impact compaction procedure and the current Hveem standard procedure, an additional test series was initiated to study the change in the characteristics of laboratory-prepared specimens of the Dubai materials with increased compactive effort with the kneading compactor.

Effect of Increased Compactive Effort on Laboratory-Compacted Specimens

To attempt to duplicate the increased bulk specific gravities obtained in the wheel tracks of the outer lane, laboratory-prepared mixtures were subjected to additional compactive efforts in the kneading compactor. One series of specimens with the design asphalt content (4.3 percent) was prepared. To ascertain the influence of reduced asphalt content in mixture stability under the same circumstances, another series with an asphalt content of 4.1 percent (only 0.2 percent lower) was prepared.

Both mixtures were subjected to additional numbers of tamps in the kneading compactor, holding the compaction pressure constant at 3.5 MPa (500 lb/in.^{2}). For the mix containing 4.3 percent asphalt, additional specimens were prepared at 300, 600, and 1,200 tamps, whereas at 4.1 percent asphalt, 300, 600, 1,200, and 2,400 tamps were used. Infrared lamps, directed onto the compaction molds, were used to keep the specimens hot during the extended compaction process.

Stabilometer tests were performed on the compacted specimens at 60°C (140°F). Only two specimens were prepared under each condition since materials were limited. Figure 6 illustrates the influence of the number of tamps on the specific gravity, air void, and stabilometer values.

In Figure 6 it can be seen that the Hveem stability value of the mix with 4.3 percent asphalt decreased with an increasing number of tamps. For the mix with 4.1 percent asphalt the stability value increased with increased compactive effort to 600 tamps. However, at 1,200 tamps the stability value dropped to a level less than that obtained at the bulk specific gravity associated with 150 tamps and dropped still further with an increase in the number of tamps to 2,400. Moreover, at the increased compactive efforts, asphalt appeared on the surfaces of the specimens (flushing).

To ascertain the compactive effort in kneading compaction comparable to that obtained in the wheelpaths of the outer lane of Dubai–Hatta Highway over the 10-month period, Figure 7 was prepared. The curve labeled 150 tamps is based on the bulk specific gravity data reported in Figure 5. The specific gravity-versus-asphalt content curves for the other compactive efforts were interpolated from the data shown in Figure 6 for specimens containing 4.1 and 4.3 percent asphalt.

The bulk specific gravity values for the cores were also plotted in Figure 7. From this analysis it would appear that a compactive effort corresponding to about 1,200 tamps, rather than 150 tamps, would be required to assess the stability characteristics of the mix in the particular situation encountered with the exceedingly heavy axle loadings in Dubai, where no legal load limit is in place.

When compacting specimens in the laboratory to this number of tamps there is a possibility of excessive fracture and degradation of the aggregate. To determine this probability for the material used in the study, gradations after extraction were determined on specimens subjected to both 150 and 2,400 tamps of the kneading compactor. These results are plotted in Figure 8. Note that there is a slight increase in the fines for the mix subjected to 2,400 tamps; otherwise, the gradations are essentially the same.

RUTTING ANALYSIS

The rutting observed in the outer lane in the Dubai-bound direction provided an opportunity to use the analytically based procedure suggested by Shell (*1*) and modified by Finn et al. (*2*) to estimate the amount of rutting by using the results of the creep tests shown in Figure 4 and the traffic data presented in Table 3. Table 3 was prepared from the available traffic information and summarizes the total number of equivalent 9-metric ton (20,000-lb) axle load repetitions applied daily to various sections of the Dubai–Hatta Highway. This tabulation shows that, in general, the greater numbers of equivalent axle loads are in the Dubai-bound direction, particularly at the Al Hibhab roundabout where, for example, the equivalent single axle loads (ESALs) are 1,220 per day in the Dubai direction and only 296 per day in the Hatta direction.

However, whereas the numbers of axle load applications have a bearing on the depth of rutting whenever an asphalt concrete has the propensity to deform, a more significant factor is the tire contact pressure. Unfortunately, information on tire pressure was not avail-

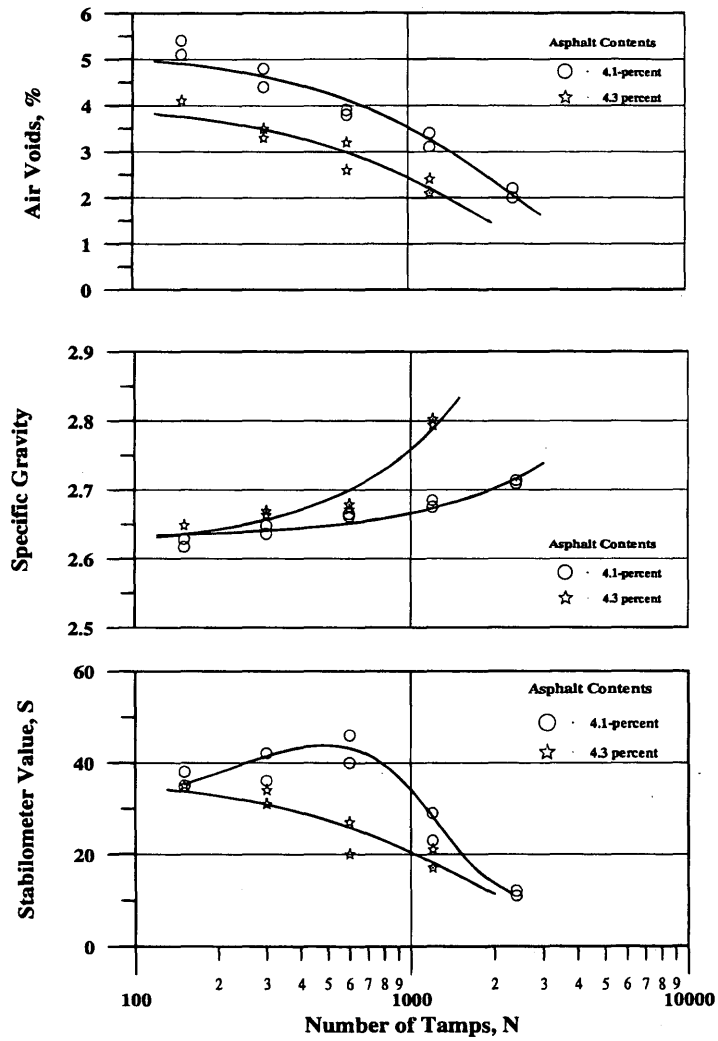

FIGURE 6 Influence of the number of tamps on specific gravity, air void, and stability values.

able at the time of the study. It is known, however, that for steel-belted radial tires the contact pressure on the pavement can reach levels of 1.8 times the air pressure in the tire for a tire loading exceeding that for which the tire was designed, for example, a tire designed for 4.5 metric tons (10,000 lbs) carrying 9 metric tons (20,000 lbs) of loading due to axle overloading (*3*).

In this connection from a review of the traffic data, overloading of the trucks that use the Dubai–Hatta Highway is quite common if one assumes that the "normal" load is 9 metric tons (20,000 lbs) for a single axle and 15 metric tons (33,000 lbs) for a tandem axle. For example, at the Al Hibhab roundabout in the Dubai direction, the data for three-axle trucks indicated that 30 of the 34 tandem axles were loaded to 21 metric tons (46,000 lbs) or greater, with 5 of the 30 trucks with tandem-axle loads of 40 metric tons (88,000 lbs).

By using the creep data in Figure 4 and the relationship (*2*)

$$\Delta h_1 = C_M h_1 \left(\frac{\sigma_{ave}}{S_{mix}}\right) \quad (1)$$

where

h_1 = thickness of the asphalt-bound layer,
σ_{ave} = average stress in the asphalt-bound layer,
S_{mix} = the value of the mix stiffness determined as described elsewhere (*4*), and
C_M = correction factor for the so-called "dynamic effect," which takes account of differences between static (creep) and dynamic (rutting) behavior (this factor is dependent on the type of mix and has been found empirically to be in the range 1 to 2),

a rut depth of about 10 mm (0.4 in.) was estimated over a 10-month period for a traffic level of 1,000 trucks per day with tire contact pressures of up to 1.4 MPa (200 lb/in.^{2}), daytime atmospheric conditions that result in pavement temperatures of 49°C to 60°C (120°F to 140°F) year around, and a seasonal range of axial creep moduli of 83 to 138 MPa (12,000 to 20,000 lb/in.^{2}) at a loading time of approximately 2,000 sec.

MEASURES TO IMPROVE ASPHALT CONCRETE MIX RUTTING RESISTANCE

Although it was beyond the scope of the investigation to evaluate alternatives that could mitigate rutting in this particular situation,

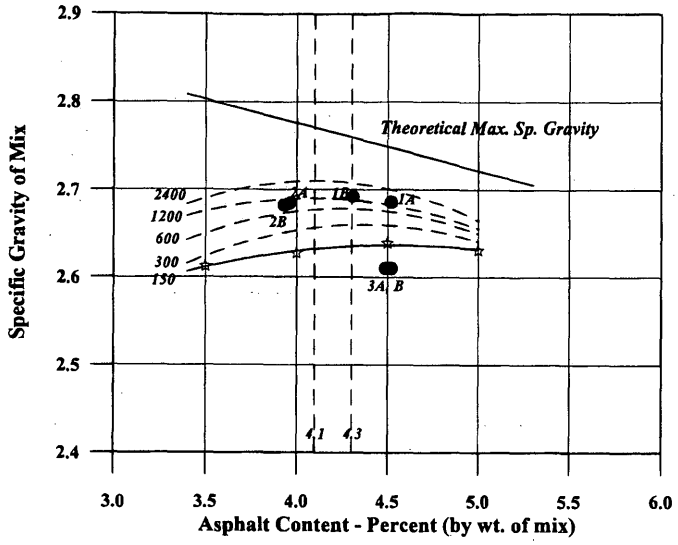

FIGURE 7 Effect of asphalt content and number of tamps on specific gravity values.

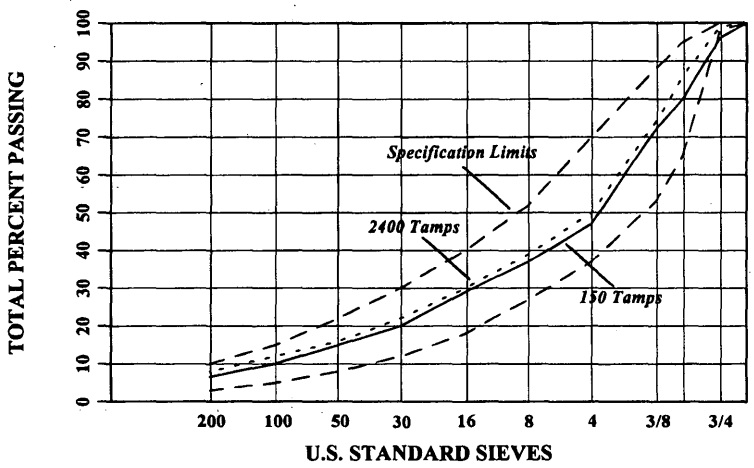

FIGURE 8 Extracted aggregate gradations of specimens subjected to 150 and 2,400 tamps at 3.5 MPa (500 lb/in.^{2}) in the kneading compaction.

some measures that may be taken to improve the rutting resistance of mixes include modification of aggregate gradation to incorporate a higher proportion of the large particles, use of additives and modifiers, and use of mechanistic and performance-based mix design methodologies. One such mix design methodology developed under the Strategic Highway Research Program (SHRP) is briefly described in the next paragraph.

The present study was conducted before the completion of the SHRP Asphalt Research Project A-003A. The authors, all of whom were associated with the A-003A research endeavor, suggest that the methodology for permanent deformation analysis developed in the A-003A study provides an improved way to analyze the performance of a project such as the one described here. The approach uses the repetitive simple shear test equipment developed during Project A-003A and the methodology reported elsewhere (*5*).

Briefly the procedure is as follows:

1. Estimate the traffic applied to the project to the time of the evaluation. One procedure would be to express the traffic in terms of ESALs.

2. Determine the critical temperature, T_c, for the site. [Deacon et al. (*6*) provide a methodology for doing this.]

3. Convert the total ESALs applied to the equivalent number at T_c, that is,

$$\text{ESALs}_{Tc} = \text{ESALs} \times \text{TCF} \quad (2)$$

where TCF is the temperature correction factor.

4. To convert the ESALs at T_c to an equivalent number of repetitions in the laboratory test, it is necessary to multiply the ESALs_{Tc} by a shift factor [the suggested shift factor is about 0.04 (*5*)]. This value is termed N'.

5. Select a value of shear strain γ_p', from the relationship

$$\text{Rut depth (in.)} = k(\gamma_p') \quad (3)$$

which was determined from finite-element analyses of representative pavement structures (*5*). A value of the coefficient k of 10 to 11 can be used for comparatively thick asphalt concrete layers. For an investigation of the type reported here the prescribed value of

TABLE 3 Summary of Daily Equivalent 9-Metric Ton (20,000-lb) Single Axle Loads at Roundabouts Along Dubai–Hatta Highway

Roundabout	2-axle	3-axle	4 to 7-axle	Total
Bu Kidra				
Dubai	34	621	177	832
Hatta	8	143	120	271
Rashidiya				
Dubai	29	341	220	790
Hatta	24	108	302	434
Awir				
Dubai	1	454	301	756
Hatta	3	56	75	134
Al Hibhab				
Dubai	2	898	320	1220
Hatta	6	158	132	296
Madam				
Dubai	0	561	736	1297
Hatta	19	35	119	173

the rut depth would correspond to that measured at the time of the investigation.

6. Plot N' determined in Step 4 and γ_p' determined from Step 5 as shown in Figure 9.

7. Perform the repeated-load, constant-height simple shear test at T_c on representative specimens of the mix used in the project.

8. Plot the results of the γ_p versus N determined from a simple shear test on the plot (Figure 9).

9. If the curve of γ_p versus N determined from the simple shear test does not pass through the plotted point (γ_p', N') adjust the shift factor used in Step 4.

10. To design an adequate mix for the site, plot the permanent shear strain associated with a prescribed rut depth and the design traffic demand termed N_{demand} (determined according to Steps 3 and 4 but using the adjusted shift factor obtained in Step 9) as shown in Figure 9.

11. Select a mix whose γ_p-versus-2 N relationship determined in a constant-height simple shear test at T_c passes through or to the right of (γ_p'', N_{demand}) (Figure 9).

SUMMARY

This paper presents a case study of early rutting of an asphalt concrete pavement in a hot desert environment. Although it was properly designed and constructed by accepted conventional design

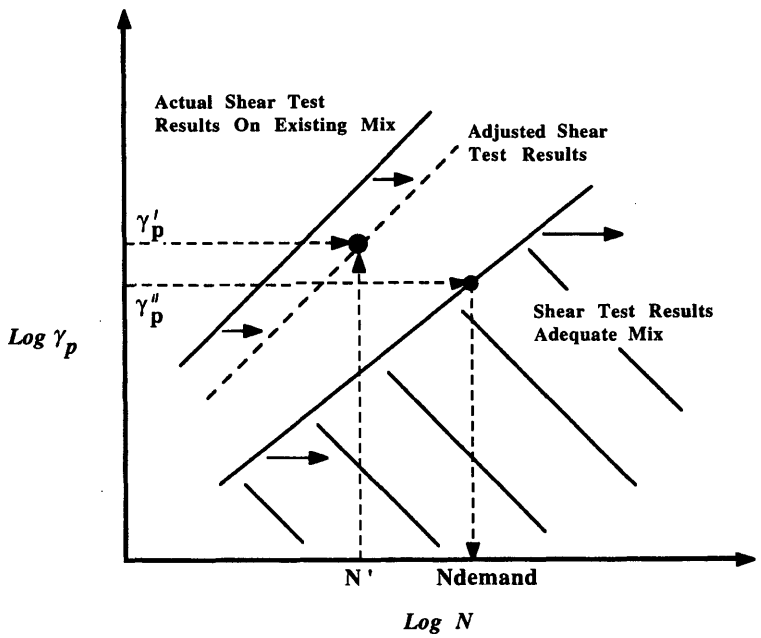

FIGURE 9 Schematic of permanent shear strain versus stress applications in constant-height simple shear test.

methods generally applicable to heavy-duty asphalt pavement, a section of the four-lane divided Dubai–Hatta Highway in the Dubai Municipality of the United Arab Emirates experienced premature rutting a mere 10 months after being opened to traffic.

An investigation to determine the most probable cause for this early rutting revealed the shortcomings not only of the present conventional methods of asphalt concrete mix design (Marshall and Hveem), which are empirically related to the rutting resistance, but also of the procedure for the fabrication of test specimens in the laboratory, which compares more realistically to the field condition. Asphalt mix design methods must be able to account for unconventional traffic loading and environment if engineers are to rely on laboratory-generated mix designs and their associated job-mix formulas to produce rut-resistant asphalt concretes.

Traffic survey information for the project indicated that the traffic loads imparted to the asphalt concrete pavement far exceeded the legal loads for which the Marshall and Hveem mix design parameters have empirically been correlated to rutting. Under this severe loading condition, the asphalt concrete was compacted to a degree far beyond that which was expected from design considerations for the conventional legal traffic load, leading to premature rutting.

Use of creep testing to establish creep modulus-versus-time relationships appeared to characterize the asphalt concrete mix response in a more fundamental way, suggesting that mechanistic analysis has the potential to permit estimates of deformation under any set of loading and environmental conditions. Its limited use in the present study confirmed that the rutting that did occur was to be expected for the existing unconventional loading conditions for the given environment.

Subsequent to this case study an improved method for the evaluation of mix performance was developed as part of SHRP Project A-003A. Unfortunately, no additional materials were available to permit the samples in this particular project to be evaluated by the new methodology. Nevertheless, the authors have provided a brief outline of the proposed approach and recommend its use as part of future case studies of the type described here.

ACKNOWLEDGMENT

The authors thank civil engineers Khalil I. Awad, managing director, and Osama A. Humaid of Almulla Construction Company, Ltd., Dubai, United Arab Emirates, for sponsoring the study and contributing their constructive comments and observations.

REFERENCES

1. Shell Pavement Design Manual. Shell International, London, England, 1978.
2. Finn, F. N., C. L. Monismith, and N. F. Markevich. Pavement Performance of Asphalt Concrete Mix Design. *Proc., The Association of Asphalt Paving Technologists*, Vol. 52, 1983.
3. Yao, P. A Comparative Study of the Effect of Truck Tire Types on Road Contact Pressure. Paper SP-765. Society of Automotive Engineers, Inc., Nov. 1988.
4. van de Loo, P. J. The Creep Test: A Key Tool in Asphalt Mix Design and in the Prediction of Pavement Rutting. *Proc., Association of Asphalt Paving Technologists,* Vol. 47, 1978, pp. 522–557.
5. Sousa, J. B., J. A. Deacon, S. Weismann, J. Harvey, C. L. Monismith, R. B. Leahy, G. Paulsen, and J. Coplantz. Permanent Deformation Response of Asphalt-Aggregate Mixes. Report SHRP-A-414. Strategic Highway Research Program, National Research Council, Washington, D.C., 1994.
6. Deacon, J. A., J. Coplantz, A. Tayebali, and C. L. monismith. Temperature Considerations in Asphalt-Aggregate Mix Analysis and Design. Presented at 73rd Annual Meeting of the Transportation Research Board, Washington, D.C., Jan. 1994.

Publication of this paper sponsored by Committee on Strength and Deformation Characteristics of Pavement Sections.

National Study of Asphalt Pavement Rutting in Saudi Arabia

H. I. AL-ABDUL WAHHAB, M. N. FATANI, A. S. NOURELDIN, A. BUBSHAIT, AND I. A. AL-DUBABE

Premature rutting has occurred on a number of recently built highways in Saudi Arabia. The Ministry of Communications, in an effort to solve the problem, has initiated a number of studies and has started to replace the affected pavement. The aim of the present study was to identify possible factors that may relate to rutting and to recommend maintenance and repair criteria for existing rutted pavements. The study covers 19 sections of 11 major highways. Results indicate a direct relationship between rutting and the percentage of air voids, the percentage of voids in mineral aggregate, the percentage of voids filled with asphalt, the resilient modulus at 25°C, and asphalt viscosity. These properties were used as bases for determination of maintenance criteria as well as the criteria for mixes required to resist rutting on Saudi roads.

The Kingdom of Saudi Arabia has invested more than US $25 billion in road construction over the last 20 years. The Kingdom has undergone an extremely rapid rate of development in many directions. The construction of thousands of kilometers of freeways, expressways, and low-volume roads has played an important role in such development. Growth in socioeconomic and industrial sectors has been encouraged, resulting in the generation of a great deal of heavy vehicle transportation in cities and between cities.

These rapid development rates have generated extremely large traffic volumes, especially those of heavy trucks, on the roadway network. The roadway capacity can properly accommodate these volumes. However, noticeable rutting problems have appeared during the last 10 years.

In an attempt to avoid the spread of the rutting problem on the prestigious Saudi roadway network, a 5-year NCHRP project entitled Evaluation of Permanent Deformation of Asphalt Concrete Pavements in Saudi Arabia was initiated in July 1987. The objectives of this research project were

1. To identify factors that may relate to rutting,
2. To recommend criteria for repairing existing rutted pavements,
3. To recommend ways and means of minimizing rutting in future constructions projects, and
4. To select a model for identifying rutting potential in different asphalt concrete mixes.

This paper summarizes the results of some phases of the study and provides preliminary recommendations for ways to obtain rut resistance on pavements bearing today's heavy traffic loads.

H. I. Al-Abdul Wahhab and A. Bubshait, Civil Engineering Department, King Fahd University of Petroleum and Minerals, Dhahran 31261, Saudi Arabia. M. N. Fatani, King Abdulaziz University, Jeddah, Saudi Arabia. A. S. Noureldin, Ministry of Communications, Riyadh, Saudi Arabia. I. A. Al-Dubabe, Saudi Aramco, Saudi Arabia.

STUDY SECTIONS

Nineteen test sections located on 12 major highways (Table 1) were selected such that

1. Three regions of the Kingdom were represented (Eastern, Central, and Western),
2. Weigh stations were present to monitor truck weights,
3. Traffic characteristics and tire pressures could be monitored easily and accurately,
4. Sections on roads without rutting problems were represented, and
5. Nonrutted segments (rut depth less than 1 cm) of roads with rutting problems were represented.

Each test section was 1 km in length and two to three standard traffic lanes wide (depending on road classification). The rut depth measurements obtained on the selected rutted sections ranged from 1.5 to 7.0 cm.

Field investigations and laboratory characterizations were conducted at each test section for both the truck lane (outer right slow lane) and the passing lane (outer left passing lane).

RUTTING DISTRESS LOCATION

Full-depth, full-width saw-cut trenches together with full-depth, full-width continuous corings obtained from rutted sections indicated that rutting distress was localized only in the top 10 cm of asphalt-bound layers on the truck lane under the wheelpaths (Figure 1).

The occasional presence of rutting in the middle lane (six-lane dual carriageways) was observed when the presence of severe rutting in the truck lane caused discomfort to the users of that lane. The middle lane in this case became, in practice, the truck lane.

The amount of rut depth under the left wheelpath was smaller than that under the right wheelpath (Figure 1). This may be attributed to the surface slope and the relatively low lateral support provided by the shoulder adjacent to the right wheelpath compared with the lateral support provided by the traffic lane adjacent to the left wheelpath.

TRAFFIC CHARACTERISTICS

Traffic counters and weigh stations located on the selected study sections were used to monitor traffic characteristics. The monitoring process resulted in the following major observations:

TABLE 1 Study Sections

Region	Non-Rutted Sections	Rutted Sections	Thickness, cm BWC[a]	BBC[b]	ASB[c]	Total
East (4 roads)	E1N	–	5	13	12	30
	E3N	E2R	5	13	12	30
	E5N	E4R	5	19	12	36
	E6N	–	5	19	12	36
Central (4 roads)	C2N	C1R	5	20	12	37
	C3N	–	5	20	12	37
	C5N	C4R	5	20	12	37
	C6N	–	5	10	12	27
West (4 roads)	W1N	W2R	5	15	12	32
	W3N	W4R	5	15	12	32
	W5N	W6R	5	15	12	32
	W7N	–	5	13	12	30
Total	12 Sections	7 Sections				

[a]BWC : Bituminous Wearing Course, 19 mm top aggregate size
[b]BBC : Bituminous Base Course, 38 mm top aggregate size
[c]ASB : Aggregate Subbase, Selected Material

1. Heavy truck (exceeding legal limits) traffic represented more than 25 percent of total traffic on all test sections.
2. Sixty percent of the truck traffic used the roadways between 9:00 a.m. and 4:00 p.m. During this time of day in the hot season (May to September), the air temperature regularly exceeds 40°C (104°F) and pavement temperatures exceed 60°C (140°F).
3. Up to 20 percent of individual axles had loads in excess of limits set by the Ministry of Communications (Figure 2).
4. Almost all truck traffic used the slow lane except when passing.
5. More than 50 percent of the tires tested had tire air pressures in excess of 8.43 kg/cm^2 (120 lb/in.^{2}), and more than 95 percent of the tires tested had tire pressures in excess of 4.92 kg/cm^2 (70 lb/in.^{2}). Some inflated tires had pressures of up to 12 kg/cm^2 (170 lb/in.^{2}), as illustrated in Figure 3. It should be noted that the Asphalt Institute pavement design method (*1*) assumes that loads are transmitted to the pavement when the contact pressure is 4.92 kg/cm^2 (70 lb/in.^{2}). In addition, the current 1993 AASHTO guide (2) also assumes that tire pressure is in the vicinity of 5 kg/cm^2.
6. A heavy truck classified as 2S2 was identified as the one associated with the most gross weight and axle load limit violations (Figure 2).

CLIMATIC CHARACTERISTICS

Temperature sensors were installed at various depths of the pavement sections to monitor air temperature, pavement surface temperature, and pavement temperature at depths of 2, 4, 8, and 16 cm and at the bottom of the bituminous layers. The monitoring process resulted in a data base of temperature measurements at the specified locations for 24 hr a day for a period of 2 years. The following are the major observations from this temperature-monitoring process:

1. Roads in Saudi Arabia are generally exposed to extremely high temperatures for long periods of time.
2. The pavement temperature approaches 70°C (158°F) in the hot summer months (May to September), during which time the air temperature approaches 50°C (122°F).
3. The highest temperature occurs at the middle of the bituminous wearing course (at a depth of 2 cm from the pavement surface).
4. The pavement surface temperature is slightly less than that of the middle of the bituminous wearing course apparently because of surface winds (Figure 4).

Although nothing can be done to alter these harsh climatic conditions, allowing a slightly larger air void content in the bituminous wearing course may help by providing more ventilation for the bituminous wearing course and hence reducing pavement temperature. Also, the end of construction and the opening of the road to traffic should not be scheduled during the summer months (May to September), when the pavement temperature is the highest and asphalt consistency is the lowest.

Figure 5 shows the monthly average temperature distributions during the hours of the day for the months of December (coldest) and July (hottest), respectively. Figures 6 and 7 illustrate the regression relationships between pavement surface temperature (or temperature at a depth of 4 cm) and air temperature during the months of December and July, respectively. In addition, Figure 8 provides the monthly variation in air temperatures in the cities of Riyadh (Central Region) and Dhahran (Eastern Region), respectively.

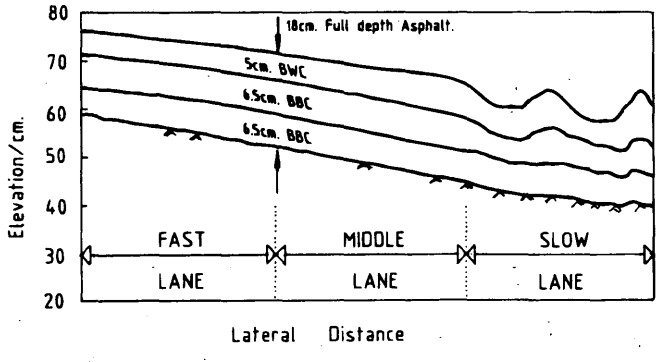

FIGURE 1 Pavement cross section at Test Section E2R.

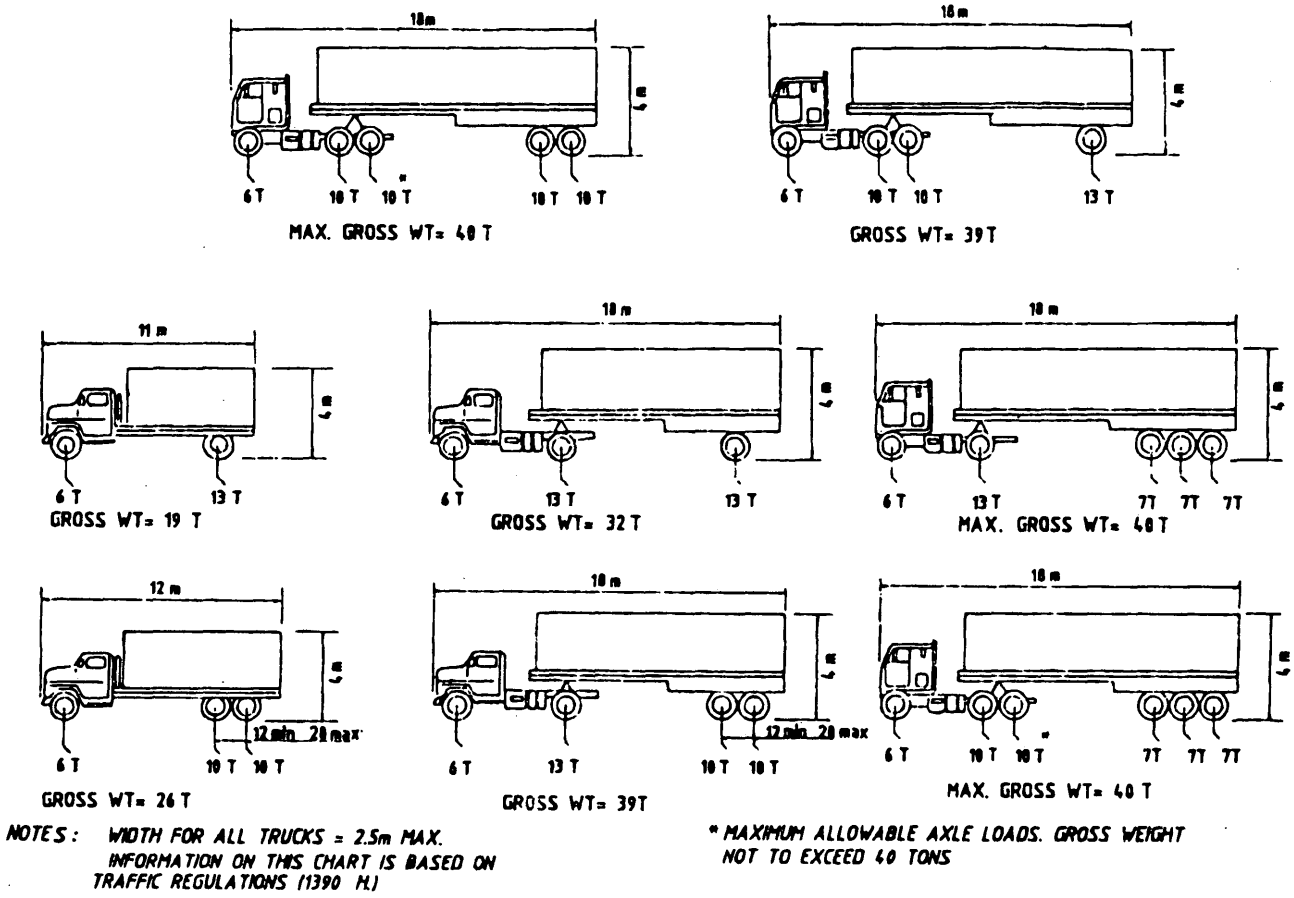

FIGURE 2 Truck classification scheme.

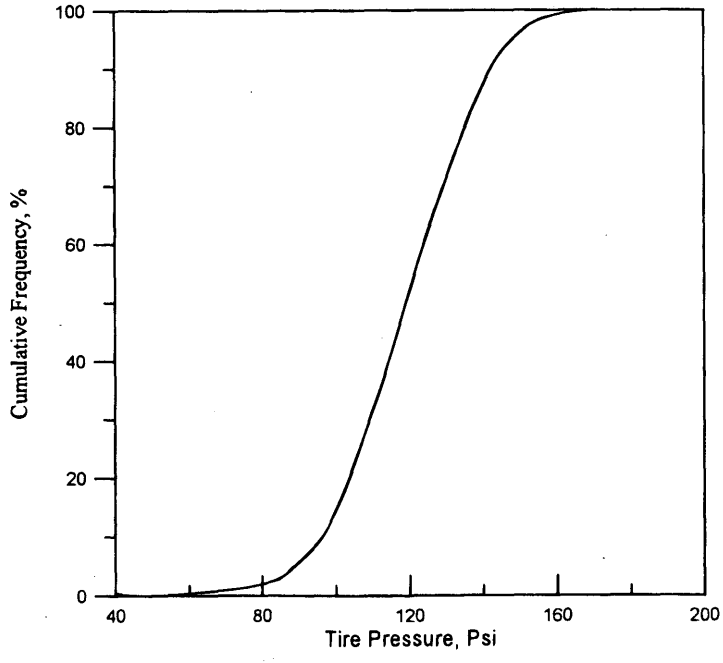

FIGURE 3 Tire pressure data.

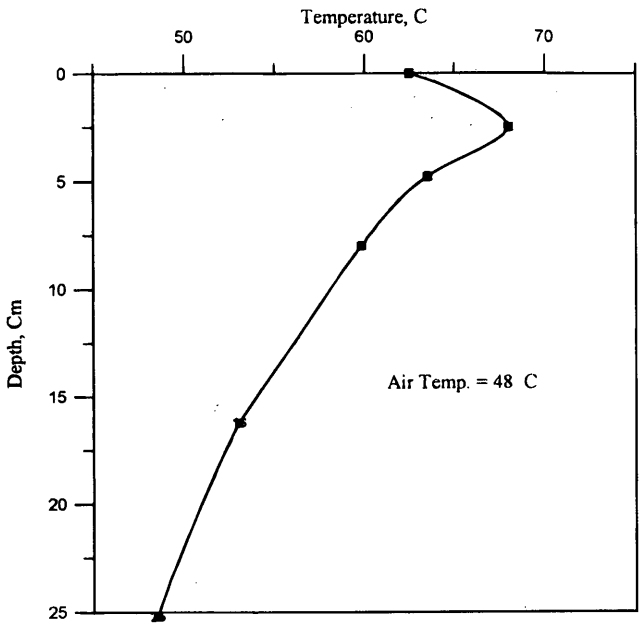

FIGURE 4 Temperature gradient during the hottest time of the year in a 25-cm, full-depth asphalt.

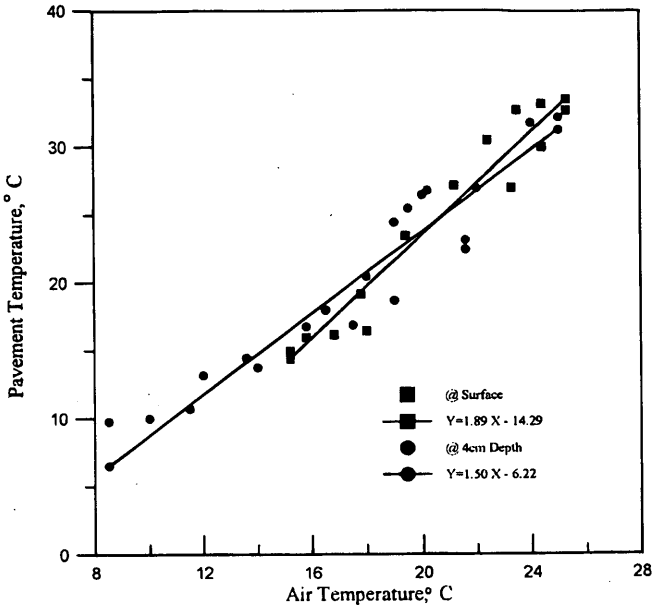

FIGURE 6 Surface temperature–air temperature relationship during December.

ASPHALT CEMENT CHARACTERISTICS

Asphalt cement samples were extracted from slabs obtained from the study sections by using ASTM D 2172 and were recovered by using ASTM D 1856. Consistency characteristics [penetration (PEN), absolute viscosity (ABSVS), kinematic viscosity (KINVS), and softening point (SFT)] were tested according to ASTM D 5, ASTM D 2171, STM D 2170, and ASTM D 36, respectively. This process was performed for the bituminous wearing course and the bituminous base course.

Asphalt cement consistency characteristics were statistically compared as follows:

1. Between the fast and slow lanes within the rutted sections,
2. Between the fast and slow lanes within the nonrutted sections, and
3. Between the fast lanes of the rutted sections and the fast lanes of the nonrutted sections.

The first and second comparisons indicated no statistically significant differences. This generally means that the asphalt cement

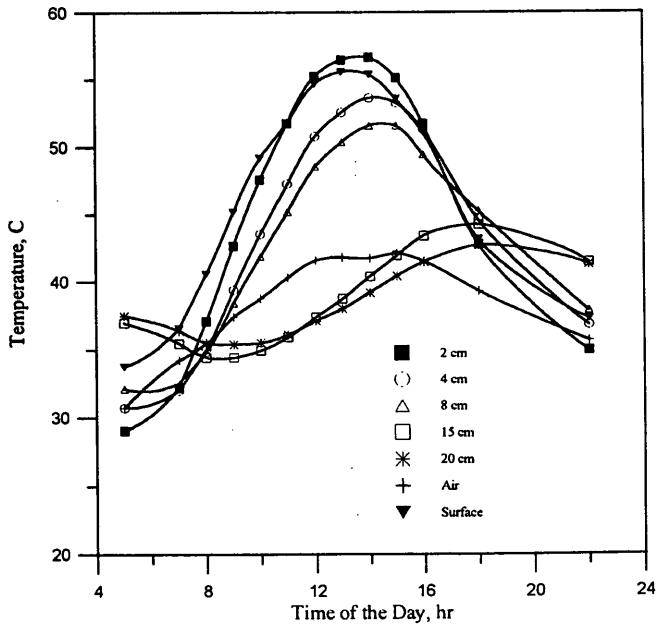

FIGURE 5 Average pavement temperatures during July in a 20-cm, full-depth asphalt.

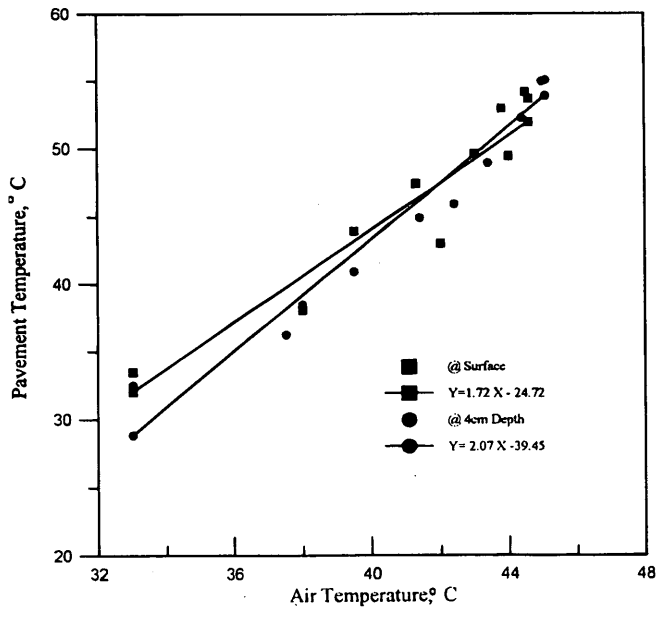

FIGURE 7 Surface temperature–air temperature relationship during July.

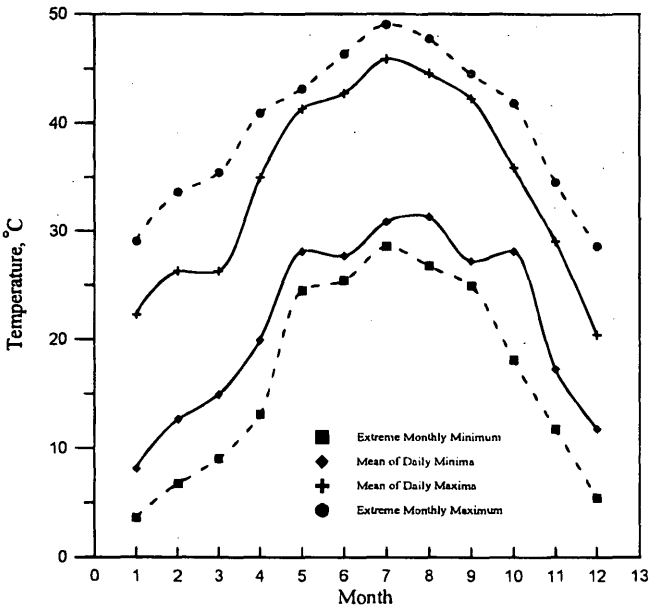

FIGURE 8 Monthly variation in air temperature for Riyadh (Central Region).

consistency characteristics were statistically identical within the same section whether it was a rutted section or a nonrutted section.

However, the third comparison indicated that significant differences exist for the bituminous wearing course only (asphalt samples extracted from the bituminous base course did not indicate statistically significant differences). Asphalt cement extracted from cores obtained from the bituminous wearing course of the fast lanes of the rutted sections was statistically softer than asphalt cement extracted from cores obtained from the bituminous wearing course of the fast lanes of nonrutted sections (Table 2). The expression *softer* means a higher level of penetration, a lower softening point, a lower viscosity, and a lower stiffness (Table 2).

AGGREGATE CHARACTERISTICS

Aggregate samples were extracted from slabs obtained from the study sections by using ASTM D 2172. Gradation analysis was conducted by using ASTM C-136 (Tables 3 and 4). The extracted aggregate, which was limestone for the Eastern and Central Regions and granite for the Western Region, was also examined to determine the surface area, hump value, and amount passing No. 200. These characteristics were obtained for both the bituminous wearing course and the bituminous base course.

TABLE 2 Asphalt Cement Consistency Characteristics for the Bituminous Wearing Course

	Mean		
Variable	Non-Rutted	Rutted	P-Value[a]
PEN	21.01	27.03	0.022
SFT	67.25	62.52	0.011
KINVS	1724.44	1339.58	0.034
ABSVS	81295.55	35645.50	0.011

[a]P-Value: Probability of Equal Means

These aggregate characteristics were statistically compared in exactly the same manner described previously for asphalt cement. The statistical comparisons indicated no significant differences.

MIX DESIGN PARAMETERS

Bulk specific gravities (GMB) of cores obtained from the study sections were obtained by using ASTM D 2726. The maximum theoretical specific gravities (GMM) were determined by using ASTM D 2041. The asphalt content (extracted) was determined by using ASTM D 2172, and its specific gravity was determined by using ASTM D 70. The bulk specific gravities (GSB) of the extracted aggregates were determined in accordance with ASTM C-127 and ASTM C-128. Percent voids in mineral aggregate (VMA), percent air voids (AV), and percent voids filled with bitumen (VFB) were computed in accordance with the Asphalt Institute Mix Design Manual (*3*).

The mix design parameters of the fast lanes of rutted sections (representing original construction conditions) were statistically compared against those parameters of fast lanes nonrutted sections. The comparison was made separately for the bituminous wearing course (BWC) and the bituminous base course (BBC). The comparison indicated (Tables 5 and 6) that

1. The GMB values of cores taken from fast lanes of rutted sections were significantly higher than the GMB values of cores taken from fast lanes of nonrutted sections. This was true for BWC and BBC.
2. The in situ percent VMA and percent AV of fast lanes of rutted sections were significantly lower than the in situ percent VMA and percent AV of fast lanes of nonrutted sections. This was true for BWC. For BBC the percent AV followed the same trend, but the percent VMA showed no significant difference.
3. The percent VFB in cores obtained from fast lanes of rutted sections was significantly higher than the percent VFB in cores obtained from fast lanes of nonrutted sections. This was true for both BWC and BBC.
4. Other mix design parameters (asphalt content, maximum specific gravity, GMM, and GSB) did not show any significant differences.
5. The statistical risk of rutting is minimized (the probability of rutting becomes minimal) when
   a. The in situ AV exceeds 5 percent, the in situ VMA exceeds 13 percent, or the in situ VFB is less than 60 percent for BWC (19-mm top aggregate size) and
   b. The in situ AV exceeds 5 percent, the in situ VMA exceeds 12.5 percent, or the in situ VFB is less than 50 percent for BBC (39-mm top aggregate size).

STRENGTH AND STIFFNESS PARAMETERS

Stability, strength, and stiffness parameters [Hveem stability, diametral resilient modulus (0.1 Hz at 25°C, 40°C, and 50°C), Marshall stability, Marshall flow, Shell creep at 40°C and indirect tensile strength] were used to statistically compare the fast lanes of rutted sections and fast lanes of nonrutted sections (representing original construction conditions). The diametral resilient modulus values of cores obtained from the fast lanes of nonrutted sections were significantly higher than the resilient modulus values of cores

TABLE 3 Wearing Course Aggregate Gradations, Resilient Modulus, and Hveem Stability for Nonrutted Sections

Sieve Size	Road Section											
	C2N	C3N	C5N	C6N	E1N	E3N	E5N	E6N	W1N	W3N	W5N	W7N
37.5 mm	100.0	100.0	100.0	100.0	100.0	100.0	100.0	100.0	100.0	100.0	100.0	100.0
25.0 mm	100.0	100.0	100.0	100.0	100.0	100.0	100.0	100.0	100.0	100.0	100.0	100.0
19.0 mm	100.0	98.3	100.0	95.7	100.0	100.0	100.0	100.0	100.0	100.0	98.4	99.3
12.5 mm	89.2	88.5	88.3	82.9	93.7	96.5	92.3	83.3	91.0	87.7	84.8	93.0
9.0 mm	76.9	78.9	76.4	73.5	81.4	80.4	90.0	71.8	79.9	71.4	71.6	85.5
4.75 mm	58.5	62.2	56.8	53.7	53.9	54.2	56.0	60.2	63.5	51.0	55.6	66.8
2.36 mm	45.2	47.1	42.2	43.6	42.0	41.5	45.2	46.0	51.8	38.2	42.6	47.5
2.00 mm	42.4	44.1	39.2	40.7	40.2	39.5	43.2	42.8	48.8	35.7	39.8	44.1
1.18 mm	35.4	35.7	31.6	32.9	35.9	34.4	39.4	34.9	40.2	29.3	32.6	35.9
0.600 mm	27.5	26.1	25.1	25.4	30.8	29.4	35.2	27.7	32.0	23.2	25.6	27.2
0.425 mm	23.5	22.4	22.2	22.1	25.5	25.3	31.5	24.0	28.2	20.7	22.7	23.0
0.300 mm	18.7	19.3	18.8	18.6	22.5	21.7	25.4	19.3	23.6	18.0	19.7	18.8
0.180 mm	14.1	16.4	14.6	14.6	17.1	16.0	17.9	14.8	17.7	14.6	16.1	14.9
0.150 mm	11.4	13.4	12.4	11.4	14.7	13.6	15.2	12.9	14.8	13.0	14.0	13.6
0.075 mm	5.9	5.5	7.7	5.0	9.2	8.2	11.4	8.3	8.5	9.3	8.8	10.9
Resilient modulus @ 25°C, 10^4 kg/cm^2	8.2	8.4	8.6	10.0	7.1	8.0	7.1	10.0	8.5	8.2	3.5	10.0
Hveem stability %	41	39	42	40	35	45	38	42	50	53	35	42

taken from the fast lanes of rutted sections (Table 7). Other parameters showed no statistically significant differences.

IDENTIFICATION OF RUT-RESISTANT MIXES

Asphalt mixes with a wide range of gradations, various binders [asphalt concrete (AC) 60/70, AC 40/50, and Novophalt and Polybelt modified asphalts], and various filler (limestone dust)-to-binder ratios were characterized by the French Central Bridge and Pavement Laboratory wheel tracking test as a pavement rutting simulator. Test procedures were those described elsewhere (*4,5*). In addition to the wheel tracking test, the mixes were characterized by the Hveem stability, Marshall stability, resilient modulus at 25°C, and indirect tensile strength tests.

Based on the assumption that rut-resistant mixes in the field will also be rut resistant during the wheel track test, the following results were obtained:

TABLE 4 Wearing Course Aggregate Gradations, Resilient Modulus, and Hveem Stability for Rutted Sections

Sieve Size	Road Section						
	C1R	C4R	E2R	E4R	W2R	W4R	W6R
37.5 mm	100.0	100.0	100.0	100.0	100.0	100.0	100.0
25.0 mm	100.0	100.0	100.0	100.0	100.0	100.0	100.0
19.0 mm	100.0	100.0	100.0	100.0	100.0	100.0	100.0
12.5 mm	87.0	91.2	95.8	87.4	94.6	86.7	87.2
9.0 mm	73.3	75.8	82.2	76.8	85.9	75.6	74.4
4.75 mm	56.2	53.9	57.4	53.0	67.5	52.4	55.4
2.36 mm	43.7	37.7	45.0	40.3	52.3	44.8	42.4
2.00 mm	41.2	35.4	43.0	38.1	48.7	41.9	39.6
1.18 mm	34.3	30.2	38.5	33.7	39.2	34.0	32.5
0.600 mm	26.9	23.7	33.0	29.0	31.0	26.3	25.8
0.425 mm	22.7	19.7	28.7	25.2	27.9	23.2	22.9
0.300 mm	17.5	15.6	22.2	18.9	24.5	19.9	19.6
0.180 mm	12.2	11.6	12.8	11.8	19.9	15.9	15.4
0.150 mm	8.3	9.5	10.3	9.4	17.4	14.1	13.4
0.075 mm	4.0	5.1	7.9	5.9	11.3	9.9	8.3
Resilient modulus @ 25°C, 10^4 kg/cm^2	4.8	6.0	5.2	5.1	8.0	7.0	2.7
Hveem stability %	38	34	33	38	52	42	34

TABLE 5 Mix Design Characteristics for Bituminous Wearing Course

Variable	Mean		P-Value
	Non-Rutted	Rutted	
AC, %	4.615	4.989	.190
GMB	2.387	2.427	.027
GMM	2.518	2.513	.915
AV, %	4.838	3.457	.000
GSB	2.609	2.590	.717
VMA, %	12.717	10.974	.000
VFB, %	59.942	69.573	.000

1. For the same asphalt binder and different aggregate characteristics, the Hveem stability test is the best indicator of rut-resistant mixes (best correlated with the wheel tracking test in identifying rut-resistant mixes). This might explain why the Hveem stability test was not capable of distinguishing between rutted and nonrutted sections in the field (fast lane versus fast lane) whose aggregate characteristics were statistically identical.
2. For the same aggregate characteristics but different asphalt binders, the modulus of resilience test (followed by the indirect tensile strength test) is the best indicator of rut-resistant mixes (best correlated with the wheel track test in identifying rut-resistant mixes). This might also explain why the modulus of resilience test was capable of distinguishing between rutted and nonrutted sections in the field (fast lane versus fast lane) whose aggregate characteristics were statistically identical and whose asphalt properties were different.
3. The arrangement described in Table 8 was suggested as a subjective identification of rut-resistant mixes.
4. Based on the criterion that the lower the rut depth measured by the wheel track test the better the rut resistance,
   a. Mixes (surface or base) prepared us with AC 40/50 and then mixes prepared with AC 60/70 + 7 percent Polybelt, AC 60/70 + 4 percent Polybelt, and AC 60/70 only (control) were, respectively, the most rut-resistant mixes.
   b. The filler effect was statistically significant in improving the rut resistance of base course mixes. This was not the case for wearing course mixes that showed little or no improvement.

SUBGRADE SOIL CHARACTERISTICS

Many well-known pavement design methods assume that pavement rutting is a subgrade problem that is reflected on the pavement surface. Among these are the Asphalt Institute method (*1*) and the AASHTO method (*2*). It was therefore essential to investigate the subgrade characteristics of the study sections to detect correlations (if any) between subgrade strength (or weakness) and pavement rutting.

TABLE 6 Mix Design Characteristics for Bituminous Base Course

Variable	Mean		P-Value
	Non-Rutted	Rutted	
AC, %	4.194	4.245	.831
GMB	2.334	2.392	.007
GMM	2.496	2.504	.865
AV, %	4.447	3.484	.038
GSB	2.543	2.569	.609
VMA, %	12.063	11.636	.454
VFB, %	48.553	64.780	.000

TABLE 7 Resilient Modulus Values (10^4 kg/cm^2 at 25°C) for Bituminous Wearing Course and Bituminous Base Course

Layer	Percentile	Non-Rutted	Rutted
Wearing Course	25 percentile	4.15	3.09
	Mean	5.00	4.03
	75 percentile	5.53	4.98
Base Course	25 percentile	4.84	2.90
	Mean	5.15	3.82
	75 percentile	6.00	5.03
Combined	25 percentile	4.46	2.97
	Mean	5.14	3.88
	75 percentile	5.85	5.03

The results of that investigation indicated that the rutting observed in all study sections was not initiated in the subgrade and reflected on the surface. In addition, it was noted that the soil classification of the subgrades under pavement layers in all study sections in the Eastern, Central, and Western Regions was A-1-a, A-1-b, A-2-4, A-2-5, or A-2-6. The presence of silt or clay (A-2-4, A-2-5, and A-2-6) occurred mainly in study sections within the Eastern Region.

This should not imply, however, that quality control measurements for subgrade preparation can be eased. Figure 9 illustrates the importance of quality control on density achieved in the field and its effect on subgrade strength as represented by the California Bearing Ratio (CBR) for the study sections. It can be seen that a 1 percent reduction in density achieved results in a drop of at least 8 percent in the in situ CBR achieved.

EMPIRICAL OBSERVATIONS

The following are some statistical empirically relevant observations extracted from the study:

1. The total rut depth per 1 cm of thickness of bituminous layers was 0.15 cm.
2. The bulk specific gravity of the aggregate used in the pavement layers was highest in the Western Region (mountainous terrain); this was followed by the Central Region (hilly terrain) and then the Eastern Region (level terrain).
3. The quality control of construction of non-asphalt-bound layers (subbase and subgrade) represented by percent compaction and CBR was highest in the Central Region (where the capital, Riyadh, is located); this was followed by the Western Region (where the second capital, Jeddah, and the Holy Cities are located) and then the Eastern Region.

CONCLUSIONS

The following conclusions are reached on the basis of the data obtained in the present study:

1. Rutting observed from trench cuts or continuous coring occurred in the top 10 cm of the asphalt-bound layers.

TABLE 8 Subjective Identification of Rut-Resistant Mixes

Rut Resistance	Rut Depth Wheel Track Test mm/10,000 Cycles		Hveem Stability		MR, 25°C 10^4 kg/cm^2
Very good	< 2.0	or	> 47	and	> 3.3
Good	2.0-3.5	or	43-47	and	3.0-3.3
Fair	3.5-5.0	or	37-43	and	2.6-3.0
Poor	> 5.0	or	< 37	and	< 2.4

2. Pavement rutting in Saudi Arabia is mainly caused by the compound effect of heavily loaded trucks with high tire pressures and long periods of hot weather.

3. In situ air void contents above 5 percent are needed to decrease the probability of premature rutting of asphalt-bound layers (surface and base).

4. In situ VMAs of at least 13 percent for a 19-mm bituminous wearing course and at least 12.5 percent for a 38-mm bituminous base course are needed to decrease the probability of premature rutting of asphalt-bound layers.

5. Mix design volumetric parameters (GMB, percent AV, percent VMA, and percent VFB) are related to pavement rutting.

6. Combined testing of laboratory-compacted cores to determine the resilient modulus at 25°C (ASTM D 4123) and then the Hveem stability (for the same specimen) can be used to subjectively identify rut-resistant mixes as described here.

RECOMMENDATIONS

The following recommendations can be made on the basis of the data obtained during the study phases:

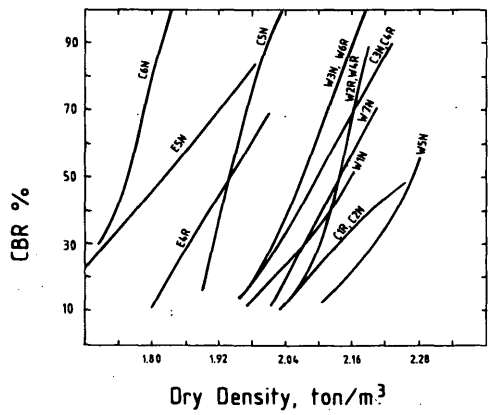

FIGURE 9 CBR-density relationship for the study sections.

1. Greater emphasis should be placed on the monitoring of truck gross weight and axle load limits, especially those trucks classified as 2S2, which have a history of violating load limits.

2. An approach to monitoring and controlling tire pressures and setting standards and penalties (similar to those for gross weight and axle load violations) is needed.

3. Whenever feasible the end of construction and the opening of new roads to traffic should not be scheduled during (or just before) the months of May to September.

4. Quality control of construction materials should include the monitoring of asphalt cement temperature versus consistency characteristics.

5. Whenever possible, polymer-modified asphalt or hand asphalt grade (AC 40/50) is preferred over AC 60/70.

6. A minimum softening point for the asphalt mastic (asphalt + filler) of at least 65°C should be specified.

ACKNOWLEDGEMENT

The authors thank King Abdulaziz City for Science and Technology, the Ministry of Communications, King Fahd University of Petroleum and Minerals, and King Abdulaziz University for valuable support of this research project.

REFERENCES

1. *Thickness Design—Asphalt Pavements for Highways and Streets*. MS-1. The Asphalt Institute, 1981.
2. *AASHTO Guide for Design of Pavement Structures*. AASHTO, Washington, D.C., 1993.
3. *Mix Design Methods for Asphalt Concrete and Other Hot Mix Types*. MS-2. The Asphalt Institute, 1984.
4. *Tracking Rutting Test*. Laboratoire Central des Ponts et Chaussees, Paris, Dec. 1981.
5. King, G. N., H. W. King, O. Harders, and P. Chaverot. Influence of Asphalt Grade and Polymer Concentration on the High Temperature Performance of Polymer Modified Asphalt. AAPT, 1992.

Publication of this paper sponsored by Committee on Strength and Deformation Characteristics of Pavement Sections.

Development and Preliminary Investigation of Rolling Dynamic Deflectometer

J. A. BAY, K. H. STOKOE II, AND J. D. JACKSON

Nondestructive testing (NDT) is an important part of optimizing any pavement management system. At this time in the United States NDT is performed at discrete points on the pavement to evaluate the properties of the pavement layers. Techniques such as the falling weight deflectometer (FWD), Dynaflect, and spectral-analysis-of-surface-waves are used. A new technique is described. It is called the rolling dynamic deflectometer (RDD) and is a large truck on which a servo-hydraulic vibrator is mounted. The vibrator is used to apply large vertical dynamic loads [up to a total load of 147 kN (33,000 lb)] to rolling wheels that come into contact with the pavement. A receiver wheel located midway between the loading wheels is used to monitor the dynamic deflections. The truck is driven at a slow speed [about 5 km/hr (3 mph)], and continuous profiles of pavement flexibility are measured under heavy traffic conditions. Descriptions of the equipment, calibration results, and test procedures are presented. Several examples involving tests of flexible pavements and comparisons with FWD results are included. The results show that the RDD can be used to (a) determine uniformity along pavement sections, (b) measure differences in average flexibility between different sections, and (c) observe nonlinearities in a given pavement section.

Nondestructive testing (NDT) techniques have been used for several decades in the field to determine the properties of pavement systems. The most common techniques used in the United States are the falling weight deflectometer (FWD), the Dynaflect, and the spectral-analysis-of-surface-waves techniques (*1–5*). Each of the methods requires the equipment to be stationary during testing. Therefore, it is difficult or impossible to obtain continuous or nearly continuous profiles either longitudinally or laterally along the pavement. To overcome this limitation of sampling at discrete points a rolling dynamic deflectometer (RDD) has been developed. With the RDD rapid measurement of continuous profiles of pavement flexibility or stiffness under heavy traffic and overload conditions can be performed. This device can move down the pavement at speeds of 3 to 6 km/hr (2 to 4 mph) and can continuously record pavement deflection under significant static and large dynamic loads. This deflectometer represents a one-of-a-kind piece of equipment. In the following paragraphs a description of the device is given, calibrations of the loading and monitoring systems are presented, and examples of test data are provided. Several field studies with flexible pavements, including comparison with results obtained with the FWD, are also presented.

DESCRIPTION OF RDD

The RDD is shown in Figure 1. This device consists of a large truck with a gross weight of about 195 kN (44,000 lb) on which a servo-hydraulic vibrator is mounted. The vibrator has a 33-kN (7,500-lb) reaction mass that is used to generate vertical dynamic forces as large as 310 kN (70,000 lb) over a frequency range of about 5 to 100 Hz. When the reaction mass is driven by the hydraulic system as illustrated in Figure 2, the resulting vertical dynamic force is applied to two sets of loading wheels that contact the pavement. Simultaneously, the hydraulic system can be used to apply a constant hold-down force to the loading wheels ranging from 65 to 180 kN (15,000 to 40,000 lb) through a system of air springs. This system is under modification so that hold-down forces ranging from 13 to 180 kN (3,000 to 40,000 lb) can be applied.

The static and superimposed dynamic forces are transferred to the pavement through two sets of dual loading wheels as shown in Figure 2. The use of wheels to transfer the load permits continuous loading to be applied while the complete system is moving. The wheels are quite rigid in that they have a solid aluminum rim that is coated with hard urethane. This type of wheel was selected to minimize the resonances that might occur with pneumatic wheels loaded in this manner. Each wheel is 457 mm (18 in.) in diameter and 127 mm (5 in.) wide. A total force (static plus dynamic) of 150 kN (33,000 lb) can be applied to the pavement surface through the loading wheels at this time. However, the wheels could be modified to allow a peak-to-peak force as large as 310 kN (70,000 lb) to be applied if it ever became desirable. The reaction mass and servohydraulic system are already capable of generating this force level. This point is rather important, because it highlights the fact that the gross weight of the truck does not control the force output. Rather, the driving force is coming from the inertial force created by the reaction mass moving at high frequencies.

The servohydraulic vibrator is capable of generating many types of dynamic loading functions. For instance, transient (like the FWD), steady-state (at any frequency from 5 to 100 Hz), swept-frequency, chirps, or random-noise types of loads can be generated. In the initial study steady-state excitation superimposed on a constant static load was used, as illustrated in Figure 3. Dynamic deflections of the pavement surface (due only to the peak-to-peak dynamic loading) are then recorded midway between the two sets of loading wheels. These deflections are recorded with an accelerometer located on a set of two receiver wheels as shown in Figure 2. Two wheels were used to support the receiver (accelerometer) simply for stability during movement. Wheels were again used in this part of the rolling device as an inexpensive way of accomplishing continuous measurements. Wheels similar to the loading wheels, but slightly smaller [30 mm (12 in.) in diameter and 76 mm (3 in.) wide], were used. The twin receiver wheels, hereafter termed *receiver wheel* for convenience, are isolated from the loading mechanism and truck by the support arm shown in Figure 1.

Department of Civil Engineering, College of Engineering, The University of Texas at Austin, Austin, Tex, 78712-1076.

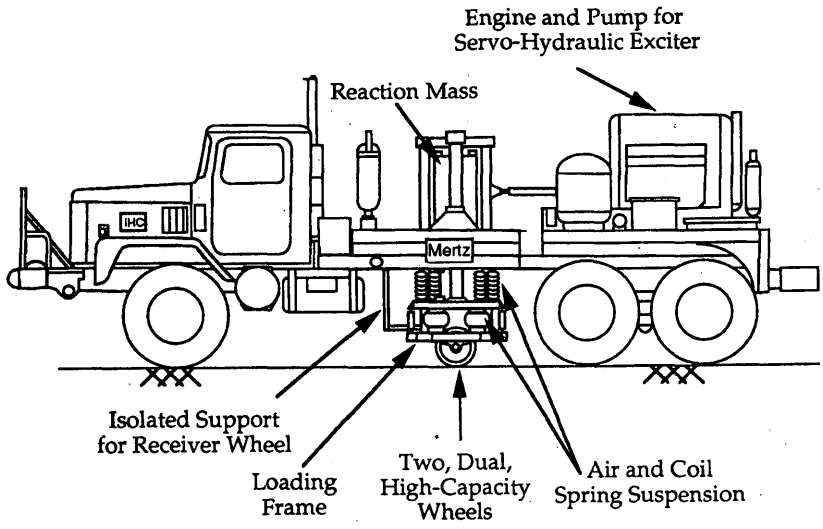

FIGURE 1 Basic components of RDD used to measure continuous pavement flexibility profiles.

The basic idea is to drive the truck at a slow speed along the pavement while applying dynamic loading and simultaneously measuring the resulting dynamic deflections. The accelerometer on the receiver wheel monitors only the dynamic motion; it does not monitor any motion resulting from the static load. In the initial studies measurements have been performed at about 5 km/hr (~3 mph), loading frequencies ranging from 20 to 40 Hz have been used, and only one measurement point (midway between the loading wheels) has been used. There is no reason, however, why multiple measurement points at various distances from the loading wheels could not be monitored.

EQUIPMENT CALIBRATION

To conduct stiffness or flexibility measurements while rolling, it is critical to perform dynamic calibrations of the equipment used to measure both forces and displacements. Any equipment resonances that fall within the range of excited frequencies will affect the dynamic response of the measurement systems and must be accounted for in the analysis of the recorded data. A set of weigh-in-motion (WIM) load cells were used to calibrate the static and dynamic loads applied in RDD testing (*6*). A velocity transducer (geophone) was

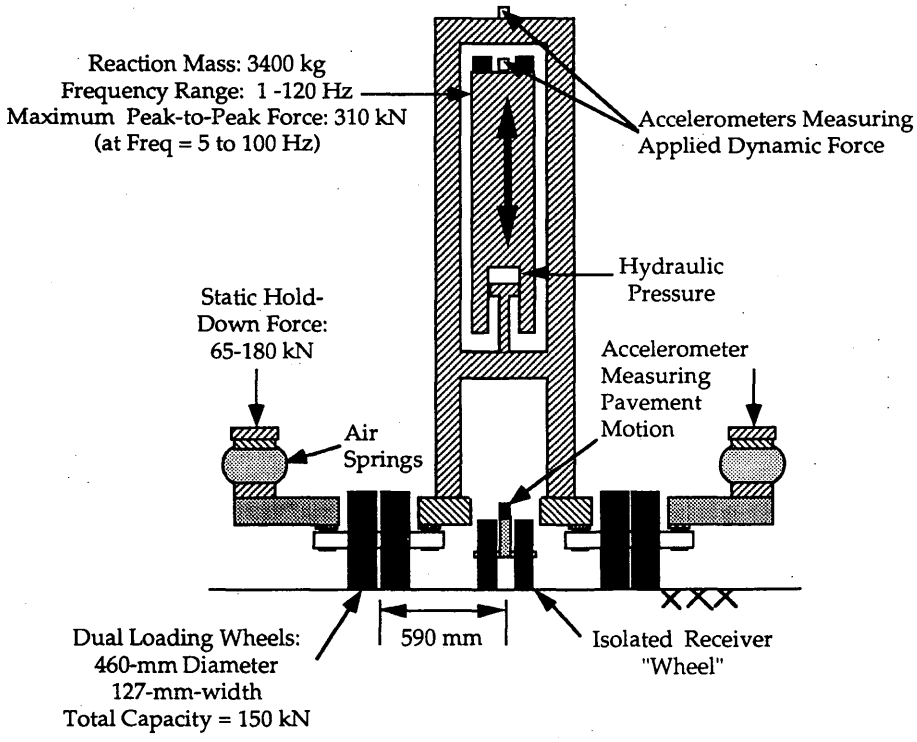

FIGURE 2 Front cross-sectional view of dynamic loading and monitoring systems of RDD.

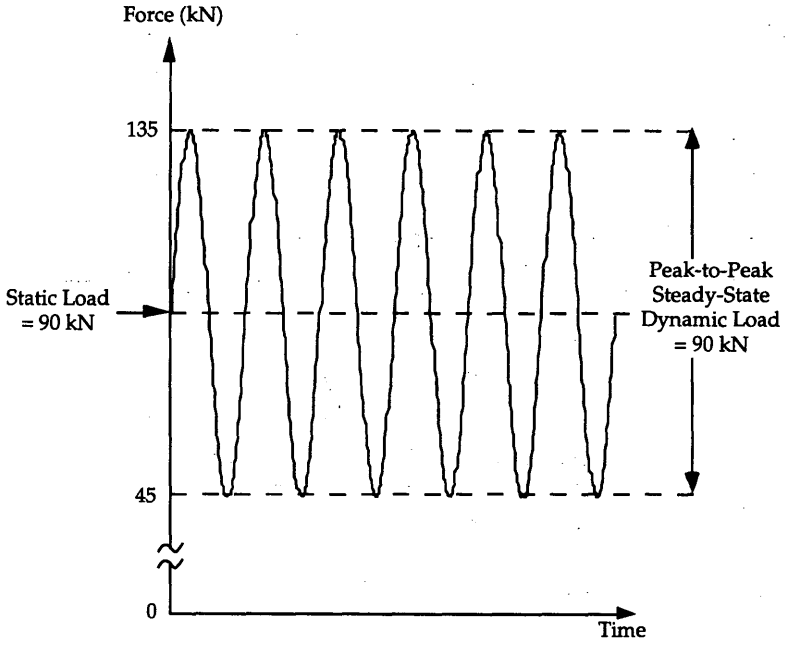

FIGURE 3 Example of combined static and steady-state dynamic loads applied continuously by RDD.

used to calibrate the receiver wheel, and an accelerometer was used to measure the dynamic displacements.

Static Force Calibration

The simplest calibration was the calibration of static load applied to the loading wheels. The static load is a combination of the dead weight of the reaction-mass-load-frame system and the force applied through the hydraulic cylinders. The static force was calibrated by comparing the pressure in the hydraulic cylinders with the force measured with the WIM load cells. This calibration curve is shown in Figure 4(*a*). With no hydraulic pressure in the cylinders a force of 55 kN (12,300 lb) was measured. This represents the dead weight of the reaction-mass-load-frame system. The pressure control valve used on the RDD system applies a minimum of 1380 kPa (200 lb/in.^{2}), and a lifting force cannot be applied with the hydraulic system while driving the reaction mass. Therefore, the lowest static force that can be applied at present is about 67 kN (15,000 lb). Future modifications will make it possible to apply much lower static loads.

Dynamic Force Calibration

The dynamic force applied by exciting the reaction mass is measured by two accelerometers, one on the reaction mass and a second on the loading frame, as shown in Figure 2. From Newton's second law it can be determined that the dynamic force applied to the pavement through the loading wheels, F_d, is equal to the sum of the accelerations of these two parts times their masses as

$$F_d = A_1 \times M_1 + A_2 \times M_2 \quad (1)$$

where A_1 and M_1 are the acceleration and mass of the reaction mass, respectively, and A_2 and M_2 are the acceleration and mass of the combination of the loading frame and the wheels, respectively. To measure the dynamic force the signals from each accelerometer were amplified with a gain proportional to the mass of the respective system, one signal was inverted, and the two signals were summed with a differential amplifier. To generate a calibration curve the combined outputs of the two accelerometers were divided by the dynamic force measured with the load cells, because the RDD was driven at various frequencies. This calibration curve is shown in Figure 4(*b*). The calibration curve is quite uniform up to 47 Hz. Above 47 Hz the performance of the system could not be evaluated because of resonances in the load cells. Further work is required to calibrate the RDD at higher frequencies. However, the frequency range shown in Figure 4(*b*) was satisfactory to perform the initial studies described here.

Receiver Wheel Calibration

Dynamic displacements created by the RDD are measured on the pavement surface with an accelerometer mounted on the axle of the two rigid receiver wheels shown in Figure 2. This system acts like a single-degree-of-freedom damped spring-mass system, with the urethane coating on the wheels acting as the damped spring. Therefore, it is expected that the response of this system will vary with frequency and will have a single resonant peak. To measure this response a velocity transducer with a known calibration was secured to the pavement surface between the receiver wheels, and the pavement was driven at a series of frequencies with the RDD while it was stationary. The outputs of the geophone and accelerometer were both measured. In the frequency domain, the output of the geophone was converted from velocity to acceleration in g's by the following equation:

$$\text{acceleration} = \frac{\text{geophone output} \times \text{calibration factor} \times i2\pi f}{9.81 \text{ m/sec}^2/\text{g}} \quad (2)$$

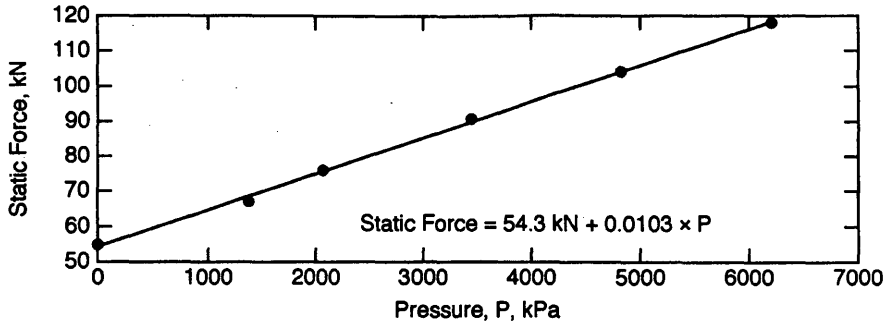

a) Calibration of Applied Static Force

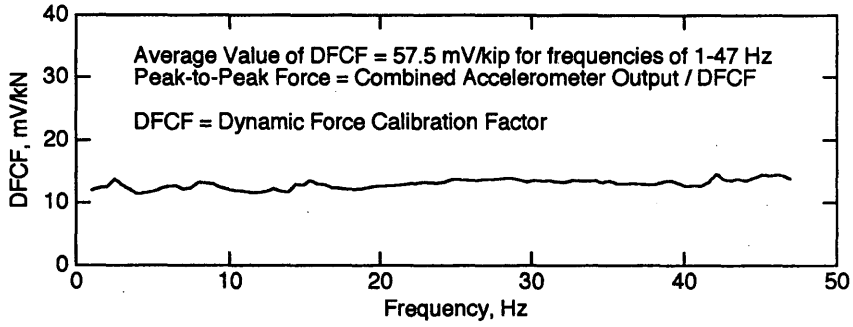

b) Variation of Dynamic Force Calibration Factor, DFCF with Loading Frequency for the Applied Dynamic Load

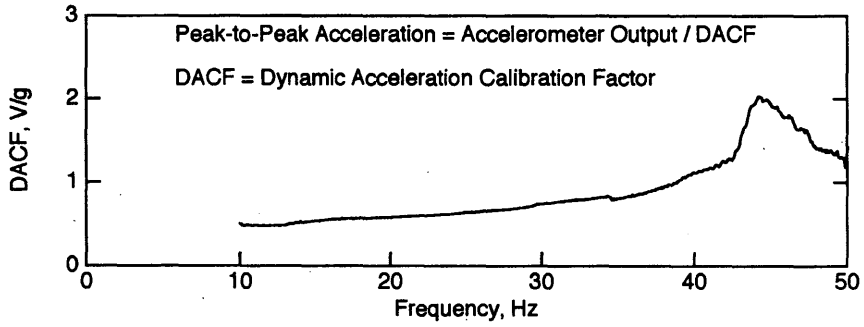

c) Variation of Dynamic Acceleration Calibration Factor, DACF with Loading Frequency for the Receiver Wheels

FIGURE 4 Calibration factors associated with load and displacement measurements using RDD.

This result was divided by the output of the accelerometer to determine the calibration curve. This resulting curve is shown in Figure 4(*c*). Below 10 Hz the accelerometer output becomes unstable. However, over the range of frequencies of interest in most pavement testing, the receiver wheel is quite well behaved and acts as a single-degree-of-freedom system with a resonance around 44 Hz. The calibration curve shown in Figure 4(*c*) was applied to all displacement measurements in the frequency domain.

TESTING AND ANALYSIS PROCEDURES

Testing Procedure

The RDD is designed to move along a pavement at velocities of 3 to 6 km/hr (2 to 4 mph) while generating large dynamic loads with the servohydraulic system and applying them to the pavement through the loading wheels. The pavement motions are measured at the isolated receiver wheel, which rolls along the pavement at the midpoint between the loading wheels. Currently, the position of the RDD along the testing axis is determined by knowing the velocity of the truck and the elapsed time. This is only suitable for continuous profiling over short sections of pavement (less than about 30 m). Very long sections of pavement could be profiled continuously by incorporating a distance measuring device, which is contemplated for future adaptations.

In the present configuration the operator must control four parameters when profiling with the RDD. The first parameter is the velocity of the truck. Currently, this is very important because it is used to determine the testing location with time. However, the vehicle velocity also controls the magnitude of the noise generated by the loading and receiver wheels rolling on the rough pavement surface. Initial experience indicates that velocities of 5 km/hr (3 mph)

or less provide adequate signal-to-noise ratios for the reasonably heavy loads and the close measurement point used. The second parameter is the static force, F_s, applied to the loading wheels. As discussed previously the static force cannot be set at less than 65 kN (15 kips) until further modifications to the hydraulic system are completed. With the modifications the static force can be varied from 13 to 180 kN (3,000 to 40,000 lb). Considerations in selecting a static force involve the third parameter, the dynamic force, F_d. This force is controlled by regulating the flow of hydraulic fluid through the servovalve. The possible range of dynamic force is 9 to 310 kN (2,000 to 70,000 lb) peak to peak.

Three criteria must be met in selecting the static and dynamic forces. First, one must satisfy

$$F_s - \frac{F_d}{2} > 4.5 \text{ kN} \tag{3}$$

This criterion ensures that the loading wheels will be in constant contact with the pavement. The second criterion is

$$F_s + \frac{F_d}{2} \leq 150 \text{ kN} \tag{4}$$

which ensures that the capacity of the loading wheels will not be exceeded. The third criterion is

$$F_s + \frac{F_d}{2} < \text{pavement capacity} \tag{5}$$

This criterion ensures that the pavement will not fail under testing. Unfortunately, the authors have not always been successful with this criterion in their initial tests. One reason is that higher dynamic forces provide larger pavement motions that result in higher signal-to-noise ratios. The desire to create very large signals resulted in overloading one flexible pavement.

The last parameter that the operator must select is the operating frequency of the RDD. The RDD is capable of operating at frequencies of from 5 to 100 Hz. The choice of an operating frequency is not a simple one. Considerations in selecting an operating frequency include site resonances due to shallow bedrock, frequency dependencies in the pavement materials, desired depth of sampling, and the frequency content of rolling and vehicle noises. Site resonances and frequency dependencies can be identified by exciting the RDD with broadband excitation (transients, swept-sines, or chirps) while it is stationary and measuring the response spectra. Up to this point frequencies around the predominant frequency of 30 Hz often found in FWD measurements have been used.

Analysis Procedure

The procedure used to analyze RDD data is illustrated by stepping through the procedure for a typical measurement. The example measurement is from tests at the Texas Transportation Institute (TTI) testing facility at Texas A&M University. The pavement used in this example is designated Section 10. Details about this flexible pavement and the other ones tested at TTI are provided in Table 1 and in a report by Scrivner and Michalak (*7*).

Figure 5 contains time records of force and acceleration that were measured while rolling across Section 10 and operating the RDD at

TABLE 1 Layer Thicknesses and Materials of the Flexible Pavements at TTI Facility Tested with RDD

Section Number	Layer Thickness			Material Type		
	Surface	Base	Subbase	Base	Subbase	Subgrade
9	127 mm (5 in.)	102 mm (4 in.)	102 mm (4 in.)	Crushed Limestone	Crushed Limestone	Sandy Gravel
10	25 mm (1 in.)	305 mm (12 in.)	102 mm (4 in.)	Crushed Limestone	Crushed Limestone	Sandy Gravel
11	25 mm (1 in.)	102 mm (4 in.)	305 mm (12 in.)	Crushed Limestone	Crushed Limestone	Sandy Gravel
12	127 mm (5 in.)	305 mm (12 in.)	305 mm (12 in.)	Crushed Limestone	Crushed Limestone	Sandy Gravel
14	25 mm (1 in.)	305 mm (12 in.)	102 mm (4 in.)	Crushed Limestone with 4% Cement	Crushed Limestone with 4% Cement	Sandy Gravel
15	25 mm (1 in.)	102 mm (4 in.)	305 mm (12 in.)	Crushed Limestone with 4% Cement	Crushed Limestone with 4% Cement	Sandy Gravel
16	127 mm (5 in.)	305 mm (12 in.)	305 mm (12 in.)	Crushed Limestone with 4% Cement	Crushed Limestone with 4% Cement	Sandy Gravel
29	76 mm (3 in.)	203 mm (8 in.)	203 mm (8 in.)	Crushed Limestone with 2% Lime	Crushed Limestone with 2% Lime	Sandy Gravel

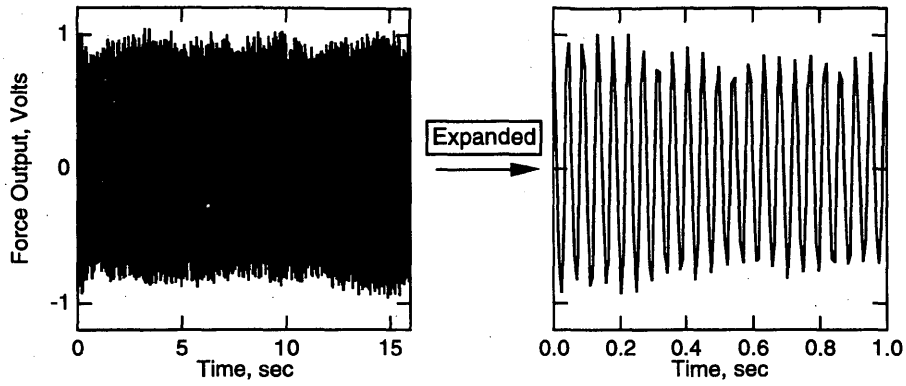

a) Dynamic Force Applied to Pavement Surface

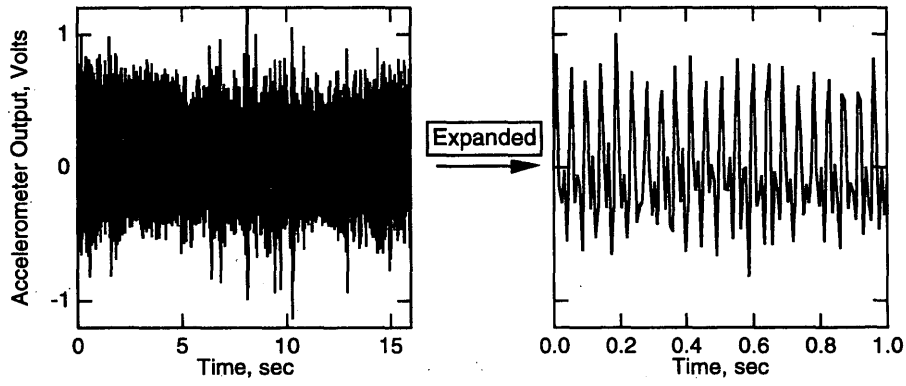

b) Motion of Pavement Surface Measured with Receiver Wheels

FIGURE 5 Typical time records from RDD operating at 22 Hz and traveling 7 m along flexible pavement Section 10 at TTI test facility.

22 Hz. The complete time record for a 7-m-long, continuous profile is shown along with one for an expanded portion. The force output is quite monochromatic, with little harmonic distortion or rolling noise. The accelerometer output exhibits significant amounts of harmonic distortion and rolling noise. However, the effects of this distortion and noise are greatly reduced in the process of converting the acceleration measurement to a displacement measurement, as will be discussed.

To analyze the data it is necessary to isolate the components of force and displacement at the operating frequency (22 Hz). This can be done in several ways. One method would have been to filter the signals through a notch-pass analog filter. Another method would be to use digital filters. Each of these methods has limitations. The method that was finally used was spectral analysis with the Fast Fourier Transform (FFT). By using the FFT the data were separated into the frequency components, and measurements were made not only at the operating frequency but also at frequencies around the operating frequency. Measurements at these additional frequencies permitted quantification of the noise level and allowed evaluation of measurement quality.

The spectral analysis procedure applied to the excitation force is illustrated in Figure 6. The force output shown in Figure 6(*a*) is that for the same record given in Figure 5. The time record is divided into a number of sections. Each section is determined by multiplying the time record by the weighting function shown in Figure 6(*b*). This function is a Hanning window, which is commonly used in spectral analysis. The effect of using the Hanning window (weighting function) is to average the measurement over a region in which more weight is applied to the center of that region. By using the window shown and the velocity at which the RDD was moving, the data were effectively averaged over about a 0.6-m (2-ft) interval. Successive measurements are analyzed by using overlapping weighting functions so that all data are used equally. The weighted force output for one section is shown in Figure 6(*c*). An FFT is performed on this time record, transforming it into the frequency domain. The magnitude of the resulting frequency function is shown in Figure 6(*d*). At this point the dynamic force calibration factor (DFCF) shown in Figure 4(*b*) is applied to the data to convert from units of voltage to units of peak-to-peak force. This conversion is shown in Figure 6(*e*), and a peak-to-peak loading force of 69.0 kN (15,500 lb) is measured at 22 Hz. Only noise at frequencies close to the measurement frequency could adversely affect the force-level measurements. To analyze this noise level the same spectrum shown in Figure 6(*e*) is plotted in Figure 6(*f*) by using a vertical logarithmic scale. The average noise level measured at frequencies of ±5 Hz from the operating frequency were considered. The average noise level in this frequency range (17 to 27 Hz) was found to be 0.36 kN (80 lb). Therefore, the actual driven force would be 69.0 ± 0.36 kN (15,500 ± 80 lb).

The same procedure is shown in Figure 7 for the displacement measurement. The procedure is identical except when converting from units of volts in the frequency domain to units of displacement

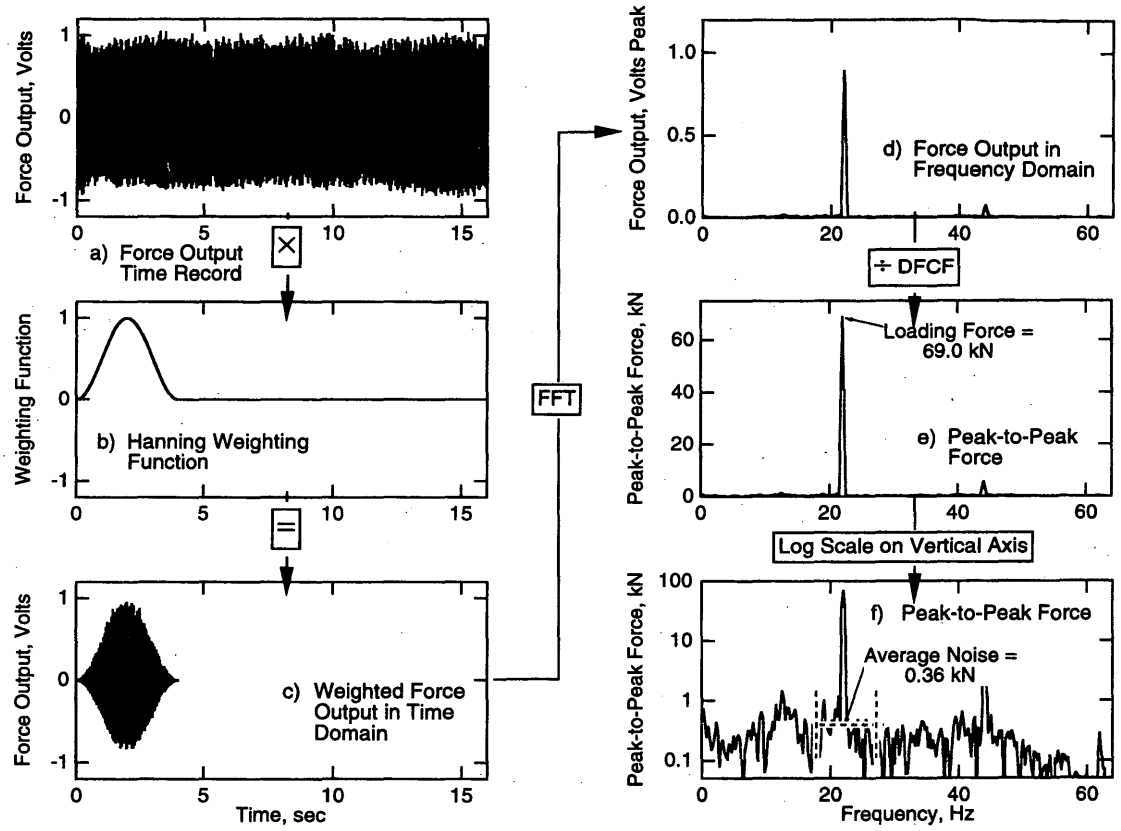

FIGURE 6 Sample calculation of dynamic force applied when RDD was operating at 22 Hz.

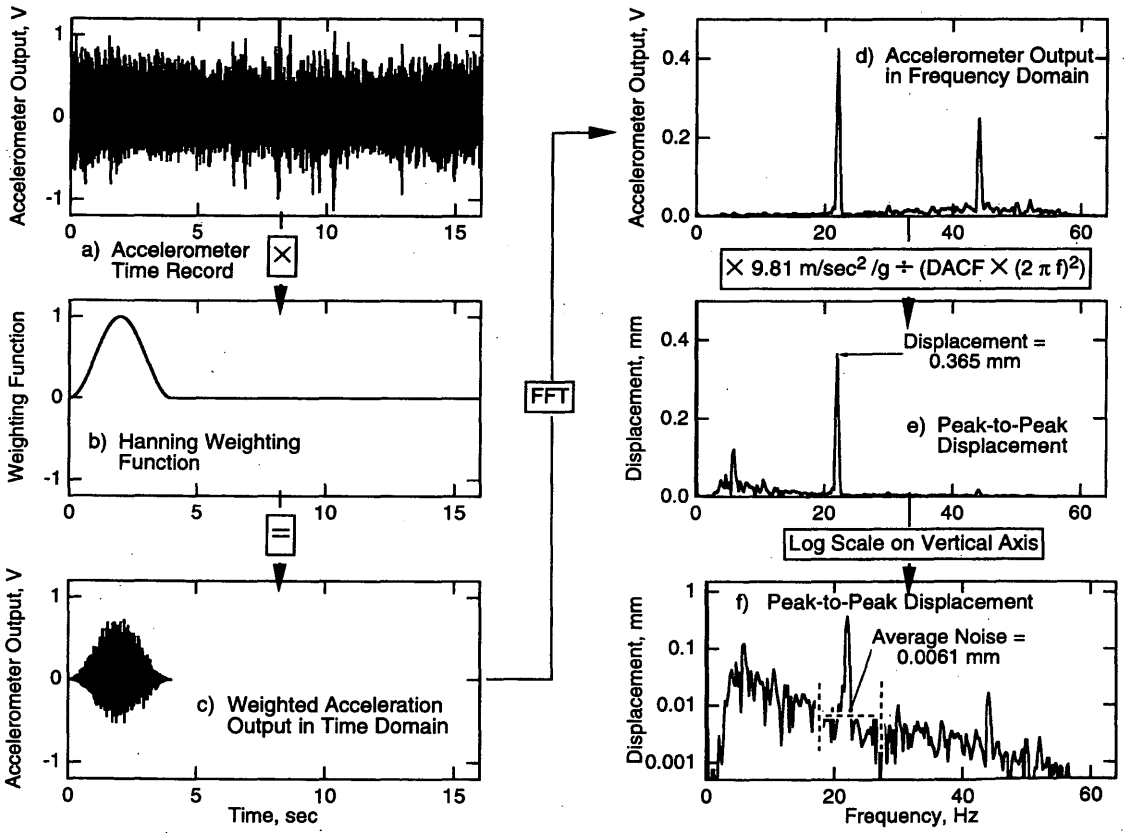

FIGURE 7 Sample calculation of dynamic displacement measured with receiver wheel when RDD was operating at 22 Hz.

in meters. In this case the displacement was found to be 0.365 mm (0.0144 in.), with an average noise level of 0.0061 mm (0.00024 in.) The rolling noise has much more of an effect on the displacement measurement than on the force measurement. However, both measurements are high-quality measurements, as shown by signal-to-noise ratios in excess of 50.

To quantify a property of the pavement system, the flexibility is calculated next. Flexibility is the inverse of stiffness. Therefore, higher flexibility indicates a softer pavement system and lower flexibility indicates a stiffer system. Flexibility is defined as follows:

$$\text{flexibility} = \frac{\text{dynamic displacement}}{\text{dynamic force}} \quad (6)$$

By using 25 successive Hanning weighting functions with the records in Figure 5, successive values of force, displacement, flexibility, and average noise levels were calculated for the time records measured at Section 10. These values are plotted in Figure 8. The flexibility profile shown at the bottom of Figure 8 reveals that the section is quite uniform longitudinally.

RDD RESULTS AT TTI FLEXIBLE TEST SECTIONS

A series of tests was performed with the RDD at the TTI pavement test facility. At that facility a number of flexible pavement sections have been constructed with different materials and thicknesses of pavement, base, and subgrade. RDD profiling was performed at eight of these test sections. Table 1 contains the materials and layer thicknesses of the sections where the tests were performed. The objectives of the testing were (a) to determine uniformity along the longitudinal centerline of each section, (b) to observe differences in average flexibility between the different sections, and (c) to observe nonlinearities in the pavement sections. FWD tests were also performed concurrently at some of the pavement sections to compare those results with the results of the RDD test. Most RDD tests were performed at an operating frequency of 22 Hz. However, a few tests were performed at 40 Hz to observe the effect of frequency. All testing was performed with a static force of 67 kN (15,000 lb).

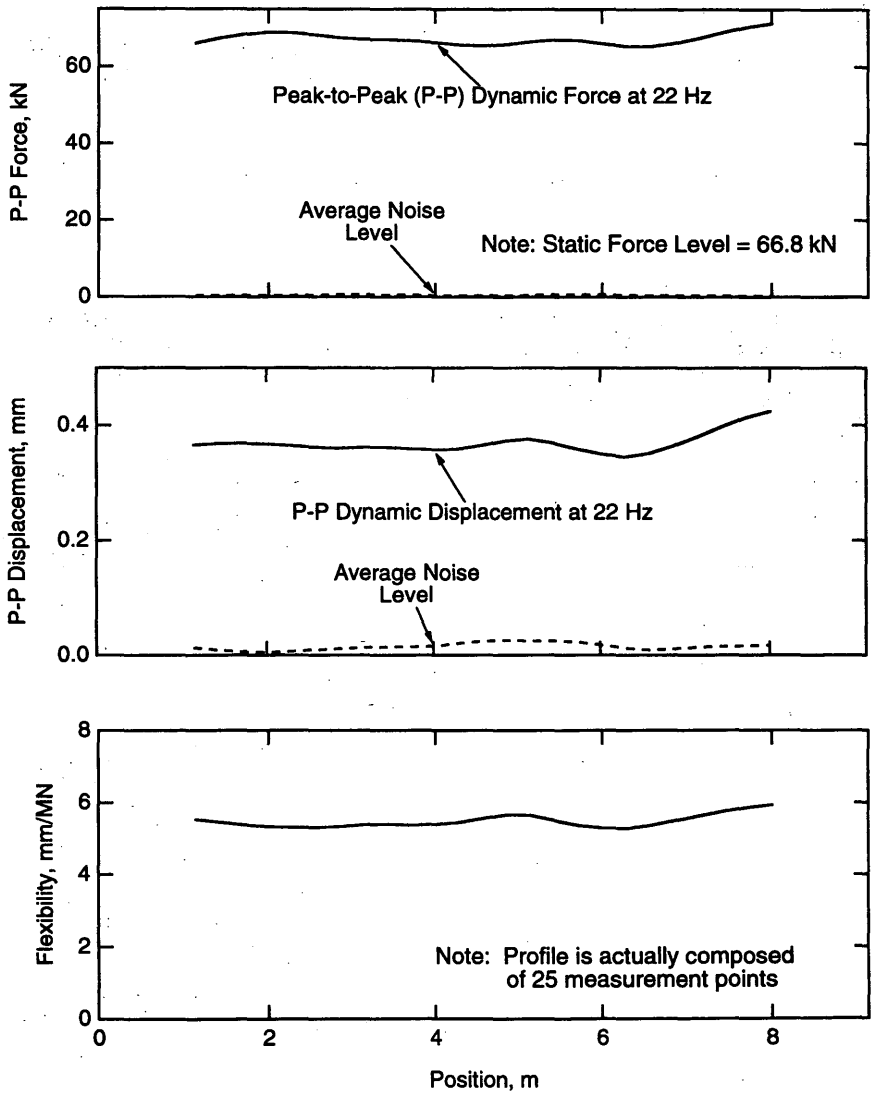

FIGURE 8 Continuous profiles of flexible pavement Section 10 at TTI test facility determined with RDD operating at 22 Hz with high dynamic force level.

Variability Within Pavement Sections

One of the major benefits of the RDD is that continuous measurements of pavement flexibility can be performed. This makes the RDD especially well suited for studying the variability (longitudinally or laterally) of pavement systems. This benefit is demonstrated by the continuous profile of Section 10 shown in Figure 8. Another approach that can be used to observe longitudinal variability is to normalize the flexibility measured continuously by dividing by the average flexibility determined over the entire section at one load. This was done for Sections 9, 10, and 16 at the TTI test facility. These normalized profiles are shown in Figure 9. Sections 9 and 10 are quite uniform, with less than 5 percent variation along the longitudinal axis. On the other hand, Section 16 exhibits a high degree of variation in the longitudinal direction, with more than a 60 percent variation in the 6-m-long section.

FWD measurements were also performed on Sections 9, 10, and 16 at the locations noted in Figure 9. These test locations were selected before the RDD profiles were determined. The FWD results from Sections 9 and 10 should properly characterize the whole section as shown by the continuous profiles. However, the average stiffness of Section 16 would be grossly overestimated by using only the FWD results at the location tested, because that location is not representative of the entire section. This result demonstrates the powerful tool that RDD testing represents in determining bounds in pavement characterization and the limitations of using discrete tests. Comparisons of RDD and FWD results are presented in a later section.

Comparison Between Flexibility Profiles of Different Pavement Sections

RDD profiling was performed at two different dynamic force levels on eight different pavement sections. Testing was nominally performed at peak-to-peak force levels of 33.5 and 67 kN (7,500 and 15,000 lb). However, in practice higher and lower force levels were generated at some pavements because of the lack of experience with the equipment. To compare the flexibilities of the pavements at one force level, interpolation was used to determine a flexibility representative of a dynamic force level of 67 kN (15,000 lb). These results, along with a graphical representation of the pavement layers, are shown in Figure 10. These results are very consistent, with thicker and stiffer pavement materials yielding lower flexibilities

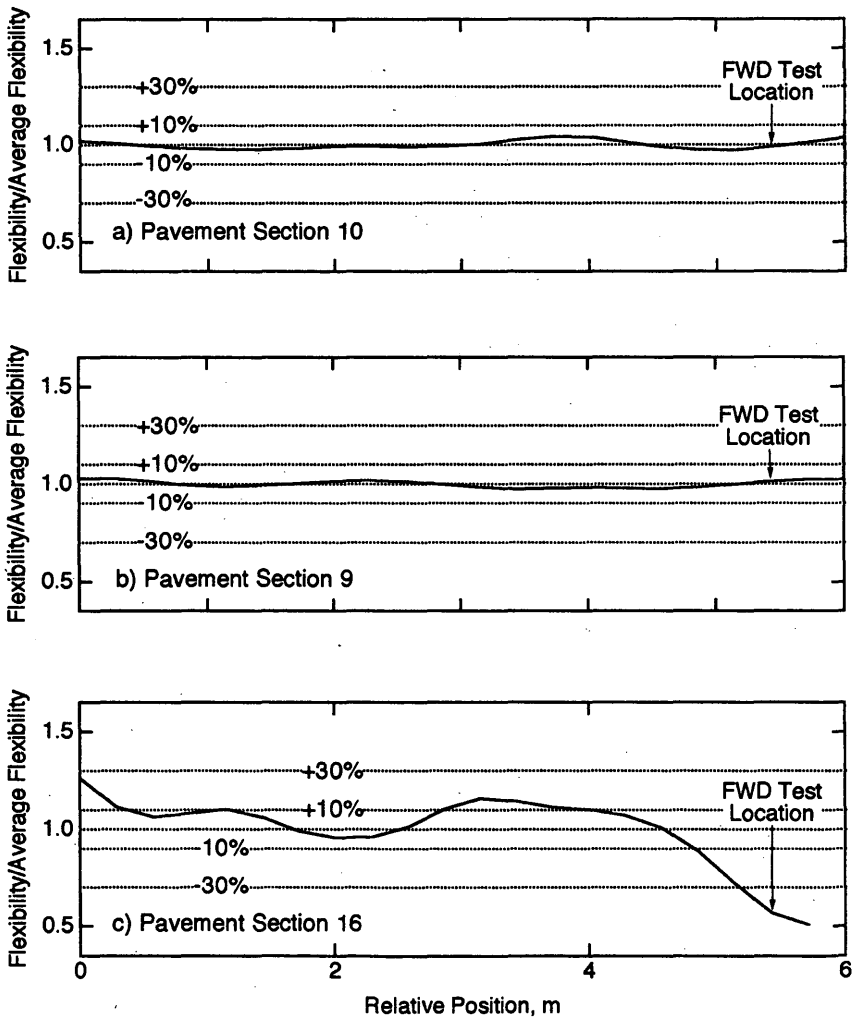

FIGURE 9 Continuous profiles of normalized flexibility for three flexible pavement sections at TTI test facility measured with high dynamic force level with RDD operating at 22 Hz.

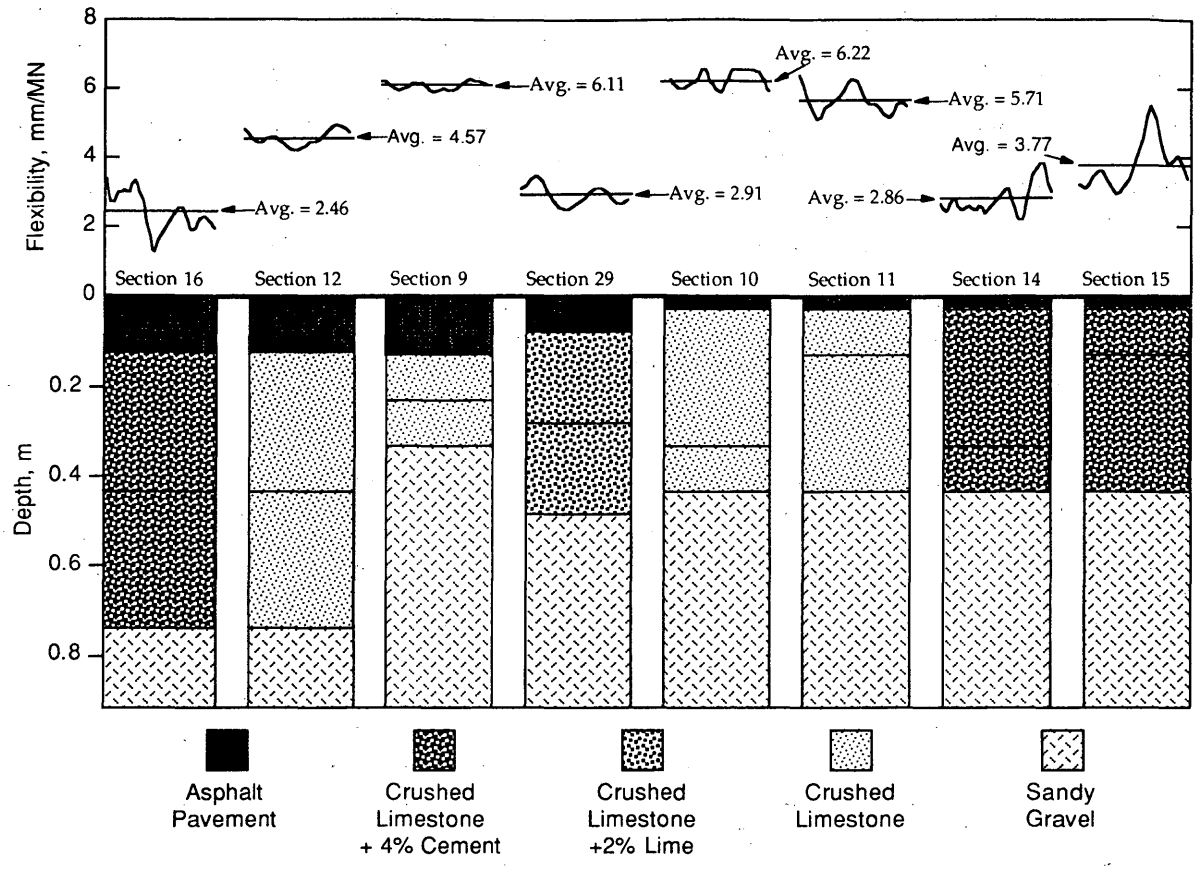

FIGURE 10 Flexibility and pavement profiles of eight flexible pavement sections at TTI test facility determined with RDD operating at 22 Hz and 67 kN (15,000 lb).

and with the flexibilities of similarly constructed sections being similar. Plotting at the horizontal scale shown accentuates the longitudinal variations in these sections.

Effect of Dynamic Force Level

Another benefit of the RDD is that testing can be performed with heavy loads. Profiles of dynamic force level and flexibility are shown in Figure 11 for three pavement sections at TTI. Tests were performed at two different dynamic force levels at each pavement section, with the upper level being near or above nominal allowable loads. These profiles show some nonlinear effect, with higher force levels yielding higher flexibilities. This effect is especially pronounced in Section 9. However, the high force level at this section was inadvertently applied at a much higher dynamic force level than was applied at the other sections. This level probably caused the excessive nonlinearity. The results demonstrate the capability of investigating nonlinear pavement response with the RDD.

Comparison Between RDD and FWD Results

FWD tests were performed at three load levels at several of the TTI test sections within 1 hr of RDD testing. The distance from the center of the receiver wheel to the center of the loading wheels is nearly 0.6 m (2 ft) in the RDD. Therefore, comparisons were made between deflections measured with the RDD and deflections measured with the FWD at Measurement Station 3 at a distance of 0.6 m (2 ft) from the center of the loaded area. Comparisons of FWD and RDD flexibilities for a range of dynamic loads are shown in Figure 12. In addition to the RDD tests discussed previously, stationary tests using broadband excitation with very low loads [about 1.3 kN (300 lb) of dynamic force] were also performed. These results are plotted along with the RDD results in Figure 12. The flexibility measured with the FWD is consistently lower than the flexibility measured with the RDD operating at 22 Hz. However, both tests show the same basic nonlinearity with dynamic load level. A few RDD tests were performed at an operating frequency of 40 Hz. These results are also plotted in Figure 12. A substantial difference between the results of the 22- and 40-Hz tests was found, indicating a significant effect of frequency on the measurements. The FWD applies a broadband, transient loading function, with the frequency content depending on the mass being dropped and the properties of the pavement. With the RDD a single monochromatic frequency is being applied. In view of the effect of frequency observed in 22- and 40-Hz tests, it should not be expected that the RDD and FWD would give the same results.

Further work needs to be done to understand the relationship between the results of FWD and those of RDD. The frequency content of the FWD must be characterized for the pavement being tested, and the effects of steady-state RDD loading on the pavement response must be determined. However, the consistency between FWD and RDD results in this preliminary study suggests that this research is very promising.

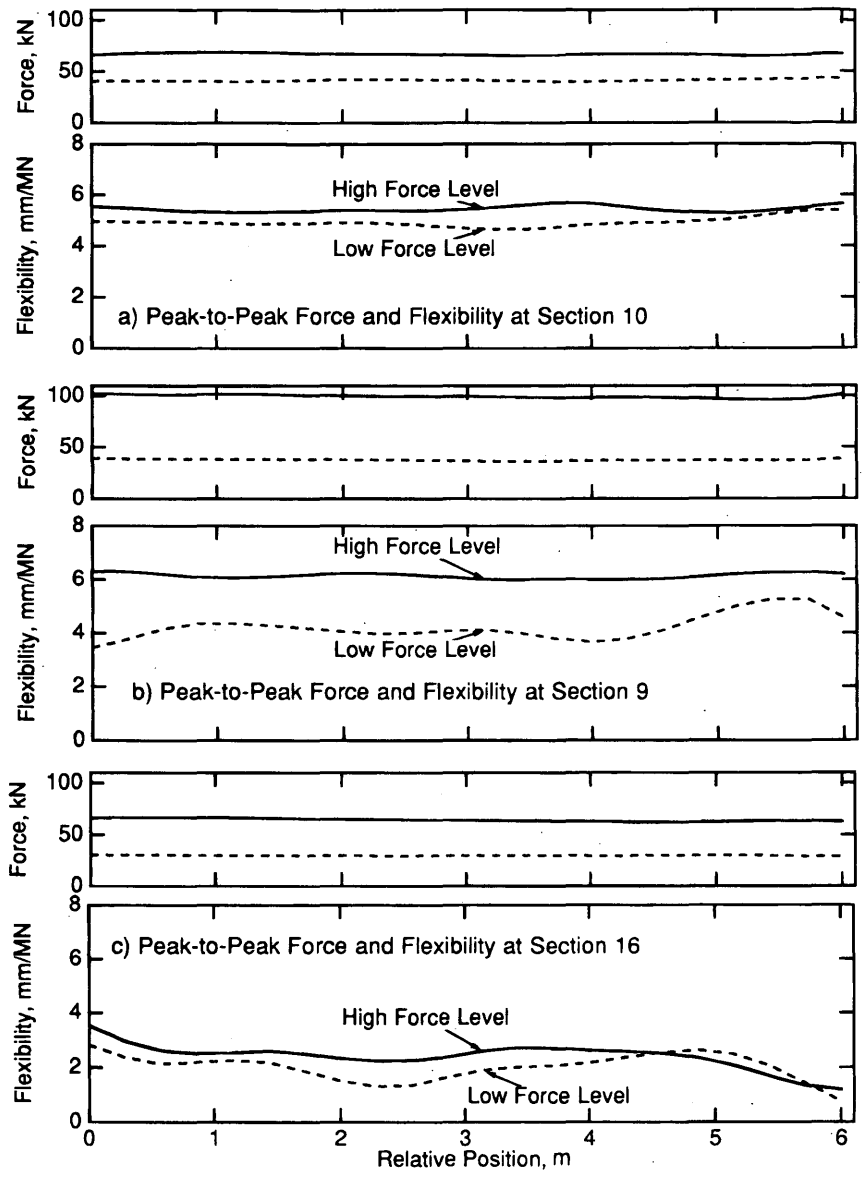

FIGURE 11 Continuous profiles of force level and flexibility for three flexible pavement sections at TTI test facility measured at two dynamic force levels with RDD operating at 22 Hz.

SUMMARY

An RDD has been developed. With the RDD continuous profiles of pavement flexibility or stiffness can be measured under heavy loads. The RDD uses a servohydraulic vibrator to apply static hold-down and vertical dynamic forces to two sets of dual loading wheels. A total force (static plus dynamic) of 147 kN (33,000 lb) can be applied to the pavement surface while the RDD is moving at velocities of 3 to 6 km/hr (2 to 4 mph). Dynamic deflections of the surface are continuously recorded with an accelerometer located on a set of receiver wheels positioned midway between the loading wheels.

The loading and monitoring systems of the RDD have been calibrated, and initial testing has been performed at the TTI pavement test facility. Eight flexible pavement sections covering a range of flexibilities have been successfully tested. Loading frequencies of 22 and 40 Hz have been used with a wide range in dynamic loads. With the RDD measurements were made of longitudinal variability within each section, differences in flexibility between sections, and nonlinearities in flexibility at several sections. Finally, a comparison of the measurements obtained by the RDD and FWD show that the flexibilities measured by both methods are consistent and closely related.

ACKNOWLEDGMENTS

The authors thank TTI at Texas A&M University for the use of their testing facility. Their cooperation in allowing collection of data at their facility is greatly appreciated. The authors also thank the Texas Department of Transportation for financial support. Clyde Lee of the University of Texas provided valuable assistance and equipment to

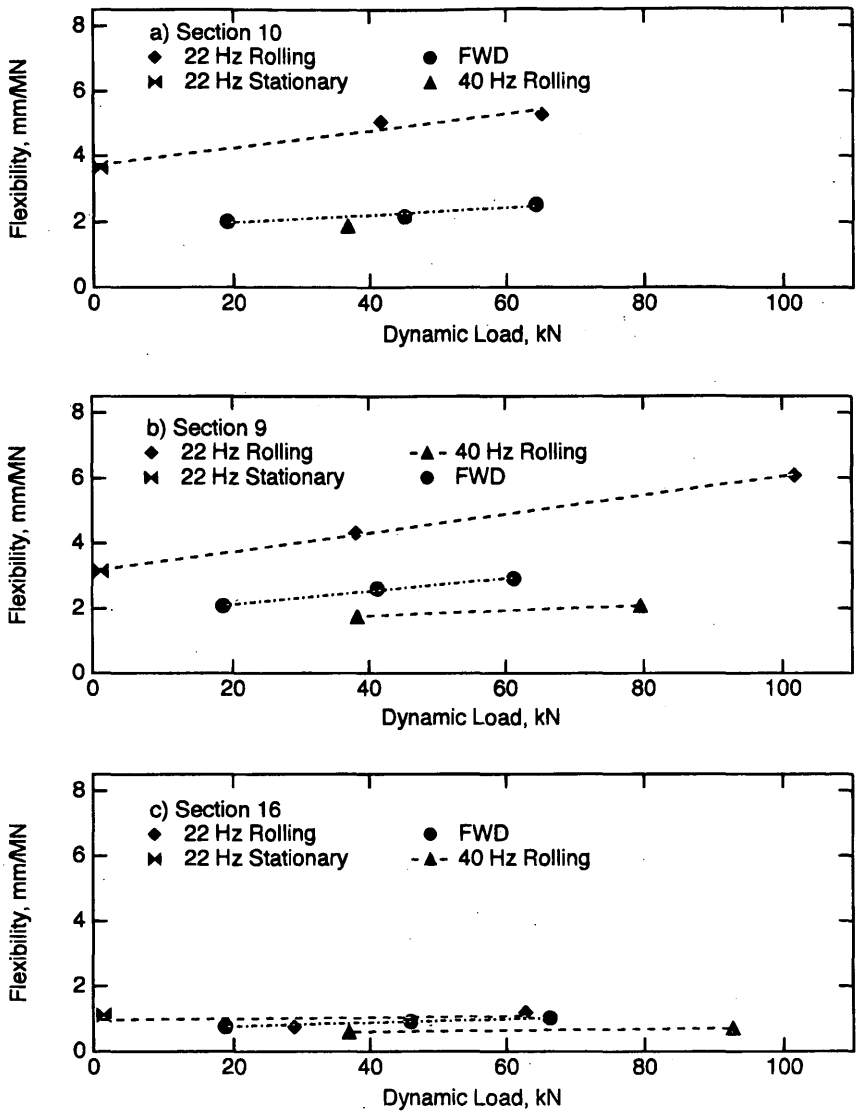

FIGURE 12 Comparison of flexibilities determined at several dynamic force levels using FWD and RDD operating at two different frequencies on three flexible pavement sections at TTI test facility.

calibrate the RDD. The authors thank the U.S. Air Force Office of Scientific Research for support in purchasing the large truck and servohydraulic vibrator. John Bedenbender and Heavy Quip Corp. provided valuable advice on the design of the RDD. The authors appreciate the efforts of those who helped to construct the RDD, James Stewart, Larry Larson, and Bernard Tippie. Homer Ward and Laurence Stienbach of the University of Texas Department of Utilities and Energy Management made construction of the RDD possible on the limited budget by providing the authors with the services of their skilled employees. Their assistance is sincerely appreciated.

REFERENCES

1. Scrivner, F. H., G. Swift, and W. M. Moore. A New Research Tool for Measuring Pavement Deflection. *Highway Research Record 129*, HRB, National Research Council, Washington, D.C., 1966, pp. 1–11.
2. Bohn, A., P. Ullidtz, R. Stubstad, and A. Sorensen. Danish Experiments with the French Falling Weight Deflectometer. *Proc., University of Michigan Third International Conference on Structural Design of Asphalt Pavements*, Vol. 1, Sept. 1972, pp. 1119–1128.
3. Tholen, O., J. Sharma, and R. L. Terrel. Comparison of the Falling Weight Deflectometer with Other Deflection Testing Devices. In *Transportation Research Record 1007*, TRB, National Research Council, Washington, D.C., 1984, pp. 12–20.
4. Nazarian, S., and K. H. Stokoe II. Use of Surface Waves in Pavement Evaluation. In *Transportation Research Record 1070*, TRB, National Research Council, Washington, D.C. 1986, pp. 132–144.
5. Nazarian, S., K. H. Stokoe II, R. C. Briggs, and R. B. Rogers. Determination of Pavement Layer Thicknesses by SASW Method. In *Transportation Research Record 1196*, TRB, National Research Council, Washington, D.C., 1989, pp. 133–150.
6. Lee, C. E., B. Izadmehr, and R. B. Machemehl. *Demonstration of Weigh-in-Motion Systems for Data Collection and Enforcement*. Center for Transportation Report 557-1F, Study IAC (84-85)-1024. The University of Texas at Austin, Dec. 1985.
7. Scrivner, F., and C. H. Michalak. *Linear Elastic Layered Theory as a Model of Displacements Measured Within and Beneath Flexible Pavement Structures Loaded by the Dynaflect*. Research Report 123–25. Texas Transportation Institute, Texas A&M University, College Station, 1974.

Publication of this paper sponsored by Committee on Strength and Deformation Characteristics of Pavement Sections.

Temperature Correction of Deflections and Backcalculated Asphalt Concrete Moduli

Y. RICHARD KIM, BRADLEY O. HIBBS, AND YUNG-CHIEN LEE

A temperature correction procedure for deflections and backcalculated asphalt concrete (AC) moduli for flexible pavements in North Carolina is presented. The data used in developing this procedure were collected from four pavements in the Piedmont area of North Carolina with various types of layer materials and thicknesses. Four trips, one in each season, were made to each of these pavements so that deflections in the maximum range of temperatures could be obtained without significant structural deterioration of the pavements. During each trip deflection testing was conducted on an hourly basis for 1 full day per test section. Pavement surface and depth temperatures were measured at the time of deflection testing with a falling weight deflectometer. The measured deflection and temperature values were used to validate the temperature correction procedure presented in the 1993 *AASHTO Guide for Design of Pavement Structures*. It was found that the AASHTO procedure produced significant errors in the corrected deflections. The main reasons for these errors were that the AASHTO mean temperature cannot account for the difference in temperature-depth gradients during heating versus cooling cycles and that the AASHTO temperature correction factors overcorrect the deflections at higher temperatures. A new temperature correction procedure for deflections and backcalculated moduli was developed on the basis of the fact that the middepth temperature of the AC layer is an effective AC layer temperature. The accuracy of this procedure was validated with deflection and surface temperature data collected from four other pavement sections in North Carolina.

The overlay design analysis in the 1993 *AASHTO Guide for Design of Pavement Structures* (*1*) introduces nondestructive dynamic deflection testing as a means of evaluating the in situ structural capacity of existing pavements. Two general approaches to carrying out this evaluation are the pavement layer moduli prediction technique and the direct structural capacity prediction technique. The first approach backcalculates the in situ moduli of all the layers by using the deflection basin measured from falling weight deflectometer (FWD) testing. The second technique determines the overall structural capacity of the pavement from the subgrade modulus and the peak deflection at the center of the loading plate of the FWD.

In either of the approaches deflection measurements or backcalculated layer properties must be corrected to a particular type of loading system and a standard set of environmental conditions for use in the overlay design analysis. Loading system-related factors are the type of nondestructive testing device, the frequency of loading, and the load level. The most important environmental factor affecting the surface deflections of flexible pavements is the temperature of the asphaltic layers.

The 1993 AASHTO guide (*1*) presents a temperature correction procedure for FWD deflections and backcalculated asphalt concrete (AC) moduli (Figure 1). A set of curves, originally developed by Southgate and Deen (*2*) and modified empirically by using AASHO Road Test data, was recommended in the AASHTO guide to correct the measured deflection at a test temperature to a deflection value at a standard temperature of 21°C (70°F). This procedure determines the effective temperature of the AC layer by calculating the mean value of temperatures from the near surface, the midlayer, and the bottom of the AC layer. These temperatures are predicted from the sum of the measured pavement surface temperatures and the average air temperature for the previous 5 days by using the relationships presented in Figure 1. It has been reported by many practitioners that the AASHTO procedure is inaccurate, especially at temperatures over 38°C (100°F) (*3*).

Johnson and Baus (*3*) recently developed an alternative technique based on the AC temperature-stiffness relationships developed by Ullidtz (*4*) and the elasticity relations used in Appendix PP of the AASHTO guide (*1*) to calculate the composite modulus of multilayered pavements. Although the proposed method by Johnson and Baus (*3*) was reported to provide more consistent results than the AASHTO procedure, the development of a more accurate method

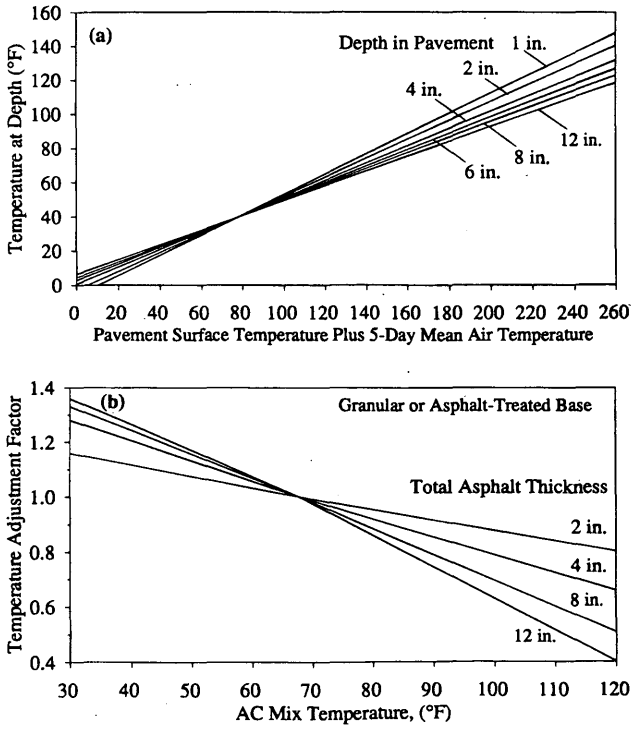

FIGURE 1 AASHTO temperature correction procedure (*1*): (*a*) prediction of pavement depth temperatures; (*b*) temperature adjustment factors for pavements with granular or asphalt-treated base [1 in. = 25.4 mm; °C = (°F − 32)/1.8].

Y. R. Kim and Y.-C. Lee, Box 7908, Department of Civil Engineering, North Carolina State University, Raleigh, N. C. 27695-7908. B. O. Hibbs, FHWA, Washington, D.C. 20590.

of estimating pavement temperatures was recommended as the most important future research topic.

Based on the urgent need to develop a more realistic temperature correction procedure for the overlay designs in North Carolina, research was conducted at North Carolina State University in which a new temperature correction procedure for FWD deflections and backcalculated AC moduli was developed by means of periodic FWD testing and temperature measurements from pavement sections in service. This procedure is based on the middepth temperature of asphaltic layers as an effective temperature and has two parts: (a) prediction of the AC middepth temperature and (b) adjustment of the measured deflections or backcalculated AC moduli to a reference temperature. In this paper field data collected from the test sections are first used to check the accuracy of the AASHTO procedure, and the newly developed temperature correction factors are presented along with a summarized description on the entire temperature correction procedure. Then this procedure is validated with the deflection and surface temperature data collected from four pavement sections in North Carolina. A prediction method for the AC middepth temperature cannot be included here because of space limitations; a description of the method can be found elsewhere (*5*).

TEST SITE SELECTION

Four test sites with pavement characteristics and at geographic locations that would highlight the factors under investigation were chosen in the Piedmont area of North Carolina: three on US-421 north of Siler City and one on US-70 east of Clayton. The major selection criteria were the thicknesses of the AC layers, the types of base course materials, and the structural conditions of these pavements. The compositions of the four sections are summarized in Table 1.

TEMPERATURE GAUGE INSTALLATION

To determine the change in temperatures within the AC layer during the testing period a method had to be devised to repeatedly measure temperatures from various depths of the AC layer without direct influence from ambient air conditions. This was achieved by first coring a 75-mm (6-in.)-diameter hole through the entire depth of the AC layer. After the core was removed a drill with a pivoting nose was placed in the 75-mm core hole to horizontally drill holes for the thermocouples. The thermocouple holes were placed in the AC layer from top to bottom at intervals of 25 to 50 mm (1 to 2 in.), depending on the depth of the section.

Epoxy was injected into each horizontal hole, and then the thermocouple attached to strands of insulated wire was injected. These thermocouples were checked in the laboratory by comparing the readings from the individual thermocouples at 25°C (77°F). The wires were taken across the pavement through a trench slit cut transversely from the core hole to the pavement edge. The wires were carried to the shoulder until it reached a junction box where the wire end connections were stored. The core hole was backfilled with hot mix, and the trench in the pavement was filled with epoxy. The wire end connections were plugged into a switch box and a digital meter that displays the temperatures given by each thermocouple. Air and pavement surface temperatures were determined with an infrared thermometer.

FIELD TESTING AND DATA COLLECTION

In each test section two areas with minimum damage were selected to avoid any errors due to location-specific variations in the strengths or stiffnesses of the pavements. In each area one temperature hole was installed and two locations were marked for FWD testing, one in the outer wheelpath and the other in the center of the outer lane. The test sections were an average of 24 m (80 ft) in length.

Testing was conducted during each season of the year (early September, October, early February, and late May). FWD deflections, temperatures (air, pavement surface, and depth), and climatic data were collected on an hourly basis over an entire day for each section. The underlying assumption was that this testing plan would allow evaluation of the effects of temperature change on deflection measurements by keeping other variables (such as the moisture contents of subsurface layers, damage state of the AC layers, and aging) relatively constant. In addition to the field temperature data, the highest and lowest air temperatures for the previous 5 days before each FWD test were acquired from the National Climatic Data Center.

FWD testing was conducted at four points in each test section, two under the wheelpath and two at the lane center, to evaluate the effect of damage in the AC layer on the temperature correction of deflections. Four different load levels, 2722, 4082, 4990, and 7711 kg (6,000, 9,000, 11,000, and 17,000 lb), were used to study the effects of load level on backcalculated moduli of different types of layer materials.

TABLE 1 Compositions of Pavement Test Sections

	Thickness, mm (in.)			
	Section 17	US 70	Section 13	Section 20
Surface Course	51 (2.0)	51 (2.0)	51 (2.0)	51 (2.0)
Binder Course	38 (1.5)	89 (3.5)	38 (1.5)	38 (1.5)
Asphalt Base	-[a]	-	102 (4.0)	140 (5.5)
Aggregate Base	203 (8.0)	279 (11.0)	-	-
Lime-Stabilized Subgrade	178 (7.0)	-	178 (7.0)	-
Total AC Layer	89 (3.5)	140 (5.5)	191 (7.5)	229 (9.0)
Subgrade Type	A-7	A-3	A-6	A-7

[a]Data not applicable.

DISCUSSION OF RESULTS

Temperature Measurements

Figure 2 presents the change in temperature gradients recorded in May from a 140-mm (5.5-in.)-thick AC layer (US-70 section). Surface temperatures moved considerably, whereas temperatures at lower depths maintained greater consistency, resulting in cone shapes on the pavement depth-versus-temperature graph. It must be noted here that the slope of the temperature gradients changes as the time of day moves from the heating cycle (before 2 p.m.) to the cooling cycle (after 2 p.m.). The significance of this observation is that one may get vastly different middepth temperatures if the change in the slope of the temperature-pavement depth curves is not taken into consideration. For example, although the surface temperatures measured at noon and at 4:02 p.m. in Figure 2 are essentially the same, the middepth temperatures differ by 7°C (13°F). Therefore, a meaningful pavement temperature prediction method requires the time of FWD testing as an input variable and a means of accounting for the temperature gradient along pavement depths.

When determining the effective temperatures of the AC layer at different times of the same day, the AASHTO mean temperature becomes a function of pavement surface temperature only, because the average air temperature for the previous 5 days remains constant for FWD testing within the same day. The problem of using the AASHTO mean temperature in correcting deflections will be presented later by analyzing deflection-temperature data obtained from the same day. In the present study the temperature at the middepth of the AC layer was selected as the effective temperature.

Validation of AASHTO Temperature Correction Procedure

One of the major strengths of the present study is the availability of deflection and temperature data at various depths measured at different times of the same day. The data from US-70 and Section 20 were used to check the accuracy of the AASHTO temperature-deflection correction procedure. Figure 3(*a*) presents the results from the AASHTO procedure. The first point to be made from Figure 3(*a*) is the increasing trend of the corrected deflections as the mean temperature increases. This trend is more significant in Section 20, which has a thicker AC layer [229 mm (9 in.) compared with 140 mm (5.5 in.) in US-70]. Since it was assumed that other variables affecting the deflection measurements except the temperature remained almost constant during a day, the corrected deflections should theoretically be the same for different times (and therefore different mean temperatures) of the same day if the correction procedure is accurate. The significantly different corrected deflections shown in Figure 3(*a*) indicate the problems with the AASHTO temperature-deflection correction procedure.

Another important observation can be made by comparing points A and B in Figure 3(*a*). Points A and B represent the data collected from the US-70 section in May 1993 at noon and 4:02 p.m. of the same day, respectively. The measured temperatures of this trip were presented earlier (Figure 2). Since the surface temperatures at these times were about the same and the average air temperature for the previous 5 days remains constant during the same day, the AASHTO mean temperatures for Points A and B are essentially the same. However, the corrected deflections are significantly different because the AASHTO mean temperature cannot account for the difference in temperature gradients in the heating versus cooling cycle of a day, which was demonstrated earlier (Figure 2). This difference in temperature gradients results in different effective temperatures of the AC layer and therefore different deflection values.

The same corrected deflection data in Figure 3(*a*) were plotted against the measured middepth temperatures in Figure 3(*b*). Although the variation in corrected deflections was reduced by using the middepth temperature, a strong temperature dependency of the corrected deflections was still observed. Some improvement in Points A and B was made in Figure 3(*b*). In general, the use of the middepth temperature improved the AASHTO-corrected deflection-versus-pavement temperature relationship, but not to a satisfactory level. The discrepancies shown in Figure 3(*b*) may be because the AASHTO mean temperature, which is heavily dependent on the surface temperature, was used to calculate the temperature

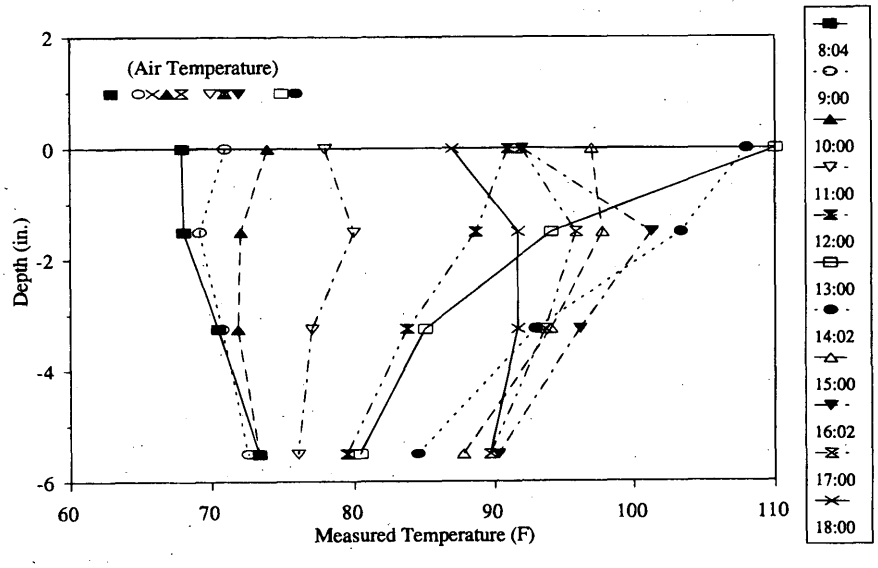

FIGURE 2 Temperature change monitored on US-70 section in May 1993.

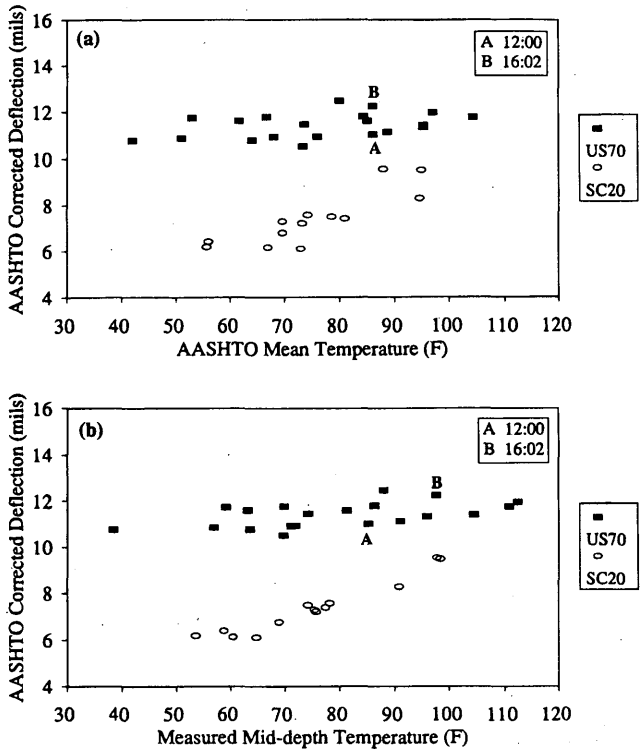

FIGURE 3 *(a)* **AASHTO-corrected deflection versus AASHTO mean temperature;** *(b)* **AASHTO-corrected deflection versus measured middepth temperature (1 mil = 25.4 μm).**

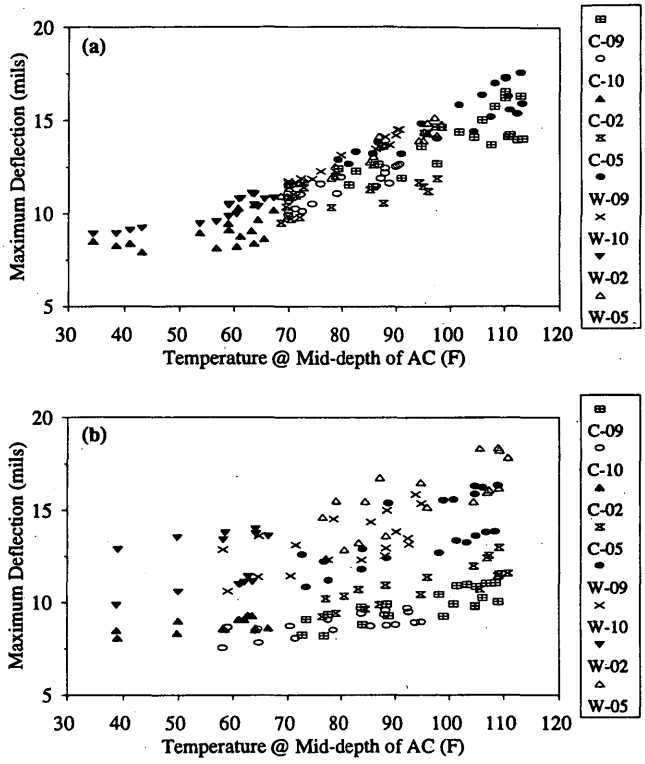

FIGURE 4 Maximum deflection versus middepth temperature: for *(a)* **US-70;** *(b)* **Section 17 (C, W, and numbers represent lane center, wheelpath, and months, respectively).**

adjustment factors and because the relationships used to determine temperature adjustment factors are inaccurate.

Temperature Correction of FWD Deflections

Maximum deflection values under 4082-kg (9,000-lb) load drops are plotted in Figure 4(*a*) against the middepth temperatures of the AC layer for the US-70 section. Two variables contributed to the variation of the maximum deflections in Figure 4(*a*). One was different damage levels between the lane center and the wheelpath, and the other was random variations in pavement stiffnesses and strengths between the two FWD testing areas within the same section. This location-specific structural difference may be due to variations in layer thicknesses, compaction, material properties, moisture conditions of sublayers, and so forth. Nevertheless, it was found that the increasing trends of the maximum deflection versus the middepth temperature from each trip were superposed quite nicely, as long as the superposition was performed on the deflection data from the same FWD testing location.

The largest deflection variation was observed from Section 17 with an 89-mm (3.5-in.)-thick asphaltic layer [Figure 4(b)]. The primary reason for this variation is due to the differences in structural conditions between the two FWD testing areas and between the lane center and the wheelpath, the effect of which is probably amplified in sections with thin AC layers.

Temperature correction factors for FWD deflections can be developed by calculating the deflection ratios by dividing the measured deflection value at a specific temperature by the deflection at 20°C (68°F). Since there existed some variation in the measured deflections at a constant temperature, as shown in Figure 4, a regression curve had to be developed to pick up the representative deflection for a specific temperature. The AASHTO correction curves express the relationship between temperature correction factor and temperature as a linear function. A more detailed study of the measured deflections as a function of the middepth temperature, however, suggested that the relationship is better expressed as a nonlinear function. Knowing that the temperature correction factor must be equal to 1 at the reference temperature of 20°C (68°F), it was found that the following equation represents the relationship fairly well:

$$D_{68} = 10^{\alpha(68 - T)} \times D_T \quad (1)$$

where

D_{68} = adjusted deflection to the reference temperature of 20°C (68°F),
D_T = deflection measured at temperature T (°F),
$\alpha = 3.67 \times 10^{-4} \times t^{1.4635}$ for wheelpath and
$= 3.65 \times 10^{-4} \times t^{1.4241}$ for lane center,
t = thickness of AC layer (in.), and
T = the AC layer middepth temperature (°F) at the time of FWD testing.

By using this relationship the temperature correction factors for deflections under the 4082-kg (9,000-lb) FWD load were calculated and are plotted in Figure 5(*a*) for different locations (wheelpath versus lane center) and for various AC layer thicknesses. Figure 5(*a*) indicates that the difference in deflections between the lane center and the wheelpath observed from Figure 4 has been significantly reduced by using the deflection ratio. Also, the pavements with thicker AC layers demonstrated a greater temperature dependency of the deflection ratio.

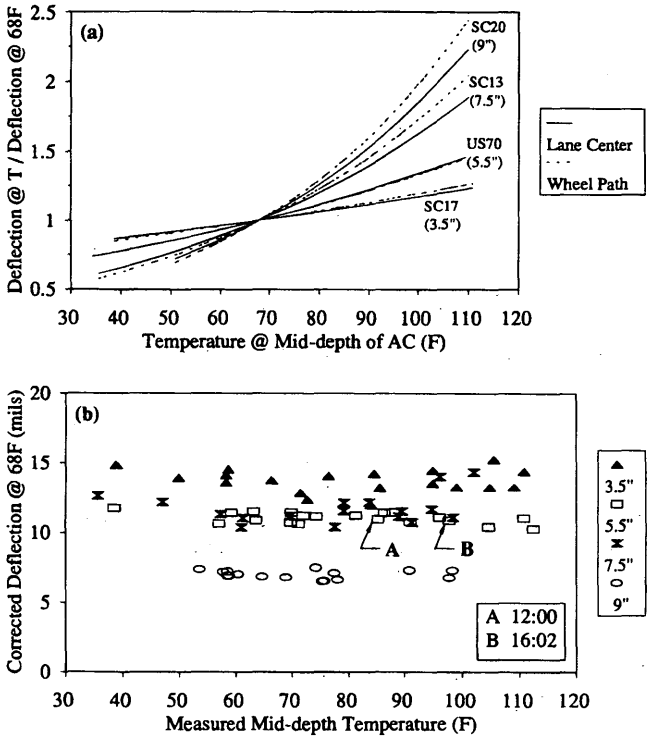

FIGURE 5 (*a*) Temperature correction factors for deflections; (*b*) corrected deflection versus middepth temperature using the deflection correction factors.

The temperature correction curves generated by Equation 1 were used to recalculate the corrected deflections presented in Figure 3. The corrected deflections were then plotted against the middepth temperatures in Figure 5(*b*) for all four seasons. Overall, the corrected deflections for the individual section were relatively constant, regardless of the middepth temperature. Points A and B displayed almost the same corrected deflections, demonstrating the accuracy of the new temperature correction procedure. Compared with Figures 4(*a*) and 4(*b*) resulting from the AASHTO procedure, substantial improvement has been made in Figure 5(*b*).

Effect of Load Level on Backcalculated Moduli

The layer moduli were backcalculated from measured deflection basins by using the MODULUS 4.0 program. Moduli values backcalculated from the 4082-kg (9,000-lb) load drop on the US-70 section are plotted in Figure 6 against the middepth temperature as an example showing typical variation in backcalculated AC moduli.

The backcalculated AC moduli were relatively the same, regardless of the FWD load levels. However, the moduli of the aggregate base course increased as the FWD load increased [Figure 7(*a*)]. This trend can be explained by the well-known effect of confining pressure or bulk stress on the modulus of granular materials. The moduli of lime-stabilized subgrade tended to decrease as the load increased [Figure 7(*a*)]. It was found that the effect of the FWD load level on the subgrade modulus was different, depending on the location of the test sections [Figure 7(*b*)]. Subgrade moduli from all of the Siler City sections (Sections 13, 17, and 20) decreased as FWD load increased, whereas the reverse trend was observed from the Clayton section (US-70). Further investigation on subgrade type provided the reason for these trends. As shown in Table 1, subgrades in the Siler City sections are classified as A-6 or A-7, indicating highly plastic clayey materials, whereas the subgrade in the Clayton section is A-3 soil, which is a granular sandy material. Therefore, the same effect of stress state as described earlier for the granular base course can be expected for the granular subgrade of the Clayton section. However, unlike the effect for granular materials, the modulus for fine-grained soils rapidly decreases as the deviator stress is increased up to a certain value and then increases very slightly with increasing deviator stress. This explains the conflicting trends in Figure 7(*b*).

Temperature Correction of Backcalculated AC Moduli

The relationship between the modulus ratio versus the middepth temperature was found to be similar for all sections (Figure 8), although larger discrepancies were found at lower temperatures. It is noted that the backcalculation for Section 17 required a fixed analysis because of the thin surface layer. This analysis determines the AC

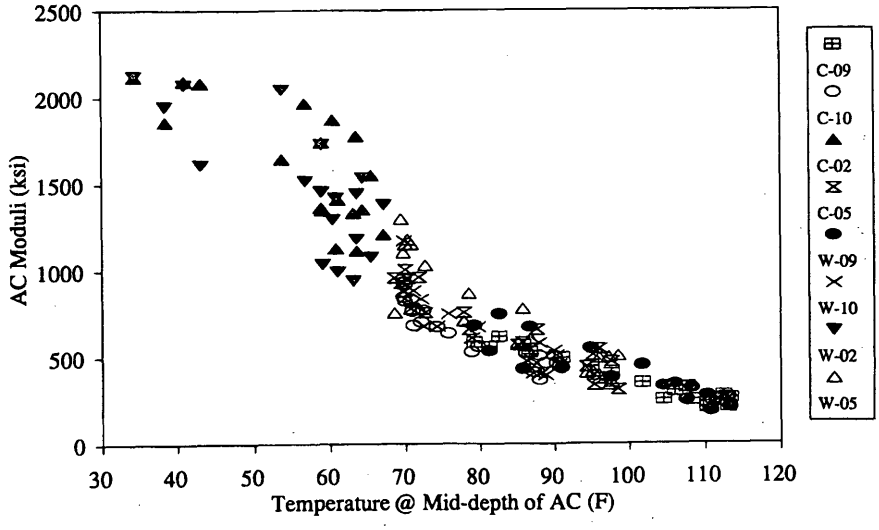

FIGURE 6 Backcalculated AC moduli as a function of middepth temperature from US-70 (1 ksi = 6.89 MPa).

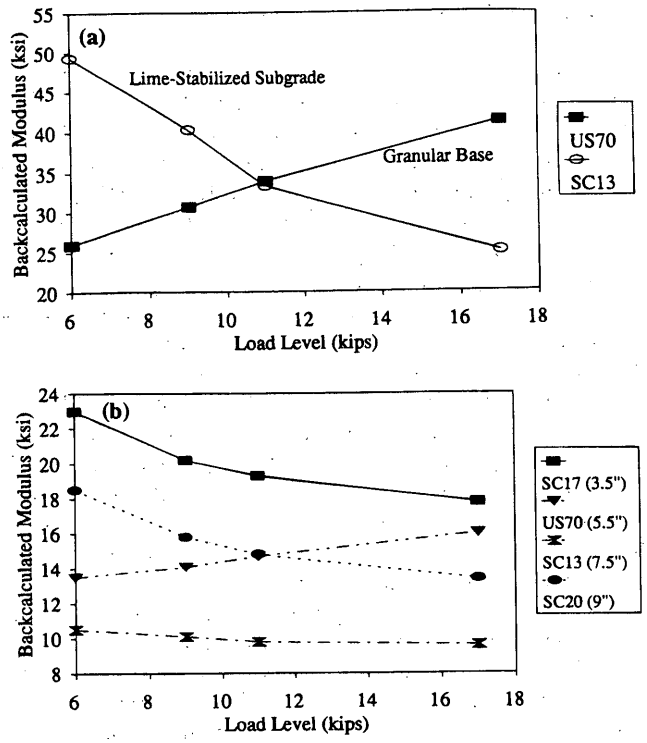

FIGURE 7 Effects of load level on backcalculated moduli: (*a*) granular base and lime-stabilized subgrade; (*b*) unbound subgrade.

modulus on the basis of the aggregate type and temperature by using the modulus-temperature relationship developed from laboratory testing and already resident in the MODULUS program. Therefore, it seemed that the AC modulus-versus-temperature relationship in the MODULUS program represents the temperature dependency of the mixtures investigated in the present study quite well.

Because the stiffness of AC is a strong function of temperature, only by specifying the corresponding temperature will the measured stiffness be meaningful. Therefore, it is important to adjust the measured modulus to a reference temperature. Since the modulus ratio curves in Figure 8 are similar for all seasons of the four test sections, the following relationship can be derived on the basis of regression analysis.

$$E_{68} = 10^{0.0153(T-68)} \times E_T \quad (2)$$

where

E_{68} = corrected AC modulus to the reference temperature of 20°C (68°F),
E_T = backcalculated AC modulus from FWD testing at temperature T (°F), and
T = the middepth temperature (°F) of the AC layer at the time of FWD testing.

A similar equation for temperature correction of AC moduli was recently reported by Baltzer and Jansen (*6*), except their power coefficient is 0.010 in English units. The slight difference between these two coefficients may be due to pavement location-specific factors as well as the type of backcalculation program used in the analysis.

NEW TEMPERATURE CORRECTION PROCEDURE FOR FWD DEFLECTIONS

In this section the temperature correction procedure developed in the present study is summarized. This procedure was developed with the purpose of creating a method that could be implemented in a computer program with easily obtainable input data. Input data for the method consist of

1. Surface temperature measured at the time of FWD testing by an infrared thermometer.
2. Thickness of the AC layer.
3. Time of day. The actual time of day that the individual FWD drop was performed should be recorded and then rounded off to the nearest hour for computer input.
4. Location of FWD test (wheelpath or lane center).
5. Measured FWD deflections and the load level of FWD drop.

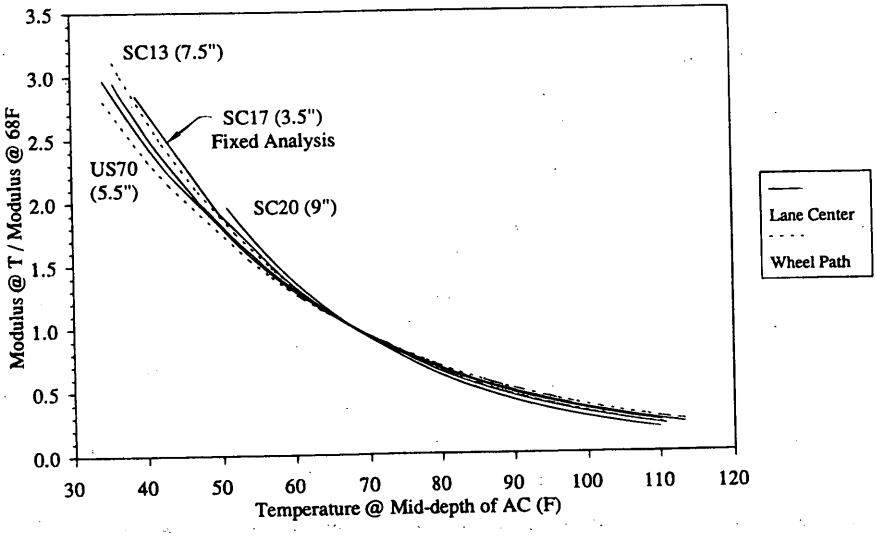

FIGURE 8 Temperature correction factors for backcalculated AC moduli.

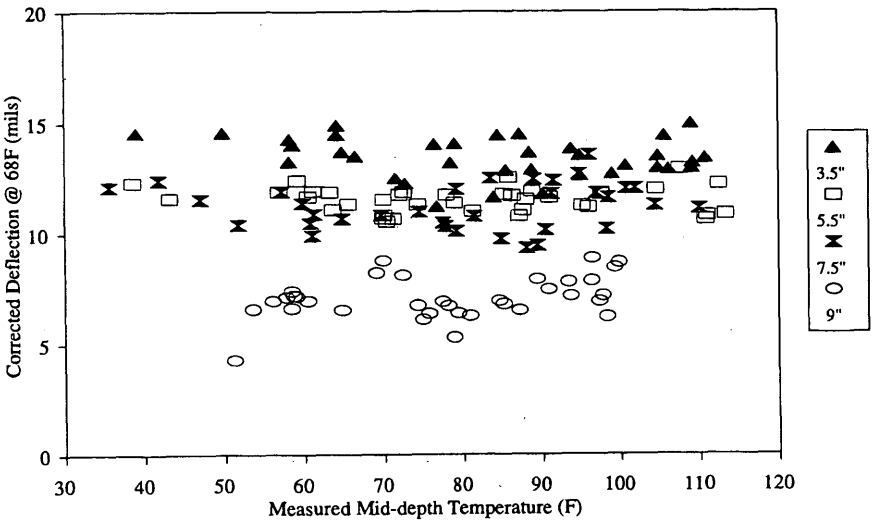

FIGURE 9 Corrected deflections using the predicted middepth temperature versus measured middepth temperature.

The reference temperature and the FWD load level were set to 20°C (68°F) and 4082 kg (9,000 lb), respectively. In the following the temperature correction procedure is described stepwise.

1. Calculate the middepth of the AC layer from the thickness of the AC layer.
2. Predict the AC middepth temperature by using the pavement surface temperature and the time of day. Details on the prediction method for the AC middepth temperature are discussed elsewhere (*5*).
3. Use the predicted middepth temperature to calculate the adjusted deflection by using Equation 1.

VALIDATION OF NCDOT PROCEDURE

To test the accuracy of the entire procedure the deflection and surface temperature data measured in the project were first used. The stepwise procedure described earlier was applied to the measured surface temperature for the known time of day to predict the middepth temperature. The predicted middepth temperature was input to the temperature correction charts to determine the corrected deflection for 20°C (68°F). The results were plotted against the measured middepth temperature (Figure 9). Compared with Figure 5(*b*), which displays the same data except that the deflections were corrected by using the measured middepth temperatures, a larger variation is observed in Figure 9. This is due to errors involved in predicting the middepth temperature from the surface temperature. In general the results show relatively constant corrected defection values at changing middepth temperatures.

The validation results in Figure 9 are somewhat expected because the same data have been used both in developing the temperature correction factors and in the validation study. Therefore, the North Carolina Department of Transportation (NCDOT) procedure must be validated with data that were not included in the development of the correction factors. Additional data were obtained from Sections 1, 2, and 3 of the Siler City test road, the AC layer thicknesses of which were 89, 51, and 140 mm (3.5, 2.0, and 5.5 in.), respectively. The data included a yearly range of FWD deflections for each section and corresponding surface temperatures. The NCDOT correction procedure was applied to the data, and the results were plotted in Figure 10. Again, the procedure provided a constant value of corrected deflections except the four points in Section 3 at the high temperature range in Figure 10(*c*). These FWD drops were performed on the same day in May 1991, which was the first set of data available for this section. Some errors may have been caused by using an inconsistent method of surface temperature collection on this day

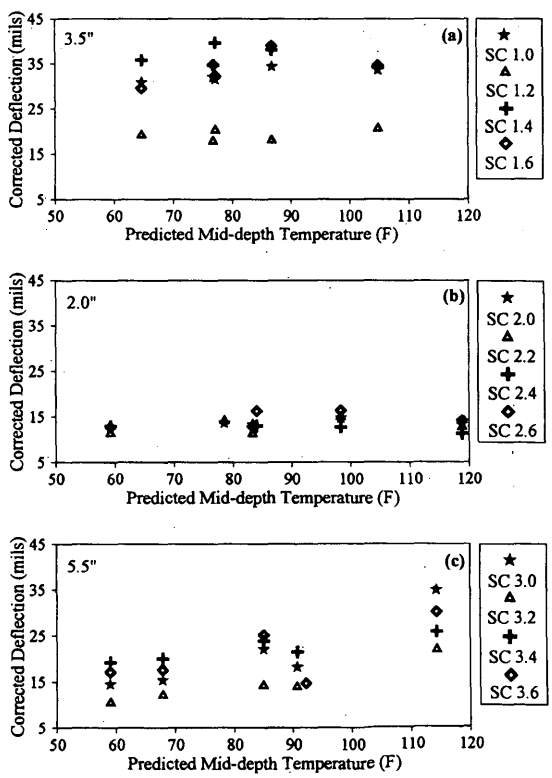

FIGURE 10 Validation of NCDOT procedure with data from Siler City: (*a*) Section 1; (*b*) Section 2; (*c*) Section 3.

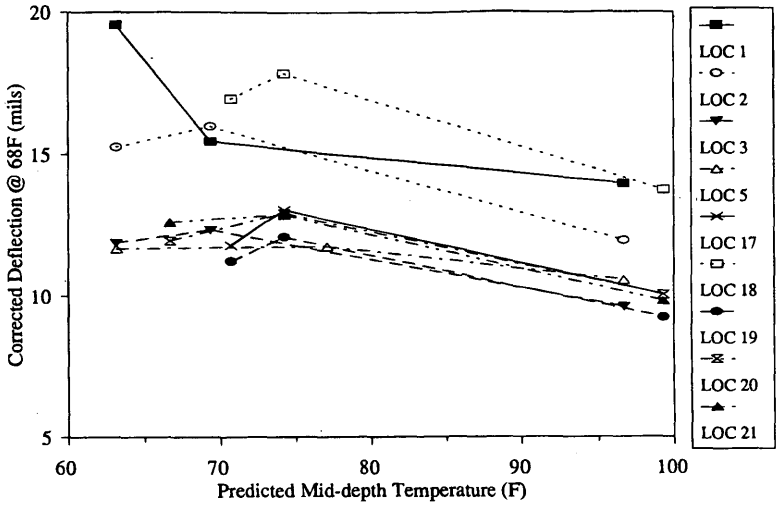

FIGURE 11 Validation of NCDOT procedure with data from Black Mountain.

compared with the methods used on the following trips, such as holding the thermocouple onto the pavement versus using an infrared thermometer. In developing the NCDOT procedure an infrared thermometer was used to measure the surface temperature throughout the entire study. It was found during the study that the measurements made with the thermocouple were different from the ones made with an infrared thermometer and that the thermocouple results would be more inconsistent because they were dependent on how the thermocouples were attached or held to the pavement.

To further add credibility to the NCDOT procedure, this method was applied to FWD data from Black Mountain, North Carolina. The results are displayed in Figure 11. The results again demonstrate the horizontal relationship between the corrected deflections and the middepth temperatures that the correct procedure should provide. Results for certain locations or sections were better than those for other locations; however, this was found to be a result of the fact that some sections were highly distressed and the meaningful temperature correction of deflections is not achievable. Overall, the results were positive, but the small variations could have resulted from climatic differences between the Black Mountain area (western area) and the Piedmont area, the pavements of which were used to develop the NCDOT procedure. Although the study has significantly improved the accuracy and reliability of the deflection-temperature correction procedure, some weaknesses remain mainly because the data were obtained from a limited number of pavements in fairly good condition and in the central area of North Carolina. The coefficients and basic relationships used in the recommended procedure could be sensitive to local climatic conditions and states of pavement damage. Calibration or generalization of the recommended procedure for different climatic regions in North Carolina and for different states of pavement damage is needed to take full advantage of the results of the study.

CONCLUSIONS

The measured deflection and pavement temperature data collected in the present study demonstrate the problems related to using the AASHTO mean temperature as the effective temperature of the AC layer. These inaccurate results were obtained because the difference in temperature-depth gradients in the heating versus cooling cycles could not be considered. In addition, the temperature adjustment factors from the AASHTO procedure overcorrected the deflections at higher temperatures, resulting in an increase in the corrected deflections as the mean temperature of the pavement increases.

The North Carolina temperature correction procedure based on the temperature at the middepth of the AC layer was found to greatly improve the accuracy of the temperature-deflection correction. The temperature correction procedure for deflections was validated with data collected from four other pavement sections. Future research efforts should be concentrated on accurately predicting the middepth temperature from the air or surface temperature and improving the accuracy of the proposed procedure for pavements in other climatic regions of North Carolina and for pavements with different damage states.

ACKNOWLEDGMENTS

This research was sponsored by NCDOT and FHWA. The authors thank NCDOT engineers in the Pavement Management Unit and Geotechnical Unit for excellent cooperation in installing gauges and FWD testing. Thanks are also due to Earl H. Inge for assistance in the validation analysis of the field data.

REFERENCES

1. *AASHTO Guide for Design of Pavement Structures*. AASHTO, Washington, D.C., 1993.
2. Southgate, H. F., and R. C. Deen. Temperature Distribution within Asphalt Pavements and Its Relationship to Pavement Deflection. In *Highway Research Record 261*, HRB, National Research Council, Washington, D.C., 1969.
3. Johnson, A. M., and R. L. Baus. Alternative Method for Temperature Correction of Backcalculated Equivalent Pavement Moduli. In *Transportation Research Record 1355*, TRB, National Research Council, Washington, D.C., 1992.
4. Ullidtz, P. *Pavement Analysis*. Elsevier, New York, 1987.
5. Kim, Y. R., B. O. Hibbs, Y. C. Lee, and E. H. Inge. *Asphalt Paving Material Properties Affected by Temperature*. Final Report. North Carolina Department of Transportation, April 1995.
6. Baltzer, S., and J. M. Jansen. Temperature Correction of Asphalt-Moduli for FWD-Measurements. *Proc., 4th International Conference on Bearing Capacity of Roads and Airfields*, Vol. 1, Minneapolis, Minn., 1994.

Publication of this paper sponsored by Committee on Strength and Deformation Characteristics of Pavement Sections.

Considerations of Saturated Soil Conditions in Backcalculation of Pavement Layer Moduli

DAVID E. NEWCOMB, DAVID A. VAN DEUSEN, YAN JIANG, AND JOE P. MAHONEY

The need to account for stiff underlying soil and rock layers has long been recognized in pavement layer modulus backcalculation. Recently, it has been suggested by other researchers that there is a need to separately characterize and incorporate materials below the water table when backcalculating moduli. This discussion is continued by presenting means for determining the depth to the water table and how to assign an appropriate modulus to this material. Results compare the depths to the water table determined by a reflection survey with those obtained by using regression equations developed for deflection testing. It was found that in the case of asphalt concrete over granular base materials, both approaches produced depths close to water table depths in open standpipes. However, there was considerable discrepancy between the depths when the testing was performed on a full-depth asphalt pavement. An appropriate modulus for soil beneath the water table could be determined by minimizing the error between measured and theoretical deflections. It was found that over a time period from fall to spring both the depth to the water table and the modulus of this material did not remain constant. As a result it was concluded that there is a need to determine the depth to the water table and the modulus of the material below the water table each time that deflection testing and deflection analysis are performed.

For a number of years pavement researchers have recognized the importance of accounting for a stiff sublayer when backcalculating the elastic moduli of pavement layers (*1–3*). The presence of such a layer has been attributed to shallow rock formations or to stiff soil layers within about 6 m of the pavement surface. The need to account for the stiff material is often recognized only when there is a poor fit between measured deflection basins and theoretically generated deflections in the backcalculation process. Early in the practice of backcalculation the method used to approach this problem was to assign an arbitrarily high modulus value to a layer at some arbitrary depth if the actual depth was not known. Researchers such as Uddin et al. (*2*) and Rohde et al. (*3*) have devised a means for estimating the depth to the stiff layer based on deflection testing.

Although rock layers and layers of hardened soils definitely constitute stiff underlying materials, it has been argued that saturated soils may respond in a similar, but softer, manner under certain conditions (*4,5*). The discussion of the effects of saturated soil on the backcalculation of layer moduli is continued in this paper. Three methods of determining the depth to the groundwater table (GWT) were tried with data from three pavement test sections at the Minnesota Road Research Project (Mn/ROAD). These included a deflection method, a body wave method, and a method that obtained readings from open standpipes in the test sections. A means of determining the appropriate modulus of material below the GWT is presented, and a comparison is made between backcalculation results assuming a semi-infinite subgrade and those for which the saturated soil is considered to be a separate layer.

A moisture content gradient exists in many soil formations, and it increases with depth to the point of saturation at the GWT or perched groundwater table level, as shown in Figure 1. Provided that there is sufficient time to dissipate the pore water pressure, the material beneath the GWT will behave in a compressible manner when it is subjected to loading since the water will flow into nearby unfilled voids. In this case the response of the soil would indicate that it is soft. The time to dissipate the pore water pressure is a function of the sizes of the voids, the sizes of the soil particles, and the time of loading. Under a dynamic impulse load produced by fast-moving traffic or falling weight deflectometer (FWD), the loading time is very short, which in a well-compacted, fine-grained material will not allow for the dissipation of pore water pressure. Since the bulk modulus of water itself is fairly high compared with the stiffness of soils at relatively low confining pressures the saturated soil behaves as a hard material (*6*). The result will be a reflection of the waves generated by the impulse load from the GWT back to the surface, making it appear as if the material below the GWT is stiff because of its incompressibility. In either case (soft or stiff) the response of the material below the water table would be different from that of the soil above it.

BACKGROUND AND MEANS FOR DETERMINING DEPTH TO SATURATED LAYERS

Deflection Measurement Method

Rohde et al. (*3*) proposed a means of estimating the depth to a rigid underlying layer by the use of regression equations applied to FWD measured deflections. The equations are based on solutions of layered elastic theory involving different thicknesses of asphalt surfacing and depths to a rigid layer. The equations relate the inverse of depth to rigid layer to deflection basin parameters such as surface curvature index, base damage index, and base curvature index as well as a parameter that is determined by the point at which the slope of the steepest portion of the deflection basin intersects a surface displacement of zero. The basis for this approach is that if the subgrade is truly a linear elastic semi-infinite medium, the lower portion of the deflection basin would form a straight line instead of curving up when displacement is plotted against the inverse of the distance from the center of the load, as shown in Figure 2.

The method proposed by Rohde and associates (*3*) is incorporated in the latest versions of the MODULUS (*7*) and EVERCALC (*5*) moduli backcalculation procedures. MODULUS has been adopted as the backcalculation technique of choice for the Long-

D. E. Newcomb and D. A. Van Deusen, Department of Civil Engineering, University of Minnesota, Minneapolis, Minn. 55455. Y. Jiang, ERES, Inc., Savoy, Ill. 61874. J. P. Mahoney, Department of Civil Engineering, University of Washington, Seattle, Wash. 98195.

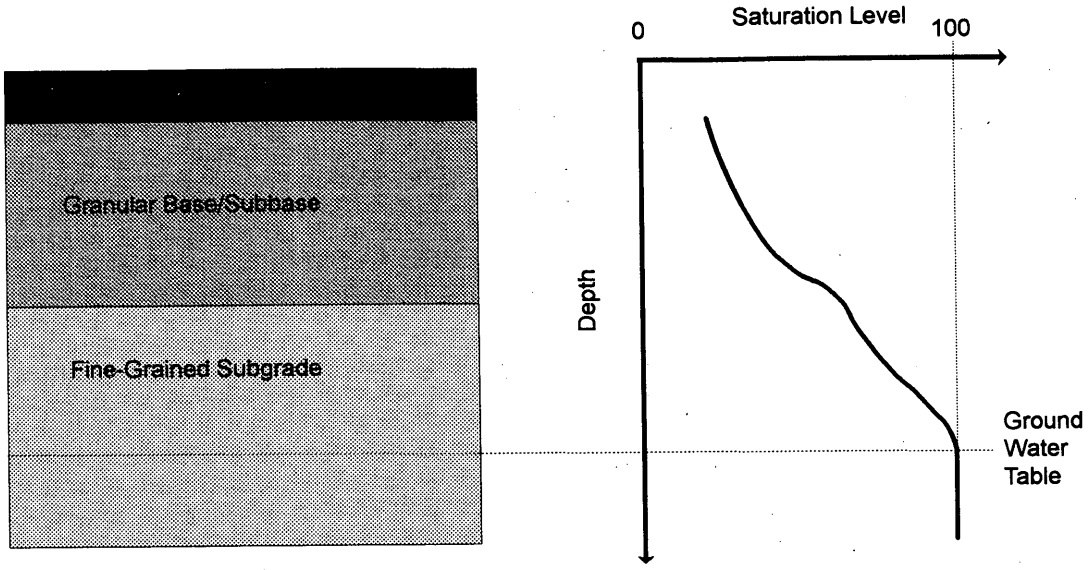

FIGURE 1 Moisture gradient in pavement over high GWT.

Term Pavement Performance study initiated by the Strategic Highway Research Program and subsequently continued by FHWA. EVERCALC was developed by the University of Washington for use by the Washington State Department of Transportation.

Mahoney et al. (*4*) reported that this approach to determining the depth to stiff layer worked well in determining the depth to saturated soil, although they cautioned that their results were not conclusive.

Reflection Survey Method

One method used at the Mn/ROAD site to locate the depth to saturated soil involved a geophysical technique known as a reflection survey for analyzing the propagation of surface and reflected waves (*8*). The test setup used to accomplish this is illustrated in Figure 3(*a*). A source (*S*) such as a drop hammer or sledgehammer was used to generate the wave, and an accelerometer was used as a receiver (*R*). The theory for this methodology is described elsewhere (*8*), and a brief summary will be presented.

The wave front of the *P*-wave is hemispherical, as shown in Figure 3(*a*), but ray theory is used to simplify the representation of the traveling waves. This means that the wave path is represented by a ray perpendicular to the wave front and parallel to the direction of wave propagation. Two paths along which the wave energy travels from *S* to *R* can be followed. The direct-wave path on the surface can be described by the travel-time equation

$$t_d = \frac{x}{v_{p1}}$$

where t_d is the travel time of the direct wave and x is the distance between the source and the receiver. The other path is the reflected

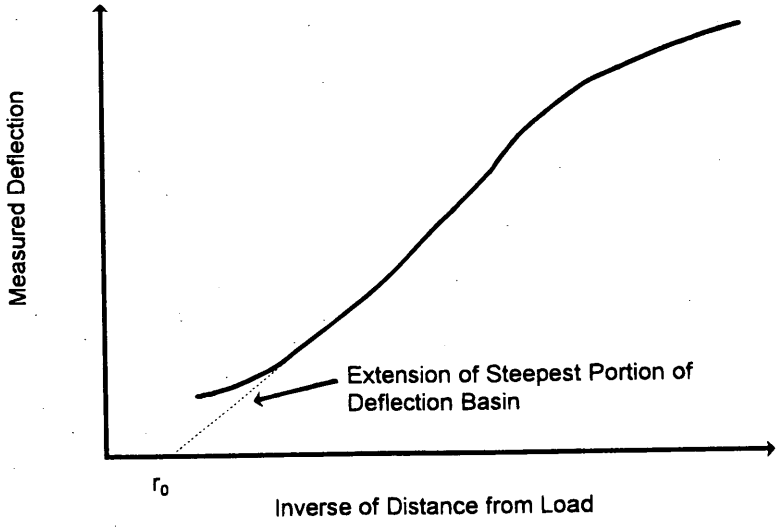

FIGURE 2 Establishing deflection basin parameter for finding depth to rigid layer (*3*).

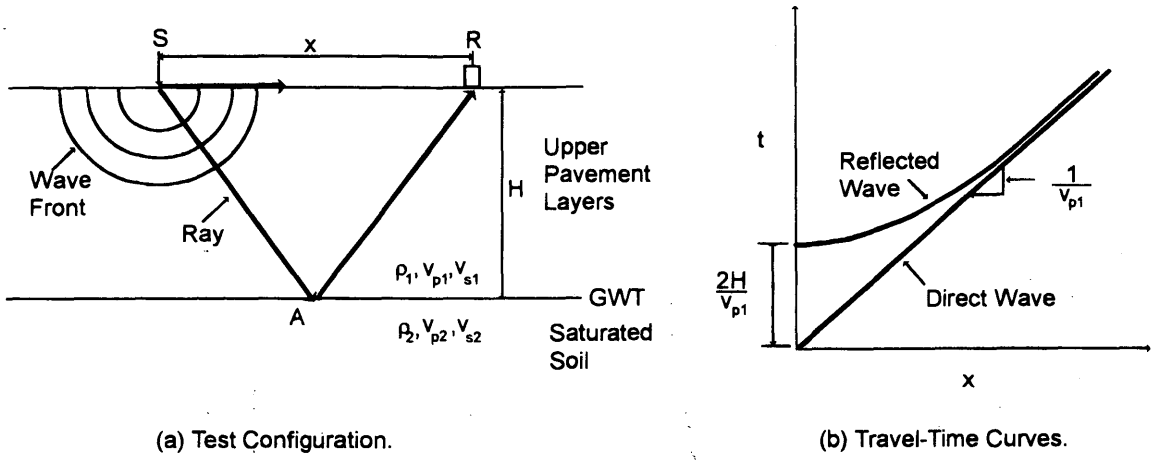

(a) Test Configuration. (b) Travel-Time Curves.

FIGURE 3 Principles of reflection survey.

wave, and it is composed of the ray from S to the interface A, where material properties change significantly, and back to the surface at R. The reflected wave travel time equation is

$$t_r = \frac{\sqrt{x^2 + 4H^2}}{v_{p1}}$$

Figure 3(*b*) shows the travel-time curves for the direct and reflected waves. For very small values of x, t_r is $2H/v_{p1}$, and for very large values of x, t_r approaches t_d.

To perform a reflection survey, the arrival times for the direct and reflected waves are recorded at the source and at several distances from the source, after which the travel times are plotted. For a layer in which the velocity is not a function of depth, both v_{p1} and H can be found. If v_{p1} is known, H can be solved by using the time difference $\Delta t = t_r - t_d$:

$$H = \frac{1}{2}\sqrt{(\Delta t v_{p1})^2 + 2x\Delta t v_{p1}}$$

A reflection survey can be used to detect the GWT level below a pavement, assuming that the material properties change significantly at that plane. An example of this is shown in Figure 4, in which Δt is determined as a change in the amplitude and frequency of the accelerometer signal.

This approach has limitations, the most important being that the reflected P-wave arrives at the receiver after the receiver has already been excited by the direct waves. This is because the stiff layers in the upper portion of the pavement produce higher velocities for the direct waves. Thus, it is not always easy to distinguish clearly the exact arrival time of the reflected wave. One check that can be made is whether H is greater than the total thickness of the pavement structure, presuming that it is above the water table.

RESEARCH APPROACH

Site Conditions

Data were obtained from three test sections at Mn/ROAD to investigate the effects of saturated soil conditions on the backcalculation of layer moduli. These pavements are designated as TS 1, TS 2, and TS 4, and the structural sections are shown in Figure 5. Each test section is approximately 150 m in length. TS 1 and TS 2 are asphalt concrete (AC) over a granular base, whereas TS 4 is a full-depth asphalt pavement. The geology of the site is such that there are no rock ledges or very stiff soil layers down to a depth of at least 30 m. The subgrade soil is characterized as being a highly plastic silty clay. The water table in this portion of the Mn/ROAD facility is high because of a nearby retention pond that has had water in it since the start of roadway construction. Each Mn/ROAD section has an open standpipe located approximately in the center of the test section offset in the shoulder 5.7 m from the centerline of the roadway.

Testing

Deflection testing was accomplished with a Dynatest Model 8000 FWD in the fall of 1993 and spring of 1994. Deflection measurements were normalized to a 40-kN load for the purposes of presenting these results. Backcalculation of layer moduli was performed by using EVERCALC version 3.3. The actual plan thicknesses of the asphalt concrete and granular base and subbase layers were used in the backcalculation process. For asphalt concrete over granular base and subbase layers, no attempt was made to subdivide the subgrade beyond differentiating the depth to the water table. In the full-depth pavement previous research (*9*) has indicated the need to consider the top portion of the subgrade to a depth of 1140 mm as a separate layer to account for the vertical variation in subgrade modulus.

Reflection surveys of the test sections were performed in the fall of 1993 by the techniques described above. At the same time readings from open standpipes were taken to make comparisons.

RESULTS

Depth to Saturated Layer

Comparisons of the three methods for determining the depth to the saturated layer are presented in Figure 6. The agreement between these techniques is excellent in TS 1, in which all three methods indicated a depth of between 1.8 and 2.0 m for the saturated layer. In TS 2 the reflection survey predicted the depth to be about 2.3 m, whereas the deflection method estimated it to be at about 1.9 m and the standpipe reading was 1.6 m. The largest disparity in the results

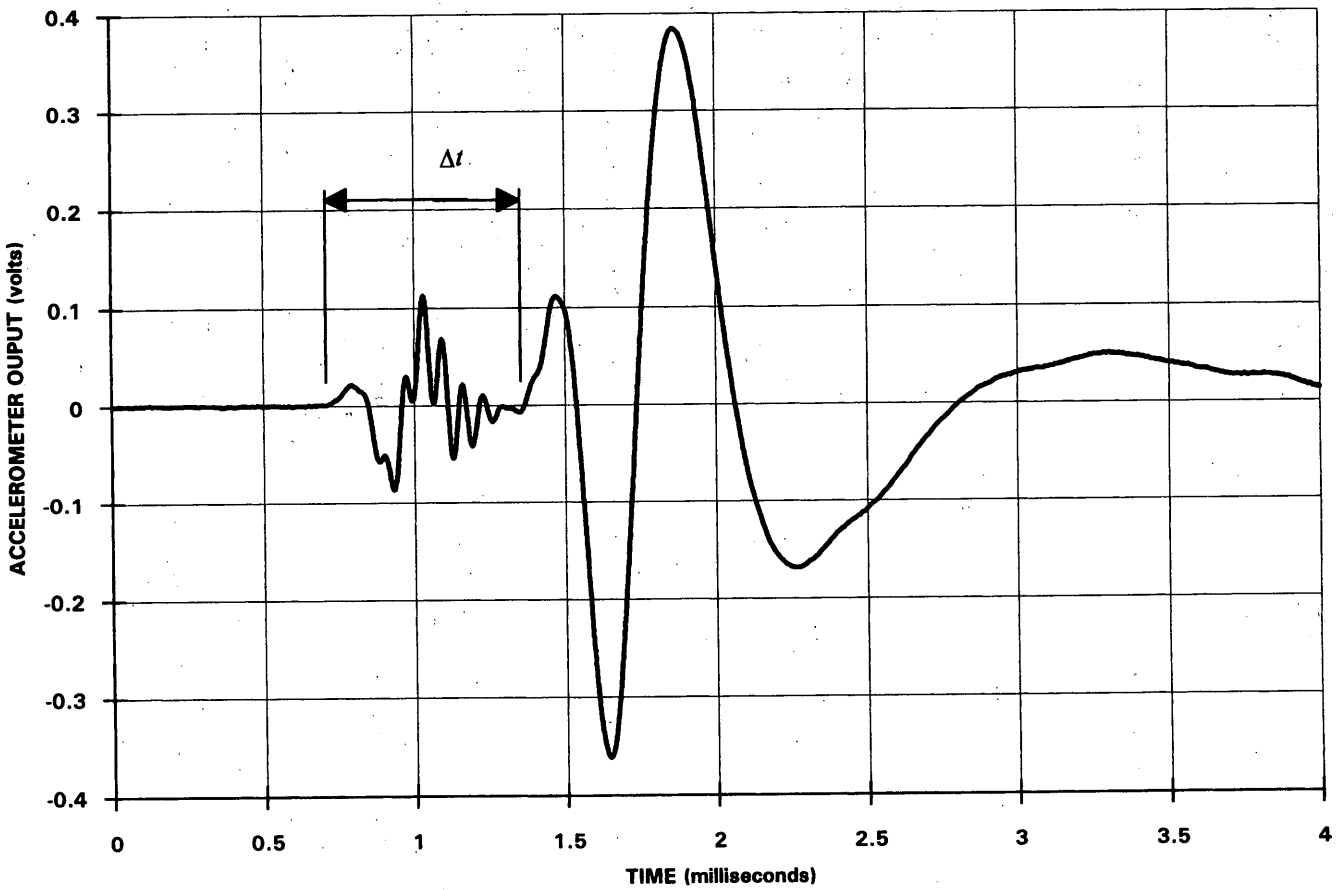

FIGURE 4 Example of accelerometer output from reflection survey.

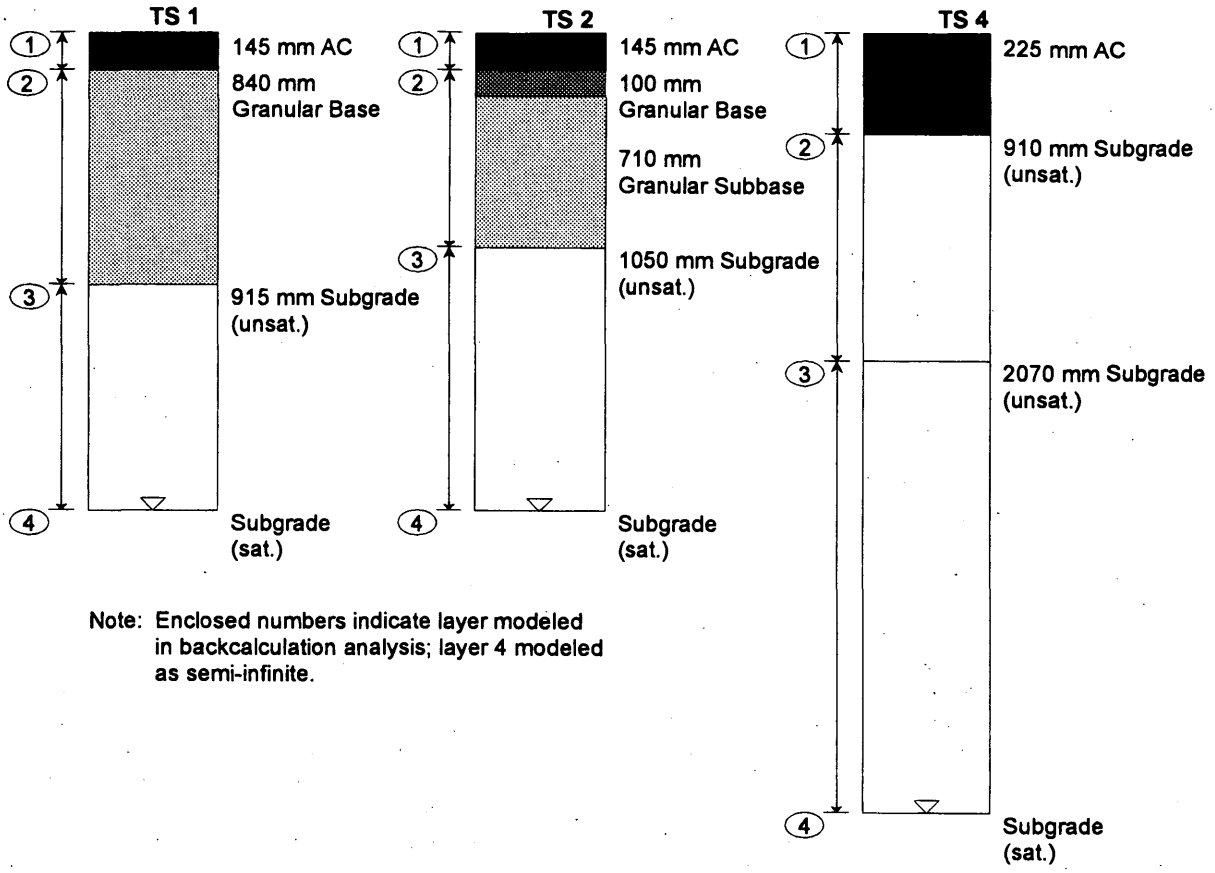

FIGURE 5 Pavement structures and layer configurations investigated at Mn/ROAD.

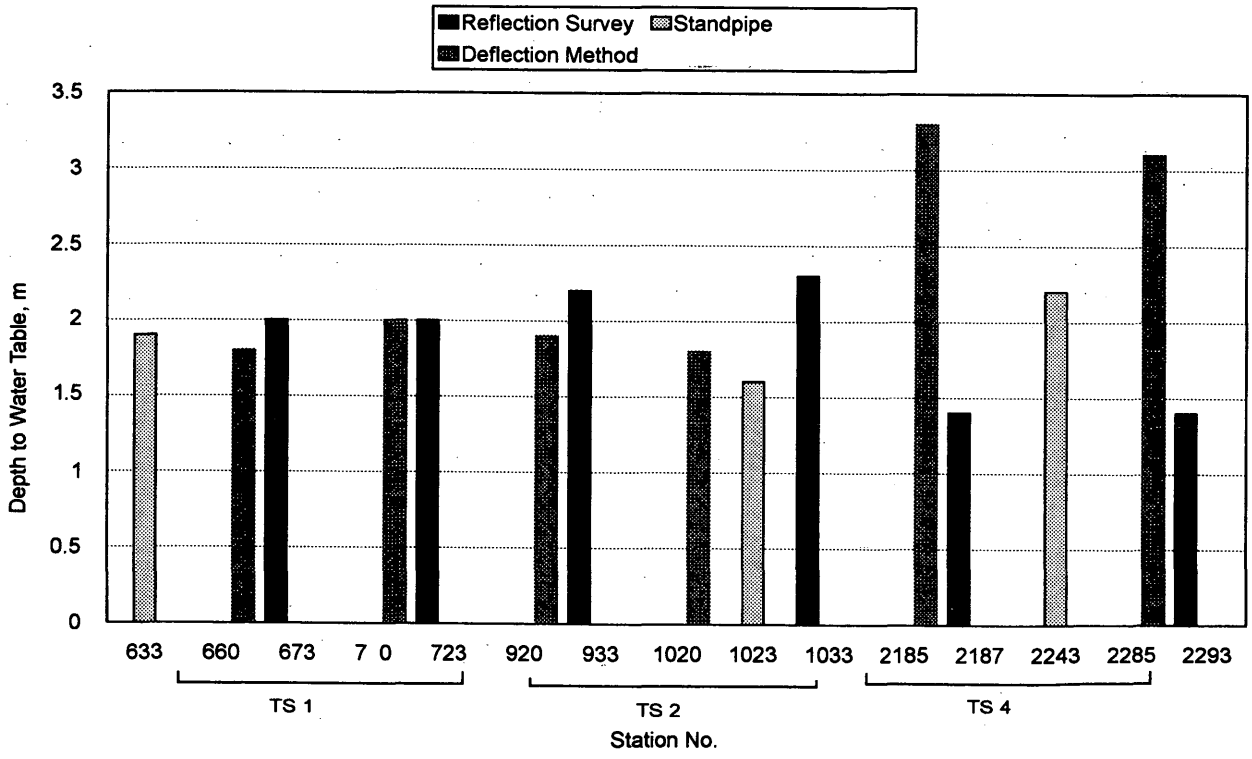

FIGURE 6 Comparison of depths to water table.

occurred in TS 4, in which the equations of Rohde et al. (*3*) put the GWT at 3.2 m and the reflection survey technique suggests that it is at 1.4 m, with the standpipe indicating 2.2 m.

Although some rather large differences may be noted for the different techniques used to estimate the depth to a saturated soil condition, it is encouraging that all three detected a condition of saturated soils near the surface. The differences might be explained both in terms of location and test methods. It should be pointed out that the difference in locations for the FWD test points and the observation wells were in excess of 15 m in some instances, although the difference in locations for the FWD and reflection surveys were all less than 4 m. In TS 4, in which the largest difference between the deflection and reflection survey methods occurred, it is perhaps the nonlinear response of the subgrade that is responsible for the difference. The reflection survey was carried out with a light hammer, and the response of the subgrade may have been relatively stiff in this instance compared with that from the heavy FWD load; thus, the stiff layer appeared to be closer to the surface. It should be remembered that TS 4 is a full-depth asphalt concrete section, so the subgrade was much shallower in this pavement, which means that the nonlinearity of the soil is more prominent in the results.

To investigate how the depth to the stiff layer might change with time, the approach that used the equations of Rohde et al. (*3*) was applied to data gathered in the spring of 1994 at the same test locations. The data in Table 1 show how the depth to saturated conditions changed between the fall and spring. It can be seen that the depth increased for TS 1 and TS 2 but decreased for TS 4. This coincided with increased in situ moisture content readings taken with time domain reflectometers (TDRs) during the same time periods for TS 2 and TS 4. The implication from this is that the depth to GWT or perched GWT is not necessarily constant and that it should be determined each time that deflection testing is performed on a pavement.

Effects on Backcalculation

Since saturated soil will not behave in the same manner as a very stiff layer such as a rock ledge, the appropriate modulus for this layer must be determined. This can be done by isolating the saturated layer during the backcalculation analysis. Two different backcalculation approaches were used for the three test sections, as shown in Figure 5. In the first approach the presence of the saturated layer was neglected so that a three-layer system was being modeled. For the second approach the medium below the calculated depth to the GWT was modeled as semi-infinite; the configurations of the upper three layers were the same as those for the first approach. The modulus of the (saturated) half-space was determined by allowing the modulus value to vary over a range of fixed values, whereas the moduli of the upper layers were left as open parameters. The best estimate for the modulus of the saturated layer was taken to be the one that returned the minimum error between the backcalculated and measured deflections. In the present study, the measure used was the root mean square (RMS) error, and its significance is discussed elsewhere (*10*). It is considered desirable to achieve a fit between measured and theoretical deflections such that the RMS error is less than 1 percent. Figure 7 shows how the RMS changed with the modulus used for the saturated layer for one of the test points in TS 4. In this case the saturated layer modulus for the minimum RMS was about 105 MPa. By using this approach to identify the modulus of the saturated layer, a comparison was made between moduli backcalculated by a normal blind technique in which the subgrade is considered a semi-infinite half-space and one in which the depth to and modulus of the saturated layer are taken into account.

Table 2 provides the results of the backcalculation comparisons. In almost every instance some reduction of the RMS occurred when the saturated layer was considered separately. This improvement in the fit ranged from relatively small (0.03 percent) to moderate (0.53 percent). The reader may note that the backcalculated modulus values of the granular pavement layers are consistently lower than those of the subgrade, particularly in the fall of 1993. At first this may seem strange, but some discussion of why this may have occurred should help to explain why this is not as unreasonable as it seems. First, the thicknesses of the base layers in TS 1 and TS 2 are substantial (840 and 810 mm, respectively), as shown in Figure 5. The calculated bulk stress at the midpoint of these base thicknesses is relatively low at less than 35 kPa. When this value is used in constitutive equations developed for laboratory-tested granular materials at Mn/ROAD (*11*), the predicted modulus of the granular materials is about 95 MPa, which compares well with the values for Layer 2 given in Table 2. Likewise, the deviatoric stress at the top of the subgrade is very small (less than 14 kPa). An examination of laboratory results showed that at this level of deviator stress the subgrade had a resilient modulus of about 152 MPa at optimum moisture content and one of about 97 MPa at a moisture content 2 percent over the optimum (*11*). Again, when compared with the laboratory-determined values, the backcalculated subgrade moduli are not unreasonable. In the fall there were instances of extremely high subgrade moduli, but the soil was dry during this time of year, so it could be expected to be stiffer.

TABLE 1 Changes in Depth to GWT with Time

Test Section	Station No.	Depth to Saturated Soil, m	
		Fall 1993	Spring 1994
1	660	1.7	2.2
	710	2.0	2.4
2	920	1.9	2.3
	1020	1.8	2.2
4	2185	3.3	2.8
	2285	3.1	3.0

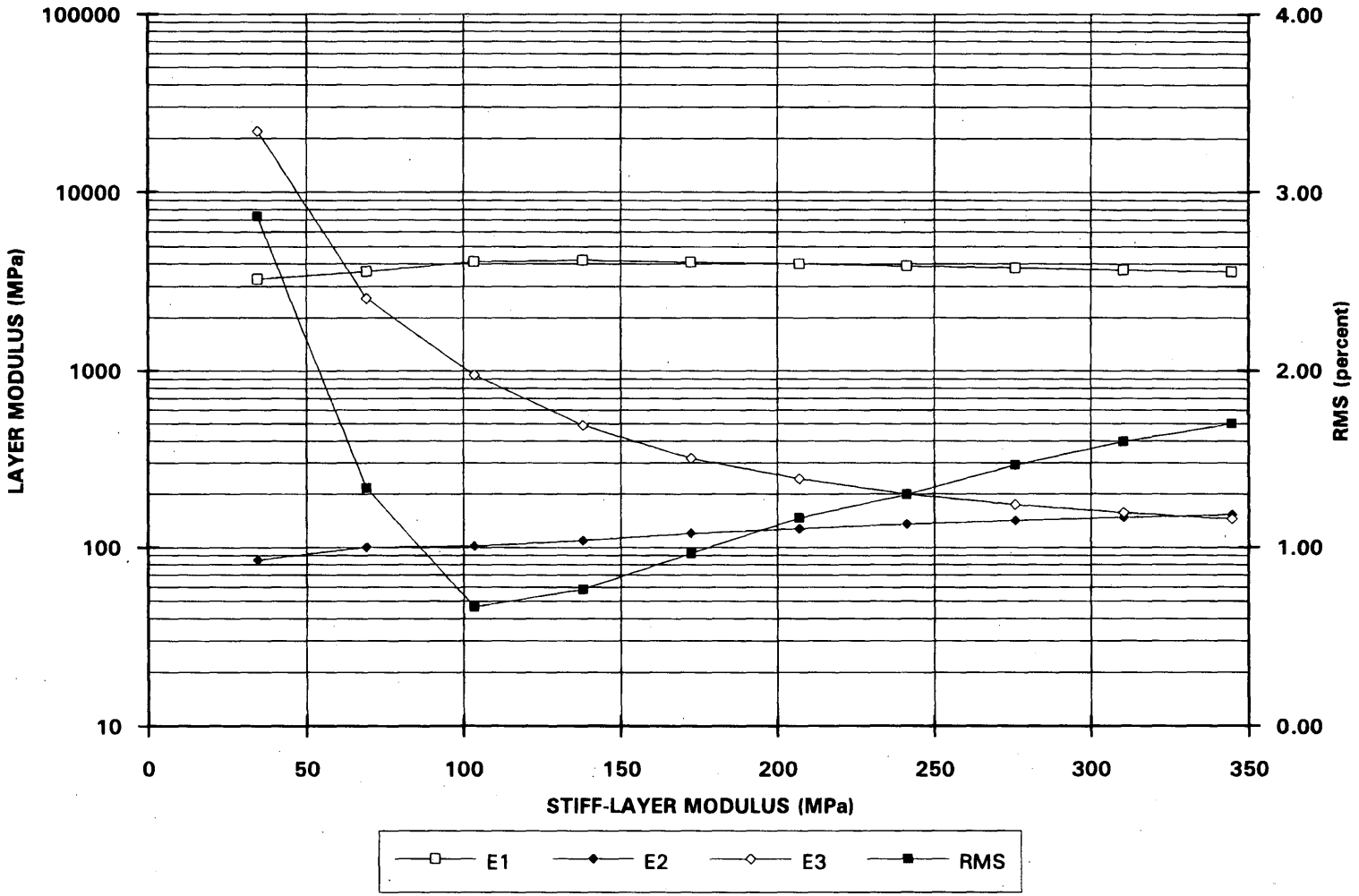

FIGURE 7 Variation in layer moduli and RMS with fixed saturated layer modulus.

TABLE 2 Results of Backcalculation

Test Section	Station No.	Date	Account for Sat. Layer?	Layer Moduli, MPa				RMS
				E_1	E_2	E_3	E_4	
1	660	Fall 93	Yes	3397	93	391	172	0.60
			No	3036	105	194		1.03
	710	Fall 93	Yes	4259	107	169	207	0.40
			No	4404	102	197		0.33
2	920	Fall 93	Yes	4956	92	395	172	0.37
			No	4407	108	200		0.40
		Spring 94	Yes	6881	154	81	345	0.77
			No	9299	103	197		0.80
	1020	Fall 93	Yes	3907	94	287	172	0.57
			No	3603	104	188		0.93
		Spring 94	Yes	6037	141	76	345	0.87
			No	8214	94	199		1.10
4	2185	Fall 93	Yes	4111	102	951	103	0.67
			No	3944	132	222		1.20
		Spring 94	Yes	7453	85	160	276	0.93
			No	7782	75	232		1.03
	2285	Fall 93	Yes	3982	102	646	138	0.67
			No	3615	127	224		0.87
		Spring 94	Yes	6793	101	136	276	0.73
			No	7265	84	213		1.10

It should also be noted that the stiffness of the saturated layer did not remain constant from the fall to the spring. In TS 2 the saturated layer stiffness increased from 172 MPa in the fall to 345 MPa in the spring, whereas in TS 4 it increased from 120 to 276 MPa. As mentioned earlier this coincides with increased in situ moisture content measurements made with TDR probes. There is a suggestion that the stiffness of the material in the saturated layer does not remain constant over time, so that in addition to determining the depth to the stiff layer, the modulus of the stiff layer should also be backcalculated each time that deflections are measured.

SUMMARY

Accounting for the saturated layer is important in the backcalculation process to better represent the structural section of pavements. The properties of this layer may differ significantly, being either stiffer or softer, from those of the overlying soil. Locating the depth of the saturated layer in areas where reliable water table level data are not available may be done by either reflection survey or by the method of Rohde et al. (*3*). It seems that some refinement may be needed in both of these methods to obtain reliable agreement with observation well data. The reflection survey technique uses a low impulse load, which may cause conditions not representative of those under traffic. On the other hand the equations of Rohde et al. (*3*) were developed for a very stiff layer (6900 MPa), so they are outside of their limits when considering saturated materials with moduli on the order of 345 MPa. The stiffness of the saturated layer should be varied to investigate which modulus value minimizes the error between measured and theoretical deflection basins.

ACKNOWLEDGMENTS

The authors gratefully acknowledge the financial and technical contributions of the Minnesota Department of Transportation in performing this work. The FWD testing and laboratory testing of the soils were performed by Mike Miezwa and Neil McGee, respectively. Supporting TDR data were provided by Craig Schrader.

REFERENCES

1. Rohde, G. T., R. E. Smith, and W. Yang. Inclusion of Depth to a Rigid Layer in Determining Pavement Layer Properties. *Proc., 3rd International Conference on the Bearing Capacity of Roads and Airfields*, Trondheim, Norway, 1990, pp. 475–486.
2. Uddin, W., A. H. Meyer, and W. R. Hudson. Rigid Bottom Considerations for Nondestructive Evaluation of Pavements. In *Transportation Research Record 1070*, TRB, National Research Council, Washington, D.C., 1986, pp. 21–29.

3. Rohde, G. T., R. E. Smith, and T. Scullion. Pavement Deflection Analysis on Sections Where the Subgrades Vary in Stiffness with Depth. *Proc., 7th International Conference on Asphalt Pavements*, Nottingham, England, 1992, pp. 280–295.
4. Mahoney, J. P., B. C. Winters, N. C. Jackson, and L. M. Pierce. Some Observations About Backcalculation and Use of a Stiff Layer Condition. In *Transportation Research Record 1384*, TRB, National Research Council, Washington, D.C., 1993, pp. 8–14.
5. Pierce, L. M., N. C. Jackson, and J. P. Mahoney. Development and Implementation of a Mechanistic, Empirically Based Overlay Design Procedure for Flexible Pavements. In *Transportation Research Record 1388*, TRB, National Research Council, Washington, D.C., 1993, pp. 120–128.
6. Richart, F. E., Jr., J. R. Hall, Jr., and R. D. Woods. *Vibrations of Soils and Foundations*. Prentice-Hall, Inc., Englewood Cliffs, N.J., 1970.
7. Rohde, G. T., and T. Scullion. *Improvements to the MODULUS Program*. Research Report 1123-3F. Texas Transportation Institute, Texas A&M University, College Station, 1990.
8. Jiang, Y. *Determination of In Situ Pavement Moduli Using High Frequency Body Waves*. MCE Project Report. Department of Civil Engineering, University of Minnesota, 1994.
9. Van Deusen, D. A., and D. E. Newcomb. Strains Due to Load in Frozen and Thawed Flexible Pavements. *Proc., 4th International Conference on the Bearing Capacity of Roads and Airfields*, University of Minnesota, Minneapolis, 1994, p. 695.
10. Lee, S. W. *Backcalculation of Pavement Moduli by Use of Pavement Surface Deflections*. Ph.D. dissertation. University of Washington, Seattle, 1988.
11. Cochran, G. R. Minnesota Department of Transportation Experience with Laboratory MR Testing. *Proc., Workshop on Resilient Modulus Testing*, Oregon State University, Corvallis, March 1989.

Publication of this paper sponsored by Committee on Strength and Deformation Characteristics of Pavement Sections.

Backcalculation of Flexible Pavement Moduli From Dynamic Deflection Basins Using Artificial Neural Networks

ROGER W. MEIER AND GLENN J. RIX

The falling weight deflectometer (FWD) test measures the response of a pavement system to a transient load applied at the pavement surface. A limitation of existing, widely used techniques for backcalculating pavement layer moduli from FWD results is that they are based on a static analysis of pavement response. Previous studies have shown that significant errors in moduli can accrue from the discrepancy between this static assumption and the dynamic nature of the FWD test. Dynamic solutions for pavement response are available, but their computational complexity makes them impractical for use in conventional backcalculation programs that use gradient search or data base techniques. This limitation has been overcome by applying artificial neural network technologies to the backcalculation problem. An artificial neural network has been trained to backcalculate pavement layer moduli for three-layer flexible pavement systems with synthetic dynamic deflection basins. The dynamic pavement response was calculated by using an elastodynamic Green function solution based on a stiffness matrix formulation of the pavement system. The computational efficiency of the trained neural network means that moduli can be backcalculated with a speed that is several orders of magnitude greater than that which can be achieved by conventional gradient search and data base approaches. This is significant because it demonstrates the feasibility of backcalculating pavement layer moduli from dynamic deflection basins in real time.

Falling weight deflectometer (FWD) tests are widely used to assess pavement layer moduli in a nondestructive manner. An FWD test is performed by applying an impulse load to the pavement via a circular plate and measuring the resulting pavement deflections at several radial distances from the plate. The test data are usually summarized as a deflection basin formed from the peak deflections at each measurement location. Pavement layer moduli are then backcalculated from these experimentally determined deflection basins. This is usually accomplished by matching a theoretically calculated deflection basin to the experimental deflections. Most FWD users employ one of two approaches to match deflection basins: (a) a gradient search approach (*1*) in which pavement layer moduli are iteratively adjusted until the theoretical and experimental deflection basins agree within a predefined tolerance and (b) a data base approach (*2*) that uses a combination of pattern searching and interpolation to calculate a theoretical deflection basin from exemplars within a predefined data base of basins.

A limitation of conventional gradient search and data base approaches is that they are based on static deflection basins calculated by using multilayer, linear elastic theory [e.g., WESLEA (*3*)]. The FWD test is inherently a dynamic test because of the impulse-type load applied to the pavement and the resulting inertial forces and resonances within the pavement system. Figure 1 illustrates the difference between static and dynamic deflection basins for a pavement profile with varying depth to bedrock. This pavement profile has a 23-cm (9-in.) asphalt layer over a 30-cm (12-in.) granular base course. The elastic moduli of the asphalt, base, and subgrade are 7×10^6, 7×10^5, and 7×10^4 kPa (10^6, 10^5, and 10^4 lb/in.^{2}), respectively. Notice that the static deflection basins [Figure 1(*a*)] are strongly influenced by the depth to bedrock, whereas the dynamic deflections [Figure 1(*b*)] are nearly independent of the depth to bedrock. The differences between the static and dynamic displacements can result in significant errors in the backcalculated layer moduli if the backcalculation program uses static deflections (*4–8*).

The computational expense of calculating dynamic deflections hinders their use in backcalculation programs that use either a gradient search or data base approach. Meier and Rix (*9*) proposed the use of artificial neural networks as a fundamentally different approach to backcalculating pavement layer moduli from experimental deflection basins. An artificial neural network is a highly interconnected collection of simple processing elements that can be taught to approximate any continuous functional mapping through repeated exposure to examples of that mapping. Meier and Rix (*9*) trained an artificial neural network to backcalculate pavement layer moduli for a three-layer flexible pavement system using synthetic static deflection basins generated by WESLEA. The trained neural network was able to backcalculate moduli more than 3 orders of magnitude faster than the conventional backcalculation program WESDEF (*1*), which also uses WESLEA. This significant increase in speed makes it possible to backcalculate pavement layer moduli in real time.

In this paper we extend the artificial neural network approach described previously (*9*) to incorporate dynamic deflection basins. The objective is to develop a backcalculation procedure that is based on dynamic deflection basins but that still permits pavement layer moduli to be determined in real time. This is possible because the computational efficiency of the trained neural network is independent of the computational complexity of the algorithms used to create the training data (i.e., the dynamic deflections).

ARTIFICIAL NEURAL NETWORKS

Artificial neural networks are a computational paradigm completely different from the conventional serial computing introduced by Von Neumann. Instead of the linear sequence of relatively complex tasks

R. W. Meir, Mobility Systems Division, U.S. Army Engineer Waterways Experiment Station Geotechnical Laboratory, 3909 Halls Ferry Road, Vicksburg, Miss. 39180-6199. G. J. Rix, School of Civil and Environmental Engineering, Georgia Institute of Technology, Atlanta, Ga. 30332-0355.

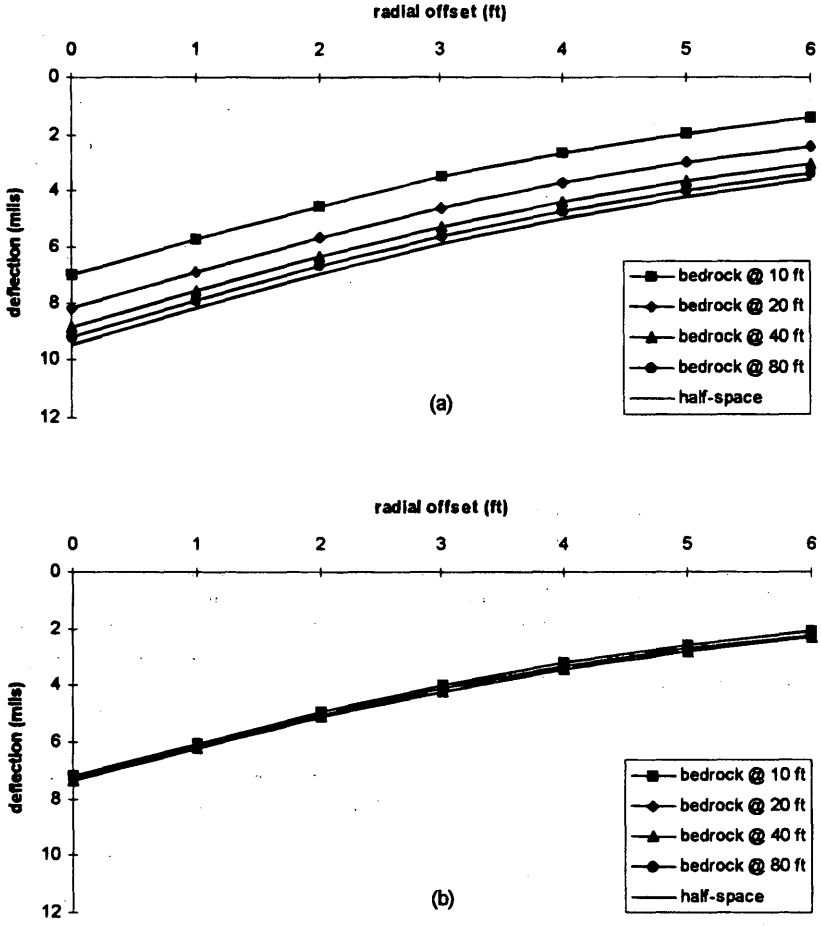

FIGURE 1 Static (*a*) and dynamic (*b*) deflection basins as a function of depth to bedrock.

that typifies most algorithmic procedures, artificial neural networks process information in parallel using a large number of operationally simple but highly interconnected processing units. The processing units themselves have certain functional similarities to biological neurons, and their organization bears at least superficial resemblance to the organization of neurons in the brain. This explains the terminology associated with neural computing.

All artificial neural networks are essentially mappers (*10*): for a given input they produce output in accordance with a mapping relationship encoded within their structure. The most common network architecture used for functional mapping (i.e., a unique mapping of real-valued inputs onto real-valued outputs) is the multilayer, feed-forward network. These networks consist of several layers of processing elements (Figure 2). The processing elements pass information, often equated with a signal pattern, from the input layer of the network through a series of hidden layers to the output layer. The signals travel between processing elements along connections whose strengths can be adjusted to amplify or attenuate the signal as it propagates. Each processing element sums the impinging signals to determine a net level of excitation. A nonlinear activation function provides a graded response to that excitation. The element then passes on the response to each of the processing elements in the next layer (Figure 3). The distribution of connection strengths throughout the network uniquely determines the output signal pattern that results from a given input signal pattern. In that respect the connection strengths encode the mapping relationship.

The neural network gains its knowledge through training. A supervised learning method is commonly used to train feed-forward networks. In supervised learning a set of training data (consisting of pairs of input-output patterns exemplifying the mapping to be learned) is presented to the network one example at a time. For each example the input pattern is propagated through the network and the resulting output pattern is compared with the target output. A learning algorithm is used to incrementally adjust the connection weights to reduce the differences between the calculated and the target out-

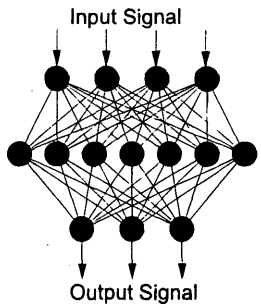

FIGURE 2 Architecture of a multilayer, feed-forward artificial neural network.

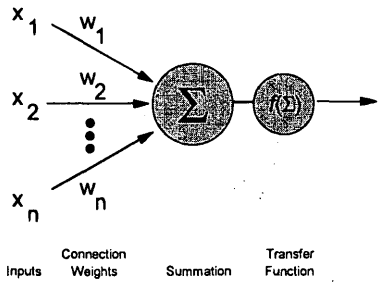

FIGURE 3 Basic processing element for a multilayer, feed-forward artificial neural network

puts. This ability to self-adjust is an essential feature of neural computing. It would be impossible to manually establish the connection weights needed to perform any but the simplest of mappings.

Once it is trained the network will provide an approximate functional mapping of any input pattern onto its corresponding output pattern. This process is extremely fast because the input pattern is propagated once through the network, a task that only involves passing weighted sums through the sigmoidal logistic function.

CALCULATING DYNAMIC PAVEMENT RESPONSE

The best way to train a neural network to map deflection basins onto their corresponding pavement layer moduli would be to use experimentally determined deflection basins along with independently measured pavement layer moduli. Lacking sufficient quantities of such data over a broad range of layer moduli and thicknesses, synthetic deflection basins can be obtained by solving the forward problem with many different combinations of pavement layer properties. A neural network can then be taught to map these synthetic deflection basins back onto their corresponding layer moduli. The latter approach is taken in this paper. This use of synthetic deflection basins to train the artificial neural network is, in principle, analogous to the use of synthetic deflection basins in all conventional basin matching programs. The following sections describe the methodology used to generate the synthetic deflection basins.

Fourier Superposition Analysis

The dynamic response of a pavement system to the transient loads imposed by the FWD can be analyzed by the principles of Fourier superposition. The first step in Fourier superposition is to decompose the transient loading pulse $p(t)$ into its frequency components, $P(\omega)$, by means of a forward Fourier transform. The next step is to develop a transfer function, $H(\omega)$, that establishes the steady-state response of the pavement system to a unit harmonic excitation at a specified frequency. For the purpose of FWD analysis the appropriate harmonic excitation is a vertical disk load applied at the pavement surface and the required pavement response is the vertical deflection of the pavement surface at some radial distance r from the center of the load. This transfer function is multiplied by the Fourier transform of the applied loads to obtain the response of the pavement in the frequency domain. Finally, the desired pavement deflection history $u(t)$ is obtained by performing an inverse Fourier transform on the calculated frequency-domain response.

The computer implementation of this method requires that the transient loading pulse be discretized into a finite number of applied loads

$$p_j = p(j\Delta t), j = 0, 1, \ldots, N - 1$$

separated by a constant time interval Δt. These loads can then be transformed into an equivalent number of complex-valued harmonic excitations

$$P_n = P(n\Delta\omega), n = 0, 1, \ldots, (N - 1)/2$$

using a forward fast Fourier transform (FFT) algorithm. These harmonic loads will be separated by a constant frequency interval

$$\Delta\omega = \frac{2\pi}{N\Delta t}$$

where N is the number of points in the discretized loading pulse.

The transfer function is evaluated for each discrete frequency and is multiplied by the appropriate frequency component of the loading pulse to obtain the pavement response in the frequency domain:

$$U_n = H(n\Delta\omega) \times P_n, n = 0, 1, \ldots, N - 1$$

These displacement components are then transformed back into the time domain by using an inverse FFT:

$$u_j = u(j\Delta t), j = 0, 1, \ldots, (N - 1)/2$$

This piecewise-linear deflection history represents the deflection pulse measured in the FWD test.

Development of Discretized Loading Pulse

The dynamic load imparted to the pavement by the FWD is generated by a free-falling mass hitting a steel plate. A rubber pad beneath the plate uniformly distributes the load to the pavement, and a series of rubber buffers above the plate decelerates the falling mass and conditions the loading pulse. Typical FWD loading pulses for a flexible pavement are illustrated by the light lines in Figure 4.

For programming convenience and computational flexibility a functional analogue to the FWD loading pulse that could be easily varied in both amplitude and duration was desired. Foinquinos et al. (*4*) and Chang et al. (*5*) used a triangular approximation to the loading pulse. Lukanen (*11*) suggests the use of a haversine:

$$p(t) = \frac{P}{2}\left(1 - \cos\frac{2\pi t}{T}\right) \quad (1)$$

where P is the peak amplitude and T is the duration. Both functional approximations were investigated for use in generating synthetic deflection basins.

The four measured loading pulses indicated by the light lines in Figure 4 were normalized to a unit load and were averaged to arrive at a sample FWD loading pulse (indicated by the heavy line in Figure 4). That sample pulse is compared with a triangle and a haversine in both the time and the frequency domains in Figure 5. Both functional analogues were made to have the same duration (26.5 msec) and peak amplitude (1.0) as the average measured pulse.

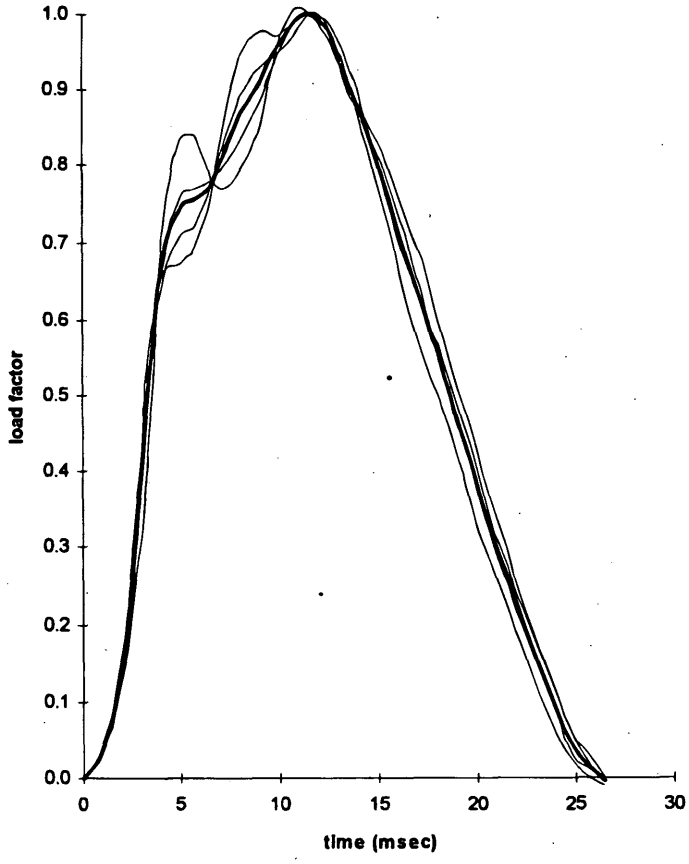

FIGURE 4 Measured FWD loading pulses and average pulse for four drop heights (*11*).

Figure 5 shows that the frequency-domain magnitude plots for all three curves are remarkably similar (especially at frequencies below 75 Hz, where all three curves essentially drop to zero) despite the fact that neither of the functional analogues captures the first peak in the time domain. Since all of the calculations in the Fourier superposition analysis occur in the frequency domain, both analogues appear to be suitable surrogates for the measured pulse. Both the triangle and the haversine have slightly lower DC (zero-frequency) values because the total impulse (the area under the force-time curve) is slightly less. The total impulse for the normalized measured pulse is 17.4 msec and the total impulse for the functional analogues is 16.0 msec. To preserve the total energy of the measured FWD pulse, the peak amplitudes of the analogues have to be increased by approximately 9 percent (17.4/16.0 = 1.09).

The haversine was chosen over the triangle for the present study because it better approximates (at least aesthetically) the shape of the sample load pulse and is slightly better behaved in the frequency domain. The perfectly straight sides of the triangular pulse and the sharp discontinuity at its peak result in spurious higher-frequency components that do not exist in the haversine or the measured pulse. Figure 6 compares the measured FWD pulse with an adjusted haversine analogue given by

$$p(t) = 0.545\left(1 - \cos\frac{2\pi t}{26.5}\right) \quad (2)$$

Again, despite the apparent differences in the time domain, there is very close agreement in the frequency domain over the range of 0 to 75 Hz. At frequencies above 75 Hz the magnitudes of both pulses hover near zero, anyway, so any differences are immaterial.

At a frequency of $0.5T^{-1}$, which is equal to 75.47 Hz, the FFT of the haversine pulse has a magnitude identically equal to zero. It would be convenient to use this as a frequency cutoff to limit the bandwidth that must be considered in the Fourier superposition analysis. Because the computational costs incurred in the analysis vary in direct proportion to the number of frequencies that must be analyzed, it was important to either minimize the bandwidth or maximize the frequency interval. To show the feasibility of using a bandwidth-limited analysis, an FFT was performed on the haversine analogue, and all of the components at frequencies higher than 75.47 Hz were set to zero. An inverse FFT was then performed to recover the time-domain loading pulse. The solid line in Figure 7 represents the original haversine, and the symbols show the inverse FFT of the bandwidth-limited function. This shows that little is lost by limiting the bandwidth.

The haversine shown in Figure 7, which was calculated at 32 discrete points in the time domain by using Equation 2, was accepted as the functional analogue of the FWD loading pulse. As a result the Fourier superposition analysis was performed at 31 discrete frequencies. Because the FFT of the haversine load pulse is zero at the

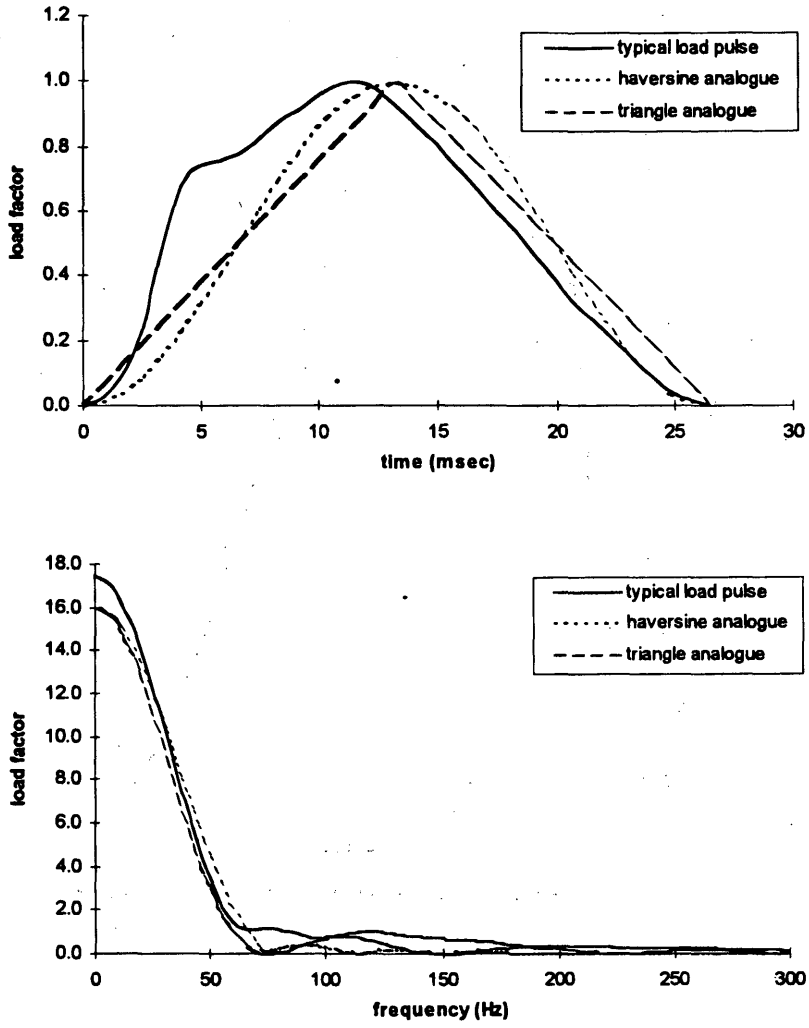

FIGURE 5 Typical load pulse and functional analogs in time (*a*) and frequency (*b*) domains.

32nd point (which corresponds to the frequency of 75.47 Hz) there was no need to develop a solution for that frequency.

Green Function Solution for Transfer Function

The fundamental (Green function) solution for the propagation of waves in layered elastic media was first presented by Thomson (*12*) and was later corrected by Haskell (*13*). Their solution, which has since become known as the Haskell-Thomson formulation, is based on the use of transfer matrices in the frequency-wave number domain that relate the displacements and internal stresses at a given layer interface to those at neighboring layer interfaces. Kausel and Roesset (*14*) developed a complementary solution based on stiffness matrices (analogous to those used in matrix structural analysis) that relate the external loads applied at the layer interfaces to the displacements at the layer interfaces. Those stiffness matrices are a function of both frequency and wave number. Both formulations are, however, computationally inefficient because the matrix elements involve transcendental functions.

Kausel and Peek (*15*) describe a Green function solution based on a discretization (sublayering) of the medium. That solution, described briefly below, is based on the premise that if the sublayer thickness is small relative to the wavelength of interest, it is possible to linearize the transcendental functions and reduce them to algebraic expressions. For most problems the increased efficiency of the algebraic formulation more than compensates for the increased computational requirements of the discretized solution (in which the size of the stiffness matrices increases in direct proportion to the number of sublayers).

Consider a horizontally layered pavement system. The stiffness matrix for each layer is given by the quadratic expression

$$\mathbf{K} = \mathbf{A}k^2 + \mathbf{B}k + \mathbf{G} - \omega^2\mathbf{M} \tag{3}$$

where k is the wave number, ω is the circular frequency, and the matrices $\mathbf{A}$, $\mathbf{B}$, $\mathbf{G}$, and $\mathbf{M}$, which are given by Kausel and Roesset (*14*), are functions of the material properties λ (Lame's constant), G (elastic shear modulus), and ρ (mass density) and the sublayer thicknesses h.

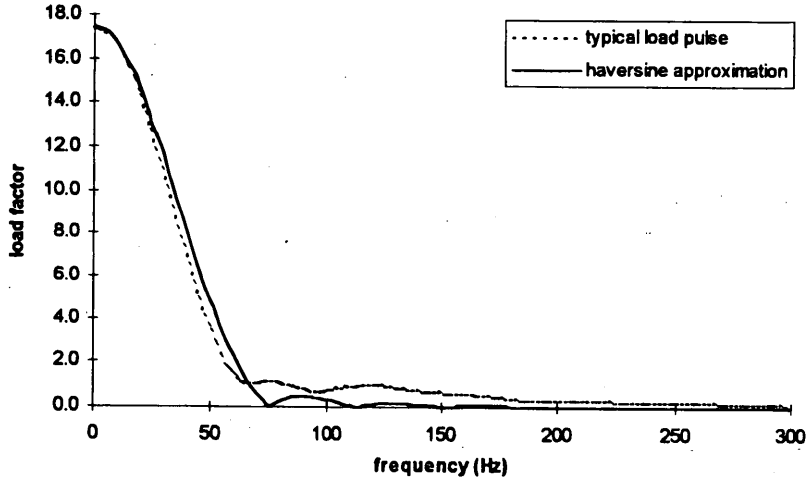

FIGURE 6 Comparison between typical load pulse and adjusted haversine analogue.

The global stiffness matrix for the pavement system as a whole is obtained by overlapping the stiffness matrices of the various layers. A numerical expedient suggested by Hull and Kausel (*16*) can be applied at the bottom of the layered system to account for the presence of a half-space instead of rigid rock. The global displacements $\bar{\mathbf{U}}$ can then be related to the global forces $\bar{\mathbf{P}}$ through the assembled global stiffness matrix:

$$\mathbf{K}\bar{\mathbf{U}} = \bar{\mathbf{P}} \tag{4}$$

The natural modes of wave propagation for the layered system are obtained by setting the load vector $\bar{\mathbf{P}}$ equal to zero. This produces the following quadratic eigenvalue problem:

$$(\mathbf{A}k^2 + \mathbf{B}k + \mathbf{G} - \omega^2\mathbf{M})\,\phi = 0 \tag{5}$$

where the eigenvectors ϕ are the displacement vectors for each natural mode of propagation. This problem yields $6L$ eigenvalues (modes) k_j with corresponding eigenvectors (mode shapes) ϕ_j, where L is the total number of sublayers. Only $3L$ of the eigenvectors correspond to waves that propagate away from the applied load. Of those, $2L$ correspond to Rayleigh waves and the remainder correspond to Love waves. Since the latter do not contribute to the vertical deflections produced by a vertical load they can be ignored. Thus, there are really only $2L$ modes of wave propagation of interest here. For those modes of propagation the quadratic eigenvalue problem reduces to a linear problem (albeit with a nonsymmetric characteristic matrix) that can be solved by the inverse power method (*17*). The Green function solution for the vertical surface displacements is expressed in terms of these $2L$ mode shapes:

$$H(\omega) = R\sum_{l=1}^{2L} \phi_w^l \phi_w^l I_{1l} \tag{6}$$

where R is the radius of the vertical disk load, ϕ_w^l is the vertical component of the lth eigenvector,

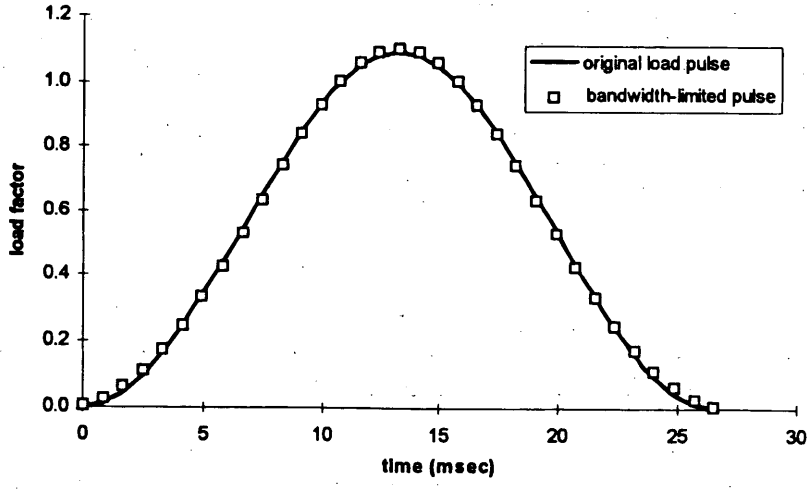

FIGURE 7 Comparison between original and bandwidth-limited haversine analogues.

$$I_{1l} = \frac{\pi}{2ik_l} J_0(k_l r)H_1^{(2)}(k_l r) - \frac{1}{Rk_l^2}, \quad \text{for } 0 \le r \le R$$

and

$$I_{1l} = \frac{\pi}{2ik_l} J_1(k_l r)H_0^{(2)}(k_l r), \quad \text{for } r > R$$

The functions J_0 and J_1 are Bessel functions of the first kind and orders zero and one, respectively. The functions $H_0^{(2)}$ and $H_1^{(2)}$ are Hankel functions of the second kind and orders zero and one, respectively.

Computer Implementation

Sanchez-Salinero (*18*) implemented the Green function solution described earlier in a FORTRAN computer program. That program was modified to perform the Fourier superposition analysis of the FWD test to obtain the dynamic deflection basins needed to train an artificial neural network. The program performs the following computations for each frequency of analysis:

1. Determine the maximum depth of interest,
2. Discretize the pavement system to the maximum depth of interest,
3. Assemble the global stiffness matrix (Equation 3),
4. Solve the eigenvalue problem (Equation 5) to obtain the propagation modes,
5. Evaluate the transfer function (Equation 6) at each radial distance of interest, and
6. Multiply the results by the FFT of the loading pulse to obtain the deflection components.

For the present study the maximum depth of interest at each frequency was assumed to be twice the length of the Rayleigh waves propagating at that frequency. The global stiffness matrix is assembled by using the half-space approximation of Hull and Kausel (*16*) below that depth. As was shown in Figure 1, the deflection basins obtained from a dynamic analysis of the pavement response are insensitive to bedrock depth for all depths in excess of approximately 3 m (10 ft). As a result the deflection basins produced here will be valid for all but the shallowest depths to bedrock.

Once the global stiffness matrix has been assembled, the eigenvalue problem (Equation 5) is solved by using the inverse power method to obtain the outward-propagating Rayleigh modes. The eigenvalues and their corresponding eigenvectors are used in the solution of the Green function at each radial distance of interest (i.e., each FWD sensor location). These solutions (given by Equation 6) are multiplied by the appropriate frequency component of the loading pulse to obtain the deflection components in the frequency domain. An inverse FFT is then used to recover the deflection pulses in the time domain. Finally, a synthetic deflection basin is assembled from the deflection pulses by finding the peak deflection at each sensor location.

TRAINING THE ARTIFICIAL NEURAL NETWORK

Backpropagation neural networks are universal approximators, but training times increase rapidly with increasing problem complexity. This places some practical limits on the mappings that can be learned. Instead of trying to train a network to handle a variable number of pavement layers, in the present study the choice was made to train a neural network to backcalculate moduli for a three-layer profile. Each three-layer profile consisted of an asphalt concrete (AC) surface layer, an unstabilized granular base course, and a soil subgrade. The thicknesses and moduli of the AC and base layers and the modulus of the subgrade were randomly selected from uniform distributions within the limits given in Table 1. Because a half-space approximation was used in the Green function solution, the thickness of the subgrade is infinite. Synthetic deflection basins were calculated for a nominal dynamic load of 40 kN (9,000 lb) based on Strategic Highway Research Program-recommended sensor spacings of 0, 20, 30, 45, 60, 90, and 150 cm (0, 8, 12, 18, 24, 36, and 60 in.). For pavement profiles or sensor spacings that differ from these assumed conditions, additional neural networks could easily be trained by the same methodology presented here.

The synthetic deflection basins in the training set are intended to represent deflection basins that would be measured in the field. Typical test specifications for the FWD test (*19*) require a systematic error no greater than 2 percent of the measured deflection and a repeatability error no greater than 2 μm (0.08 mils). As illustrated in a previous study (*20*), these potential inaccuracies can be accommodated by introducing random noise during training, a technique known as noise injection. The random noise was added to each of the seven deflections in each training example just before presenting it to the network. In this way, even though the training basins were constantly reused, the added noise was different every time. The random variates were drawn from uniform distributions whose limits were equal to the larger of ±2 percent of the ideal deflection or ±2.5 μm (±0.1 mils). The latter was made slightly larger than the test specification to permit some room for error.

The study used the same network architecture used previously (*9*) for mapping static deflection basins with noise injection. Despite the increased fidelity of the model used to create the training data, both networks map nine-element vectors of pavement deflections and layer thicknesses onto three-element vectors of pavement moduli. Since this complexity of the mapping task is essentially the same, the same network architecture, which uses two hidden layers with 15 neurons apiece, should suffice.

TABLE 1 Pavement Layer Properties Used To Train the Neural Networks

Layer	Layer Modulus (MPa)[a]	Layer Thickness (cm)[b]	Poisson's Ratio
Asphalt	1725 - 20,685	5 - 30	0.325
Base	35 - 1035	15 - 75	0.35
Subgrade	35 - 345	3050	0.35

[a] 1 MPa = 0.145 ksi
[b] 1 cm = 0.394 in

Network training proceeded by iteratively presenting the training examples to the network. Each pass through the set of 10,000 examples constituted a training "epoch." During each epoch the first 9,750 examples were used to train the network. The remaining 250 examples were set aside to test the network at the conclusion of training. (Neural networks should never be tested with the same data that were used to train them. It is important that the network be able to generalize beyond the training examples instead of simply memorizing them.) At first the mean squared output error drops rapidly as the training epochs are completed [Figure 8(*a*)]. With further training the output error asymptotically approaches some minimum level. Network training continued until it was clear that the computational expense of continued training outweighed any further increases in network accuracy.

At the conclusion of training the 250 deflection basins previously set aside were used to check the accuracy of the network. As with the other 9,750 deflection basins, random noise was added to these test basins to better simulate real measurements. Tests to determine the repeatability of FWD measurements (*21*) have shown that individual transducers have a standard deviation of ±1.95 μm. Because this error is random, it can be lessened by replicating the test and averaging the results. Irwin et al. (*21*) recommend that three to five replicates be conducted for each test. The amount of noise added to each deflection was therefore established by averaging five random variates drawn from a Gaussian distribution with a mean of zero and a standard deviation that was rounded off to ±2 μm (0.08 mils). Because these random variates were drawn from a Gaussian distribution instead of the uniform distribution used to train the network, it is possible that some of these test basins contained more noise than was present in the training set.

Figures 8(*b*), 8(*c*), and 8(*d*) compare the target and computed moduli for the asphalt, base, and subgrade layers, respectively, for the 250 test basins. The neural network clearly learned the mapping from deflection basins to subgrade moduli extremely well, despite the presence of noise. It also learned the mapping from deflection basins to asphalt moduli very well, although there was a slight tendency toward underestimation for the stiffer pavements. Considering that the base moduli are always the hardest to backcalculate, the network has done a very good job with those, too. Figure 9(*a*) shows that the base modulus error is less than 15 percent for more than 80 percent of the pavement profiles. Figures 9(*b*), 9(*c*), and 9(*d*) collectively show that the 20 percent of the profiles with the greatest

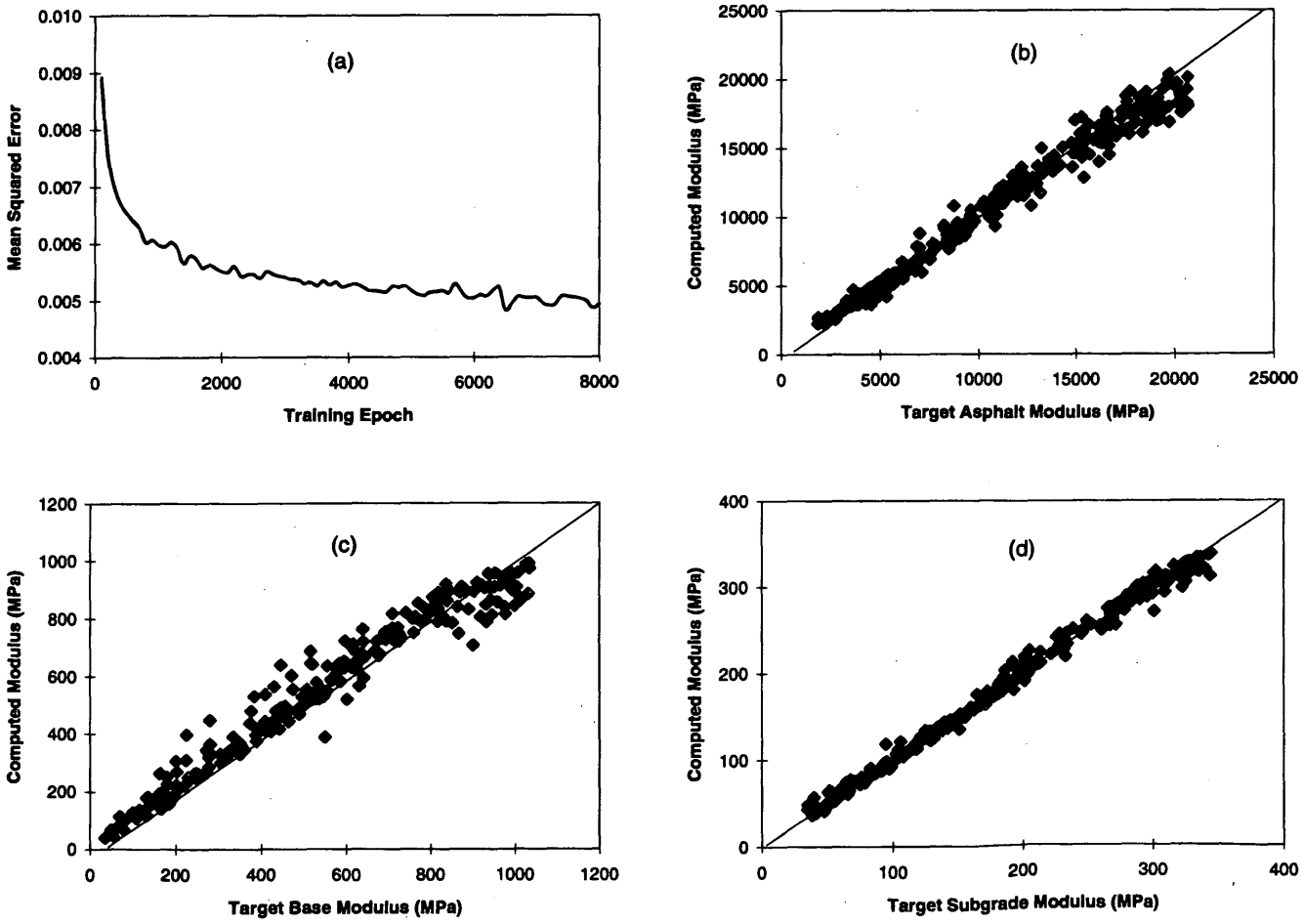

FIGURE 8 Training progress (*a*) and testing results for asphalt (*b*), base (*c*), and subgrade (*d*) moduli.

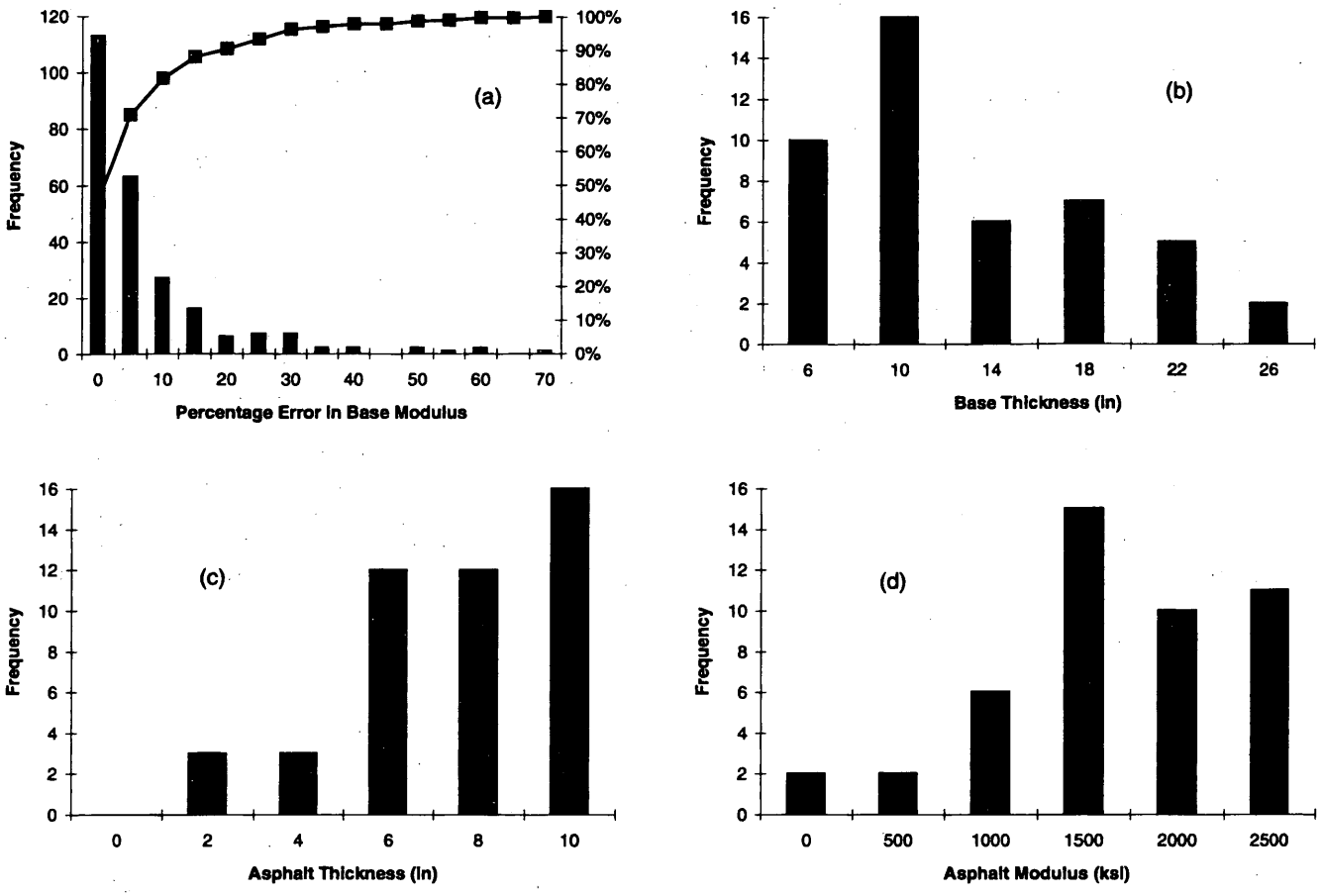

FIGURE 9 Error distribution and pavement layer property distributions for 80th percentile errors.

base modulus error tend to have a relatively rigid (thin, stiff or both) asphalt layer and a relatively thin base course. The rigidity of the surface layer makes the thin base layer essentially invisible, a problem inherent to the FWD test itself.

SUMMARY AND CONCLUSIONS

A previous study (*9*) showed that an artificial neural network could be trained to backcalculate pavement layer moduli from FWD deflection basins. That study used synthetic deflection basins calculated by using a static analysis of pavement response. In the present study an artificial neural network was successfully trained to backcalculate pavement layer moduli from synthetic deflection basins calculated by using a dynamic analysis of pavement response based on Green functions. Because the FWD test is inherently dynamic, these dynamic deflection basins are a significantly better analogue for the experimental results that would be obtained in the field.

Because the computational efficiency of the trained neural network is independent of the computational complexity of the algorithms used to create the training data, this neural network takes no longer to run than those in the previous study, and it still runs in real time. The authors know of no other method for backcalculating pavement layer moduli from dynamic deflection basins in real time.

ACKNOWLEDGMENTS

The information presented herein, unless otherwise noted, was obtained from research conducted by the U.S. Army Engineer Waterways Experiment Station. The authors acknowledge the advice and support provided throughout the study by Albert J. Bush III and Don R. Alexander of the Waterways Experiment Station. The authors acknowledge the assistance and encouragement provided by José M. Roesset of the University of Texas at Austin and Eduardo Kausel of the Massachusetts Institute of Technology.

REFERENCES

1. Bush, A. J., III. *Nondestructive Testing for Light Aircraft Pavements, Phase II: Development of the Nondestructive Testing Methodology*. Report FAA-RD-80-9-II. FAA, U.S. Department of Transportation, 1980.
2. Uzan, J., R. L. Lytton, and F. P. Germann. General Procedure for Backcalculating Layer Moduli. In *Nondestructive Testing of Pavements and Backcalculation of Moduli* (A. J. Bush III and G. Y. Baladi, eds.). ASTM 1026. ASTM, Philadelphia, 1989, pp. 217–228.

3. Van Cauwelaert, F. J., D. R. Alexander, T. D. White, and W. R. Barker. Multilayer Elastic Program for Backcalculating Layer Moduli in Pavement Evaluation. In *Nondestructive Testing of Pavements and Backcalculation of Moduli* (A. J. Bush III and G. Y. Baladi, eds.). ASTM 1026. ASTM, Philadelphia, 1989, pp. 171–188.
4. Foinquinos, R., J. M. Roesset, and K. H. Stokoe II. Response of Pavement Systems to Dynamic Loads Imposed by Nondestructive Tests. Presented at 73rd Annual Meeting of the Transportation Research Board, Washington, D.C., 1993.
5. Chang, D. W., V. Y. Kang, J. M. Roesset, and K. H. Stokoe II. Effect of Depth to Bedrock on Deflection Basins Obtained with Dynaflect and FWD Tests. In *Transportation Research Record 1355*, TRB, National Research Council, Washington, D.C., 1990, pp. 8–16.
6. Davies, T. G., and M. S. Mamlouk. Theoretical Response of Multilayer Pavement Systems to Dynamic Nondestructive Testing. In *Transportation Research Record 1022*, TRB, National Research Council, Washington, D.C., 1985, pp. 1–7.
7. Shao, K.-Y., J. M. Roesset, and K. H. Stokoe II. *Dynamic Interpretation of Dynaflect and Falling Weight Deflectometer Tests on Pavement Systems*. Research Report 437-1. Center for Transportation Research, University of Texas at Austin, Aug. 1986.
8. Ketchum, S. A. Dynamic Response Measurements and Identification Analysis of a Pavement During Falling Weight Deflectometer Experiments. In *Transportation Research Record 1415*, TRB, National Research Council, Washington, D.C., 1993, pp. 78–87.
9. Meier, R. W., and G. J. Rix. Backcalculation of Flexible Pavement Moduli Using Artificial Neural Networks. Presented at 73rd Annual Meeting of the Transportation Research Board, Washington, D.C., 1993.
10. Wasserman, P. D. *Advanced Methods in Neural Computing*. Van Nostrand Reinhold, New York, 1993.
11. Lukanen, E. O. Effects of Buffers on Falling Weight Deflectometer Loadings and Deflections. In *Transportation Research Record 1355*, TRB, National Research Council, Washington, D.C., 1993, pp. 37–51.
12. Thomson, W. T. Transmission of Elastic Waves Through a Stratified Soil Medium. *Journal of Applied Physics*, Vol. 21, No. 1, Feb. 1950, pp. 89–93.
13. Haskell, N. A. The Dispersion of Surface Waves on Multilayered Media. *Bulletin of the Seismological Society of America*, Vol. 43, No. 1, Feb. 1953, pp. 17–34.
14. Kausel, E., and J. M. Roesset. Stiffness Matrices for Layered Soils. *Bulletin of the Seismological Society of America*, Vol. 71, No. 6, Dec. 1981, pp. 1743–1761.
15. Kausel, E., and R. Peek. Dynamic Loads in the Interior of a Layered Stratum: An Explicit Solution. *Bulletin of the Seismological Society of America*, Vol. 72, No. 5, October 1982, pp. 1459–1481.
16. Hull, S. W., and E. Kausel. Dynamic Loads in Layered Half-Spaces. *Proc., Fifth Engineering Mechanics Division Specialty Conference*, Laramie, Wyo., New York, ASCE, 1984.
17. Young, D. M., and R. T. Todd. *A Survey of Numerical Mathematics*, Vol. II. Dover Publications, Inc., New York, 1973, pp. 918–920.
18. Sanchez-Salinero, I. *Analytical Investigation of Seismic Methods Used for Engineering Applications*. Ph.D. thesis, University of Texas at Austin, May 1987.
19. Standard Test Method for Deflections with a Falling-Weight-Type Impulse Load Device. In *Annual Book of ASTM Standards*, Vol. 04.03, ASTM, Philadelphia, 1993, pp. 566–568.
20. Matsuoka, K. Noise Injection into Inputs in Back-Propagation Learning. *IEEE Transactions on Systems, Man, and Cybernetics*, Vol. 22, No. 3, 1992, pp. 436–440.
21. Irwin, L., W. Yang, and R. Stubstad. Deflection Reading Accuracy and Layer Thickness Accuracy in Backcalculation of Pavement Layer Moduli. In *Nondestructive Testing of Pavements and Backcalculation of Moduli* (A. J. Bush III and G. Y. Baladi, eds.). ASTM 1026. ASTM, Philadelphia, 1989, pp. 229–244.

The views of the authors do not purport to reflect the position of the Department of the Army or the U.S. Department of Defense.

Publication of this paper sponsored by Committee on Strength and Deformation Characteristics of Pavement Sections.

Evaluation of Roller-Compacted Concrete Pavements Using Nondestructive Load Testing

CHUNG-LUNG WU AND H. A. (ALAN) TODRES

Nondestructive load testing was carried out to study the behavior of roller-compacted concrete (RCC) pavements located at Moran and Conley Terminals, Boston, Massachusetts. Tests were conducted in late October 1990 with a Dynatest 8081 heavy weight deflectometer. Loads were applied at various locations on each of the 11 selected test sections. Measured deflections were first used to estimate the in situ pavement parameters. The estimated values were then used, in conjunction with a concrete pavement analysis program, to evaluate the structural performances of the pavement sections. Also, load transfer efficiency across joints and cracks was evaluated, and laboratory tests were performed on cores taken from the pavements. From the study it was found that RCC generally possessed engineering properties similar to those of conventional concrete. However, the RCC modulus of elasticity appeared to be lower than that of portland cement concrete. Large variations in load transfer efficiency were observed. The structural performance of the RCC pavement test sections in the study appeared to be adequate.

Since the first large-scale construction of roller-compacted concrete (RCC) pavement in British Columbia, Canada, in 1976 the use of RCC pavements has gained great popularity in recent years. The primary uses of RCC as paving material have been for off-highway facilities and for heavy-duty secondary roads. It is generally agreed among pavement engineers that it is less expensive to construct RCC pavements than asphalt concrete (AC) and portland cement concrete (PCC) pavements, and savings of 30 percent can usually be expected. The maintenance costs for RCC pavements are also less than those for AC pavements. Another important advantage over AC pavements offered by RCC pavements is their resistance to chemical attack from hydraulic fluid, fuel, and other hydrocarbons.

Because RCC was a relatively new material and no specific design methods were available, most of the RCC pavements were designed following the guidelines used for designing conventional PCC pavements. This was based on the assumption that RCC possesses engineering properties similar to those of PCC. As part of a research effort sponsored by the Portland Cement Association (PCA) to advance the technology for RCC pavements, nondestructive load testing was conducted to evaluate the RCC pavements at Moran and Conley Terminals, Boston, Massachusetts. The objective of this research work was to study RCC pavement behavior under loading, and thus to assess the suitability of using conventional pavement thickness design procedures for RCC pavements.

Construction Technology Laboratories, Inc., 5420 Old Orchard Road, Skokie, Ill. 60077.

BACKGROUND

The use of RCC pavement was pioneered in North America by the U.S. Army Corps of Engineers. In 1975 a test section of 3.7 × 32.0 m (12 × 105 ft) was placed by the Waterways Experiment Station as part of a street in Mississippi (*1*). However, the first large-scale construction of RCC pavement, a 16,000-m^2 (4-acre) log-sorting yard, took place in British Columbia, Canada, in 1976 (*2*). The pavement slabs, with a thickness of 355 mm (14 in.), were placed in two lifts. Slab thickness design was based essentially on engineering judgment and experience obtained from cement-stabilized base. No joints other than construction joints were provided. Slabs were allowed to crack naturally, and the spacing was generally in the range of 12 to 18 m (40 to 60 ft).

Following the success of the first application, several other log-sorting yards in British Columbia were constructed with RCC. All of the pavements had the same thickness, 355 mm (14 in.), as the first pavement, and the same design concept used for the first pavement was used. Usually, the remainder of the structural system consisted of a 150-mm (6-in.) granular subbase placed over a consolidated subgrade. The design method for RCC pavements currently used in Canada is the PCA's airport thickness design procedure.

In the United States the first production project of RCC pavement, a test section 71.4 m (234 ft) long by 6.1 m (20 ft) wide, was constructed at Fort Stewart, Georgia, in July 1983 (*3,4*). The pavement had a slab thickness ranging from 230 to 330 mm (9 to 13 in.) and currently serves as an access from a tracked-vehicle parking area to a series of tank trials. In July 1984 a 15 000-m^2 (18,000-yd^2) RCC parking area was constructed at Fort Hood, Texas. This 255-mm (10-in.)-thick pavement was designed to carry 54 000-kg (120,000-lb) tracked vehicles as normal traffic.

Because of their early success, RCC pavements have been used on several large-scale projects since 1985. These projects include the following:

- An aircraft parking apron at Portland International Airport, Portland, Oregon, 1985 (*5*).
- An intermodal yard (Rennick Yard) at Denver, Colorado, 1986 (*6*).
- An army base at Fort Drum, New York, 1988 and 1989 (*7*).
- Various projects at Tasmania, Australia, 1986 and 1987 (*8*).
- High-speed test sections near Melbourne, Australia, 1988 and 1989 (*9*).

The use of conventional rigid pavement design procedures for RCC pavements was based on the assumption that RCC possesses engineering properties similar to those of PCC. This assumption

was later justified by strength testing conducted on cores and laboratory specimens obtained from various RCC pavements. However, RCC is likely to show lower density, and hence lower strength, in the areas near construction joints, where compaction is often less effective because of a lack of edge support.

In a laboratory study to evaluate RCC material properties, Tayabji and Okamoto (*10*) also concluded that the engineering behavior of RCC was similar to that of conventional normal-weight concrete. Based on that study a pavement thickness design procedure for RCC was developed (*11*). This procedure essentially followed the same concept used in conventional rigid pavement design, with the substitution of a different fatigue curve. The specific RCC fatigue relationship, which was similar to the PCC fatigue relationship, was developed from RCC beams sawed from full-scale RCC test panels.

FIELD AND LABORATORY TESTING

Description of Test Sections

Both Moran and Conley Terminals are located at Boston Harbor, Massachusetts, serving as container storage and transshipping yards. RCC pavements were designed to support the weights of the containers as well as the equipment used to transport them. The primary transporting device used at Moran is a special-purpose front-end loader, the Marathon LeTourneau Letro-Porter (nicknamed Hurdy-Gurdy at the site). This is an extremely heavy machine with a maximum rated single wheel load of about 400 kN (90,000 lb). Several Letro-Porters were in use at Moran at the time of testing. Subsequently, one was transferred to Conley, which up to then had been solely a tractor and trailer operation.

It was reported that the Moran RCC pavements consisted of an RCC layer of 380 mm (15 in.), a 230-mm (9-in.) gravel subbase, and a compacted subgrade. RCC slabs were constructed in three lifts of 140, 140, and 100 mm (5.5, 5.5, and 4 in.) from bottom to top. No transverse contraction joints except construction joints were provided during construction. Instead, the slabs were allowed to crack naturally. It was somewhat surprising to note that very long crack spacing (greater than 30.5 m or 100 ft) was not uncommon at the Moran RCC pavement site. Both the construction joints and cracks showed widely different performances. Some have remained in relatively good condition, whereas others have badly deteriorated. Slab width varied, ranging from 4.3 to 8.2 m (14 to 27 ft).

Four RCC pavement sections were selected for testing. They were designated Slabs M1 through M4. Slab dimensions were about 30.5 × 4.9 m (100 × 16 ft), 30.5 × 8.2 m (100 × 27 ft), 39.0 × 8.2 m (128 × 27 ft), and 30.5 × 4.6 (100 × 15 ft) for Slabs M1, M2, M3, and M4, respectively. Although Slabs M1, M2, and M3 were enclosed by construction joints and cracks, two sides of Slab M4 were adjacent to an area of asphalt pavement, thus approximating the free-edge condition. Deflections for determination of load transfer efficiency (LTE) were also measured at locations throughout the site. LTE was defined as the deflection measured at the unloaded side divided by that measured at the loaded side, expressed as a percentage.

The design thickness of the Conley RCC slab was 455 mm (18 in.), constructed in three lifts of 165, 165, and 125 mm (6.5, 6.5, and 5.0 in.) from bottom to top. A 200-mm (8-in.)-thick dense graded, crushed stone base was placed under the RCC slab. The subgrade material was mainly composed of sand, silt, and cobbles.

Seven RCC pavement sections, designated Slabs C1 through C7, were selected for testing. Dimensions for Slabs C1 to C7 were 19.5 × 5.1, 29.0 × 3.7, 36.3 × 5.1, 15.3 × 4.8, 15.3 × 5.1, 44.5 × 5.6, and 44.5 × 5.8 m (64 × 16.7, 95 × 12, 119 × 16.7, 50 × 15.8, 50 × 16.7, 146 × 18.3 and 146 × 19 ft), respectively. Additional locations were also chosen for load transfer deflection measurements.

Dynamic Load Testing

Tests were performed in late October 1990. A Dynatest 8081 heavy weight deflectometer (HWD) was used to provide the dynamic loads in the tests. The HWD is a device similar to a falling weight deflectometer, which delivers an impulse load to the pavement surface through a loading plate. However, the HWD has a much higher load capacity [greater than 265 kN (60 kips)], which is needed to generate realistically measurable pavement responses in such thick sections. The diameter of the loading plate is 450 mm (17.7 in.). Dynamic loads were applied at positions along both longitudinal and transverse joints and along transverse lines 4.9 m (16 ft) from the transverse joints. Loads were also placed at adjacent slabs along the transverse joints. This was done to evaluate if the LTE would stay the same with loads applied at different sides of the joints.

Deflections were measured by velocity transducers placed at the center of the loading area and outward to 1.5 m (5 ft) at 0.3-m (1-ft) intervals. A sensor was also placed at the opposite side of the load, 0.3 m (1 ft) from the loading center. Four different load levels, approximately 90, 155, 200, and 265 kN (20, 35, 45, and 60 kips), were used for each load position. Two drops were performed for each load level. The typical loading and sensor layouts are displayed in Figure 1. Each load position was identified by a station number, such as S1.1, S3.1, and S12.2. Additional load transfer measurements were conducted on different types of joints on slabs located through the Moran and Conley RCC sites.

The weather was cloudy and cool and the RCC pavement surface temperature varied between 9°C and 11°C (48°F and 52°F) during the entire testing process.

Laboratory Testing

Three RCC cores were taken from each slab tested at Moran Terminal, whereas two cores were taken from each of the RCC test slabs tested at Conley Terminal. The diameter of the cores was 95 mm (3.75 in.). After initial examination of bonding between lifts and measurements of specimen lengths, all of the cores were cut into either two or three pieces. Laboratory tests were then conducted on all prepared cores to determine the unit weight, compressive strength, split tensile strength, and RCC modulus of elasticity. The direct shear test was also performed on a few specimens from the Moran RCC pavement. All of the tests conducted followed the standard procedures of ASTM.

ANALYSIS OF TEST RESULTS

Estimation of K and E_c from HWD Deflection Measurements

By using the backcalculation procedure ECOPP developed at Construction Technology Laboratories, Inc. (*12*), RCC pavement pa-

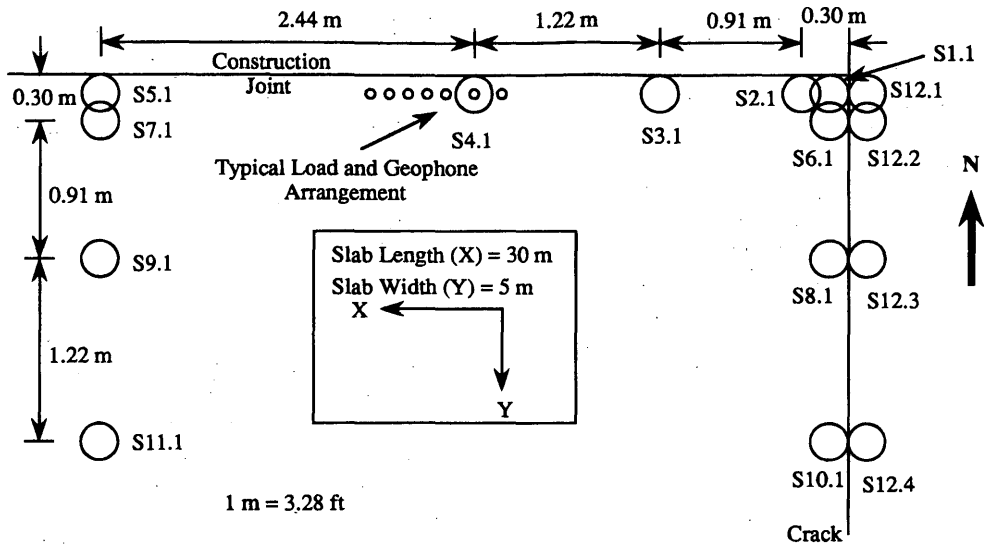

FIGURE 1 Typical HWD testing plan.

rameters were estimated on the basis of the deflections measured at the center load positions. In this procedure regression equations were developed from theoretical deflection data to estimate the RCC elastic modulus (E_c) and the modulus of subgrade reaction (K).

HWD deflections should be used with caution when attempting to backcalculate pavement material properties. It is a well-known fact that the temperature differential in a concrete slab will cause it to curl. When the top of the slab is warmer than the bottom, it will curl up at the slab interior and lose partial contact with the subbase or subgrade. Since deflections measured at slab interiors are usually used for the backcalculation process, the results might be misleading if deflections were collected under this situation.

To verify a complete support from the layer underneath, four load levels were used for each load position on the slabs. Slab M4 was excluded from the analysis since it was not subjected to a center load condition. An examination of the load-deflection characteristic for the center load position (S11.1) was made for each of the test slabs. It was observed that although a linear load-deflection relationship existed for Moran test slabs, Conley test slabs exhibited nonlinear behavior under center load conditions. The measured center load deflections are listed in Table 1.

Although showing some nonlinearity, attempts were still made to estimate the Conley RCC pavement parameters from the HWD deflections, and large variations in the estimated values were observed, especially for the lower load levels. However, for the two higher load levels, the estimated values showed some consistency. It was believed that the larger loads might have restored the pavement support condition, and the deflections under them were used in the analysis.

Actual average RCC slab thicknesses measured from cores were 400, 370, and 375 mm (15.8, 14.5, and 14.8 in.) for Slabs M1, M2, and M3, respectively, and they were 440, 510, 505, 470, 470, 480, and 470 mm (17.3, 20.0, 19.8, 18.6, 18.5, 18.9, and 18.6 in.) for Slabs C1 through C7, respectively. Table 2 lists the estimated elastic moduli and moduli of subgrade reaction for the RCC slabs at different loads. In general, the estimated values at different load levels were close to one another except those obtained at the 90-kN (20-kip) load level on Slab M1, which were excluded from the analysis. The average estimated RCC elastic moduli compared favorably with laboratory-measured values determined from cores except for the values for Slab C3, which were also excluded from further analyses.

By using predicted RCC moduli and moduli of subgrade reaction, the deflection basins for the four different loads were computed and compared with measured values. It was observed that the computed and measured deflection basins matched well at distances 3 ft or more from the loads. They did not match well close to the loads. Computed deflections were always greater than the measured ones. The discrepancy might be attributed to the stress-dependent behavior of subgrade material. It was hypothesized that the subgrade was stiffer when it was closer to the load center than away from it.

Following the concept of resilient modulus of soil and using a trial and error process, as described previously (*12*), variable moduli of the subgrade reactions for the RCC pavements were determined. The adjusted moduli of the subgrade reactions are displayed in Table 3. A typical comparison of the deflections computed by the concrete pavement analysis program JSLAB with adjusted K values and the measured deflections is shown in Figure 2. The deflection basins matched well with each other (Figure 2). Thus, the estimated values were considered satisfactory in representing in situ pavement material properties.

Analysis of RCC Pavement Response Data

Similar to the behavior of conventional concrete pavements, for all of the test slabs corner loads were observed to produce the highest maximum deflections, whereas the smallest maximum deflections occurred at interior loading conditions. In general, the deflections measured at the joint center or the slab edge were between these two cases. At the highest load level of 265 kN (60 kips), the interior maximum deflections were 58, 42, and 41 percent of the corner maximum deflections for Slabs M1, M2, and M3, respectively. The interior deflection measurement location in Slab M4 was only 0.6 m (2 ft) inward from the edge and, therefore, was not considered representative for a true interior loading condition. For Conley test sec-

TABLE 1 Measured HWD Deflections Under Center Load Condition

Slab No.	Load (kN)	Deflection (microns)						
		Distance from Loading Center (m)						
		0.0	0.3	0.6	0.9	1.2	1.5	-0.3
M1	87	111	99	89	81	72	62	96
	158	180	169	150	140	125	109	164
	200	237	217	195	180	159	139	212
	268	298	274	246	226	201	175	267
M2	91	96	86	77	70	62	54	86
	164	174	154	138	127	114	100	151
	203	216	193	174	161	143	126	191
	282	279	243	218	199	177	155	241
M3	89	124	114	103	94	83	73	112
	160	219	198	181	170	150	133	195
	199	277	249	228	213	189	169	246
	267	351	312	283	258	232	207	302
C1	97	70	62	58	53	51	46	62
	176	125	108	100	95	87	78	107
	220	149	136	125	117	108	97	134
	292	180	167	150	140	131	116	164
C2	87	78	70	64	62	57	51	70
	157	136	122	112	104	98	87	124
	201	163	152	139	127	120	107	153
	265	196	183	170	157	142	128	184
C3	91	73	72	68	64	60	54	73
	166	146	127	115	109	101	90	125
	207	173	157	145	136	124	112	155
	281	211	191	176	165	149	131	190
C4	87	82	77	71	66	64	58	76
	157	144	132	123	118	108	100	133
	203	173	164	147	143	131	121	163
	268	209	196	178	170	156	142	196
C5	89	89	79	73	72	65	59	79
	161	158	139	128	121	111	103	136
	199	185	173	158	150	137	124	170
	275	219	207	186	172	160	146	204
C6	88	75	76	69	65	59	52	75
	157	147	132	121	116	104	93	130
	200	173	165	150	141	130	115	160
	264	217	197	181	169	153	137	191
C7	88	65	66	60	56	53	47	66
	162	147	117	107	100	92	81	116
	202	163	144	137	127	111	100	143
	275	198	178	165	152	134	117	174

1 kN = 225 lbf, 1 micron = $3.937*10^{-5}$ in., 1m = 3.28 ft

tions, at the highest load level of 265 kN (60 kips), the interior maximum deflections were 14, 17, 36, 34, 31, and 23 percent of the corner maximum deflections for Slabs C1 to C7, respectively, excluding Slab C3. These values were considerably lower than those found for Moran RCC slabs. It was also noted that, with similar RCC moduli and subgrade stiffnesses and thicker slabs, Conley RCC slabs had larger maximum corner deflections than Moran RCC slabs. This was explained by the much lower LTE values found in the Conley RCC pavements.

From the cores taken from the four slabs, average slab thicknesses were 400, 370, 375, and 410 mm (15.8, 14.5, 14.8, and 16.2 in.) for Slabs M1, M2, M3, and M4, respectively. However, with the greatest-slab thickness, corner deflections in Slab M4 were greater than those in the other three slabs. Among other factors that affect pavement deflection under loading, an important element might be the fact that Slab M4 was adjacent to a stretch of asphalt pavement, and the corner was more or less free.

The same load could cause a very different deflection, depending on which side of a joint it was placed, as evidenced by those measured along the transverse joints of Slabs M1 and M2. A ratio of close to 2:1 was noted. Also, a nonlinear load-deflection characteristic existed in stations with the higher deflections (Stations 12.1 and 12.2 for Slab M1 and stations 12.1 to 12.4 for Slab M2). This might be an indication that certain pavement defects, such as voids under the slabs and cracks in the slabs, existed in the pavement system.

Maximum deflections along the transverse joints, longitudinal joints, and transverse lines 4.9 m (16 ft) from the joints are plotted in Figure 3 and Figure 4 for the Moran and Conley test slabs, re-

TABLE 2 Measured and Estimated Pavement Parameters

Slab No.	Load (kN)	Estimated ℓ (mm)	Estimated Subgrade Modulus (MPa/m)	Estimated RCC Modulus (MPa)	Measured RCC Modulus (MPa)	Difference (%)
M1	89	909*	104*	12,928*	17,741	11.0
	156	1029	97	19,839		
	200	1018	97	18,829		
	267	1022	103	20,414		
	Avg.	1023	99	19,694		
M2	89	892	128	18,944	19,399	-0.3
	165	872	132	17,887		
	205	923	123	20,960		
	280	870	145	19,547		
	Avg.	889	132	19,335		
M3	89	976	87	17,505	16,083	14.9
	160	1009	84	19,154		
	200	1010	83	19,113		
	267	960	96	18,129		
	Avg.	989	88	18,475		
C1	222	1027	158	24,580	23,313	11.2
	289	1029	174	27,285		
	Avg.	1028	166	25,932		
C2	200	1148	117	18,167	20,867	-3.9
	267	1199	119	21,951		
	Avg.	1173	118	20,059		
C3*	205	1057	120	13,966	20,045	-29.0
	280	1031	138	14,479		
	Avg.	1044	129	14,223		
C4	205	1119	110	19,252	17,263	17.6
	267	1122	120	21,344		
	Avg.	1120	115	20,298		
C5	200	1103	104	17,359	19,428	-2.4
	276	1101	124	20,571		
	Avg.	1102	114	18,965		
C6	200	1186	102	21,230	18,067	2.7
	262	1046	126	15,890		
	Avg.	1116	114	18,560		
C7	200	1080	126	18,936	20,221	-6.3
	276	1038	147	18,951		
	Avg.	1059	137	18,943		

Note: * excluded from further analyses
1 kN = 0.225 kip, 1 mm = 0.0394 in., 1 MPa = 0.145 ksi, 1 MPa/m = 3.684 pci

spectively. Deflections were expressed as percentages of the maximum values for that particular series. For example, maximum values would occur under edge loading when loads were moving along the transverse lines. The distance from the corner or the joint was expressed in units of l (radius of relative stiffness). It was observed that, except for deflections along the transverse joint in Slab M1, the deflection ratio decreased as the load moved inward from the joints. The rate of deflection ratio decrease also decreased with increasing distance from the corner or joint. Excluding data from Slab M1 transverse joint loads, regression lines were developed for these three series of deflections. Although showing some scatter, with the coefficient of determination in the range of between 0.700 and 0.900, a decent relationship between the deflection ratio and the distance from the joint exists. It is also interesting to note that the three regression lines for Moran test slabs were very close to one another, suggesting that the relationship may be unique, regardless of the position of deflection measurements. However, the three regression lines were different for Conley RCC test sections.

Deflection measurements for LTE determination were made on Slabs M1 to M3, Slabs C1 to C7, and at other locations throughout the two RCC sites. Tests were conducted at 51 locations at Moran RCC sites and 66 locations at Conley RCC sites. The joints tested included construction joints and cracks in both longitudinal and transverse directions. LTE measurements were taken from both sides of the joints, and four load levels were used.

Earlier studies by the U.S. Army Corps of Engineers have revealed widely scattered LTE values on various RCC pavements. Therefore, joints with zero load transfer were generally assumed for RCC pavement thickness design. Similar variability in LTE values was observed in Moran and Conley RCC pavements. For Moran test sections the LTE values ranged from 18 to 87 percent, with an average value of 49 percent and a coefficient of variation of 40 per-

TABLE 3 Adjusted Modulus of Subgrade Reaction

Slab No.	Load (kN)	Adjusted Modulus of Subgrade Reaction (MPa/m)		
		Distance up to 0.9 m from load	Distance of 0.9 to 1.5 m from load	Distance above 1.5 m from load
M1	156	143	97	67
	200	145	97	66
	267	156	103	70
	Average	148	99	68
M2	89	202	128	83
	165	213	132	91
	205	193	123	87
	280	244	145	101
	Average	213	132	90
M3	89	133	87	61
	160	122	84	57
	200	123	83	58
	267	152	96	68
	Average	132	88	61
C1	222	203	158	131
	289	225	174	146
	Avg.	214	166	138
C2	200	150	117	98
	267	148	119	96
	Avg.	149	118	97
C4	205	138	110	89
	267	153	120	97
	Avg.	146	115	93
C5	200	128	104	86
	276	157	124	104
	Avg.	143	114	95
C6	200	124	102	82
	262	160	126	102
	Avg.	142	114	92
C7	200	161	126	98
	276	192	147	113
	Avg.	176	137	106

1 m = 3.28 ft, 1 kN = 0.225 kips, 1 MPa/m = 3.684 pci

cent. Similar LTE values were observed for both the shrinkage cracks and the construction joints. The average LTE was 48 percent for cracks, with a coefficient of variation of 44 percent, and 51 percent for construction joints, with a coefficient of variation of 37 percent. The LTE values for Conley pavements showed an even larger variation compared with those for the Moran slabs. They ranged from 12 to 100 percent, with the majority being less than 50 percent. The average LTE was 36 percent, with a coefficient of variation of 56 percent.

No trend in the LTE values at different points along a joint could be found. Some had similar LTE values across the joint, such as the transverse joint of Slab C2, and some showed different behaviors, such as the transverse joint of Slab C7. Therefore, it is essential to specify the locations of measurement when dealing with LTE determinations.

Analysis of Laboratory Test Data

Three cores were taken from each of Slabs M1 to M4, and two cores were taken from each of Slabs C1 to C7. All of the cores had a nominal diameter of 95 mm (3.75 in.). The core thicknesses were close to one another within each slab except for Slab C1, which had a 140-mm (5.5-in.) difference in length. However, some variations in thickness were noted between slabs. For Moran test sections the layers were found to be fully bonded for most of the cores, whereas the layers of half of the Conley cores were found to be separated. The interfaces between lifts could not be easily identified for the bonded specimens. All of the cores were cut into either two or three pieces after initial examination.

Direct shear tests were conducted on four cores before they were cut. The shear strengths were 6240, 2655, 1758, and 2069 kPa (905,

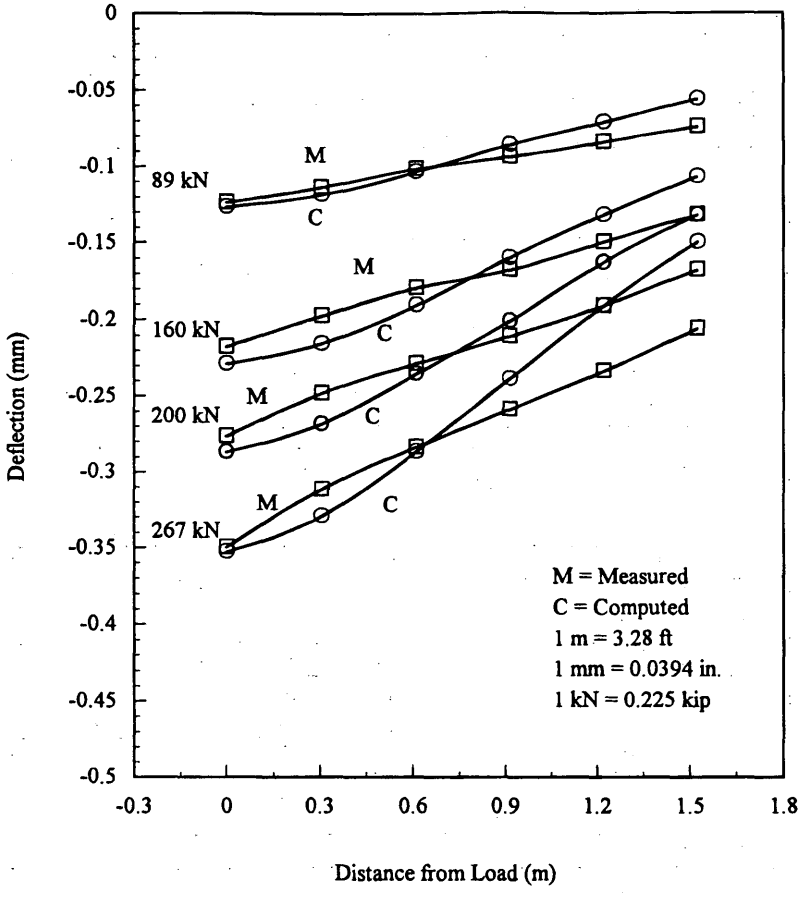

FIGURE 2 Typical comparison between measured and computed deflections.

385, 255, and 300 lb/in.^{2}) for these specimens, and the failure planes were coincident with the observed interfaces. It has been reported that for conventional normal-weight concrete constructed in a single lift, shear strength can vary from 35 to 80 percent of the compressive strength (*13*), or from 50 to 80 percent of the compressive strength (*14*). The RCC cores showed low shear strengths at the interfaces, ranging from 5 to 16 percent of the compressive strengths. Therefore, it is reasonable to hypothesize for design purposes that multi-layer construction of RCC pavements will result in weakened horizontal planes between lifts.

All prepared specimens were subjected to tests to determine the RCC modulus of elasticity and unit weight. Compressive strength and split tensile strength were also determined for selected samples. Table 4 lists all of the laboratory test results. It can be observed that the values of compressive strength, split tensile strength, and unit weight are comparable to those of conventional PCC, whereas the RCC moduli of elasticity were found to be less than the expected moduli of elasticity of PCC, with all other factors being equal.

It has been well documented that density (unit weight) is an important factor in affecting the strength of RCC. A small reduction in density will result in a significant decrease in strength (*15–17*). In this research an attempt was made to study the relationship between density and RCC strengths and elastic moduli. By using regression techniques the following equations were developed:

$$f_c' = 464 \cdot W - 63{,}189 \quad (1)$$
$$R^2 = 0.6311$$
$$n = 21$$

$$ST = 36.6 \cdot W - 4756 \quad (2)$$
$$R^2 = 0.6559$$
$$n = 50$$

where

f_c' = compressive strength (lb/in.^{2}),
W = density (pcf),
ST = split tensile strength (lb/in.^{2}), and
n = number of datum points.

Two datum points from Sample M1-2 at the middle and Sample M4-1 at the top were not used in deriving Equation 1 because of extreme values. Predicted compressive strengths and split tensile strengths ranged from 12.2 to 44.2 MPa (1,771 to 6,411 lb/in.^{2}) and from 2.5 to 5.1 MPa (368 to 734 lb/in.^{2}), respectively, for RCC, with densities being between 2240 and 2400 kg/m^3 (140 and 150 lb/ft^3). These values were comparable to those of normal-weight concrete.

Following the form of the American Concrete Institute (ACI) equation, the RCC modulus of elasticity can be estimated from its compressive strength and density by the following equation:

$$E_r = 21.6 \cdot W^{1.5} \cdot \sqrt{f_c'} \quad (3)$$
$$n = 23$$

where E_r is the modulus of elasticity of RCC (lb/in.^{2}).

Compared with the ACI equation for conventional PCC, with strength and density being equal, the modulus of elasticity of the

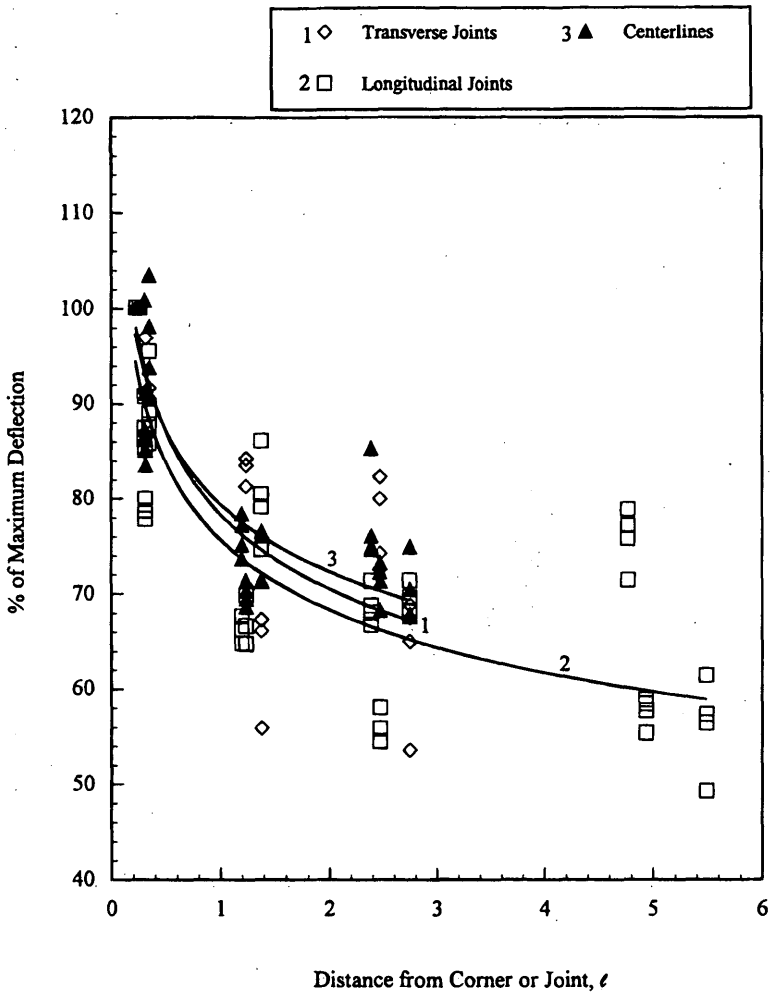

FIGURE 3 Deflection ratio versus distance, Moran Terminal.

RCC at the Moran and Conley Terminals was about 65 percent of that of regular PCC. Since the strength of RCC is comparable to that of PCC and a higher concrete elastic modulus will result in a higher stress in concrete slabs, the lower modulus of elasticity can be beneficial to RCC pavement performance.

Structural Evaluation of RCC Test Slabs

By using the estimated pavement parameters from the HWD deflection data and with the aid of the program JSLAB, the structural adequacy of the RCC slabs was assessed in two ways. In the first method the maximum stresses in the slabs caused by the anticipated traffic loads were computed. The computed maximum stresses were then used along with the RCC strengths and Miner's hypothesis to determine the number of loads that the pavements could take before failure. This number could be used to check if the design thickness was adequate. All of the loads were applied at the slab edge.

The second method, known as critical condition analysis, was based on the concept that a pavement system might fail under a single application of the worst possible condition rather than under fatigue. It had been established that a load applied at the slab edge with a high positive thermal gradient (the top warmer than the bottom) in the slab would induce the highest stress in the pavement slab. Furthermore, a free edge condition (no load transfer) was assumed in the analysis. It should be noted that instead of using variable moduli of subgrade reaction, the highest value was used for each slab because the analytical computer program could not handle both temperature gradient and variable modulus of subgrade reaction at the same time.

The tire load of a fully loaded Letro-Porter at slab edge and a temperature differential of +11°C (+20°F) were used in representing the worst possible condition. The use of +11°C (+20°F) was arbitrary since few data were available. However, with the thickness ranging from 380 to 510 mm (15 to 20 in.) and on the basis of experience with PCC pavements, it was believed that this number could realistically be achieved during summer days.

In their study Tayabji and Okamoto (*10*) developed relationships between RCC flexural strength and compressive strength for four different RCC mixes. The equations followed the form of the general ACI equation, $f_r' = C \cdot \sqrt{f_c'}$. The constant C ranged between 9.4 and 10.8 for the four RCC mixes, with an average value of 9.9, which was used in estimating the flexural strengths of the Moran and Conley RCC pavements. The fatigue equation developed in the same study was also used to predict the allowable number of load repetitions. These equations are given below:

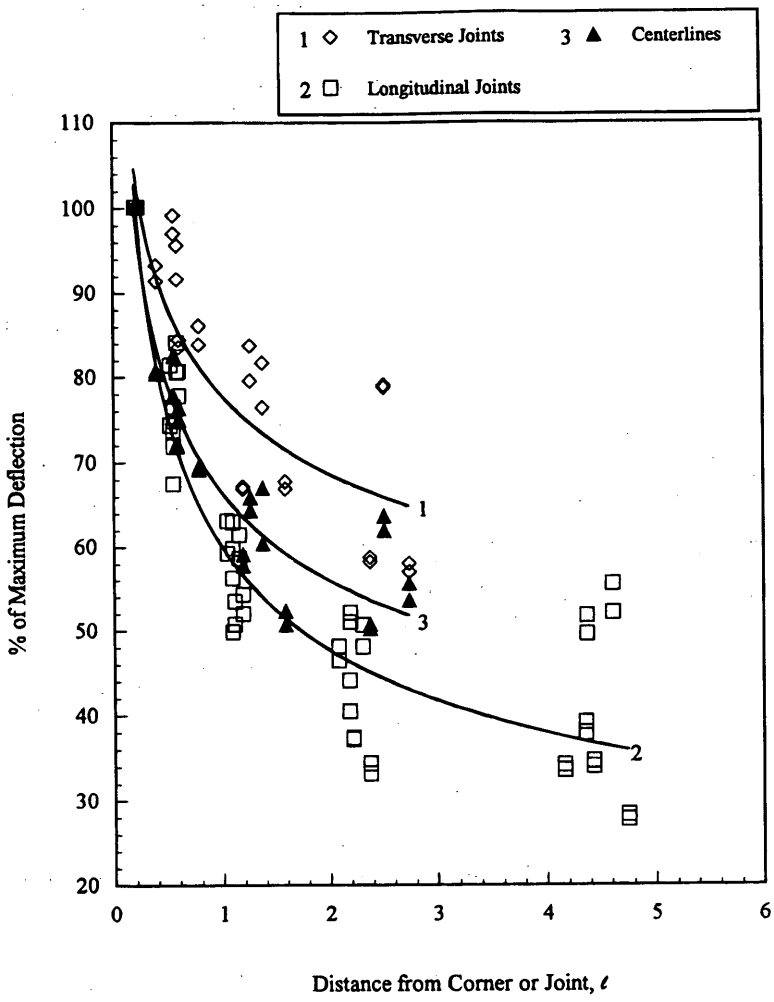

FIGURE 4 Deflection ratio versus distance, Conley Terminal.

$$f_r' = 9.9 \cdot \sqrt{f_c'} \quad (4)$$

$$SR = 118.31 - 10.73 \cdot \log (N) \quad (5)$$

where

f_r' = flexural strength (lb/in.^{2}),
f_c' = compressive strength, (lb/in.^{2}),
SR = stress to strength ratio (percent), and
N = allowable number of load repetitions.

The results of the structural evaluation are given in Table 5. The evaluation was not conducted for Slabs M4 and C1 because of insufficient data and for Slab C3 because of large errors in the estimated RCC elastic modulus. As observed, without considering the temperature effect, the stresses caused by the load ranged from 2.8 to 3.1 MPa (408 to 455 lb/in.^{2}) for the Moran test sections and from 2.0 to 2.2 MPa (288 to 323 psi) for the Conley RCC. The stress-to-strength ratios were 55, 63, and 72 percent, resulting in allowable load repetitions of 835,933, 151,822, and 20,225 for Slabs M1, M2, and M3, respectively. For a design life of 20 years, with operation 365 days a year, Slab M3 could take maximum load repetitions of about 3 times a day, whereas Slab M1 would be allowed to take more than 114 load repetitions each day at any given point. Although the structural performance of Slab M3 can be expected to be marginal, Slab M1 can be expected to last a long time. The large variations in the structural performance were mainly due to the variation observed in the actual strength of the RCC pavement and, to a lesser extent, in the thickness of the pavement.

The stress-to-strength ratio ranged from 32 to 51 percent for Conley RCC test sections. The allowable numbers of load repetitions were mostly unlimited except for Slab C2, which could take about 2 million load repetitions before failure. Therefore, the thickness design for Conley RCC slabs could be regarded as conservative.

Under the critical thermal-loading condition, stress-to-strength ratios were 80, 89, and 100 percent for Slabs M1, M2, and M3, respectively. A ratio of 100 percent would cause the slab to crack. However, this condition would probably rarely happen considering the assumption of free edge loading and a high thermal gradient in the slab. It can be predicted that Slabs M1 and M2 will perform better than Slab M3. With the stress-to-strength ratio ranging from 52 to 79 percent, it can be inferred that the Conley RCC test sections are structurally adequate. Results of the evaluation as well as laboratory tests have indicated great variability in the performances of RCC pavements and the material strengths of RCC pavements.

TABLE 4 Results of Laboratory Tests on RCC Specimens

Sample	Modulus of Elasticity (MPa)			Compressive Strength (kPa)			Split Tensile Strength (kPa)			Unit Weight (kg/m^3)		
No.	Top	Middle	Bottom	Top	Middle	Bottom	Top	Middle	Bottom	Top	Middle	Bottom
M1 – 1	16,475	20,787	17,114	*****	*****	*****	3,682	5,688	5,923	2295	2398	2387
M1 – 2	18,143	13,651	19,196	39,550	31,172	*****	*****	*****	867	2366	2409	2430
M1 – 3	17,322	18,699	18,281	*****	*****	46,569	4,358	5,509	*****	2332	2412	2414
M2 – 1	16,231	24,915	20,704	34,572	*****	35,895	*****	5,385	*****	2379	2390	2335
M2 – 2	18,185	19,362	15,044	*****	33,027	*****	4,661	*****	3,406	2363	2352	2270
M2 – 3	19,860	19,971	20,322	*****	*****	*****	4,827	5,351	4,496	2372	2395	2361
M3 – 1	19,278	17,699	15,457	*****	*****	*****	3,827	3,668	3,503	2289	2332	2244
M3 – 2	16,595	14,831	12,674	37,826	24,932	*****	*****	*****	2,006	2398	2297	2207
M3 – 3	16,522	18,298	13,394	*****	*****	21,306	3,330	4,068	*****	2324	2356	2311
M4 – 1	18,538	24,176	17,947	46,265	*****	*****	*****	6,316	5,006	2321	2430	2417
M4 – 2	17,328	22,914	20,306	*****	46,141	*****	3,158	*****	4,882	2281	2403	2379
M4 – 3	19,764	22,180	19,751	*****	*****	45,004	3,923	4,599	*****	2319	2379	2382
C1 – 1	20,864	*****	20,665	*****	*****	*****	540	*****	3,944	2356	*****	2360
C1 – 2	24,262	*****	27,459	*****	*****	*****	681	*****	3,647	2371	*****	2319
C2 – 1	16,354	19,309	21,111	*****	*****	*****	4,268	4,323	5,309	2382	2347	2408
C2 – 2	16,744	19,654	32,033	*****	*****	57,932	5,226	3,620	*****	2374	2372	2409
C3 – 1	17,066	20,252	17,208	*****	*****	*****	3,689	5,192	4,468	2366	2401	2385
C3 – 2	18,195	23,523	24,029	*****	*****	*****	4,799	5,109	5,502	2356	2392	2388
C4 – 1	19,312	15,143	17,175	35,123	21,437	29,069	*****	*****	*****	2356	2315	2308
C4 – 2	17,697	17,500	16,753	*****	*****	*****	4,378	3,441	3,434	2358	2326	2313
C5 – 1	22,439	19,041	19,828	41,480	44,328	40,812	*****	*****	*****	2352	2395	2374
C5 – 2	18,474	19,132	17,655	*****	*****	*****	4,061	5,130	3,275	2361	2401	2368
C6 – 1	14,147	20,868	17,837	*****	*****	*****	2,661	4,551	4,985	2310	2352	2339
C6 – 2	12,514	*****	24,971	22,471	*****	36,709	*****	*****	*****	2316	*****	2345
C7 – 1	11,678	*****	22,152	*****	*****	*****	4,378	*****	4,103	2390	*****	2396
C7 – 2	22,655	*****	24,399	32,462	*****	33,089	*****	*****	*****	2390	*****	2401

Note: ***** Not available

1 MPa = 0.145 ksi, 1kPa = 0.145 psi, 1 kg/m^3 = 0.0624 pcf

TABLE 5 Results of Structural Evaluation of RCC Test Sections

Slab No.	Load Only				Load & Thermal Gradient		
	Flexural Stress (kPa)	Flexural Strength (kPa)	Percent of Strength	Allowable Repetition, N	Flexural Stress (kPa)	Flexural Strength (kPa)	Percent of Strength
M1	2,813	5,137	55	835,933	4,096	5,137	80
M2	3,027	4,827	63	151,822	4,296	4,827	89
M3	3,137	4,351	72	20,225	4,351	4,351	100
C2	1,986	6,254	32	Unlimited	3,227	6,254	52
C4	2,227	4,392	51	1,997,217	3,489	4,392	79
C5	2,227	5,344	42	Unlimited	3,413	5,344	64
C6	2,151	4,475	48	Unlimited	3,303	4,475	74
C7	2,137	4,709	45	Unlimited	3,323	4,709	71

1 kPa = 0.145 psi

Therefore, it is suggested that an additional factor of safety be used in RCC pavement design.

CONCLUSIONS

From the analyses of the nondestructive load testing conducted on Moran and Conley Terminal RCC pavements, the following conclusions are drawn.

1. Estimated in situ pavement parameters, obtained by using the program ECOPP and the HWD deflection data, were considered to be reasonably accurate when compared with the values measured in the laboratory.
2. Under loading RCC pavements showed behavior similar to those of conventional concrete pavements. However, widely scattered LTE values across joints or cracks were observed. They ranged from 18 to 87 percent, with an average of 49 percent and a coefficient of variation of 40 percent, for Moran RCC slabs and from 12 to 100 percent, with an average of 36 percent and a coefficient of variation of 56 percent, for Conley RCC slabs.
3. The LTE values calculated by using deflection measurements at different locations along a joint may be quite different. Therefore, it is important to specify the exact locations in measuring and reporting LTE measurements.
4. For Moran and Conley test sections, the strengths and densities of RCC pavements were in the same range as those of PCC pavements, whereas RCC moduli of elasticity were found to be only about 65 percent of PCC moduli of elasticity, with all other factors being equal.
5. The strength of RCC was highly dependent on its density. A small reduction in density would reduce the strength considerably.
6. The RCC pavement design seemed to be adequate from the structural evaluation. However, because of the large variations in the material properties of RCC and field performance, a higher factor of safety may be needed in designing RCC pavements than in designing conventional concrete pavements.

ACKNOWLEDGMENTS

The research reported in this paper was conducted at Construction Technology Laboratories, Inc., with the sponsorship of PCA.

REFERENCES

1. Keifer, O., Jr. Paving with RCC. *Civil Engineering*. ASCE, Oct. 1987, pp. 65–68.
2. Piggott, R. W. Roller Compacted Concrete for Heavy-Duty Pavements: Past Performance, Recent Projects, and Recommended Construction Methods. In *Transportation Research Record 1062*, TRB, National Research Council, Washington, D.C., 1986, pp. 7–12.
3. Ragan, S. A. Evaluation of the Frost Resistance of Roller-Compacted Concrete Pavements. In *Transportation Research Record 1062*, TRB, National Research Council, Washington, D.C., 1986, pp. 25–32.
4. Keifer, O., Jr. Corps of Engineers Experience with RCC Pavements. *Proc., Conference on Roller Compacted Concrete II*, San Diego, Calif. Construction, Geotechnical Engineering, and Materials Engineering Divisions, ASCE, New York, 1988, pp. 429–437.
5. Abrams, J. M., J. L. Jacksha, R. L. Morton, and D. J. Irvine. Roller-Compacted Concrete Pavement at Portland International Airport. In *Transportation Research Record 1062*, TRB, National Research Council, Washington, D.C., 1986, pp. 20–24.
6. Delva, K. L. Rennick Yard RCC Pavement Design and Construction. Proc., *Conference on Roller Compacted Concrete II*, San Diego, Calif. Construction, Geotechnical Engineering, and Materials Engineering Divisions, ASCE, New York, 1988, pp. 410–418.
7. Cortez, E. R., and J. A. Gerlach. Roller-Compacted Concrete Pavement Construction at Fort Drum, New York. In *Transportation Research Record 1282*, TRB, National Research Council, Washington, D.C., 1990, pp. 8–17.
8. Brett, D. M. RCC Pavements in Tasmania, Australia. *Proc., Conference on Roller Compacted Concrete II*, San Diego, Calif. Construction, Geotechnical Engineering, and Materials Engineering Divisions, ASCE, New York, 1988, pp. 369–379.
9. Jameson, G. W., K. G. Sharp, and R. S. Rollings. An Investigation of the Use of Roller Compacted Concrete in a Heavily-Trafficked, High-Speed Application in Australia. *Proc., Fifth International Conference on Concrete Pavement Design & Rehabilitation*, Vol. 2, Purdue University, April 1993, pp. 281–292.
10. Tayabji, S. D., and P. A. Okamoto. Engineering Properties of Roller-Compacted Concrete. In *Transportation Research Record 1136*, TRB, National Research Council, Washington, D.C., 1987, pp. 33–45.
11. Tayabji, S. D., and D. J. Halpenny. Thickness Design of Roller-Compacted Concrete Pavements. In *Transportation Research Record 1136*, TRB, National Research Council, Washington, D.C., 1987, pp. 23–32.
12. Wu, C. L., H. A. Todres, and B. T. Bock. Comparison of Roller Compacted Concrete Pavement Responses to Static and Dynamic Loads. *Proc., Fifth International Conference on Concrete Pavement Design & Rehabilitation*, Vol. 2, Purdue University, April 1993, pp. 293–325.
13. Kosmatka, S. H., and W. C. Panarese. *Design and Control of Concrete Mixtures*, 13th ed. Portland Cement Association, Skokie, Ill. 1988, 5 pp.
14. Derucher, K. N., and C. P. Heins. *Materials for Civil and Highway Engineers*. Prentice-Hall, Inc., Englewood Cliffs, N.J., 1981, 137 pp.
15. Pittman, D. W. RCC Pavement Construction and Quality Control. *Proc., Conference on Roller Compacted Concrete II*, San Diego, Calif. Construction, Geotechnical Engineering, and Materials Engineering Divisions, ASCE, New York, 1988, pp. 439–453.
16. Pittman, D. W., and T. D. White. Roller-Compacted Concrete Pavements. *Proc., Third International Conference on Concrete Pavement Design & Rehabilitation*, Vol. 2, Purdue University, April 1985, pp. 107–112.
17. Todres, H. A., A. P. Jacobs, and L. S. Marzi. A New Mix Design Methodology for Roller Compacted Concrete, with Case Studies. Paper presented at *7th International Symposium on Concrete Roads*, Vienna, Austria, Oct. 3–5, 1994.

Publication of this paper sponsored by Committee on Strength and Deformation Characteristics of Pavement Sections.

Prediction of Effective Asphalt Layer Temperature

EARL H. INGE, JR., AND Y. RICHARD KIM

The most widely used method for evaluating deflection measurements for overlay design analysis is the 1993 *AASHTO Guide for Design of Pavement Structures*. Researchers and numerous users of the AASHTO overlay design procedure have challenged the accuracy of the AASHTO temperature correction procedure for deflections. In another paper presented at the 1995 TRB Annual Meeting a new temperature correction procedure was presented, and that procedure resulted in significant improvements over the AASHTO procedure. That procedure requires the middepth temperature of asphalt layers as input for the effective temperature of the layers. A new prediction method for an asphalt concrete middepth temperature on the basis of a data base approach is described. The major improvements over the AASHTO method are (a) air temperatures for the previous 5 days are not needed, which allows simpler and quicker deflection analyses in the North Carolina Department of Transportation (NCDOT), and (b) different temperature-depth gradients between the heating (morning) and the cooling (afternoon) cycles are taken into account. The comparison of the measured and predicted temperature demonstrated an acceptable degree of accuracy of this model for routine deflection analyses by state highway agencies. In addition to presenting the NCDOT temperature prediction procedure, an alternative temperature prediction model, known as BELLS equation, is also studied. Comparison of the measured pavement temperatures and the predicted values obtained by the BELLS equation showed underprediction of the one-third-depth temperatures at temperatures higher than 32°C (90°F).

The use of nondestructive deflection testing has become one of the primary means of determining the in situ structural capacities of existing pavements. Use of deflection measurements in flexible pavement design and analysis requires the adjustment of deflections to a reference temperature. The 1993 *AASHTO Guide for Design of Pavement Structures* (*1*) presents the temperature correction procedure for falling weight deflectometer (FWD) deflections. This procedure, however, has been reported to be inaccurate and impractical because of the use of the average air temperature for previous 5 days to predict pavement depth temperatures.

A research study sponsored by the North Carolina Department of Transportation (NCDOT) was recently performed by North Carolina State University. In that study a new temperature correction procedure for deflections was developed for flexible pavements in North Carolina. The procedure has been described by Kim and colleagues (this Record). One of the critical parameters to be determined by the procedure is the middepth temperature of asphalt layers, which represents the effective temperature of the layers. In this paper a data base approach to predicting the middepth temperature of asphalt concrete (AC) is presented.

E. H. Inge, Jr., Stroud, Pence, and Associates, 204A Grayson Road, Virginia Beach, Va. 23462. Y. R. Kim, Box 7908, Department of Civil Engineering, North Carolina State University, Raleigh, N.C. 27695–7908.

Similar research in dealing with temperature correction and temperature prediction was recently reported by Baltzer and Jansen (*2*) and Stubstad et al. (*3*). The major conclusion of their research was that the effective AC temperature is better represented by the one-third-depth temperature instead of the middepth temperature. By using the measured pavement depth temperatures from the Strategic Highway Research Program's Long-Term Pavement Performance Program data base, an equation, referred to as the BELLS equation, was developed as a means of predicting the one-third-depth temperature. The temperature data collected from the NCDOT study were used in checking the accuracy of the BELLS equation for predicting the one-third-depth temperature for North Carolina pavements.

MEASUREMENT OF PAVEMENT TEMPERATURES

Four pavement test sections in the Piedmont area of North Carolina were selected for use in performing FWD testing and temperature measurements. These sections are referred to as Section 17, US-70, Section 13, and Section 20. The thicknesses of the asphalt layers in these pavements are 89, 140, 191, and 229 mm (3.5, 5.5, 7.5, and 9 in.), respectively. These sections were instrumented with thermocouples at various depths of the asphalt layers. Each section was subjected to FWD testing and temperature measurements at four different seasons for a duration of 1 year. During each of the site visits the measurements were made on an hourly basis for 1 full day for each section. Details on the structural designs, instrumentation, and testing plans for these sections can be found in the paper by Kim et al. (this Record).

PREDICTION OF PAVEMENT TEMPERATURE: NCDOT PROCEDURE

The NCDOT temperature correction procedure presented by Kim et al. in this Record requires the determination of middepth temperature of the AC layer as the effective temperature. Because of the routine use and speed of FWD testing, it is desirable to predict the middepth temperature of the AC layer from readily available information without performing destructive tests. To develop a simple and accurate prediction model for the middepth temperature of the AC layer, a detailed study was carried out, using the measured data, on the change of temperature as a function of the AC layer thickness, depth in pavements, time of day, season, and so forth.

By a nondestructive technique the only two temperature parameters that can be measured are the air and pavement surface temperatures. Therefore, the temperature prediction procedure that relates

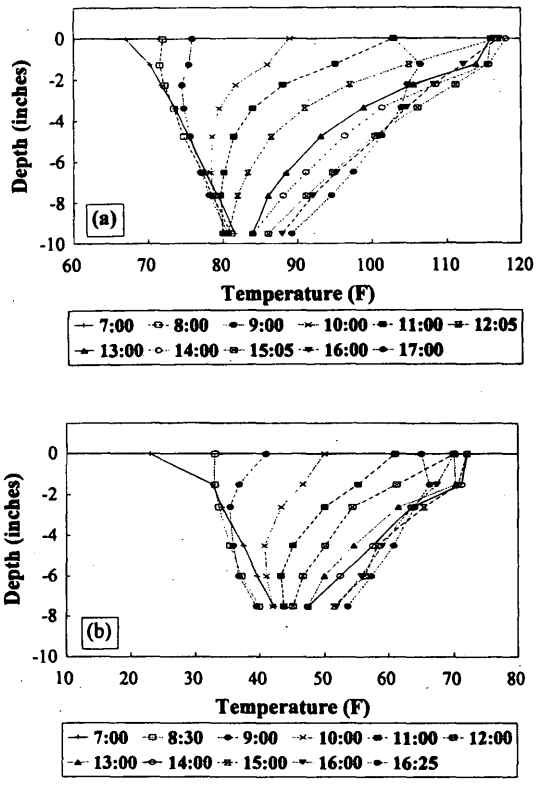

FIGURE 1 Temperature change as a function of pavement depth and time of measurement: (*a*) Section 20 in September; (*b*) Section 13 in February [1 in. = 25.4 mm; °C = (°F − 32)/1.8].

air or surface temperature to the middepth temperature is preferred for practical reasons. From the measured data a graph of pavement depth versus temperature can be plotted (Figure 1). Note in Figure 1 that surface temperatures move considerably, whereas temperatures at lower depths maintain greater consistency, resulting in cone shapes of pavement depth-versus-temperature graphs. Figure 2 displays the changes in various temperatures as a function of time of day by using the 24-hr data obtained from US-70 section [AC layer thickness of 140 mm (5.5 in.)] in May 1993. The surface temperature peaks at about 2 p.m., whereas the highest middepth and bottom temperatures occur at times somewhat delayed from that time. This delay in the peak temperature causes the change in the slope of the temperature pavement depth curves shown in Figure 1 before and after 2 p.m. The conclusion of this observation is that the slope of the temperature gradient varies with time, and neglecting it could result in significant errors in the predicted middepth temperatures. Therefore, a detailed study was carried out, using the measured temperature data, to develop a relationship between the slope of the temperature gradient and the time of day.

To investigate this relationship the temperature gradients for a particular time of day of a particular season were first grouped together, regardless of the thickness of the AC layer. Some examples are shown in Figure 3. Figures 3(*a*) and 3(*b*) contain the seasonal temperature data for four asphalt layer thicknesses. It can be observed from these figures that in most cases the temperature gradients of the four different AC layer thicknesses have similar curves. That is, the thinner pavements have the same temperature gradient shape as the thicker pavements, although the temperature gradients of the thinner pavements stop at shallower depths. This observation is very important in simplifying the temperature prediction procedure by eliminating the effect of AC layer thickness on the temperature gradient. This finding also suggests that the heat transfer mechanism in asphalt layers is the top–down process, meaning that the temperature gradients are more sensitive and more dependent on the surface temperatures than the base temperatures.

Further investigation of the effect of seasonal variation on the temperature gradient shape was done. In general, it was found that the difference in the surface temperatures between two seasons was greater than the difference in temperatures at the bottom of the AC layer between two seasons. This behavior suggested a possibility of parallel gradients for different seasons if the data were plotted on a logarithmic scale. The temperature gradients of all four sections for four seasons are presented in Figure 4 on a logarithmic scale. Since the surface temperature with a depth equal to zero could not be plotted on a log-log scale, this temperature was plotted at a depth equal to 0.1 in.

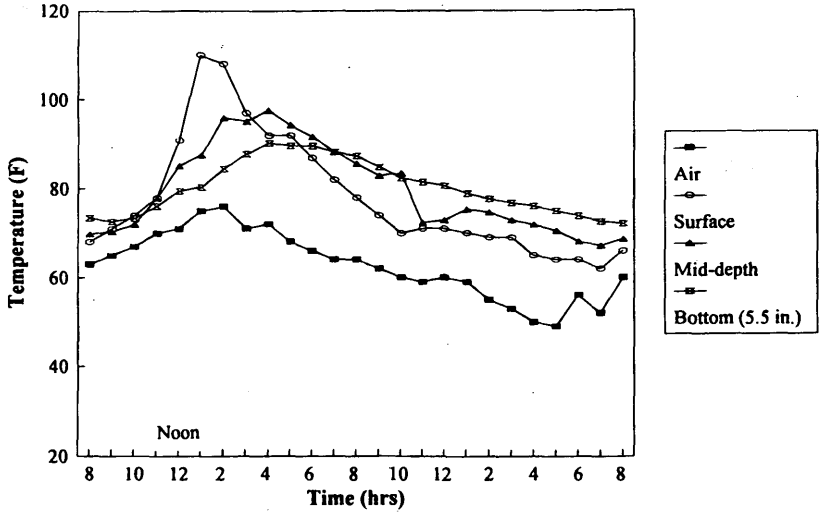

FIGURE 2 Change in temperatures during a 24-hr period measured for the US-70 Section in May 1993 [1 in. = 25.4 mm; °C = (°F − 32)/1.8]

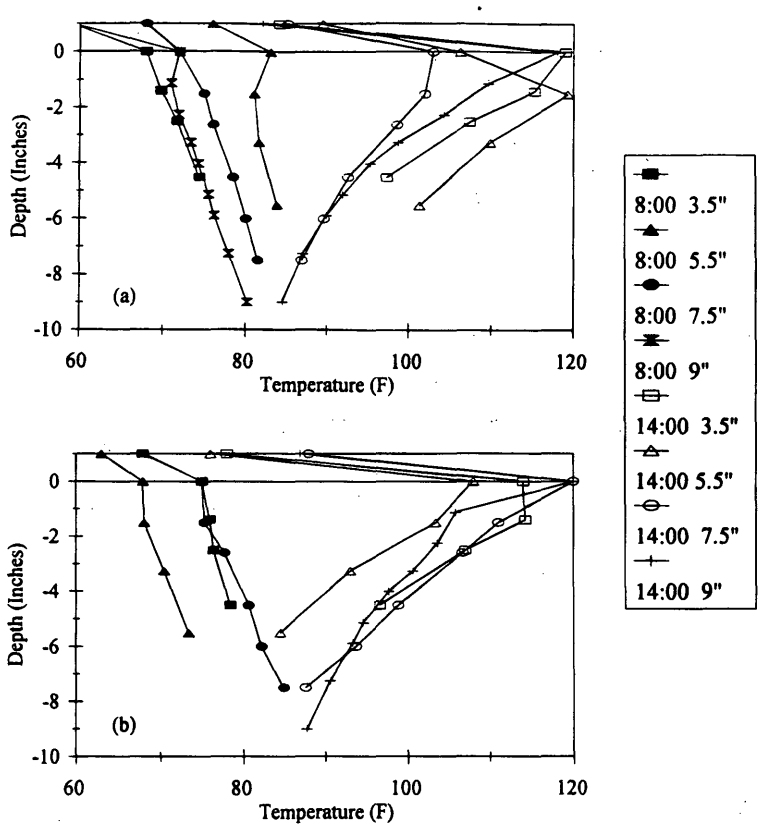

FIGURE 3 Temperature gradients for all four test sections at 8 a.m. and 2 p.m.: (*a*) September; (*b*) May [1 in. = 25.4 mm; °C = (°F − 32)/1.8].

Two important observations can be made from Figure 4. First, the temperature gradients on a logarithmic scale were composed of two straight lines, one above a depth of 38 mm (1.5 in.) depth and the other below a depth 38 mm. The significance of the 38 mm is due only to the fact that in most sections this was the depth where the shallowest thermocouple was installed. In fact, in Section 20, where the first sensor was installed at a depth of 25 mm (1 in.), depth a break in the linearity of the temperature gradient was found at a depth of 25 mm. Since the majority of the sections had first sensors at 38 mm, this depth was selected as the breakpoint for further analyses.

The second point to be made from Figure 4 is that the logarithmic temperature gradient lines are mostly parallel to each other regardless of season and time of day. This observation has a significant meaning in modeling the temperature gradient. Provided that a reference temperature gradient equation is determined for a particular time of day, one can measure the surface temperature at that time and predict the middepth temperature by shifting the reference curve to the surface temperature.

The relationship between the gradients can be proven to be parallel if the gradients are superposed when the individual gradients are all shifted along the temperature axis to one reference temperature. Since the only pavement temperature that can be measured nondestructively is the surface temperature, all of the temperature gradients at a particular time were first shifted to a reference surface temperature (Figure 5). The degree to which the gradients are superposed was not as precise as that required by the procedure. This discrepancy was due to the change in the slope of temperature gradients at 38 mm. Therefore, another shift was made to the reference 38-mm-depth temperature as shown in Figure 6. It can be seen from Figure 6 that the difference in gradients after the shift can be minimized by shifting the gradients to a reference 38-mm-depth temperature instead of a reference surface temperature. The degree to which the gradients are superposed is better, especially at depths greater than 38 mm. Use of the reference 38-mm-depth temperature also helps to minimize the effect of radiation or sunlight on the surface temperature.

Once all of the gradients were shifted to the reference 38-mm-depth temperature, as shown in Figure 6, a regression equation was derived to represent the temperature gradient shape below a depth of 38 mm for each working hour of the day (i.e., from 8 a.m. to 5 p.m.). The general form of the temperature gradient equation is

$$T_d = A \times d^B$$

where

T_d = pavement temperature at depth d,
d = pavement depth, and
A, B = regression constants.

Since the regression analyses were performed on the temperatures at depths below 38 mm from the surface, selection of the reference 38-mm-depth temperature was needed to represent an average 38-mm-depth temperature for the entire year at that particular hour of day. Regression constants and the reference 38-mm-depth temperature for each hour of the day are given in Table 1.

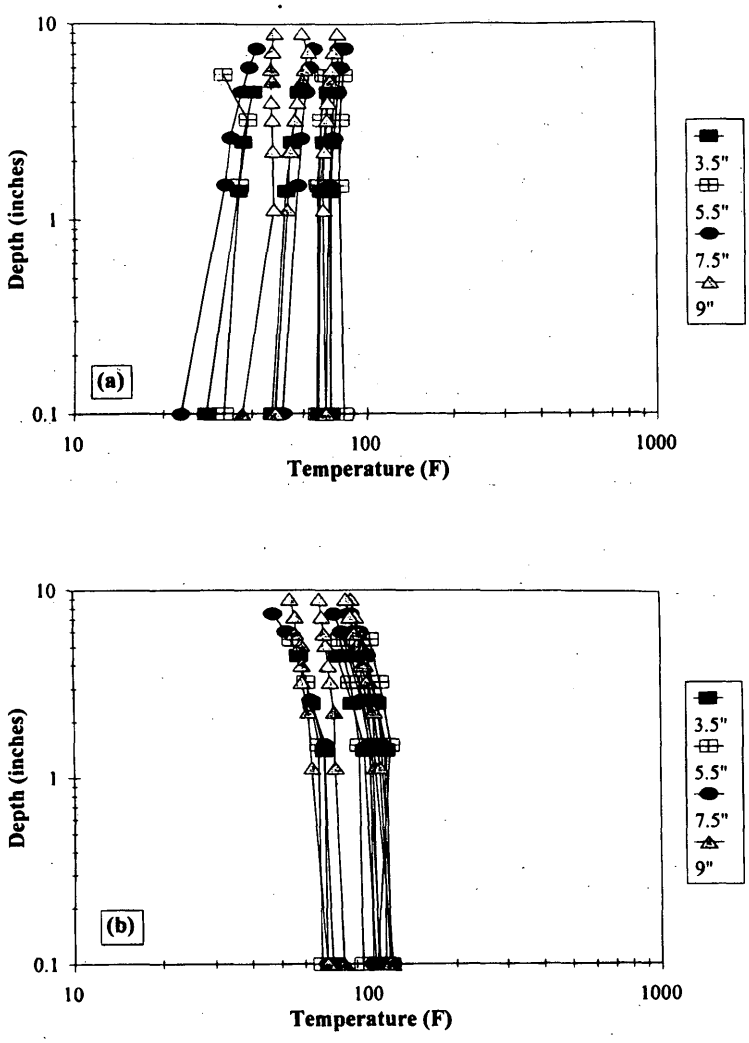

FIGURE 4 Temperature gradients for all four sections plotted on a log-log scale: (*a*) 8 a.m.; and (*b*) 2 p.m. [1 in. = 25.4 mm; °C = (°F − 32)/1.8].

Although the use of the 38-mm-depth temperature enhanced the accuracy of predicting the middepth temperature, it cannot be measured by nondestructive methods. Therefore, surface temperatures corresponding to the reference 38-mm-depth temperatures had to be determined. A reference surface temperature was selected for each hour of the day by identifying the average surface temperature when the pavement had a 38-mm-depth temperature close to the selected 38-mm-depth reference temperature given in Table 1. The reference surface temperatures for every hour of the day are also given in Table 1.

By using a measured surface temperature and the reference surface temperature, a shift factor can be developed. The shift factor is the ratio of the measured surface temperature to the reference surface temperature for a particular time. The shift factor provides a relationship between the reference gradient equation and the actual temperature gradient. By using the parallel nature of the gradients at a particular time of day, the shift factor for surface temperatures would also be a shift factor for the middepth temperature. The middepth of the asphalt layer can be substituted into the regression equation for a particular time to calculate a reference middepth temperature. The calculated middepth temperature can then be multiplied by the shift factor to obtain a final middepth temperature. An example of determining the middepth temperature by the NCDOT procedure is given below.

EXAMPLE OF MIDDEPTH TEMPERATURE PREDICTION

FWD tests were conducted at about 2 p.m. on a flexible pavement with a total AC thickness of 191 mm (7.5 in.). The measured surface temperature at the time of FWD testing was 18°C (65°F). The middepth temperature can be predicted in the following steps.

1. The general form of the temperature gradient equation is

$$T_d = A \times d^B$$

where

T_d = pavement temperature at middepth,
d = middepth, and
A, B = regression constants in Table 1.

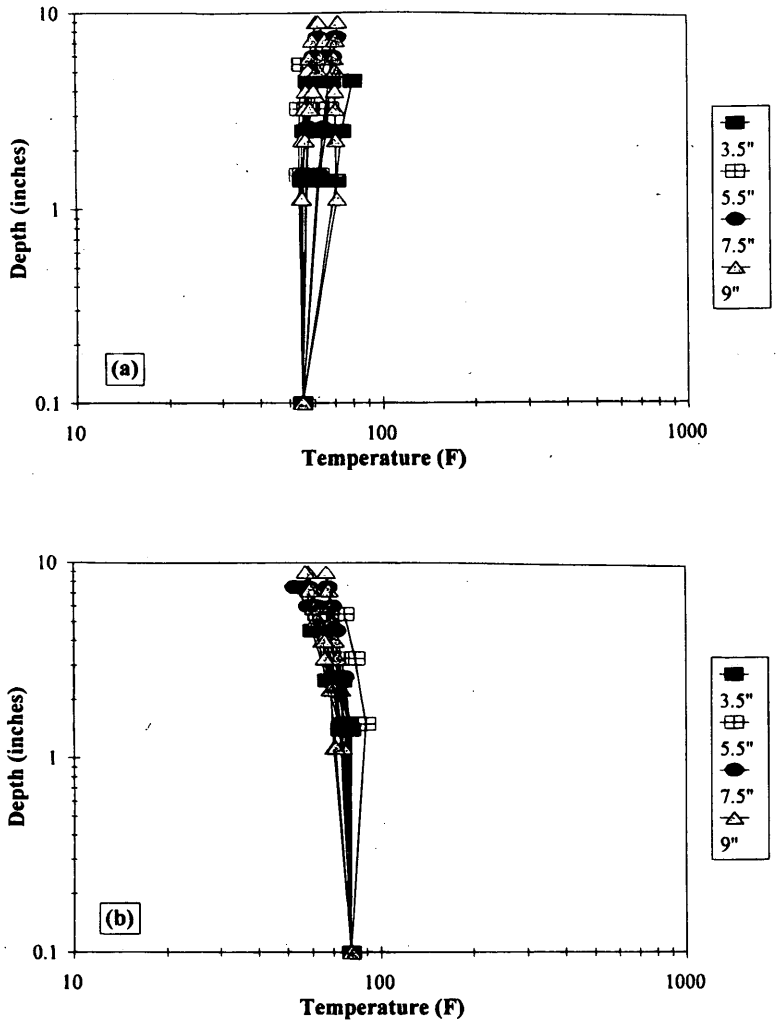

FIGURE 5 Temperature gradients shifted to a reference surface temperature: (*a*) 8 a.m.; (*b*) 2 p.m. [1 in. = 25.4 mm; °C = (°F − 32)/1.8].

In this example d is equal to 95 mm (3.75 in.) and A and B are 93.85 and −0.1173, respectively. Thus, the middepth temperature in the reference temperature gradient is 26.9°C (80.4°F).

2. Determine a shift factor by dividing the measured surface temperature (in °F) by the reference surface temperature for the time of FWD testing in Table 1. The shift factor adjusts the calculated reference middepth temperature in Step 1 to the actual middepth temperature corresponding to the input surface temperature.

Shift factor = 65/95 = 0.684

3. Multiply the calculated middepth temperature (in °F) from Step 1 by the shift factor from Step 2 to predict the actual middepth temperature.

Actual middepth temperature = 80.4 × 0.684 = 55°F

This procedure was applied to all of the measured data, and the accuracy of this method is demonstrated in Figure 7 by comparing the predicted middepth temperatures with the measured values. Actual application of this prediction method to the temperature correction procedure is presented in the paper by Kim et al. (this Record).

VALIDATION OF BELLS EQUATION

The widespread knowledge of the incorrect AASHTO procedure and the importance of temperature correction in using FWD deflections in pavement analysis have spawned various researchers to develop their own temperature correction procedures. Recently, Baltzer and Jansen (2) presented the temperature correction factors for backcalculated AC moduli and suggested that the effective AC temperature is the temperature at the one-third depth of the asphalt layer. The philosophy behind using the one-third-depth temperature instead of middepth or other depth temperatures is based on the relationships between the elastic modulus of AC and temperature. Their research showed that the variation in elastic modulus was less when it was plotted against the one-third-depth temperature. The reason for the smaller variation is that the heating and cooling of the asphalt at the one-third depth progressed at the same rate. The elastic modulus was of the same magnitude for a given temperature, independently of

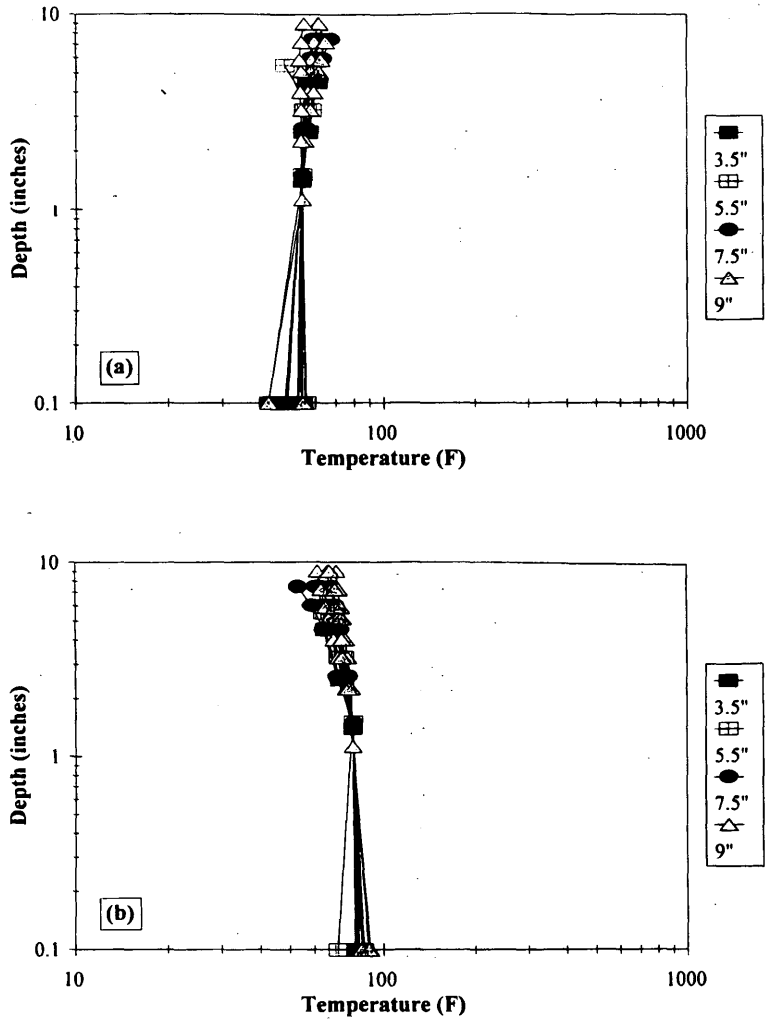

FIGURE 6 Temperature gradients shifted to a reference 38-mm (1.5-in.)-depth temperature: (*a*) 8 a.m.; (*b*) 2 p.m. [1 in. = 25.4 mm; °C = (°F − 32)/1.8].

TABLE 1 Regression Constants and Reference Temperatures for Each Hour of Day [°C = (°F − 32)/1.8]

Time of Day	A	B	Reference 38 mm Temperature (F)	Reference Surface Temp. (F)
8:00	53.79	0.0530	55	55
9:00	58.78	0.0225	60	60
10:00	65.42	-0.0283	65	70
11:00	76.83	-0.0914	75	79
12:00	83.75	-0.1433	80	86
13:00	88.61	-0.1246	85	95
14:00	93.85	-0.1173	90	95
15:00	89.27	-0.1151	85	85
16:00	83.65	-0.0926	80	80
17:00	78.20	-0.0768	75	76

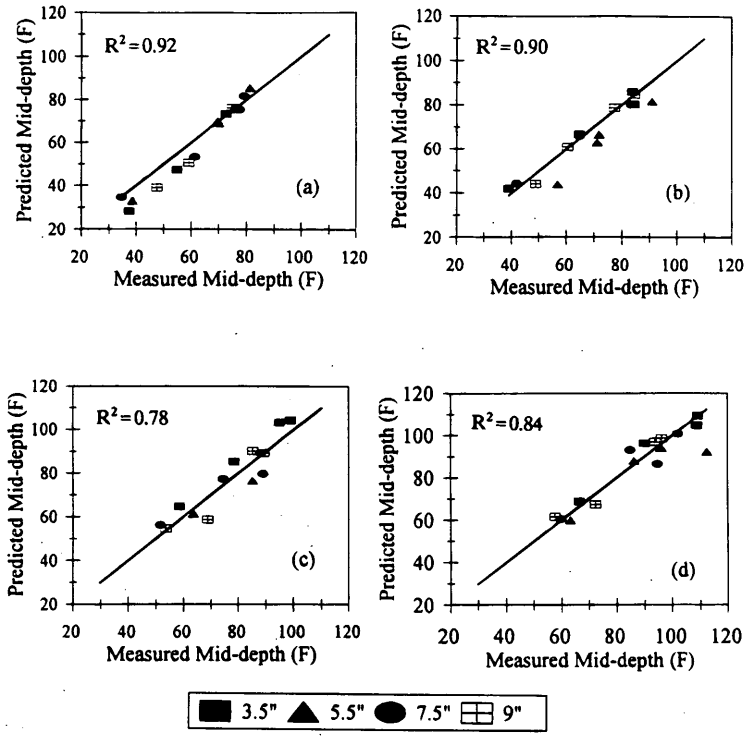

FIGURE 7 Comparison of predicted and measured middepth temperatures: (*a*) 8 a.m.; (*b*) 10 a.m.; (*c*) 12 noon; and (*d*) 2 p.m. [1 in. = 25.4 mm; °C = (°F − 32)/1.8].

whether the asphalt layer was heating or cooling. For depths other than the one-third depth, the magnitude of the elastic modulus was different for a given temperature, depending on whether the asphalt layer was in a heating or a cooling cycle. In support of Baltzer and Jansen's work, Stubstad et al. (*3*) presented the BELLS equation for the prediction of the one-third-depth temperature.

In order to validate the one-third-depth theory, maximum deflection data from the NCDOT data base were plotted against measured one-third-depth and middepth temperatures for all four pavements (see Figures 8 and 9 for examples). If the one-third-depth research claim were valid, the one-third-depth temperature would show smaller differences in the deflection values between the heating cycle in the morning and the cooling cycle in the late afternoon at the same one-third-depth temperature. Figures 8 and 9 show no improvement by using the one-third-depth temperature instead of using the middepth temperature.

The validity of the BELLS one-third-depth prediction equation was also studied. Measured values from the NCDOT data base were applied to the BELLS equation, and predicted versus measured temperatures are plotted in Figure 10. The BELLS equation resulted in a relatively small variation; however, the slope of the relationship that the BELLS equation displays is incorrect. The BELLS equation consistently underpredicts values at high temperatures and overpredicts values at low temperatures. The fact that the BELLS equation was developed on the basis of data collected mostly from northern states may present a possible reason for its poorer predictions at higher temperatures. Another possible source of this discrepancy is that the BELLS equation was developed by using the AC surface temperature measured with an infrared sensor mounted on the FWD, which could have measured the surface temperatures in the shade.

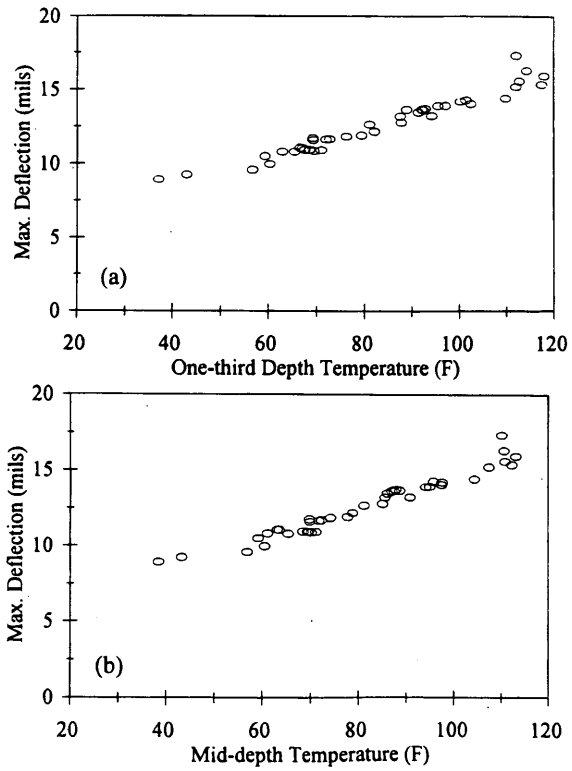

FIGURE 8 Maximum deflection versus effective AC temperature for US-70 section (140-mm-thick AC): (*a*) one-third depth; (*b*) middepth [1 mil = 0.0254 mm; °C = (°F − 32)/1.8].

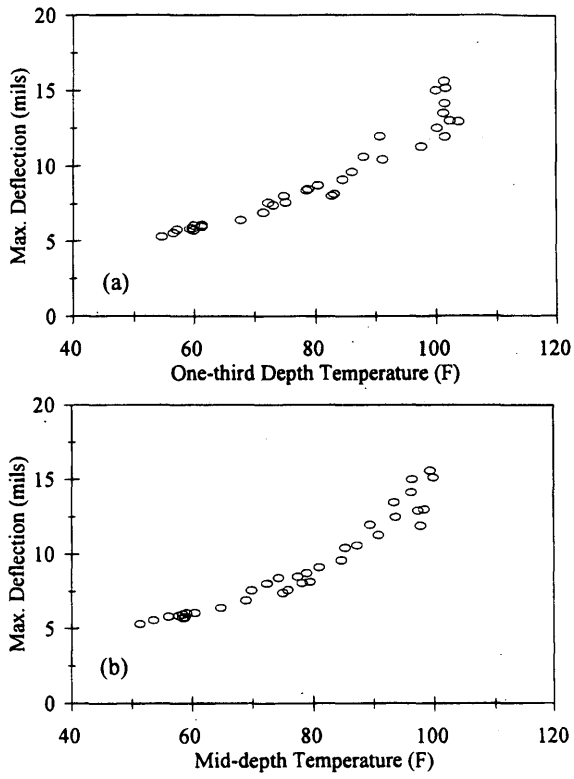

FIGURE 9 Maximum deflection versus effective AC temperature for Section 20 (229-mm-thick AC): (*a*) one-third depth; (*b*) middepth [1 mil = 0.0254 mm; °C = (°F − 32)/1.8].

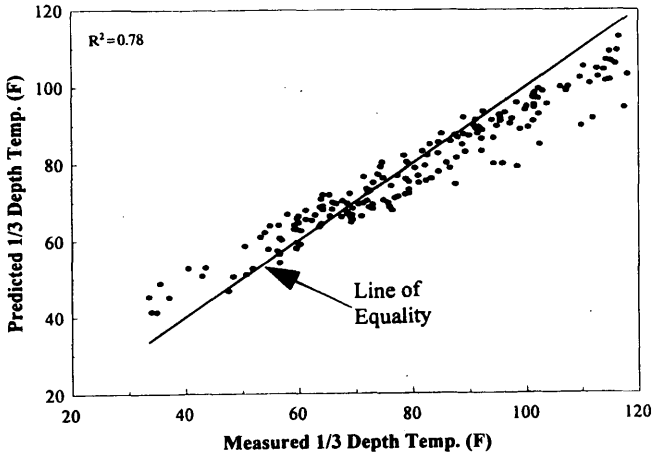

FIGURE 10 Validation of the BELLS equation using temperatures measured from pavements in North Carolina [°C = (°F − 32)/1.8].

Currently, the statewide calibration of the NCDOT procedure is conducted at North Carolina State University by testing a larger number of pavements widely spread throughout the state of North Carolina. This research will provide the necessary data to improve the temperature prediction model presented here.

CONCLUSIONS

Development of the NCDOT temperature correction procedure described in the paper by Kim et al. (this Record) produced a method that greatly improved the accuracy of the temperature-deflection correction. To supplement the NCDOT method, a temperature prediction model that predicts the middepth temperature of the AC layer was also developed. The key concept of the prediction model was the inclusion of temperature gradients along the depth as a function of the time of day. This data base approach of temperature prediction produced satisfactory results without requiring any material properties and air temperatures during the 5 days before FWD testing.

An alternate temperature prediction model, known as the BELLS one-third-depth equation, was studied by using the measured data from the North Carolina pavements. The prediction obtained by the BELLS equation showed relatively small variation, but at higher temperatures it underpredicted the measured one-third-depth AC temperature. Also, within the data base studied in this research, the AC one-third-depth temperature did not demonstrate any improvement in corrected deflection-versus-temperature relationship over the AC middepth temperature.

ACKNOWLEDGMENTS

This research was sponsored by NCDOT and FHWA. The authors thank NCDOT engineers in the Pavement Management Unit and Geotechnical Unit for excellent cooperation in installing gauges and FWD testing.

REFERENCES

1. *AASHTO Guide for Design of Pavement Structures*. AASHTO, Washington D.C., 1986.
2. Baltzer, S., and J. M. Jansen. Temperature Correction of Asphalt-Moduli for FWD-Measurements. *Proc., 4th International Conference on the Bearing Capacity of Roads and Airfields*, Vol. 1, Minneapolis, Minn. 1994.
3. Stubstad, R. N., S. Baltzer, E. O. Lukanen, and H.J. Ertman-Larsen. Prediction of AC Mat Temperatures for Routine Load/Deflection Measurements. *Proc., 4th International Conference on the Bearing Capacity of Roads and Airfields*, Vol. 1, Minneapolis, Minn. 1994.

Publication of this paper sponsored by Committee on Strength and Deformation Characteristics of Pavement Sections.

Analytical and Experimental Comparison of Heavy Vehicle Loads on Pavements

KANG-MING HSU, DONALD A. STREIT, AND BOHDAN T. KULAKOWSKI

A vehicle's vertical dynamic wheel force acting at the tire-road interface is a significant factor in causing pavement damage. Work that involved configuring a two-axle, 66,750-N (15,000-lbf) truck for dynamic wheel force measurement is described. Strain gauges were installed in a shear strain measurement mode on the axle housing of the vehicle. Inertia compensation was included when calculating tire-road forces. A 12.7-mm (0.5-in.) step and a 2-Hz sinusoid with a 12.7-mm (0.5-in.) peak-to-peak amplitude were used as inputs to a hydraulic vehicle shaker. The measured vehicle response data were in good agreement with those predicted by computer simulation.

Theoretically, a vehicle traveling on a perfectly smooth, straight, horizontal road at a constant speed will apply constant forces to the road through its tires, its static wheel loads (neglecting out-of-balance forces generated by the vehicle itself). In practice this condition never actually occurs because all roads have surface irregularities that excite the vehicle suspension system and cause a fluctuating force component on the road. This force, superimposed on the static wheel load, is frequently called the dynamic wheel force or the dynamic tire force (*1*). Knowledge of the magnitude of dynamic wheel forces is important for a variety of reasons:

1. Damage to a road structure is related to the magnitude of applied wheel forces.
2. Vibrational behaviors of highway bridges are determined by dynamic wheel forces.
3. Dynamic wheel forces applied to the road generate ground vibrations that can be an annoyance and that can cause damage to adjacent buildings.
4. A vehicle's road-holding ability is affected by the magnitude of the dynamic variations of wheel force; for instance, if the variations are large enough for a wheel to lose contact with the road surface, the vehicle's braking ability will be impaired.
5. The magnitude of the dynamic variation of wheel force is related to the forces applied to the vehicle body and hence to the ride quality of the vehicle.

These concerns, among others, are the motivating factors for the development of methods for dynamic wheel force measurement.

The force at the tire-road interface can be determined either in the pavement or on the vehicle. To continuously monitor this force directly it would be necessary to mount a continuous force-sensing instrument to the surface of a tire. Because this is not yet possible, many indirect or discrete measuring systems have been devised. Sensors have been mounted both in pavements and on trucks. Although vehicle-mounted systems do not provide direct wheel-pavement force measurement, they offer continuous force data. Vehicle-mounted systems are usually used on a long-term, continuous basis for studying the loads developed by vehicles traveling over various pavement types. One advantage of these methods is that a single instrumented vehicle can be used on numerous roads, allowing study of various surface conditions and pavement types. One disadvantage is that each vehicle in a study must be instrumented. Only vehicle-mounted systems that are generally used to measure dynamic wheel forces are considered in this paper. Typical vehicle-mounted systems are described first. Implementation of an experimental system is then described, and results from experiments and simulations are compared.

Pennsylvania Transportation Institute, The Pennsylvania State University, 201 Research Office Building, University Park, Pa. 16802.

BACKGROUND

Tire pressure as a means of monitoring wheel-pavement forces has been discussed in works by Fisher and Huckins (*2*) and Whittemore et al. (*3*). A differential tire pressure transducer is used to measure the change in tire pressure as wheel forces are applied to a tire. Transducer response can reflect wheel force. The differential pressure-load relationship is affected by tire pressure and tire volume. However, Whittemore et al. (*3*) found that the precision of this method is not acceptable because of nonlinear and phase-shift relationships between pressure change and wheel force.

Tire deflection has been related to wheel-pavement load measurement by Magnusson (*4*), Dickerson and Mace (*5*), and Hopkins and Boswell (*6*). Considering a tire as a spring, tire deflection-versus-tire load characteristics can be determined via calibration procedures. Tire deflection can then be used to calculate the wheel-pavement force. Usually, noncontact displacement transducers such as laser transducers or optical sensors are used to measure tire deflection. The load-versus-deflection relationship is usually very sensitive to tire pressure and temperature. If tire pressure or temperature changes, then such changes must be accommodated in the calculation of pavement loads.

Whittemore et al. (*3*) and others (*7,8*) have discussed the wheel force transducer method for measuring dynamic wheel-pavement loads. This system is similar to the strain-gauged axle housing system, but instead of using strain gauges a specially designed wheel force transducer is used. Different types of wheel force transducers have been developed. Usually, the wheel force transducer is designed to provide an output that is proportional to wheel loads. The advantage of this system is that it can be installed directly onto the wheels, serving as a portable measuring system available for use on many vehicles.

The strain-gauged axle housing method has been discussed by various investigators (*3,9–11*). In this method strain gauges are ce-

mented to the axle housing of a vehicle. Vertical accelerations of the axle are measured by two accelerometers installed on the vehicle axle. By adding the inertial force of the mass that is outboard of the strain gauges to the shear force sensed by the strain gauges, the force applied at the tire-road interface can be determined.

STRAIN-GAUGED AXLE HOUSING

The experimental method used in the present study is the strain-gauged axle housing method. A short summary of the instrumentation procedure is followed by descriptions of calibration procedures and wheel-pavement load calculations.

INSTRUMENTATION

Strain Gauges

The front and rear axles of a truck were instrumented. Strain gauges were cemented to the centers of two vertical surfaces of the axle housing, as close to the wheels as possible, as shown in Figure 1. In previous studies strain gauges were sometimes cemented to the top or bottom surface of the axle housing to measure normal strains due to bending. The benefit of those arrangements is that strain gauges are very sensitive to the wheel force because the maximum bending stresses occur at the top and bottom of the housing. However, if straight and steady driving is not maintained, lateral wheel forces can significantly affect strain gauge output, causing distortion of vertical wheel force measurements. In the present study strain gauges were attached to the centers of the vertical surfaces of the axle housing. They measure housing maximum shear stress and largely eliminate the effects of lateral wheel forces on vertical wheel-pavement load measurements. Strain gauge calibration showed that the shear strain gauge arrangement is sufficiently sensitive to experimentally determine vertical wheel loads on pavement.

Accelerometers

On each side of the front axle a bracket was mounted near the wheel to accommodate accelerometer mounting. On the rear axle accelerometers were mounted directly on the top centers of the leaf springs as shown in Figure 1. All accelerometers were mounted upright to measure vertical accelerations. Additionally, a thermally insulated accelerometer was installed on the right side of the rear axle adjacent to the regular accelerometer to monitor the effects of temperature on accelerometer output.

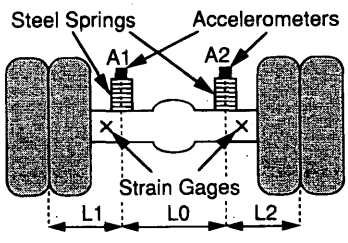

FIGURE 1 Instrumentation of rear axle.

STATIC CALIBRATION

Static strain gauge calibration was performed by progressively jacking the truck to adjust wheel load and strain gauge outputs. Wheel force was measured via a wheel scale under the tire. Five and one-half tons of dead weight were placed on the truck to increase the calibration range. Because of the difficulty of increasing the load on the front axle, the front calibration range was only from 0 to 15 570 N (3,500 lbf) on each side of the axle. The rear axle load range was from 0 to 44 480 N (10,000 lbf). Calibration results exhibited linear relationships between strain gauge output and vertical wheel force. Strain gauge calibration curves are given in Figure 2.

WHEEL-PAVEMENT LOAD FORMULATION

Tire-road forces include three components, as shown in Figure 3. In Figure 3 F_x is the traction force due to tire rolling resistance, F_y is the lateral force, which is very small and negligible compared with the other forces in the condition of straight driving, and F_z is the vertical wheel force, which causes pavement damage and affects the vibrational behavior of vehicle and road structure. F_z was the force component of interest in the present study.

The strain-gauged axle housing method requires that a strain gauge be installed at a particular section of the axle between wheel and suspension leaves. Sensor output depends on the forces transmitted from the tire-road interface to the sensor. Therefore, it is necessary to know the effects of each force on the instrumented section. During straight driving, which is typical of highway driving, lateral force is negligible. Both traction and vertical wheel force are the primary forces affecting force sensor output. Vertical wheel force

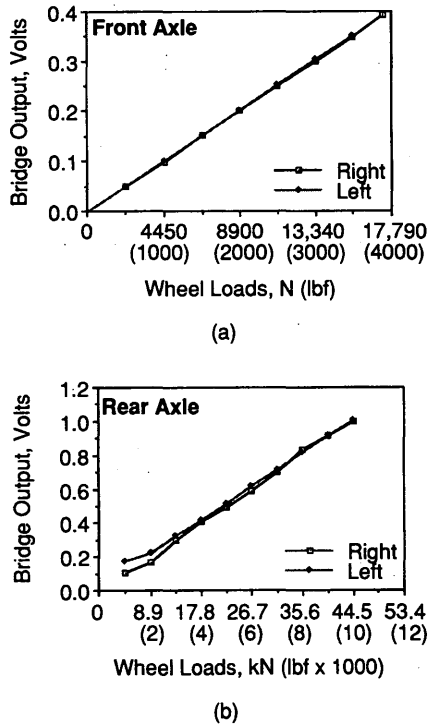

FIGURE 2 Bridge characteristics: (*a*) front axle; (*b*) rear axle.

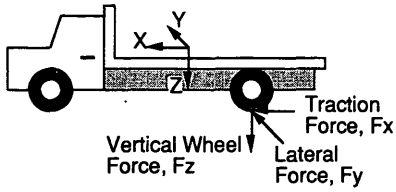

FIGURE 3 Wheel forces diagram.

causes shear and bending at the section where the sensor is installed. In addition to the shear and bending, the traction force also causes torsion. The sensing circuits used in this project were designed so that the effects of bending and torsion are largely eliminated. Therefore, the vertical shear force at the instrumented section can be determined from the strain gauge output.

In most wheel force measurement approaches, the measurement transducer is located some distance away from the point at which the force of interest is located. This is due to the difficulties involved in installing the transducer at the tire-road interface (except in instrumented pavement measuring systems). When dynamic loads vary only slowly, static calibration of the measurement system might be sufficient to determine the force applied at the tire-road interface. However, when changes of loading occur over very short time intervals, the data measured by sensors such as strain gauges or wheel force transducers are distorted by dynamic effects. Some fraction of applied force is required to accelerate the mass of the intervening structure between the point of force application and the force sensors. Adding the inertial force component of the outboard mass to that determined at the gauge location, the dynamic wheel force applied at the tire-road interface can be obtained (*12–14*). Thus, the total vertical dynamic wheel force, defined as F_z, can be expressed as

$$F_z = F_{sg} + M_{ob}A_{ob} \tag{1}$$

where

F_{sg} = force measured by strain gauges;
M_{ob} = outboard mass, which is the mass of the intervening structure between the transducer and the point of force application in this project, M_{ob} is the mass outboard of the locations of the strain gauges; and
A_{ob} = vertical acceleration of the outboard mass.

Outboard mass depends on the location of the transducer and is sometimes difficult to determine accurately. For instance, in the case of a strain-gauged axle, the outboard mass includes the tire assembly, the brake unit (drum, shoes, booster, etc.), and a part of the axle. Accurate determination of the center of the outboard mass is also important. However, the irregular shape and inhomogeneity of the outboard structure make it difficult to measure the location of the center of mass accurately. Usually, the center of mass is estimated to be at the center of the wheel or at some proximal offset. The acceleration of the center of the outboard mass is difficult to instrument directly because of axle and wheel rotation. It is therefore necessary to determine acceleration of the outboard mass geometrically with accelerometers mounted to the axle. As shown in Figure 4 the vertical acceleration of the right-hand outboard mass, A_{ob}, is calculated as

$$A_{ob} = (1 + L_2/L_0)A_2 - (L_2/L_0)A_1 \tag{2}$$

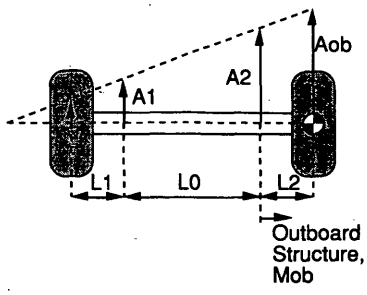

FIGURE 4 Geometric determination of acceleration.

where

A_1 = vertical acceleration measured by Accelerometer A1 in Figure 4,
A_2 = vertical acceleration measured by Accelerometer A2 in Figure 4,
L_0 = horizontal distance between two accelerometers in Figure 4,
L_2 = horizontal distance between the center of mass of the right outboard mass and Accelerometer A2, and
L_1 = horizontal distance between center of mass of the left outboard mass and Accelerometer A1.

The vertical acceleration of the left-hand side can be calculated similarly by switching the parameters A_1 and A_2 and replacing L_2 by L_1 in Equation 2.

In dynamic force measurement the closer the force sensor is to the point of force application the less the intervening structure affects the force measurement. Measurement accuracy can be increased as the effects of inertia and local bending of any nonrigid body are reduced. Also, locating the force sensor near the point of force application will minimize the unavoidable errors in the estimation of the mass and the center of mass of the intervening structure.

ADVANTAGES AND DISADVANTAGES

A major advantage of the strain-gauged axle housing method for determining dynamic wheel loads is cost. Hardware requirements for strain gauge implementation are minimal, and once it is instrumented a vehicle can be used to study many test conditions. The disadvantages of this method include the requirement of multiple strain gauges and accelerometer installation and calibration on each vehicle of interest. In addition, depending on vehicle geometry, some axles may be particularly cumbersome for strain gauge installation. Also, errors in inertial force measurement are introduced by inaccuracies in determination of the mass or the center of mass of the outboard structure, on both, and by acceleration calculation errors resulting from axle bending.

ANALYSIS OF TEST DATA

To evaluate system performance the truck was placed on a hydraulic shaker (DYNTRAC, the FHWA Dynamic Truck Actuator System), which was used to generate elevation irregularities. Two tests, a 12.7-mm (0.5-in.) step input and a 2-Hz sinusoidal input of

12.7 mm (0.5 in.) of peak-to-peak amplitude, were performed. All tests were in phase for all wheels. The sampling rate for both tests was 200 Hz. The measured data were compared with the simulation results by using the Phase 4 computer package (*15*). In the case of step input the actual DYNTRAC actuator displacement data were recorded and were used as input for simulation. For sinusoidal input the actual actuator response data were not available, and therefore, a perfect sinusoidal input was used in computer simulation. Time traces of the shear forces determined at strain gauge locations, total dynamic wheel forces, and simulation results are displayed in Plots *a*, *b*, and *c*, respectively, of Figures 5 through 8.

COMPARISON OF DYNAMIC WHEEL FORCES

To investigate the effect of wheel-axle inertia on the experimental results, Plots a and b of Figures 5 through 8 were compared. The difference between shear force (Plots *a*) at the strain gauge locations and the total dynamic wheel force (Plots *b*) is the inertial force that accelerates the outboard structure. The points labeled 1 through 10 in these plots have been identified for purposes of comparison. Equation 3 compares inertial loads (numerator in this equation) to the dynamic component of total wheel load (denominator in this equation). Values given by Equation 3 are listed in Table 1.

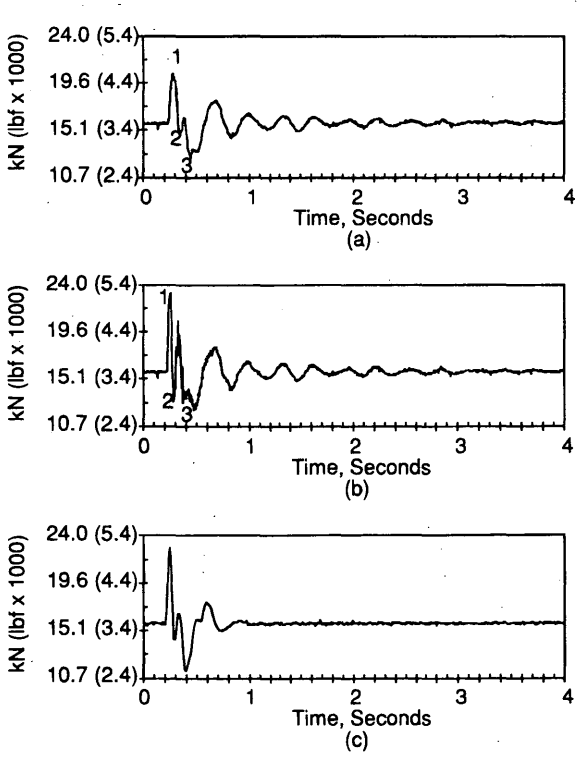

FIGURE 5 Vertical forces on front axle [127-mm (0.5-in.) step input]: (*a*) force at location of axle strain gauge; (*b*) experimental dynamic wheel force after inertial corrections according to Equation 1; (*c*) dynamic wheel force from simulation results.

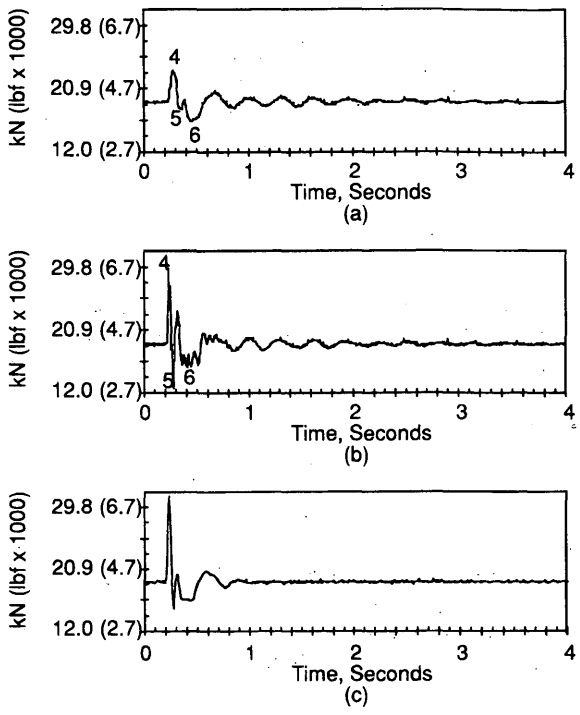

FIGURE 6 Vertical forces on rear axle [127-mm (0.5-in.) step input]: (*a*) force at location of axle strain gauge; (*b*) experimental dynamic wheel force after inertial corrections according to Equation 1; (*c*) dynamic wheel force from simulation results.

$$\text{Percent} = \left| \frac{F_i - S_i}{F_i - \overline{F}} \right| \times 100 \tag{3}$$

where

F_i = dynamic wheel force,
S_i = sensed shear force, and
$\overline{F}$ = average force.

Figures 5 to 8 and Table 1 show that in the case of sinusoidal input the inertial force is small, approximately 6 to 15 percent, because of the low excitation frequency and amplitude. Increasing the frequency or the amplitude, or both, of the excitation will largely increase this inertia effect. In the case of step input large axle acceleration resulted in a large inertial force component. For some points in step input the magnitude of this inertial force component was up to 57 to 84 percent of the amplitude of dynamic wheel force, exceeding the component of force sensed by strain gauges. The need to introduce the compensation for an inertia effect is clearly demonstrated.

When the measured dynamic wheel force and simulation results are compared, they show good agreement in shape, and the difference of magnitudes is within acceptable limits. Based on the simulation it is likely that the difference in the magnitudes in force peaks was mainly caused by the difference between the actual tire stiffnesses and those used in the simulation. In the case of step input, in addition to a resonance of about 2.5 to 3 Hz shown in the measured dynamic wheel force, a second vibration mode clearly appeared in both the measured force and the simulation result. Theoretically, both the tire stiffness and the suspension spring rate largely affect the magnitude of dynamic wheel force and its fluctuation behavior. Simulation results showed much quicker settling. Both viscous

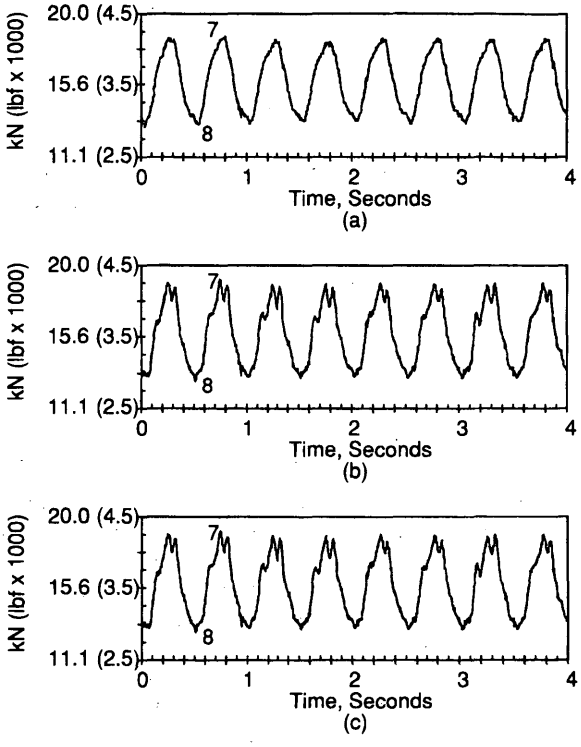

FIGURE 7 Vertical forces on front axle [sinusoidal input, 2 Hz, 63.5 mm (0.25 in.) of amplitude]: (*a*) force at location of axle strain gauge; (*b*) experimental dynamic wheel force after inertial corrections according to Equation 1; (*c*) dynamic wheel force from simulation results.

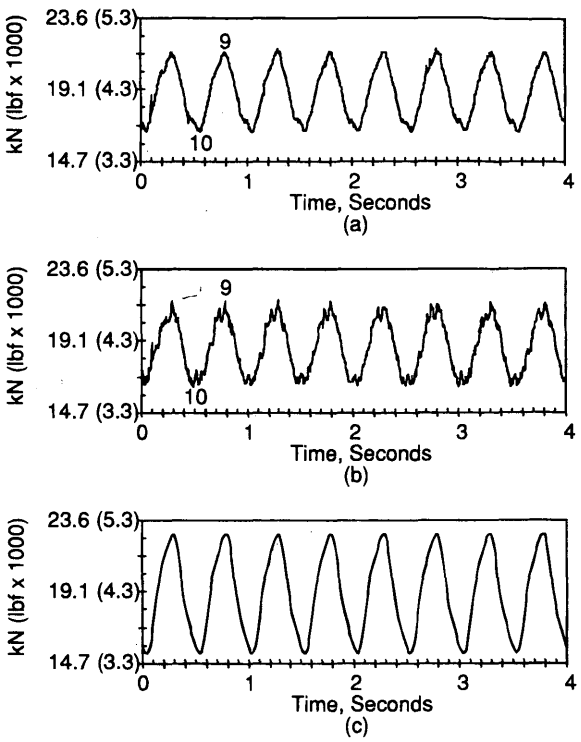

FIGURE 8 Vertical forces on rear axle [Sinusoidal Input, 2 Hz, 63.5-mm (0.25-in.) amplitude]: (*a*) force at location of axle strain gauge; (*b*) experimental dynamic wheel force after inertial corrections according to Equation 1; (*c*) dynamic wheel force from simulation results.

damping and coulomb friction affected the settling time. The comparison implied that these energy dissipation-related parameters might be too large in the simulation. Basically, computer simulation provides a theoretical value. Its results are a function of the parameters input into the program. However, some parameters are very difficult to measure. The differences between actual truck parameters and those used in the simulation result in inconsistencies between measured data and simulation results. However, a good correlation between the measured data and the simulation results has been demonstrated.

In addition to the truck parameters used in the simulation, many other factors may affect the difference between measured data and simulation results:

1. Inaccurate determination of the mass of the outboard structure will cause an error in the calculation of inertial force.
2. Inaccurate determination of the position of the center of mass of the outboard structure will cause an error in acceleration calculation, and thus, the inertial force will be distorted. This effect will be especially clear when the excitations to truck wheels are out of phase and of high roughness or frequency.
3. Geometric determination of acceleration is based on consideration of the axle moving as a rigid body. Local bending of any nonrigid body of the axle will cause the difference between the calculated and the actual accelerations. In high-frequency excitation the magnitude of this error will increase.
4. Temperature change may affect strain gauge characteristics. This effect is more important in field tests since the axle temperature may greatly increase because of braking.
5. The signal-to-noise ratio of shear strain gauge output is not large enough so that the output might be significantly affected by noise.
6. Accelerometers did not respond well in the low-frequency range.

TABLE 1 Percentage of Inertia Force of Amplitude of Dynamic Wheel Force

	Step Input			Sinusoidal Input		
Axle	Fig. No.	Data Pt.	% Diff.	Fig. No.	Data Pt.	% Diff.
Front	5	1	36.5	7	7	15.3
Front	5	2	67.8	7	8	9.5
Front	5	3	9.8	-	-	-
Rear	6	4	57.1	8	9	6.1
Rear	6	5	84.5	8	10	7.7
Rear	6	6	12.5	-	-	-

COMPARISON OF POWER SPECTRAL DENSITIES

Power spectral densities of measured dynamic wheel force and simulation results are shown in Figures 9 and 10 for a step input and Figures 11 and 12 for a sinusoidal input. Good agreement between experimental and simulation data is displayed. In the case of sinusoidal input the highest power spectral density peaks occur at 2 Hz, which is consistent with the excitation frequency. Because a perfect sinusoidal input was used in the computer simulation the difference in the power spectral density between measured data and simulation is more pronounced than in the case of step input, in which actual

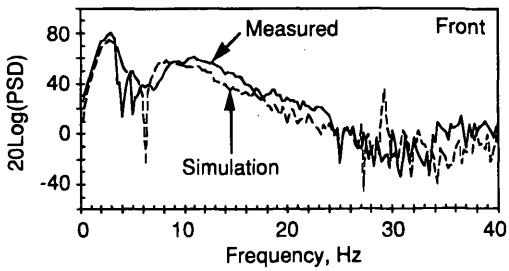

FIGURE 9 Power spectral densities of front wheel forces [127-mm (0.5-in.) step input].

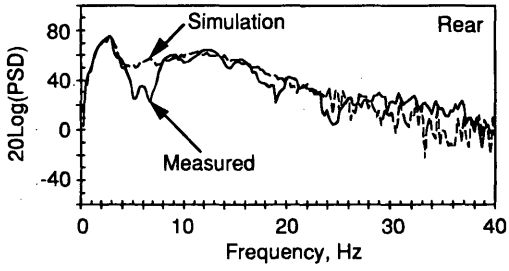

FIGURE 10 Power spectral densities of rear wheel forces [127-mm (0.5-in.) step input].

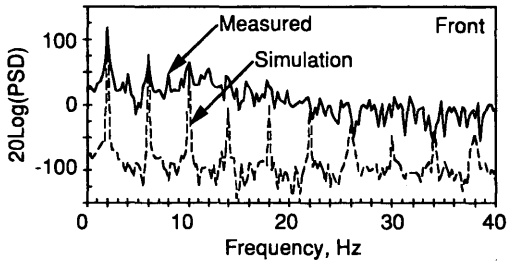

FIGURE 11 Power spectral densities of front wheel forces [sinusoidal input, 2 Hz, 63.5-mm (0.25-in.) amplitude].

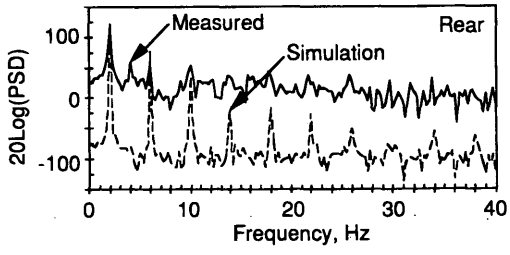

FIGURE 12 Power spectral densities of rear wheel forces [sinusoidal input, 2 Hz, 63.5-mm (0.25-in.) amplitude].

actuator output was recorded and was used as input to the computer simulation.

COMPARISON OF DYNAMIC IMPACT FACTORS

The dynamic impact factor (DIF) provides a quantitative measure of the variation of dynamic wheel forces and is defined as

$$\text{DIF} = \sqrt{\frac{\sum_{i=1}^{n} (F_i - \bar{F})^2}{(n-1)\bar{F}^2}} \tag{4}$$

where

n = number of sampled datum points,
$\bar{F}$ = average dynamic wheel force, and
F_i = dynamic wheel force at the ith datum point.

The comparison of DIFs is shown in Table 2. In the case of sinusoidal input the DIFs of the simulation results are significantly higher than those of the measured data. It is suspected that the actuator gains might be set too low, such that the amplitude of the actual actuator response was smaller than a perfect sine wave and, thus, resulted in smaller force variation. It is therefore reasonable for the measured force to have smaller DIFs. In the case of a step input, since actual actuator output was recorded for the input to the computer simulation, the DIFs of the test data and simulation results are very close.

CONCLUSIONS

Axle strain was used to determine dynamic wheel loads on pavement. Experimental data show a good correlation with analytical simulation results. Additional dynamic wheel load measurement techniques are being studied. These include dynamic wheel scales mounted on the FHWA Dynamic Truck Actuator System (DYNTRAC) and a removable wheel force transducer hub that would be mounted between a wheel and an axle. Accurate and transferable dynamic wheel force instrumentation will be used to survey the effects of vehicle parameters such as tire pressure, tire type, suspension type, and number of axles on pavement load.

During the course of the study it was of interest to know the required accuracy of the measurements of those vehicle parameters to ensure reasonable simulation results. The simulation model that has been validated experimentally as described here has been used to determine the sensitivity of dynamic wheel-pavement forces to variations in system parameters at different vehicle speeds and for different road roughness values. The results of that sensitivity analysis are reported by Lin et al.(*16*).

ACKNOWLEDGMENTS

The work reported in this paper was conducted under the sponsorship of FHWA.

TABLE 2 Comparison of DIFs

Input Function	Wheel	Test Data DIF	Simulation DIF
Step	Front	0.0626	0.0532
Step	Rear	0.0542	0.0564
Sinusoidal	Front	0.1215	0.1562
Sinusoidal	Rear	0.0871	0.1347

REFERENCES

1. Quinn, B. E., and C. C. Wilson. Can Dynamic Tire Forces Be Used as a Criterion of Pavement Condition? Highway Research Record *46*, HRB, National Research Council, Washington, D.C., 1964, pp. 88–100.
2. Fisher, J. W., and H. C. Huckins. Special Report 73: *Measuring Dynamic Vehicle Loads*. HRB, National Research Council, Washington, D.C., 1962, pp. 138–148.
3. Whittemore, A. P., J. R. Wiley, P. C. Shultz, and D. E. Pollock. *NCHRP Report 105: Dynamic Pavement Loads of Heavy Highway Vehicles*. HRB, National Research Council, Washington, D.C., 1970.
4. Magnusson, G. *Measurement of Dynamic Wheel Load*. VTI Report 279A. Swedish Road and Transport Research Institute, Linköping, Sweden, 1987.
5. Dickerson, R. S., and D. G. W. Mace. *Dynamic Pavement Force Measurements with a Two-Axle Heavy Goods Vehicle*. TRRL Supplement Report 688. Transport and Road Research Laboratory, Department of the Environment Department of Transport, Crowthorn, United Kingdom, 1981.
6. Hopkins, R. C., and H. H. Boswell. Methods for Measuring Load Transfer Through Vehicle Tires to the Road Surface. HRB Proc., Vol. 36, 1957, pp. 240–252.
7. Lysdale, C. A., and R. R. Hegmon. *Development of a Truck Wheel Force Transducer*. SAE Paper 800247. Society of Automotive Engineers, Warrendale, Pa. 1980.
8. Todd, K. B. Design Recommendations for Wheel Force Transducers. Technical Memorandum EI-TIRE-8701. Pennsylvania Transportation Institute, University Park, 1987.
9. Page, J., and J. W. Grainger. A Technique for Measuring Vehicle Dynamic Wheel Loads. *TRRL Supplement Report 98UC*, Transport Road Laboratory, Department of the Environment, Crowthorn, United Kingdom, 1974.
10. Mitchell, C. G. B., and L. Gyenes. Dynamic Pavement Loads Measured for a Variety of Truck Suspensions. Paper presented at the 2nd International Conference on Heavy Vehicle Weights and Dimensions, Kelowna, British Columbia, 1989.
11. Chi, M. C. *Analysis of Dynamic Truck-Tire Pavement Interaction*. M.S. thesis. The Pennsylvania State University, University Park, 1987.
12. Ervin, R. D., R. L. Nisonger, M. Sayers, T. D. Gillespie, and P. S. Fancher. *Influence of Truck Size and Weight Variables on the Stability and Control Properties of Heavy Trucks*. Report UMTRI-83-10/2. University of Michigan, Ann Arbor, April 1983.
13. Heath, A., and M. C. Good. Heavy Vehicle Design Parameters and Dynamic Pavement Loading. *Australian Road Research*, Vol. 15, No. 4, 1985, pp. 249–263.
14. Sayers, M., and T. D. Gillespie. Dynamic Pavement/Wheel Loading for Trucks with Tandem Suspensions. *Proc., 8th IAVSD Symposium on the Dynamics of Vehicles on Roads and on Railway Tracks*, Cambridge, Minn. 1983, pp. 517–533.
15. MacAdam, C. C., P. S. Fancher, G. T. Hu, and T. D. Gillespie. *A Computerized Dynamics of Trucks, Tractor Semi-Trailers, Doubles, and Triples Combinations: User's Manual—Phase 4*. Report UM-HSRI-80-58. Highway Safety Research Institute, Ann Arbor, Mich., 1980.
16. Lin, W.-C., Y.-C. Chen, B. T. Kulakowski, and D. A. Streit. Dynamic Wheel/Pavement Force Sensitivity to Variations in Heavy Vehicle Parameters, Speed and Road Roughness. *Heavy Vehicle Systems, International Journal of Vehicle Design*, Vol. 1, No. 2, 1994, pp. 139–155.

The findings and conclusions in this paper are those of the authors and do not necessarily represent the views of FHWA.

Publication of this paper sponsored by Committee on Strength and Deformation Characteristics of Pavement Sections.

Effect of Selecting Subgrade Resilient Modulus Values on Asphalt Overlay Design Thicknesses

KHALED KSAIBATI, JAMES M. BURCZYK, AND MICHAEL L. WHELAN

Design pavement overlay thicknesses were calculated for primary roads located in the state of Wyoming. Subgrade resilient modulus values were determined on the basis of laboratory testing at a deviator stress of 41.4 kPa (6lb/in.^{2}) laboratory testing at the actual field deviator stress, and backcalculation from deflection measurements. Several pieces of relevant field and laboratory information were also collected on all sections. Asphalt overlay thicknesses were then calculated on the basis of the *AASHTO Guide for Design of Pavement Structures*. The data analysis indicated that the three calculated resilient modulus values at each test section did not result in significantly different overlay thicknesses.

The 1993 *AASHTO Guide for Design of Pavement Structures* (*1*) requires selection a of subgrade resilient modulus (M_R). The determination of the subgrade M_R is essential for designing overlay thicknesses for existing pavement sections. If the selected design M_R value is too high, the thickness of the pavement layer will be insufficient. If the design M_R value is too low, the thickness will be too conservative and not cost-effective. The two most commonly used methods for determining subgrade M_R values are actual laboratory testing and backcalculation procedures described in the *AASHTO* Guide for Design of Pavement Structures (*1*).

Laboratory testing is normally performed with different combinations of confining and deviator pressures. A design M_R value is then selected from a plot of M_R versus deviator stress. An important aspect of choosing a design M_R value is making sure that the selected value is consistent with the assumptions made in the design performance equation for the AASHO Road Test subgrade. The AASHTO guide uses a value of 20 684 kPa (3,000 lb/in.^{2}) to represent the subgrade for the AASHO Road Test, but it does not justify its selection. This value is one of the underlying assumptions of the flexible pavement performance model. Based on a study by Thompson and Robnett (*2*), this value is appropriate when the AASHO soil is about 1 percent wet of optimum and subjected to a deviator stress of about 41.4 kPa (6 lb/in.^{2}) or more. Thompson and Robnett (*2*) also showed that M_R values from deviator stresses of less than 41.4 kPa (6 lb/in.^{2}) vary significantly, whereas M_R values from deviator stresses of more than 41.4 kPa (6 lb/in.^{2}) tend to remain constant. Therefore, when selecting an M_R value from laboratory testing, use of a zero confining pressure and a 41.4-kPa (6-lb/in.^{2}) deviator stress is suggested (*3*).

When adequate field data are available, actual field deviator stresses can be calculated. These calculations normally incorporate some assumptions about applied loadings, tire pressures, and pavement material properties and layer thicknesses. Typically, computer programs such as BISAR (*4*) can be used to determine the stresses in a pavement's subgrade soil. Design M_R values can then be determined from laboratory testing on the basis of the actual deviator stresses rather than the assumed value of 41.4 kPa (6 lb/in.^{2}).

M_R values can also be backcalculated. The AASHTO guide recommends use of the following formula to determine the resilient modulus value for subgrade soils based on deflection measurements:

$$M_R = \frac{0.24P}{d_r r}$$

where

M_R = backcalculated subgrade resilient modulus,
P = applied load,
d_r = deflection at a distance r from the center of the load, and
r = distance from center of load (sensor location).

The resulting M_R value is normally adjusted with a correction factor to make it consistent with the 20 684-kPa (3,000-lb/in.^{2}) assumption (*1*).

The University of Wyoming and the Wyoming Department of Transportation (DOT) conducted a joint research project to (a) compare actual subgrade field deviator stresses with the 41.4-kPa (6-lb/in.^{2}) deviator stress assumed in determining a design M_R value from laboratory testing and (b) determine the effect of selecting an M_R value on the design overlay thicknesses for typical pavement sections in Wyoming. This paper presents the main findings of that study.

DESIGN OF EXPERIMENT

Figure 1 shows the data collection process and overall evaluation strategies followed in the project. During the summer of 1992 and spring of 1993 several types of field data were collected on nine pavement test sections. These sections were chosen to represent typical cohesive subgrade soil conditions on primary roads throughout the state of Wyoming. The field evaluation included pavement coring, subgrade coring, and deflection measurements. Table 1 shows the locations and thicknesses of the sections included in the experiment. Pavement cores were used mainly to confirm the thicknesses of the different layers in the pavement structures. These thicknesses were then used to calculate the actual field stress conditions on the subgrade soil at each test site. Laboratory resilient modulus testing was then performed on the subgrade samples. Subgrade M_R values were then determined on the basis of the assumed deviator stress of 41.4 kPa (6 lb/in.^{2}), the actual field deviator stress,

Department of Civil and Architectural Engineering, College of Engineering, University of Wyoming, P.O. Box 3295, University Station, Laramie, Wyo. 82071.

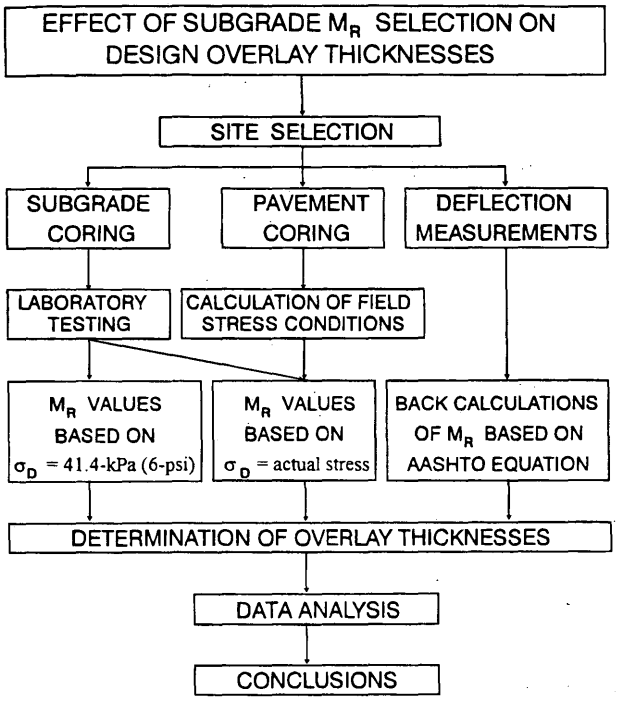

FIGURE 1 Data collection and analysis strategies.

and deflection measurements. Statistical analyses were then performed to determine if differences existed between M_R values calculated by using an assumed deviator stress of 41.4 kPa (6 lb/in.^{2}) and the actual deviator stresses. Next, these M_R values were used to calculate overlay thicknesses for all nine pavement test sections. Further analyses were then completed to examine the differences in the resulting design overlay thicknesses on the basis of laboratory M_R values and the AASHTO M_R backcalculated values.

DATA COLLECTION AND LABORATORY TESTING

Field Data Collection

Extensive field data were collected on all test sections included in the present research study. First, pavement deflection measurements were obtained by using standard loads on the Wyoming DOT's KUAB 2-m falling weight deflectometer. Pavement and air temperatures were also recorded for later use in correcting the temperature to the standard value of 21°C (70°F). Second, three pavement cores were taken from each section to examine the characteristics of the asphalt layers and to verify the thicknesses. These data were later used in the AASHTO overlay design procedures. Finally, three Shelby tube samples were taken from the subgrade at each test section. The soil samples were used to determine M_R values by laboratory testing procedures. Sieve analysis, liquid limit, plastic limit, and water content tests were also performed on the soil samples.

Resilient Modulus Testing

Laboratory soil resilient modulus tests were performed on the Wyoming DOT machine manufactured by the Interlaken Technology Corporation. This system has a Series 3300 98-kN (22-kip)-capacity test frame, a Series 3230, 16-channel data acquisition system, and a Series 3200 controller. The interim method of test for resilient modulus of unbound granular base/subbase materials and subgrade soils (Strategic Highway Research Program Protocol P46; AASHTO standard T 294-92 I) outlines the latest testing procedure. Soil samples were extracted from the Shelby tubes and were tested under Type II (cohesive) subgrade soil conditions. The amount of deformation in the soil samples was recorded by using two linear variable differential transducers (LVDTs) mounted outside of the testing chamber on the loading piston. All samples tested were 71 mm (2.8 in.) in diameter and 152 mm (6 in.) in height. These measurements, a height not less than 2 times the diameter and a minimum diameter of 71 mm (2.8 in.) or 5 times the nominal particle size, were selected in accordance with current specifications (*5*). Deformation and applied load readings were digitally recorded for the last five loading cycles. Several spreadsheets were developed to accept these data as well as the length and diameter of each sample. Figure 2 shows an example of the M_R summary spreadsheet developed for the study. The upper half of the spreadsheet shows the measured values under different testing conditions. These values include mean deviator load, mean applied deviator stress, mean recoverable deformation from each LVDT, mean resilient strain, and mean M_R value. By entering these data the M_R values were calculated automatically for each testing condition and test section. A logarithmic plot of M_R versus deviator stress was also created by using these values, as shown in the lower left-hand corner of Figure 2. In addition, a simple linear regression analysis was performed to develop a general equation for determining the M_R values as a func-

TABLE 1 Locations and Thicknesses of Test Sections

Roadway	Mile Post	Pavement Thicknesses	
		Surface (mm)	Base (mm)
US-30	48	305	305
US-30	70	140	152
US-287	416	152	152
US-26	108	127	152
US-20/26	15	127	203
US-20	163	76	64*
US-16	229	152	203*
US-16	244	58	191*
US-85	197.4	152	203**

*Asphalt Treated Base (ATB) **Cement Treated Base (CTB)

CHAMBER CONFINING PRESSURE (kPa)	NOMINAL DEVIATOR STRESS (kPa)	MEAN DEVIATOR LOAD (N)	STANDARD DEVIATION OF LOAD (N)	MEAN APPLIED DEV. STRESS (kPa)	MEAN RECOV. DEF. LVDT #1 (m)	MEAN RECOV. DEF. LVDT #2 (m)	MEAN RECOV. DEF. LVDT #3 (m)	MEAN RECOV. DEF. (m)	STD. DEV. OF RECOV. DEF. (m)	MEAN OF RESILIENT STRAIN (m/m)	MEAN OF Mr (kPa)	STD. DEV. OF Mr (kPa)
41.4	13.8	70.2855	0.3634	18.92	4.40282E-05	4.37182E-05		4.38732E-05	8.93317E-07	2.88122E-04	58720	802.1
41.4	27.6	103.9076	0.3634	25.01	9.70484E-05	9.58081E-05		9.64283E-05	8.83790E-07	6.33259E-04	39492	285.3
41.4	41.4	161.5086	0.1942	38.87	2.89595E-04	2.83394E-04		2.86494E-04	1.69844E-06	1.88145E-03	20661	138.8
41.4	55.2	201.9946	0.3071	48.61	4.25400E-04	4.11139E-04		4.18269E-04	1.29738E-06	2.74684E-03	17698	49.8
41.4	68.9	235.7035	0.4953	56.73	5.24620E-04	5.06016E-04		5.15318E-04	1.38639E-06	3.38417E-03	16763	33.0
20.7	13.8	67.5922	0.4952	16.27	4.03075E-05	4.09277E-05		4.06176E-05	4.24599E-07	2.66742E-04	60990	651.5
20.7	27.6	101.9964	0.5664	24.55	9.85986E-05	9.89087E-05		9.87537E-05	1.03994E-06	6.48530E-04	37854	385.2
20.7	41.4	201.9076	0.6444	48.59	3.95634E-04	3.88194E-04		3.91914E-04	1.29738E-06	2.57376E-03	18880	57.2
20.7	55.2	212.2464	0.5828	51.08	4.32841E-04	4.23540E-04		4.28191E-04	1.29632E-06	2.81199E-03	18166	50.7
20.7	68.9	246.9111	0.7892	59.42	5.46943E-04	5.37022E-04		5.41983E-04	8.48641E-07	3.55928E-03	16696	54.5
0.0	13.8	62.1187	0.4344	14.95	3.53466E-05	3.72069E-05		3.62768E-05	1.49104E-06	2.38235E-04	62833	2443.4
0.0	27.6	93.6561	0.3887	22.54	1.36426E-04	1.33325E-04		1.34875E-04	1.09622E-06	8.85747E-04	25449	138.3
0.0	41.4	150.5618	0.9517	36.24	3.09439E-04	3.06338E-04		3.07888E-04	3.39596E-06	2.02195E-03	17922	84.1
0.0	55.2	205.6435	0.5827	49.49	4.99194E-04	4.90513E-04		4.94853E-04	2.29954E-06	3.24978E-03	15230	57.8
0.0	68.9	251.6026	0.7139	60.55	6.59185E-04	6.46162E-04		6.52673E-04	1.55067E-06	4.28621E-03	14128	16.6

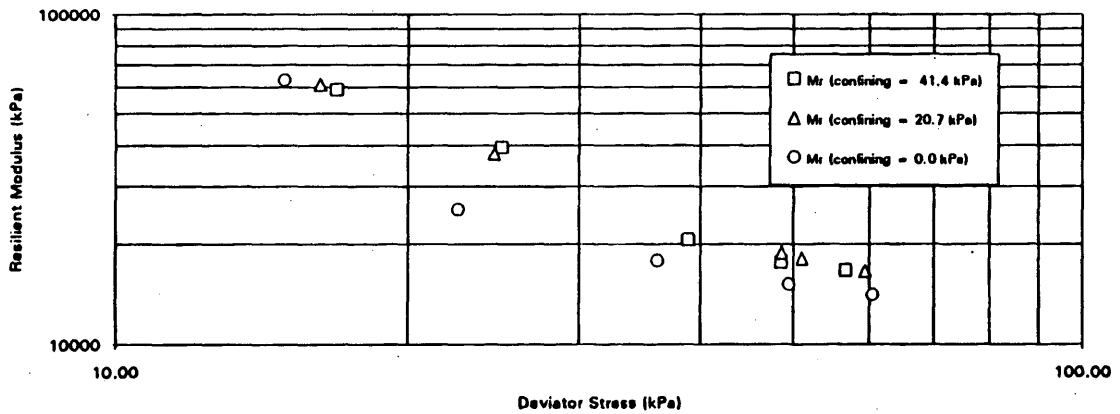

APPLICATIONS

EXPRESSION OF THE MODULUS

$$MR = 930697\ (Sd)^{-1.021}$$

STATISTICS 2

R = 0.908

SUMMARY

SAY Sd =	41.4 kPa
MR (design) =	20822 kPa
R value =	30.0
R value Specimen Height =	66.6 mm
Rcorrected =	32.0

TYPE OF SAMPLE: THAWED

FILENAME: T341511A.XLS

FIGURE 2 Summary spreadsheet for calculating subgrade M_R.

tion of the deviator stress [$M_R = f(\sigma_d)$]. After obtaining the equation a deviator stress of 41.4kPa (6 lb/in.^{2}), suggested in the literature, was substituted into the equation to determine a design M_R value. Table 2 summarizes the M_R values on the basis of the 41.4-kPa (6-lb/in.^{2}) deviator stress. Variations among samples at each test site are documented elsewhere (*6*).

Laboratory M_R Values Based on Actual Field Stresses

Actual field deviator stresses were calculated on the basis of the thicknesses and material characteristics of the different layers in each pavement test section. Table 3 summarizes the characteristics of different material types commonly used by the Wyoming DOT. The BISAR (*4*) computer program was used to calculate field deviator stresses. As shown in Figure 3, stresses were calculated on the basis of a 40-kN (9,000-lb) wheel load, a 689-kPa (100-lb/in.^{2}) tire pressure, and a three-layer pavement structure. This program computes the stresses for an n-layer pavement structure by considering the vertical and horizontal loads. Table 4 summarizes the calculated average field deviator stresses for all test sections. These actual field stresses were entered into the M_R equations developed in the laboratory testing, and M_R values based on actual stress conditions were calculated. Table 5 summarizes these M_R values.

Backcalculated M_R Values Based on AASHTO Procedure

M_R values were also determined on the basis of the AASHTO backcalculation equation described earlier. In that equation the minimum distance between the deflection sensors and the loading plate is determined with the following formula:

$$r \geq 0.7a_e$$

where r is the distance from the center of the load and a_e is the radius of the stress bulb at the subgrade-pavement interface. After backcalculating M_R values with the AASHTO equation, a correction factor of 0.33 was applied to all calculated M_R values. This correction factor is specified in the AASHTO design guide (*1*). Table 6 summarizes the backcalculated M_R values for all test sections.

Calculating Overlay Thicknesses

Several spreadsheets were developed to determine the overlay thicknesses for all test sections. The following subgrade M_R values were available for calculating overlay thicknesses: laboratory M_R based on 41.4-kPa (6-lb/in.^{2}) deviator stress, laboratory M_R based on actual field deviator stress, and backcalculated M_R based on AASHTO equation (referred to as LAB, FIELD, and AASHTO, respectively). Tables 2, 5, and 6 list these M_R values. All three sets of M_R values were used in the calculations of overlay thicknesses. The following values were used to calculate the overlays: 85 percent reliability factor, 0.45 standard deviation, and 2.5 as the change in present serviceability index. Overlay thicknesses were calculated at the following three different traffic levels: 800,000, 3,000,000, and 5,000,000 equivalent single axle loads corresponding to low, medium, and high traffic levels, respectively. All design overlay thicknesses were obtained by using a layer coefficient (a_{ol}) of 0.44. Table 7 summarizes the overlay thicknesses (D_{ol}) resulting from this analysis.

DATA ANALYSIS

Comparison Between M_R Values Calculated on the Basis of Actual and Assumed Deviator Stresses

Because laboratory M_R values were calculated by using two different stress conditions, one would want to know if there is any statistical difference between using the actual deviator stress and the assumed value of 41.4kPa (6lb/in.^{2}). Therefore, the test for differences for paired data was performed. The data were placed in two groups, granular and treated, because four of the nine sites had some type

TABLE 2 Laboratory M_R Values (in kPa) Based on 41.4-kPa (6-lb/in.^{2}) Deviator Stress

Roadway	Mile Post	$M_{R\ LAB}$
US-30	48	25793
US-30	70	52704
US-287	416	42941
US-26	108	31199
US-20/26	15	14672
US-20	163	10728
US-16	229	59495
US-16	244	46664
US-85	197.4	60019

TABLE 3 Material Properties Commonly Used by Wyoming DOT

Layer in Pavement Structure	Young's Modulus (MPa)	Unit Weight (kN/m^3)	Poisson's Ratio
Asphalt Cement Mix	2758	23.1	0.35
Granular Base	124	22.8	0.40
Cement Treated Base	5516	22.0	0.25
Asphalt Treated Base	2413	23.1	0.37

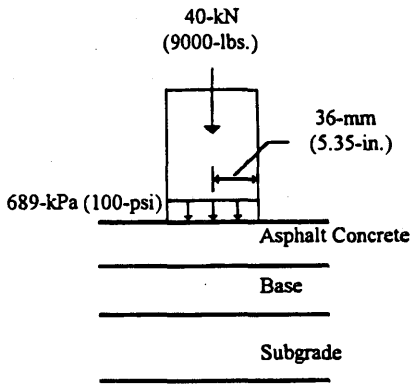

FIGURE 3 Assumptions made in calculating actual field stresses.

of treated base, either asphalt-treated base or cement-treated base. After completing this separation comparisons were performed on all the sites within each group and then by each site individually. Tables 8 and 9 summarize the results for the granular and treated sites, respectively. Both tables indicate that there is not a statistical difference between the two data sets. However, by examining the variances one would favor using the computed field deviator stresses over the assumed 41.4-kPa (6-lb/in.^{2}) values because of the reduction in the amount of variance. By determining actual deviator stresses, the resulting M_R values were more consistent with each test site.

Effect of M_R Selection on Overlay Thicknesses

With three different methods for determining M_R (AASHTO, LAB, and FIELD) it might also be of interest to know if there are any sta-

TABLE 4 Calculated Average Field Deviator Stresses (in kPa)

Roadway	Mile Post	Averaged Field Deviator Stress (σ_d)
US-30	48	13.3
US-30	70	47.7
US-287	416	41.3
US-26	108	43.5
US-20/26	15	30.4
US-20	163	41.8
US-16	229	24.6
US-16	244	49.9
US-85	197.4	14.3

TABLE 5 Laboratory M_R Values (in kPa) Based on Actual Deviator Stresses

Roadway	Mile Post	$M_{R\ FIELD}$
US-30	48	59584
US-30	70	46202
US-287	416	43003
US-26	108	30723
US-20/26	15	19733
US-20	163	16030
US-16	229	96478
US-16	244	39328
US-85	197.4	56516

TABLE 6 Backcalculated M_R Values (in kPa) Based on AASHTO Equation

Roadway	Mile Post	$M_{R\ AASHTO}$
US-30	48	22180
US-30	70	26193
US-287	416	41562
US-26	108	17099
US-20/26	15	20119
US-20	163	28758
US-16	229	51014
US-16	244	33577
US-85	197.4	59805

TABLE 7 Overlay Thicknesses (in mm) for All Test Sections

Roadway	Mile Post	Traffic Level: Low AASHTO D_{ol}	Low LAB D_{ol}	Low FIELD D_{ol}	Medium AASHTO D_{ol}	Medium LAB D_{ol}	Medium FIELD D_{ol}	High AASHTO D_{ol}	High LAB D_{ol}	High FIELD D_{ol}
US-30	48	-133	-144	-198	-88	-100	-162	-69	-82	-147
US-30	70	87	42	50	131	78	88	149	94	104
US-287	416	48	46	46	87	84	84	103	101	100
US-26	108	163	120	121	211	161	162	232	179	180
US-20/26	15	121	146	122	167	195	169	186	216	188
US-20	163	90	167	134	132	221	182	150	243	203
US-16	229	-103	-112	-138	-67	-77	-107	-51	-62	-94
US-16	244	118	97	107	158	134	146	176	150	163
US-85	197.4	-203	-203	-200	-168	-168	-165	-153	-154	-149

TABLE 8 Testing Significance of Differences Between M_R Values for Granular Base Sites

Roadway	Mile Post	M_R (41.4-kPa) Variance	M_R (field) Variance	t	df	p-value
US-30	48	4.25E+06	3.24E+08	3.11	1	0.198
US-30	70	4.33E+08	1.38E+08	1.71	3	0.184
US-287	416	8.53E+07	5.68E+07	0.403	5	0.744
US-26	108	3.08E+08	1.44E+08	0.064	7	0.951
US-20/26	15	2.20E+07	1.60E+07	6.06	5	0.002
Pooled		3.50E+08	2.49E+08	1.07	25	0.293

TABLE 9 Testing Significance of Differences Between M_R Values for Treated Base Sites

Roadway	Mile Post	M_R (41.4-kPa) Variance	M_R (field) Variance	t	df	p-value
US-20	163	3.41E+06	2.23E+06	0.916	1	0.528
US-16	229	1.42E+08	1.65E+09	1.197	1	0.443
US-16	244	4.37E+08	4.00E+08	6.084	10	0.0001
US-85	197.4	3.49E+07	4.32E+08	0.094	1	0.941
Pooled		5.31E+08	8.53E+08	0.630	16	0.537

tistical differences in the calculated overlay thicknesses due to the method used. The negative thicknesses were left in the analysis to provide a better indication of the differences among methods. A repeated measures analysis showed no evidence of differences (null hypothesis) among the methods at low, medium, or high traffic levels ($F_{2,24} = 2.16$, p-value $= 0.1367$; $F_{2,24} = 2.18$, p-value $= 0.1351$; and $F_{2,24} = 2.18$, p-value $= 0.1349$, respectively). Huynh-Feldt epsilon values were calculated to account for any model violations and to make adjustments to the denominator degrees of freedom (df). The values, 0.8690, 0.8725, and 0.8733 for the low, medium, and high traffic levels, respectively, were near 1, indicating that violations were minor.

Even though there were no differences among the methods, one might also want an idea for a given difference in thickness, if one could detect that the methods were not the same. Therefore, the power of the F test was performed to determine the probability of accepting the alternative hypothesis (H_a) that the methods are different. Suppose one is interested in determining if a maximum difference of 25.4 mm (1.0 in.) could be detected. At the low traffic level there was a 0.92 probability that differences would be detected among the three different methods. Overall, 19.1-mm (0.75-in.) maximal differences could be detected with 80 percent probability.

Besides the above test the Tukey procedure for pairwise comparisons was also completed. The following 95 percent confidence intervals were obtained (μ_3 is the treatment mean for AASHTO, μ_2 is the treatment mean for LAB, and μ_1 is the treatment mean for FIELD) for the low traffic level:

$$-0.49 \le \mu_3 - \mu_2 \le 1.01$$
$$-0.13 \le \mu_3 - \mu_1 \le 1.37$$
$$-0.40 \le \mu_2 - \mu_1 \le 1.11$$

These intervals suggest that AASHTO M_R values give the lowest overlay thicknesses. Similar results were obtained at the medium and high levels of traffic, as shown below by the 95 percent confidence intervals, respectively.

$$-0.56 \le \mu_3 - \mu_2 \le 1.17$$
$$-0.15 \le \mu_3 - \mu_1 \le 1.58$$
$$-0.45 \le \mu_2 - \mu_1 \le 1.27$$

$$-0.59 \le \mu_3 - \mu_2 \le 1.23$$
$$-0.16 \le \mu_3 - \mu_1 \le 1.66$$
$$-0.48 \le \mu_2 - \mu_1 \le 1.34$$

SUMMARY AND CONCLUSIONS

Comprehensive field and laboratory evaluations were performed on nine different sites representing typical primary roads in the state of Wyoming. M_R values were obtained from laboratory testing based on 41.4-kPa (6-lb/in.^{2}) deviator stress, laboratory testing based on actual field deviator stresses, and the AASHTO backcalculation equation based on deflection measurements. These values were then used to determine the required overlay thickness at each pavement test site. Based on the extensive data analysis performed in this research project, the following conclusions are drawn:

1. M_R values based on actual deviator stresses did not statistically differ from values based on the assumed deviator stress of 41.4 kPa (6 lb/in.^{2}). However, by computing actual deviator stresses the resulting M_R values within each testing site were more consistent.
2. The three calculated M_R values at each test section did not result in significantly different overlay thicknesses. Among the three, however, the AASHTO M_R value gave the lowest overlay thicknesses.

These conclusions are applicable to all traffic levels considered in the study. Overall, similar overlay thicknesses can be obtained by using backcalculated M_R, laboratory M_R based on a 41.4-kPa (6-lb/in.^{2}) deviator stress, or laboratory M_R based on the actual field deviator stresses.

ACKNOWLEDGMENTS

This cooperative study was funded by the U.S. DOT's University Transportation Program through the Mountain-Plains Consortium, the Wyoming DOT, and the University of Wyoming. The authors express their appreciation to Mike Farrar, Materials Staff Engineer, Wyoming DOT, for assistance in completing the study.

REFERENCES

1. *AASHTO Guide for Design of Pavement Structures*. AASHTO, Washington, D.C., 1993.
2. Thompson M. R., and Q. L. Robnett. *Resilient Properties of Subgrade Soils, Final Report—Data Summary*. Transportation Engineering Series 14, Illinois Cooperative Highway Research and Transportation Program Series 160. University of Illinois at Urbana-Champaign, 1976.
3. Elliott, R. P. Selection of Subgrade Modulus for AASHTO Flexible Pavement Design. In *Transportation Research Record 1354*, TRB, National Research Council, Washington, D.C., pp. 39–44.
4. De John, D. L., M. G. F. Peatz, and A. R. Korswagen. *Computer Program BISAR Layered Systems Under Normal and Tangential Loads*. External Report AMSR.0006.73. Konin Klijke Shell-Laboratorium, Amsterdam, 1973.
5. *Interim Specifications for Transportation Materials and Methods of Sampling and Testing*. Part II. *Interim Test Methods*. AASHTO, Washington, D.C., 1992.
6. Ksaibati, K., M. Whelan, J. Burczyk, and M. Farrar. Factors Influencing the Determination of a Subgrade Resilient Modulus Value. Mountain-Plains Consortium Report 93-19. Mountain-Plains Consortium, Fargo, N.D. 1993.

Publication of this paper sponsored by Committee on Pavement Rehabilitation.

Effective Structural Number Algorithm Enhancements to ROADHOG

KEVIN D. HALL AND QUINTIN B. WATKINS

ROADHOG is a deflection-based flexible pavement overlay design procedure used by the Arkansas Highway and Transportation Department. It uses a structural deficiency approach to overlay design modeled after the guidelines given in the 1986 *AASHTO Guide for Design of Pavement Structures*. The effective structural capacity of the existing pavement (SN_{eff}) is calculated as a function of the difference in the maximum pavement deflection and a deflection at some radial distance from the point of loading. This deflection difference is termed *delta-D*. As originally developed ROADHOG is limited to the structural thickness design of asphalt concrete (AC) overlays for existing conventional flexible pavements (AC surface, granular base, subgrade). Research has enhanced ROADHOG by adding capabilities to determine the SN_{eff} for full-depth asphalt (FDA) pavements and surface-treated pavements (STPs). These enhancements allow the use of ROADHOG for any flexible pavement. The SN_{eff} algorithm for FDA pavements uses a *delta-D* approach similar to the algorithm currently used in ROADHOG for conventional flexible payments. SN_{eff} is determined for STPs by using a deflection ratio, *delta-D/D0*, in which *D0* is the maximum pavement deflection under load. The algorithms are developed by using a comprehensive deflection basin data base generated by the finite-element pavement model ILLI-PAVE, varying surface and base course thickness and stiffness and subgrade stiffness. In both the FDA and STP algorithms the subgrade stiffness is not considered explicitly for estimating SN_{eff}. SN_{eff} estimates for surface-treated pavements also do not explicitly include the granular layer thickness of the STP. Comparisons of the new SN_{eff} algorithms with the current procedures in ROADHOG indicate that the new algorithms give more consistent and accurate estimates of the effective structural number of the existing pavement.

ROADHOG is a deflection-based structural overlay design procedure for flexible pavements developed in 1989 at the University of Arkansas for the Arkansas Highway and Transportation Department (AHTD) (*1*). AHTD designs new pavements by using AASHTO procedures, as detailed in the 1993 *AASHTO Guide for Design of Pavement Structures* (*2*). ROADHOG was developed to be compatible with AHTD new pavement design practices; thus, the structural pavement design concepts in ROADHOG are compatible with AASHTO flexible pavement design. A detailed description of the ROADHOG procedure is given by Hall and Elliott (*3*).

As originally developed the ROADHOG procedure is limited to asphalt concrete (AC) overlays of existing conventional flexible pavements (AC surface, granular base, subgrade). Recently, research was initiated to upgrade and enhance the capabilities of ROADHOG. One such enhancement is the inclusion of additional flexible pavement types as existing pavements. This paper describes the development of algorithms to determine the effective structural capacity (SN_{eff} for flexible pavements) of full-depth asphalt (FDA) pavements and surface-treated pavements (STPs).

Department of Civil Engineering, University of Arkansas, Fayetteville, 4159 Bell Engineering Center, Fayetteville, Ark. 72701.

ROADHOG OVERLAY DESIGN METHODOLOGY

ROADHOG uses a structural deficiency approach to overlay design, similar to that described in the AASHTO guide (*2*). By this approach the structural capacity required of the overlay is calculated as the difference between the structural capacity required to carry future traffic loadings and the effective structural capacity of the existing pavement. For AASHTO flexible pavement design, structural capacity is expressed in terms of a structural number (*SN*). The structural number of the overlay can be expressed in equation form, shown as Equation 1.

$$SN_{ol} = SN_f - SN_{eff} \quad (1)$$

where

SN_{ol} = structural number of overlay,
SN_f = structural number required to carry future traffic, and
SN_{eff} = effective structural number of existing pavement.

SN_f is calculated in a manner similar to that of a new pavement design. The methodology for estimating SN_{eff} in ROADHOG was originally developed by Kong (*4*). A brief synopsis of the SN_{eff} procedure contained in ROADHOG follows.

Figure 1 is an idealized representation of pavement response to an applied load, such as that applied by a falling weight deflectometer to represent a wheel load. At some distance from the applied load (*t*) the pavement surface deflection is almost entirely due to deformation within the subgrade. Directly beneath the load pavement surface deflection is due to deformations within all paving layers. Kong (*4*) suggested that the difference between two deflections, the deflection beneath the load (all layers contributing) and a deflection outside the zone of pavement influence (only subgrade contributing), could be used as a measure of pavement stiffness. If SN_{eff}

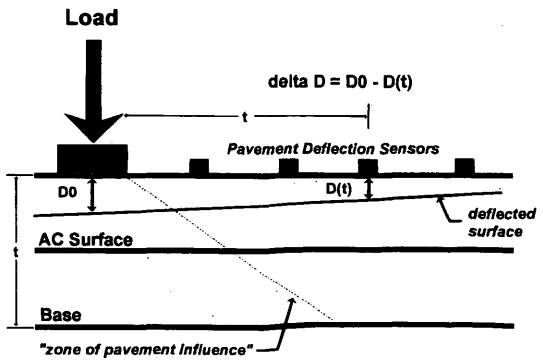

FIGURE 1 Conceptual basis for ROADHOG (*4*).

is a function of pavement stiffness (as assumed by AASHTO), then this deflection difference becomes a measure of SN_{eff}. Kong (*4*) related the SN_{eff} of a number of conventional flexible pavement configurations to a deflection difference termed *delta-D*. He estimated SN_{eff} by component analysis, in which the *SN* of a pavement is the sum of individual layer thicknesses multiplied by appropriate AASHTO layer coefficients (*2*), as shown in Equation 2.

$$SN = a_1d_1 + a_2d_2 \quad (2)$$

where

SN = structural number,
a_n = AASHTO layer coefficient of layer n, and
d_n = thickness of layer n.

Kong (*4*) calculated *delta-D* by using the maximum surface deflection under the load and the surface deflection at a distance away from the load equal to the pavement thickness. Figure 2 shows the relationship between SN_{eff} and *delta-D* for various pavement thicknesses. The *delta-D*-SN_{eff} relationship is primarily a function of total pavement thickness; Kong found the effect of subgrade stiffness to be negligible (*3*).

FDA PAVEMENT ALGORITHMS

The algorithms used to estimate SN_{eff} for FDA pavements are developed in a format similar to those used for conventional flexible pavements in ROADHOG. Three tasks are performed to establish the algorithms: (a) generate a pavement deflection data base, (b) relate SN_{eff} to *delta-D* for each pavement in the data base, and (c) compare results for FDA pavements with the conventional flexible pavement algorithms currently in ROADHOG. The third task is performed to ensure that existing algorithms are insufficient, requiring that specific SN_{eff} algorithms be established for FDA pavements.

FDA Pavement Deflection Data Base

Pavement surface deflections are generated by using the ILLIPAVE finite-element pavement model (*5*). FDA pavements are modeled as two-layer systems (AC surface, subgrade). The parameters that are varied to establish the data base are given in Table 1. Other material properties are selected after work performed by Elliott and Thompson (*6*) and Gomez-Achecar and Thompson (*7*).

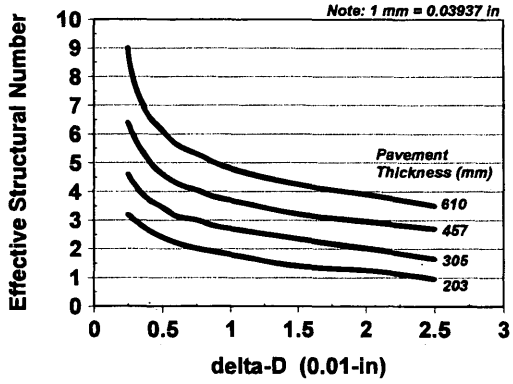

FIGURE 2 Original SN_{eff}/*delta-D* relationships (*4*).

TABLE 1 Parameters Varied To Establish FDA Pavement Data Base

Pavement Layer Property		
Asphalt Concrete		Subgrade
Thickness (mm)	Resilient Modulus (MPa)	Resilient Modulus (MPa)
152	1035	21
203	3450	52
254	10005	83
305		

NOTE: 1 mm = 0.03937 in.
1 Mpa = 0.145 ksi

FDA SN_{eff}/*delta-D* Relationship

The relationship between SN_{eff} and *delta-D* for FDA pavements is shown in Figure 3. The lines shown in Figure 3 result from regression equations fit to the *delta-D*/SN_{eff} data. The degrees of fit as suggested by the regression coefficient r^2 are 0.972, 0.984, 0.987, and 0.991 for FDA pavement thicknesses of 152 mm (6 in.), 203 mm (8 in.), 254 mm (10 in.), and 305 mm (12 in), respectively. Part of the unexplained variation in SN_{eff} (the difference between the reported r^2 value and a perfect fit of 1.0) may be attributed to the effects of AC temperature and subgrade stiffness.

Comparison with Current ROADHOG Algorithm

Figure 4 shows the SN_{eff}/*delta-D* relationship for a 254-mm (10-in.) FDA pavement calculated by using both the new FDA algorithm and the existing ROADHOG algorithm. The general trend shown in Figure 4 for the 254-mm (10-in.) FDA pavement is also observed in similar plots prepared for 152-mm (6-in.), 203-mm (8-in.), and 305-mm (12-in.) FDA pavements. The new FDA algorithms show a *delta-D*/SN_{eff} relationship that is markedly different from that relationship shown by the existing ROADHOG algorithms. This result is not unexpected. The *SN*s used to develop both *delta-D*/SN_{eff} relationships are calculated by a component analysis approach, in which the *SN* of the pavement is the sum of thicknesses (d_i) and layer coefficients (a_i) of the individual layers (*2*). For a given pave-

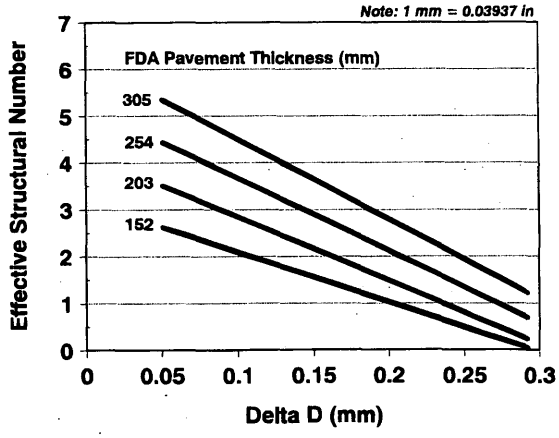

FIGURE 3 Full-depth asphalt SN_{eff}/*delta-D* relationship.

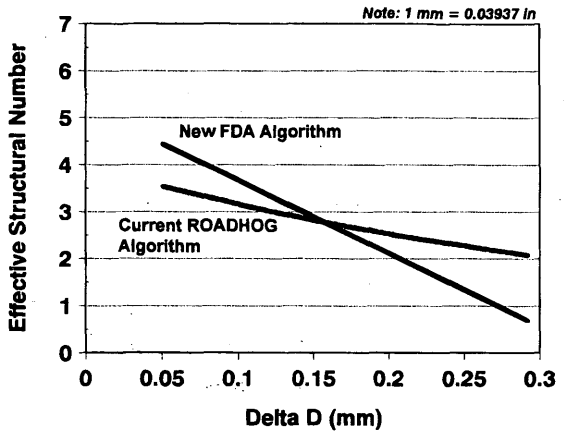

FIGURE 4 Comparison of full-depth asphalt SN_{eff} algorithms, 254-mm pavement.

ment thickness the *SN* of an FDA pavement will be calculated by using a single layer coefficient for AC; for a conventional flexible pavement, some portion of the SN will be calculated by using a layer coefficient for a granular base.

The new SN_{eff} algorithm for FDA pavements should better represent the effective structural capacity of the existing pavement for a given value of *delta-D*. The difference in SN_{eff} values between the two algorithms given in Figure 4 could result in differences in overlay thicknesses of more than 50 mm (2-in.), using a typical AC layer coefficient of 0.44. Continued use of the existing algorithms in ROADHOG could result in conservative overlay thicknesses for FDA pavements with lower *delta-D* values and inadequate overlay thicknesses for FDA pavements with higher *delta-D* values.

STP ALGORITHMS

The algorithms used to estimate SN_{eff} for STPs are developed in a format similar to those used for conventional flexible pavements in ROADHOG. Four tasks are performed to establish the algorithms: (a) generate a pavement deflection data base, (b) determine the extent to which the existing ROADHOG SN_{eff} algorithm accurately and consistently estimates the SN_{eff} of surface-treated pavements in the data base, (c) relate SN_{eff} to the deflection basin for each pavement in the data base, and (d) compare new algorithm results with the conventional flexible pavement algorithms currently in ROADHOG.

STP Deflection Data Base

Pavement surface deflections are generated by using the ILLI-PAVE finite-element pavement model (*5*). STPs are modeled as two-layer systems (granular base, subgrade). No structural contribution is assigned to the surface treatment itself. The parameters that are varied to establish the data base are given in Table 2. Other material properties are selected after work performed by Elliott and Thompson (*6*).

Existing ROADHOG Algorithm

In its current form ROADHOG estimates the SN_{eff} of a pavement on the basis of total pavement thickness and *delta-D*. Figure 5 shows the relationship between *delta-D* and SN_{eff} (as determined by ROADHOG) for STPs. The curves shown in Figure 5 represent various pavement thicknesses; the points representing 152-mm (6-in.) and 203 mm (8-in.) STPs combine to form one curve. The curves indicate that the existing ROADHOG algorithm produces inconsistent results. For the same pavement thickness [greater than 203 mm (8-in.)] identical SN_{eff} values can be produced by using different values of *delta-D*. In addition, the curves show a relationship in which *SN* increases with an increasing *delta-D*, which is not reasonable.

TABLE 2 Parameters Varied To Establish STP Data Base

Pavement Layer Property		
Granular Layer		Subgrade
Thickness (mm)	Resilient Modulus (MPa)	Resilient Modulus (MPa)
152	207	21
203	276	52
254		83
305		

NOTE: 1 mm = 0.03937 in.
1 Mpa = 0.145 ksi

Figure 6 shows the SN_{eff} determined by ROADHOG plotted against the *SN* of the STP calculated by component analysis (in this application the component analysis-based *SN* represents a known structural number). It is seen in Figure 6 that, relative to the component analysis-based *SN*, the existing algorithm in ROADHOG generally overestimates the *SN* of STPs.

It is demonstrated that the existing SN_{eff} algorithm in ROADHOG neither accurately nor consistently estimates the *SN* for STPs.

STP SN_{eff}/*delta-D* Relationship

To be consistent with current ROADHOG design philosophy it is desired that a relationship between pavement stiffness (e.g., *delta-D*) and SN_{eff} that is reasonably independent of the subgrade resilient modulus be established (*1,3*). Unfortunately, traditional SN_{eff}/*delta-D* curves prepared from STP data show strong trends relative to the subgrade modulus value used to generate the data base. Various combinations of deflection basin data were examined to establish a relationship with SN_{eff} that would minimize the effect of subgrade modulus. The best available relationship uses *delta-D* values that are modified by dividing *delta-D* by the maximum deflection *D*0.

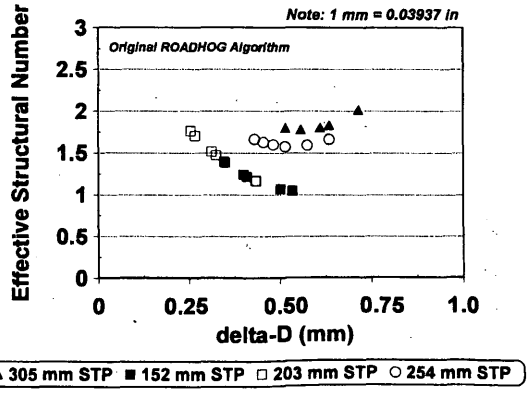

FIGURE 5 *delta-D*/SN_{eff} relationship for STP using current ROADHOG algorithm.

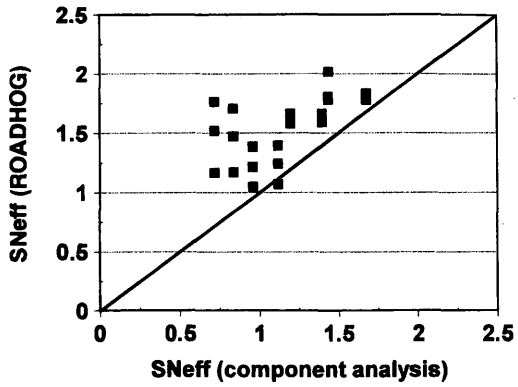

FIGURE 6 Comparison of SN_{eff} values for STPs estimated by using component analysis and current ROADHOG algorithm.

The resulting relationship between SN_{eff} and the (*delta-D/D0*) ratio for STP pavements is shown in Figure 7. In Figure 7 the thickness of the granular layer and the subgrade stiffness are not explicitly used to estimate SN_{eff}. Groupings of the data in Figure 7 are evident; these groupings represent variations in subgrade stiffness and granular layer thickness.

Comparison with Current ROADHOG Algorithm

Both the existing SN_{eff} algorithm used in ROADHOG and the regression line shown in Figure 7 relate pavement deflections to an *SN*; *SN*s used to establish the respective algorithms are calculated by using component analysis of known pavement structures. Figure 8 is a comparison of the relative abilities of the new SN_{eff}/(*delta-D/D0*) relationship and the existing ROADHOG algorithm to estimate the *SN*s of the known pavement configurations used in the study. The existing SN_{eff} algorithm in ROADHOG overestimates the structural number of STPs relative to the new deflection ratio algorithm. In addition, the ROADHOG algorithm is less consistent for STP data, as evidenced by a lower regression coefficient when fitted to a straight line ($r^2 = 0.41$ for ROADHOG versus $r^2 = 0.83$ for the new algorithm).

SUMMARY AND CONCLUSIONS

Algorithms are developed to estimate the SN_{eff} of FDA pavements and STPs on the basis of measured surface deflections. The SN_{eff} algorithms for FDA pavements are a function of the deflection difference *delta-D* as currently defined in the ROADHOG overlay design procedure. In addition, the specific SN_{eff} equation SN_{eff} used for FDA pavements depends on the thickness of the AC. For STPs SN_{eff} is a function of a deflection ratio, *delta-D/D0*, where *delta-D* is as currently defined in the ROADHOG procedure and *D0* is the maximum pavement deflection under load. The SN_{eff} equation for STPs does not explicitly consider granular layer thickness. Neither algorithm, FDA pavements nor STP, explicitly considers the subgrade resilient modulus in SN_{eff} estimation.

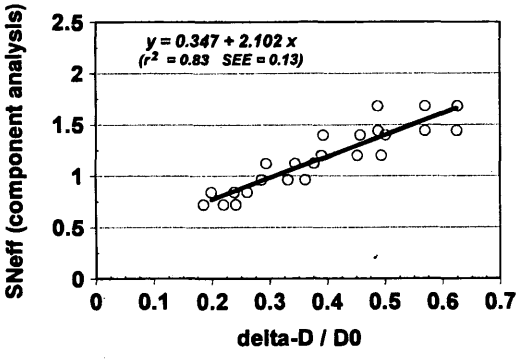

FIGURE 7 Proposed SN_{eff} algorithm for STPs.

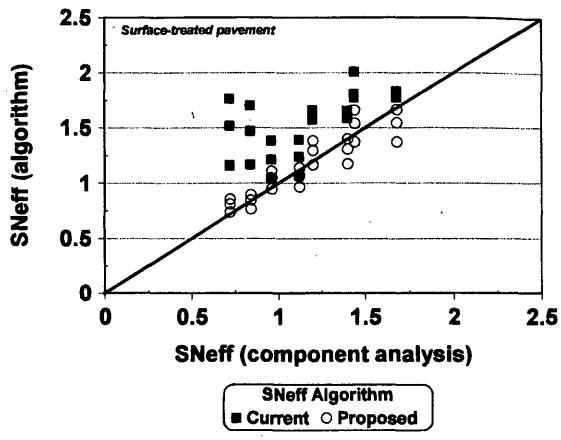

FIGURE 8 Comparison of current and proposed SN_{eff} algorithms for STPs with component analysis-based SN_{eff} values.

Comparisons of SN_{eff} values obtained by using the new algorithms with the values obtained by using current ROADHOG procedures show that the new algorithms provide better estimates of the *SN*s of modeled pavements. These results are not totally unexpected. The SN_{eff}/*delta-D* relationship in ROADHOG is based on conventional flexible pavement configurations. Relationships developed with different pavement configurations should model those configurations better than a generic relationship.

A number of items concerning these analyses must be noted. (a) Both the FDA pavements and STPs are modeled as single-layer, single-material pavements. Multiple layers above the subgrade may change the *SN* relationships shown. (b) The material properties used in the analyses are typical of those found in Arkansas. Significant deviation from the properties used in the pavement models may change the *SN* relationships that were developed. (c) Although AASHTO *SN*s and a structural deficiency approach similar to that recommended in the 1993 AASHTO guide were used in these analyses, FDA pavements and STPs were not included in the testing matrix that resulted in the original AASHTO flexible pavement design/performance equation. The *SN* concept is philosophically sound for use with FDA pavements STPs. However, these analyses do represent an extrapolation beyond the original AASHTO data base.

ACKNOWLEDGMENTS

This paper is based on the project Reliability and Design Procedure Revisions to ROADHOG, conducted by the Department of Civil Engineering at the University of Arkansas. The project is sponsored by AHTD, the U.S. Department of Transportation, FHWA, and the Mack-Blackwell National Rural Transportation Study Center.

REFERENCES

1. Elliott, R. P., K. D. Hall, N. T. Morrison, and S. H. Kong. *The Development of ROADHOG, A Flexible Pavement Overlay Design Procedure*. Final Report: TRC-8705, NDT Overlay Design. Report UAF-AHTRC-90-001. Arkansas State Highway and Transportation Department, Little Rock, 1990.
2. *AASHTO Guide for Design of Pavement Structures*. AASHTO, Washington, D.C., 1986.
3. Hall, K. D., and R. P. Elliot. ROADHOG—A Flexible Pavement Overlay Design Procedure. In *Transportation Research Record 1374*, TRB, National Research Council, Washington, D.C., 1993.
4. Kong, S. H. *Determination of Effective Structural Number in Flexible Pavement Overlay Design*. Master's thesis. University of Arkansas, Fayetteville, 1989.
5. ILLI-PAVE: A Pavement Analysis Program Provided by the Transportation Facilities Group. Department of Civil Engineering, University of Illinois at Urbana-Champaign, 1985.
6. Elliott, R. P., and M. R. Thompson. *Mechanistic Design Concepts for Conventional Flexible Pavements*. Transportation Engineering Series 42. University of Illinois, Urbana, 1985.
7. Gomez-Achecar, M., and M. R. Thompson. ILLI-PAVE Based Response Algorithms for Full-Depth Asphalt Concrete Flexible Pavements. In Transportation Research Record 1095, TRB, National Research Council, Washington, D.C., 1986.

Publication of this paper sponsored by Committee on Pavement Rehabilitation.

Microsurfacing: Solution for Deteriorated Freeway Surfaces

THOMAS J. KAZMIEROWSKI AND ALISON BRADBURY

Many of Ontario's freeway surfaces are showing signs of premature surface deterioration in the form of map cracking, raveling, and coarse aggregate loss associated with the use of 100 percent steel slag coarse and fine aggregates in the hot-mix wearing course. The majority of these freeways will require rehabilitation within the next few years. The Ministry of Transportation of Ontario has reviewed various alternatives for increasing the service lives of these pavements before major rehabilitation becomes a necessity. One alternative strategy was to use microsurfacing to seal, level, and provide a thin, durable, skid-resistant wearing surface. In 1991 the Ministry undertook two demonstration projects to determine if microsurfacing would extend the lives of freeways exhibiting this type of premature surficial deterioration. The project on Highway 401 exhibited very severe map (block) cracking and raveling. The Highway 403 project exhibited severe map (block) cracking throughout the entire length of the project and slight to moderate raveling in some areas. Two contractors using two different microsurfacing systems placed a 3-km four-lane trial section on Highway 403. On the Highway 401 project one contractor placed two 500-m sections over two lanes. The annual average daily traffic at the trial locations was approximately 15,000, with 15 to 25 percent commercial traffic. The design, testing procedures, material characteristics, construction, and short-term performance of the microsurfacing systems that were placed are described. The viability of microsurfacing as a surficial rehabilitation treatment under freeway conditions is also discussed.

In recent years many of Ontario's major freeways have begun to show signs of premature surface deterioration due to the use of steel slag coarse and fine aggregates. The Ministry of Transportation of Ontario (MTO) subsequently banned the use of steel slag as a hot-mix aggregate, but there was still a need to develop a method of extending the lives of these pavements before major rehabilitation is required. Microsurfacing appeared to be an ideal solution because it provides for a restoration of the riding surface that is both cost-effective and environmentally responsible.

In 1991 the Ministry placed a trial section of microsurfacing on a low-volume, secondary highway. The results for this test section were quite encouraging (*1*). The initial project demonstrated that microsurfacing is a viable alternative to a one-lift overlay on low-volume roadways with severe surface deficiencies and a structurally sound base but that it did not mitigate reflection cracking. In addition, it was concluded that the Ministry's high-quality hot-mix aggregates could be used in the microsurfacing mix and that the success of microsurfacing technology was dependent on quality construction practices and prudent mix design (*1*).

To determine if microsurfacing was a viable alternative to a one-lift overlay on structurally sound yet surface-distressed freeways, two projects were undertaken in the summer of 1992: one on Highway 403 and the other on Highway 401. Both highways are four-lane, divided, rural freeways that form part of Ontario's major freeway system.

Pavements and Foundations Section, Ministry of Transportation of Ontario, 1201 Wilson Avenue, Downsview, Ontario M3M 1J8, Canada.

BACKGROUND

Microsurfacing is a polymer-modified, quick-setting, cold-slurry paving system. This high-performance, thin-slurry surfacing consists of a densely graded fine aggregate, polymer-modified asphalt emulsion, water, and mineral fillers (*2*).

The polymer-modified asphalt cement allows the material to remain stable when it is applied in multi-stone thicknesses (*3*). The emulsifier is a proprietary product. Generally, the manufacturers of these emulsifiers license contractors to place their particular microsurfacing products. Micro-surfacing technology was originally developed in Germany in the late 1960s and early 1970s (*4*) and was introduced to North America in the early 1980s. The material is applied with specialized equipment that carries all of the components of the mixture, accurately measures and mixes them in a pug mill, and spreads the mixture over the width of a traffic lane as a thin, homogeneous mixture.

The use of Microsurfacing has several advantages over the use of a one-lift overlay:

- There is a significant conservation of nonrenewable resources, including asphalt cement and aggregates, since the thickness of a lift of microsurfacing is typically 9 to 12 mm, versus 40 mm for a hot-mix overlay.
- This thin surfacing does not significantly alter the road profile; therefore, the need for guiderail adjustments, the need for reductions in bridge clearances, and the need for shoulder granular material are greatly reduced (*5*).
- The cost is approximately 70 percent that of single-lift hot-mix overlay.
- Less energy is expended because the microsurfacing is applied at ambient temperatures. In addition, none of the harmful emissions often associated with hot-mix production are released (*5*).

PROJECT DESCRIPTION

The section of Highway 401 chosen for the trial is located near Chatham, Ontario, Canada, 100 km east of the Windsor, Ontario, and Detroit, Michigan, area. The Highway 403 project is located near Brantford, Ontario, Canada, 100 km west of Toronto.

Two contractors (Contractors A and B) were invited to participate on both trial projects. Contractor A was involved in both the

Highway 401 and 403 projects, and Contractor B took part in only the Highway 403 project.

The Highway 401 project consisted of two 500-m, two-lane segments placed by Contractor A. The width placed was 7.3 m, with 0.5-m partially paved shoulders on both sides.

The Highway 403 project consisted of a 3-km, four-lane section. The lanes were 3.65 m wide, with 0.5-m partially paved shoulders on both the inside and the outside lanes. Contractor A microsurfaced the westbound lanes, and Contractor B completed the eastbound lanes.

The design for both projects consisted of a scratch coat and a final surface coat of microsurfacing. The scratch coat was intended to provide transverse surface leveling by filling in distortions and minor rutting. The final coat was designed to provide a uniform, dense-graded, skid-resistant surface.

These were demonstration projects; therefore, no mix application rates were specified, but to submit a bid representatives from each contracting company made a site visit to assess the site conditions and determine the amount of material required.

EXISTING CONDITIONS

Both Highway 401 and Highway 403 are four-lane, rural freeways with fully controlled access.

A stretch of Highway 401 westbound in the Chatham area, approximately 20 km in length, has severe to very severe raveling throughout, and this has developed into potholing in a few locations. The distresses in this area consist of few moderate transverse cracks and some slight map cracking. The two 500-m sections chosen for the trial had distresses typical of this area. The annual average daily traffic (AADT) is 14,000, with 25 percent commercial traffic.

The 3-km section of Highway 403 was exhibiting map cracking that was severe to very severe throughout, moderate raveling throughout, and intermittent moderate to severe transverse cracking. The AADT is 18,000, with 15 percent commercial traffic.

SPECIFICATIONS

Specifications controlling the microsurfacing operation on this project included the following:

- The binder shall be a quick-set, polymer-modified, cationic-type CSS-1H emulsion.
- The aggregate shall be 100 percent crushed material from bedrock meeting the physical requirements for the Ministry's premium quality hot-mix aggregate.
- The contractor shall select a qualified laboratory to prepare the job mix formulae.
- The mix shall meet the following proportions: residual asphalt, 6 to 11.5 percent by dry mass; mineral filler, 0 to 3.0 percent by dry mass.
- The mixture shall be placed when the atmospheric temperature is at least 10°C and rising and between June 1 and September 15.
- The pavement surface shall be thoroughly cleaned of all debris.
- Water may be sprayed into the spreader box to facilitate spreading without harming the mix.
- Traffic shall be kept off the freshly placed mixture for a minimum of 30 min or whatever time is required to prevent damage to the surface.
- A 100-m-long, one-lane-width trial area of microsurfacing shall be placed off site before the commencement of the microsurfacing operation.

CONSTRUCTION

On the Highway 401 project a single load or stop–start method of applying the microsurfacing was used, where as the Highway 403 project specified the use of the continuous load process of application. A description of the two methods of microsurfacing has been provided previously (*1*).

Highway 401, Contractor A

The project consisted of two 500-m sections of two-lane highway; therefore, a continuous operation was not specified, as would normally have been the case for a highly trafficked and high-speed freeway.

The Highway 401 project was completed on August 18 and 19, 1992. The weather was typically sunny with overcast periods and a cool wind. The ambient temperature ranged from 15°C to 24°C. There was a heavy rainfall during the evening of the first day of construction.

Contractor A used a Scanroad single truck-mounted mixing unit to place the microsurfacing. The waiting time between loads was up to 40 min.

The depth of the scratch coat ranged from 0 to 10 mm. The deepest sections were in the right-lane wheelpaths. The left-lane wheelpaths ranged from 0 to 5 mm in depth. Potholes were not present in either of the two 500-m sections.

The edges and joints were finished with brooms. In general, the mix was very uniform, and few problems with drag or tear marks in the surface were encountered.

When early morning temperatures were cooler the portland cement content was 1.75 percent; as the temperature rose the cement content was lowered to 1.5 percent to delay the set time. Emulsion break occurred at approximately 1 min, and set time occurred at 15 min. A cement content of 1.25 percent was used at the warmest temperatures, and then the break time was 30 to 40 secs and the set time was 5 to 10 min.

Highway 403, Contractor A

Contractor A placed microsurfacing on the westbound lanes of a 3-km, two-lane section of Highway 403. The resurfacing was completed from August 24 to 27, 1992. The ambient temperature during this period ranged from 19°C to 32°C. It was generally sunny in the morning and humid, with some overcast periods.

A continuous load process was specified for this contract. To meet this requirement Contractor A attached a material transfer unit to a truck-mounted mixing unit (the same that was used on the Highway 401 project). Trucks in front of the equipment dumped the aggregate into a hopper where the aggregate was conveyed into the bin on the mixing unit. Water and emulsion were loaded into the appropriate compartments on the mixing unit from tanker trucks on the shoulder of the highway. This method caused some problems because the shoulders varied in width and were not always wide enough to carry the tanker trucks. Another problem was with gravel being kicked onto the roadway from the shoulder by these vehicles.

This larger-size gravel would cause tear or drag marks on the microsurfacing.

The contractor used brooms to feather and finish the edges and joints. The joint at the centerline was not feathered properly, creating a 25- to 50-mm ridge. This created a hazardous situation on a superelevated portion of the roadway where damming of the rainwater in the inner wheelpath area occurred. The contractor milled a 600-mm strip along the centerline, removing the ridge, and resurfaced the entire driving lane with microsurfacing for a distance of approximately 500 m.

The set time was approximately 5 min, and the break time was approximately 1 min. The contractor used either 1.25 or 1.5 percent portland cement content, depending on the ambient temperature.

The scratch and surface coats were both approximately 7 to 11 mm in depth.

Highway 403, Contractor B

Contractor B microsurfaced the eastbound lanes of a 3.0-km, two-lane section of Highway 403. The work was performed from September 1 to 9, 1992. The ambient temperature ranged from 14°C to 22°C; the weather was sunny with intermittent clouds and slight winds.

Contractor B used a continuous truck-mounted mixing unit that included two tandem trucks and an emulsion and water truck that reloaded the mixer from the front rather than from the shoulders of the road. Although this was considered to be continuous because the emulsion, water, and aggregates were added to the mixing equipment from the roadway, the paving was halted for approximately 20 to 25 min while the emulsion and water were added from the tanker trucks.

The contractor used 1 percent portland cement at all times to achieve a set time of 5 to 10 min and a break time of under 1 min.

The scratch coat was an average of 10 mm in depth, and the final coat was 8 to 10 mm in depth.

Contractor B used a small pneumatic-tired roller along the centerline to consolidate any high areas due to overlapping of the microsurfacing lifts.

Production

The application rates for both the scratch and surface coats for Contractor A on Highway 401 were 14.6 and 10.0 kg/m^2, respectively. The rates for Contractor A on Highway 403 were 12.0 kg/m^2 for the scratch coat and 10.2 kg/m^2 for the surface course. The application ranges for the final coats used are within generally acceptable rates of 8.2 to 16.3 kg/m^2 (*4*). Application rates for Contractor B were not available.

On the Highway 401 project Contractor A traveled approximately 300 to 350 m per load for both the scratch and final coats. On the Highway 403 project Contractor A was placing the microsurfacing at a rate of approximately 0.9 m/sec. Contractor B was placing microsurfacing at approximately 0.3 m/sec on the same project.

MIX DESIGN

The mix design used by both of the contractors is shown in Table 1. Contractor A used the same mix design for both the Highway 401 and Highway 403 projects. Contractor A used the Micropave system, and Contractor B used the Micromat system.

The mix design for both contractors was completed by using the International Slurry Surfacing Association (ISSA) methodology as outlined previously (*6*). For the results of mix design see Table 2. A detailed description of the mix design process used in the test sections has been provided previously (*1*).

TABLE 1 Mix Designs

	Highway 403		Highway 401	
	Contractor A	Contractor B	Contractor A	MTO Requirements
Aggregate	Dolomitic sandstone screenings 100%	Traprock screenings 100%	Dolomitic Sandstone Screenings 100%	High quality hot mix aggregate
Mineral Filler	Type 1 Portland Cement 0.2 to 1.5%	Type 1 Portland Cement 1.0%	Type 1 Portland Cement 0.2 to 1.5%	1.5% - 3.0%
Asphalt Emulsion	ASENCO 11.5±1.1%	POLYMAC 12%	ASENCO 11.5±1.1%	---
Residual Asphalt	7.4±0.7%	7.4±0.5%	7.4±0.7%	6% - 11.5%
Water	9 - 12%	11%	9 - 12%	---
Additive	As Required	As Required	As Required	---
Latex (% solids by weight of asphalt)	Latex SBR 3.0%	Natural Latex 3.0%	Latex SBR 3.0%	Min. 3.0%

MATERIAL TESTING

Aggregate

The specifications required that the aggregate meet the quality requirements of the Ministry's premium surface course hot-mix aggregate (HL-1 designation). HL-1 aggregate is a high-quality, skid-resistant, 100 percent crushed aggregate from bedrock that is used for hot-mix surfaces on heavily trafficked highways. Each contractor chose a different type of aggregate, as shown in Table 1, and test results of the aggregate are given in Table 3. The specified gradation was verified on samples taken from the stockpiles of all three trial sections. These results are shown in Table 4 and are plotted as gradation curves in Figure 1.

The gradation results indicate that the aggregate used on the Highway 403 project by Contractor A was within the specified range. The aggregate used by Contractor B was slightly out of the specified range on the 600-μm and 4.75-mm sieves.

The aggregate was also recovered from the microsurfacing samples obtained in the field. The gradation results were similar to those obtained from the stockpile samples.

TABLE 2 Test Results from Mix Designs

			Highway 403		Highway 401
Test Name	Test Number	Requirements	Contractor A	Contractor B	Contractor A
Wet Cohesion @ 30 minutes minimum (kg-cm)	ISSA TB-139	12 minimum	17.5	17.0	17.5
Wet Cohesion @ 60 minutes minimum(kg-cm)	ISSA TB-139	20 minimum	20.0	22.0	20.0
Excess Asphalt by LWT Sand Cohesion(g/m^3)	ISSA TB-109	538 maximum	473	N/A	473
Wet Stripping (%)	ISSA TB-114	Pass (90 minimum)	99	N/A	99
Wet Track Abrasion Loss					
@ 1 Hr. Soak (g/m^2)	ISSA TB-100	538 Maximum	135	291	135
Wet Track Abrasion Loss					
@ 6 Days Soak (g/m^2)	ISSA TB-100	807 Maximum	600	571	600
Lateral Displacement (%)	ISSA TB-147A	5 Maximum	4.7	2.5	4.7
Vertical Displacement (%)	ISSA TB-147A	10 Maximum	9.7	1.5	9.7
Specific Gravity after 1000 cycles of 57 kg		2.10 Maximum	2.01	2.01	2.01
Classification Compatibility	ISSA TB-144	(AAA, BAA) 11 Grade Pt. Minimum	AAA 12 Grade Pt.	BAA 11 pts.	AAA 12 Grade Pts.
Mix Time @25° (sec)	ISSA TB-113	Controllable to 120 Minimum	120	180	120

Notes:
1. Requirements as specified by "ISSA Recommended Performance Guidelines For Micro-Surfacing, A143 (Revised) Jan. 1991"
2. N/A = Not Available

TABLE 3 Aggregate Test Results

Test Name	Test Number	Requirement	Highway 403 Contractor A	Highway 403 Contractor B	Highway 401 Contractor A
Methylene Blue	ISSA TB-145 RTMII 6	Max. 15 ml	2.0	3.5	2.0
Sand Equivalency	ASTM D2419	Min. 60 units	64	75	64

TABLE 4 Aggregate Gradation from Stockpile Samples (Percent Passing)

MTO Sieve Designation (mm)	MTO Requirements	Highway 403 Contractor A (n = 1)	Highway 403 Contractor B (n = 2)	Highway 401 Contractor A (n = 1)
9.500	100	100.0	99.7	100.0
4.750	70 - 90	87.3	82.9	91.0
2.360	45 - 70	60.1	54.8	66.5
1.180	32 - 54	46.9	38.5	53.0
0.600	23 - 38	37.1	29.3	44.0
0.300	16 - 29	24.1	19.8	28.5
0.150	9 - 20	15.9	13.5	19.0
0.075	5 - 15	9.6	8.7	12.5

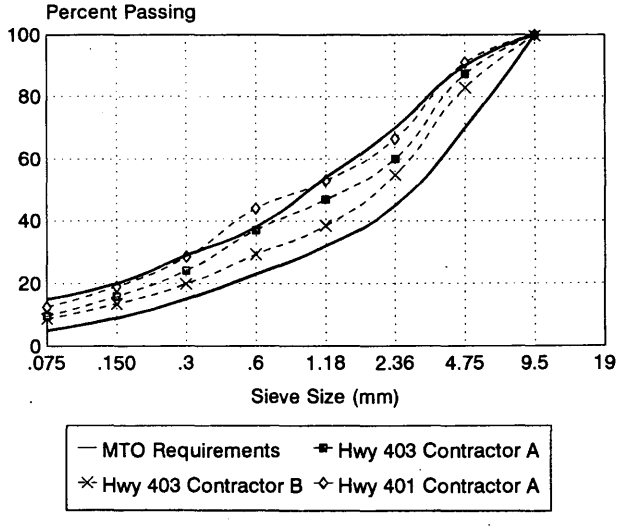

FIGURE 1 Gradation curves for aggregate used in microsurfacing.

Emulsion

Microsurfacing requires a quick-set cationic CSS-1H emulsion. The emulsifier used to produce the emulsion is a proprietary product. The manufacturer or contractor is usually licensed by the manufacturer of the emulsifier to produce the emulsion and place the microsurfacing.

The emulsion used on Highway 403 for both contractors was tested from tanker samples. The emulsions were tested to determine if they met the Ministry's requirements for a CSS-1H emulsion, as required in the specifications. Tests included softening point, penetration, kinematic viscosity, and elastic recovery. The sample from Contractor B did not meet the requirements for kinematic viscosity. The results for emulsion testing are shown in Table 5. The amount of residue was also measured, with all contractors meeting the minimum requirement of 62 percent.

The binders recovered from the field samples of microsurfacing from both contractors on the Highway 403 project were also tested to determine if they still met Ministry standards. The samples from both contractors were low in the requirements for softening point,

TABLE 5 Test Results for Polymer-Modified Emulsified Asphalt Samples

Test Name	Test Number	Requirements	Highway 403 Contractor A (n = 1)	Highway 403 Contractor B (n = 2)	Highway 401 Contractor A (n = 1)
Softening Point (°C)	ASTM D36	57°C Min.	58.0°C	57.5°C	63.9°C
Penetration @ (25°C, 100 g, 5 s, 0.1 cm)	MTO LS-200	40 - 90	85	88	N/A**
Kinematic Viscosity @ 135°C(mm^2/s)	ASTM D2170	650 Min.	994	601	N/A**
Elastic Recovery @ 10C (20 cm extension)	N/A*	Not Specified	47.5	35.4	N/A**
(Length)			20	15	
Residue Distillation (%)	MTO LS-219	62	62.7	64.0	63.9

* Proposed ASTM standard test.
** Sample not tested.

and the sample from Contractor A was low in the requirements for kinematic viscosity. The results are presented in Table 6.

The residue from the emulsion samples of Contractor A had a penetration of 85 and a kinematic viscosity of 994 mm^2/sec, yet the results from the recovered residue showed an increased penetration of 86.7 and a lower kinematic viscosity of 617 mm^2/sec, indicating that the residue is softer. The results from the emulsion used by Contractor B show the residue becoming stiffer after mixing. The penetration went from 88 to 57.5 and the kinematic viscosity went from 601 to 1188 mm^2/sec.

Samples of the emulsion and microsurfacing from the Highway 401 project were not taken.

Polymer Modifier

Contractor A used an SBR latex (synthetic polymer), whereas Contractor B used a natural latex.

The minimum amount of polymer modifier was specified to be 3.0 percent by weight of asphalt cement (Table 1). However, binder temperature susceptibility characteristics (defined in the specifications by penetration index, softening point, and kinematic viscosity) are often considered to be more important than the quantity of the polymer. In other words, a certain amount of modifier is required to achieve the desirable temperature susceptibility of the binder.

TABLE 6 Test Results for Polymer-Modified Emulsified Asphalt

Test Name	Test Number	Requirements	Highway 403 Contractor A (n = 3)	Highway 403 Contractor B (n = 2)	Highway 401 Contractor A
Softening Point (°C)	ASTM D36	57°C Min.	48.9	56.8	N/A*
Penetration @ (25°C, 100 g, 5 s) 0.01 cm	MTO LS-200	40 - 90	86.7	57.5	N/A*
Kinematic Viscosity 135°C (cSt/Sec)	ASTM D2170	650 Min.	617	1188	N/A*

* Not available; samples not tested

PAVEMENT PERFORMANCE

Pavement Condition

The pavement conditions of all three trial sections have been reviewed periodically since construction. In the summer of 1994, approximately 20 months after the work was completed, the following characteristics were noted.

Highway 401, Contractor A

This section had an excellent ride with a uniform texture throughout. There was no snowplow damage in the two 500-m sections. There was no raveling, delaminations, or deformations. All working transverse cracks had reflected through, although there was no spalling. A slight chatter, which occurred during construction, still remains. Slight buildup occurred at the centerline.

Highway 403, Contractor A

Overall, this section is in good condition, with no sign of any snowplow damage.

Slight to moderate reflection cracking, both map and transverse, was apparent, but no raveling was apparent at the cracks. Very slight chattering was still evident, and very slight longitudinal streaking was apparent because the original burlap drag was still apparent. The centerline ridge was still pronounced enough to lightly affect steering when a vehicle drives over the ridge.

Highway 403, Contractor B

This section also appeared to be in good condition, with no snowplow damage and a uniform texture.

Other distresses noted in this section were few, slight to moderate transverse reflection cracking and intermittent, slight, reflective map cracking. No occurrences of delamination, raveling, or coarse aggregate loss were found.

Rutting

Rutting surveys were done before and after construction with the Automatic Road Analyzer (ARAN). On the front bumper of the ARAN is a 3.75-m-long "smart bar" equipped with ultrasonic sensors placed at 100-mm intervals. These sensors bounce signals off the pavement and record the relative distance between the bar and the surface. These data are interpreted to give a transverse profile of the pavement lanes (*7*).

The average rut depths on the Highway 401 project are given in Figure 2. The rut depths were averaged for both 500-m sections. Although the original rut depths on this project were slight, the average rut depth in both lanes was reduced after construction. The average rut depth in lane 1 decreased to 3.3 mm from 8.5 mm, and in lane 2 it decreased to 4.9 mm from 7.9 mm. Twenty-one months after construction the rut depth in lane 1 increased slightly to 5.0 mm, and it remained unchanged at 4.2 mm in lane 2.

Figure 3 shows the average rut depths for the Highway 403 project. Before construction the rut depths in both the eastbound and the westbound lanes were similar and very slight: lane 1 at 4.6 and 5.1 mm and lane 2 at 7.6 and 6.9 mm, respectively. Results of the ARAN testing at 9 and 21 months after construction reveal that the results were very similar for the sections constructed by both contractors. The average rut depths in lane 1 remain virtually unchanged 21 months after construction, with depths of 4.5 mm in the westbound lanes and 4.3 mm in the eastbound lanes. The results of ARAN testing in lane 2 showed similar results, with an insignificant decrease in rut depth 21 months after construction: 6.1 mm in the westbound lane and at 5.8 mm in the eastbound lane.

Roughness

Before construction roughness surveys were taken with a portable Universal Roughness Device (PURD). PURD is a trailer-mounted, accelerometer-based measuring device operated at a constant speed on the highway. It uses the root mean square of the vertical acceleration of the trailer axle (PURD) to measure roughness. These are converted into a riding comfort rating (RCR) as follows (*7*):

$$RCR = 26.64 - 7.38 \cdot \log_{10}(PURD)$$

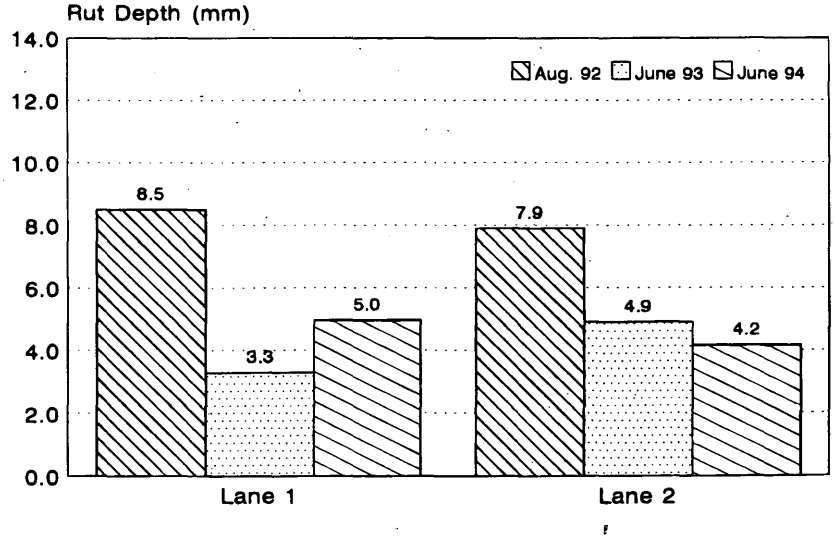

FIGURE 2 Average rut depths for Highway 401.

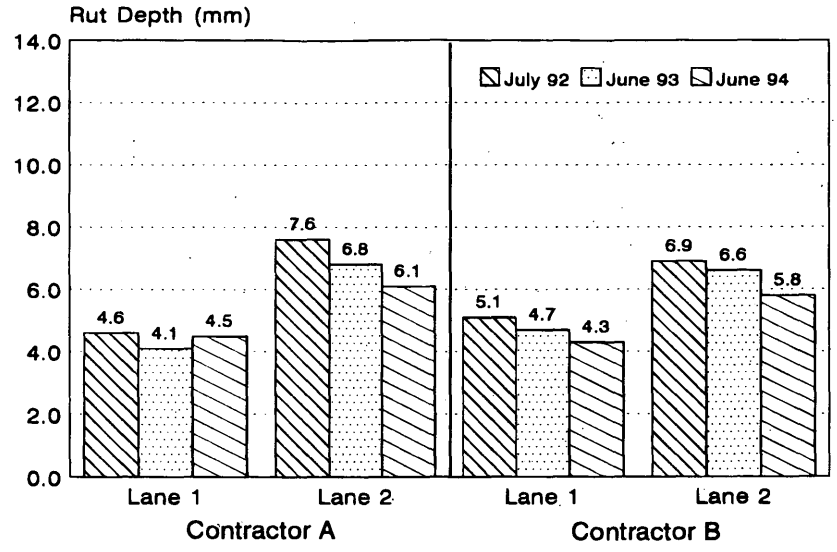

FIGURE 3 Average rut depths for Highway 403.

One of the limitations of the PURD is the inability to filter out the effect of the pavement's macrotexture from overall roughness results. This becomes a significant concern when measuring tined surfaces or surface treatments (such as microsurfacing), in which there can be an aggressive macrotexture. For this reason roughness measurements after construction were taken with a Mays Ride Meter (MRM). MRM is a road response-type measuring device that is mounted onto the rear axle of a vehicle or trailer operated at a constant speed.

MRM uses the vertical distance that the vehicle travels with respect to the rear axle in inches per mile to measure the roughness. Measurements taken with MRM are currently converted to RCR by the following transfer function:

$$RCR = 9.38 - 0.0177 \cdot (MAYS)$$

The average roughness results for the Highway 401 project are given in Figure 4 for lanes 1 and 2. The roughness results for both 500-m sections were averaged together. The RCRs before construction were 6.3 and 6.4 in lanes 1 and 2, respectively, which are in the lower end of the comfortable category. Nine months after construction the readings for lanes 1 and 2 were 7.5 and 7.6, respectively. Readings 21 months after construction are almost identical at 7.5 and 7.7 for lanes 1 and 2, respectively. The micro-surfacing improved the rides on these short sections to the upper portion of the comfortable range.

Figure 5 provides the average RCRs for both contractors on the Highway 403 project for lanes 1 and 2.

The roughnesses of the eastbound and westbound lanes before construction were very similar, with RCR of 7.4 to 7.8, putting the ride in the upper portion of the comfortable category.

The westbound lanes, Contractor A's section, showed an increase in the ride characteristics after construction. The RCR over the 21-month evaluation period places it in the middle portion of the smooth range, with an RCR of 8.8 for both lanes.

The results of the Mays roughness testing on the eastbound lanes indicated that the ride is very similar to that on the westbound lanes. The RCR in both lanes 9 months after construction was 8.3, and

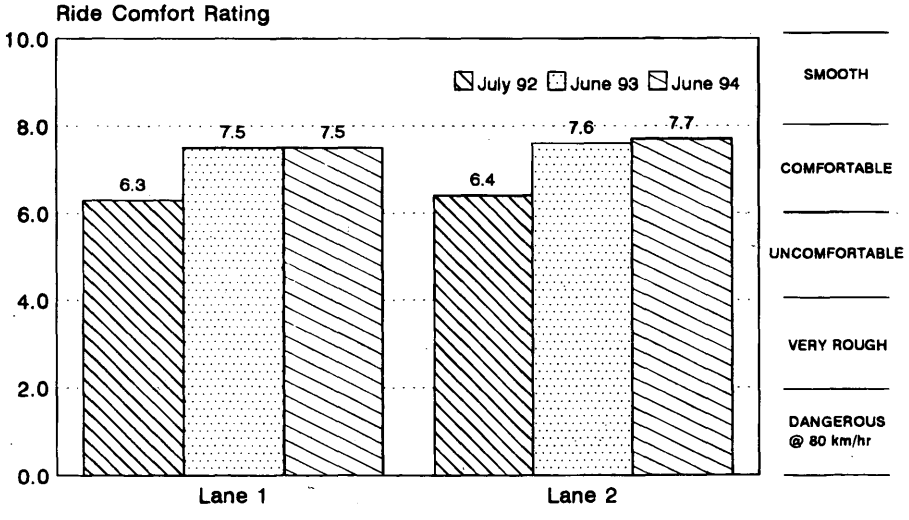

FIGURE 4 Average roughness for Highway 401.

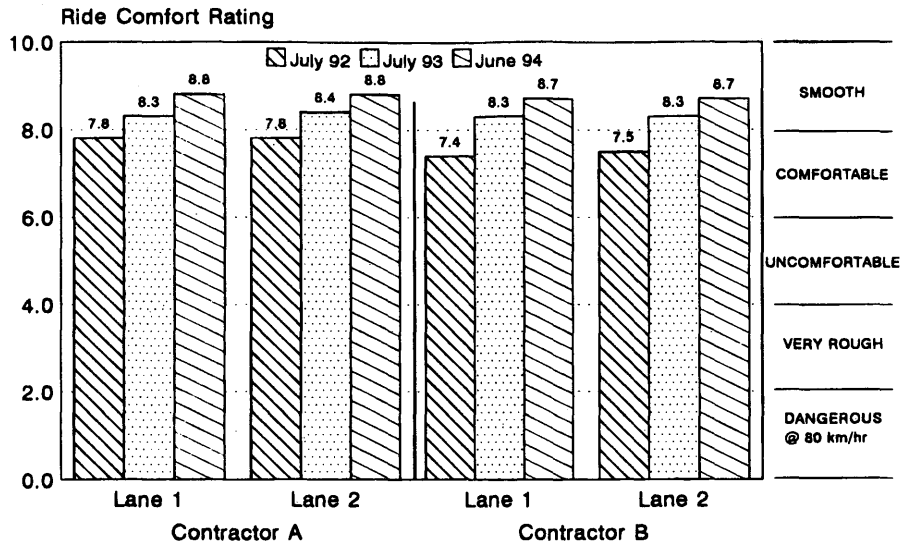

FIGURE 5 Average roughness for Highway 403.

after 21 months the RCR was 8.7, again placing the ride in the lower portion of the smooth category.

Skid Resistance

The relative skid resistance of a pavement is given in terms of a skid number (SN). This number was obtained by field measurements by using an ASTM brake force trailer (*7*).

Figure 6 shows the results of the skid resistance survey for the Highway 401 project, lane 2. It indicates that the skid resistance immediately after construction was at a high level, with an SN of 44, and the level remained high after 8 and 20 months after construction, at SNs of 45 and 53, respectively. The results for lane 1 were similar.

Figures 7 and 8 show the skid surveys for lanes 2 of both the westbound and eastbound lanes of the Highway 403 project. The westbound lane 2 (Contractor A) indicated a high skid level, with an SN of 41 before construction: Nine months after microsurfacing the value increased to an SN of 46 and remained consistent with an SN of 47 after 20 months. In lane 2 of the eastbound lanes, Contractor B's section, the results are similar to those for Contractor A's section; the original SN of 41 rose to an SN of 49 nine months after construction and fell slightly to 43 twenty months after construction.

The results of the skid testing indicate that the microsurfacing surfaces on both projects and for both contractors exhibits a high frictional resistance, similar to those of freeways with a premium-quality hot-mix surface.

CONCLUSIONS

This paper summarized the design and construction of two trial microsurfacing projects on freeways. On the basis of the short-term results of this project coupled with the positive results of the Ministry's first microsurfacing project (*1*), it appears that microsur-

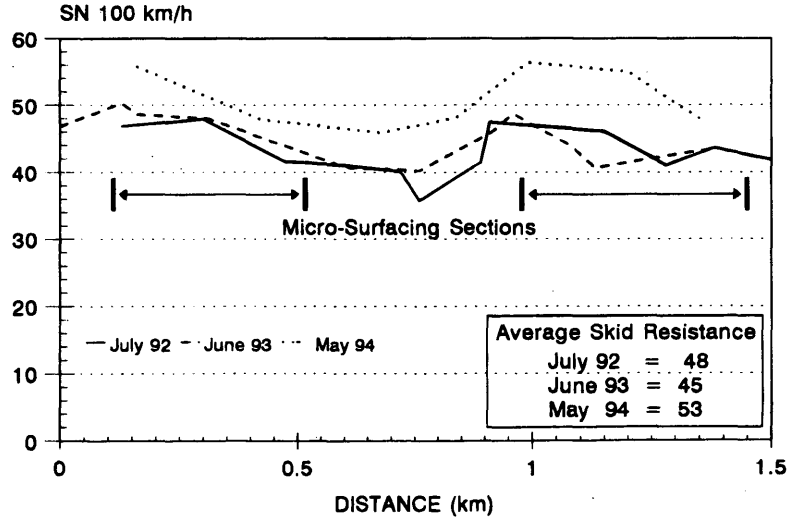

FIGURE 6 Skid resistance survey, Contractor A, Highway 401, Lane 2.

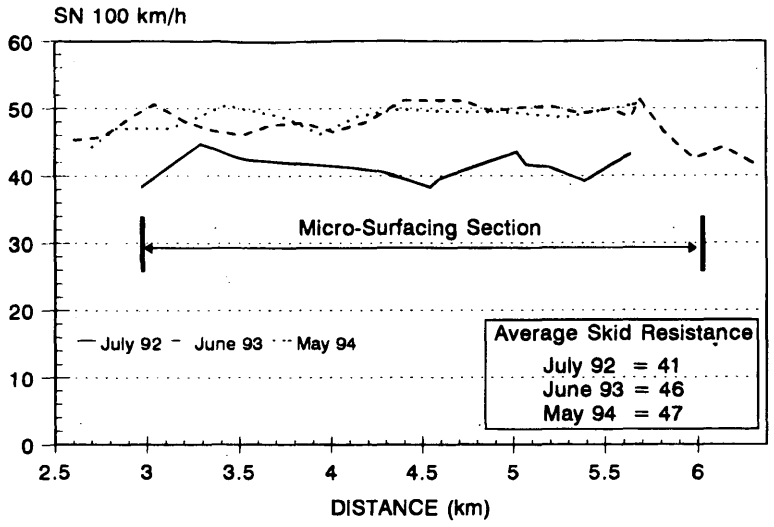

FIGURE 7 Skid resistance survey, Contractor A, Highway 403, westbound Lane 2.

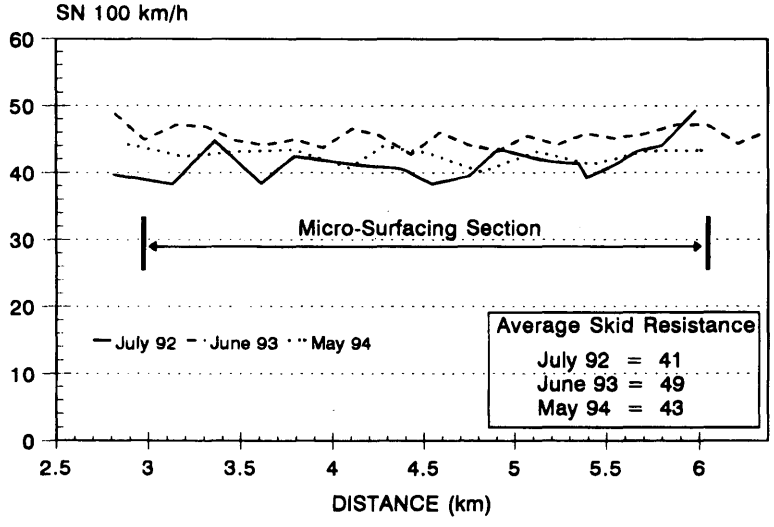

FIGURE 8 Skid resistance survey, Contractor B, Highway 403, eastbound Lane 2.

facing can provide a viable alternative rehabilitation technique for extending the pavement lives of high-speed, highly trafficked freeways suffering from severe surficial distresses.

The following short-term conclusions are made on the basis of the results of the two projects described in this paper.

- Microsurfacing provides a durable, highly skid-resistant surface comparable to the Ministry's premium hot-mix surfaces.
- Microsurfacing appears to have the potential to extend the life of a pavement suffering from the distresses associated with the use of steel slag aggregates in the wearing surface, at least in the short term.
- The microsurfacing provides a uniform surface that rides within the comfortable to smooth range on the basis of MRM testing.
- The weather conditions have a considerable effect on the constructability of microsurfacing; this underscores the need for an experienced, skilled, and knowledgeable crew that can make the slight adjustments to the mix design that may be required as the ambient weather conditions change during the operation.
- Both contractors designed and placed an acceptable microsurfacing product on both trial projects, and both projects have exhibited similar performance results to date, although it is noted that care must be taken to minimize the amount of overlap between lanes, especially on superelevated pavements.

RECOMMENDATIONS

The following areas require further study and development.

- By monitoring and testing, establish the mid- to long-term performance characteristics of microsurfacing on freeway facilities in a wet–freeze environment.

- Additional trials are required to determine the effectiveness of microsurfacing as a rut fill material and possible crack and pothole fill material.
- A quick field methodology is required to assess application rates and check on mix design.
- Rationalize quality assurance testing to characterize surface texture and mix design requirements.
- An equitable 2-year warranty specification should be developed (*8*).

REFERENCES

1. Kazmierowski, T. J., A. Bradbury, G. Jones, and J. Hajek. Effectiveness of High Performance Thin Surfacings in a Wet-Freeze Environment. In *Transportation Research Record 1392*, TRB, National Research Council, Washington, D.C. 1993, pp. 3–12.
2. Micro-Surfacing Pavement Resurfacing. International Slurry Surfacing Association, Washington, D.C.
3. Doyle, M. P., and K. R. Kramer. Comparison of Mix Design Methods to Determine Optimum Bitumen Content in Micro-Surfacing Systems. *Proc, ISSA*, Feb. 1989, pp. 85–136.
4. Pederson, C. M., W. J. Schuller, and C. D. Hixon. Micro-Surfacing with Natural Latex-Modified Asphalt Emulsion: A Field Evaluation. In *Transportation Research Record 1171*, TRB, National Research Council, Washington, D.C., 1988, pp. 108–112.
5. Reinke, G., W. R. Ballou, S. L. Engber, and T. M. O'Connell. Studies of Polymer Modified Micro-Surfacing Materials in Highway Maintenance. *Proc. ISSA*, Feb. 1989, pp. 45–83.
6. *Recommended Performance Guidelines for Micro-Surfacing*, Design Technical Bulletin A143 (revised). International Slurry Surfacing Association, Washington, D.C., Jan. 1991.
7. *Pavement Design and Rehabilitation Manual.* Report SDO-90-01. Surveys and Design Office, Ministry of Transportation of Ontario, Downsview, Ontario, Canada, 1990, Chapt. S.
8. *State of the Practice Design, Construction, and Performance of Micro-Surfacing*. FH WA, U.S. Department of Transportation, June 1994.

Publication of this paper sponsored by Committee on Pavement Rehabilitation.

Categorization of Asphalt Overlays on Broken and Seated Pavements

RAJAGOPAL S. ARUDI, KRISHNA KANDULA, ISSAM A. MINKARAH, AND MAHESH BHUPALAM

Breaking and seating (B/S) concrete pavements before the construction of an asphalt concrete overlay is a method adopted by several states to minimize the problem of reflection cracking in composite pavements. Breaking the slabs into smaller pieces decreases their effective length and reduces the thermal movements that are the root cause of the development of reflection cracking. The B/S treatment has a significant effect on the structural response and behavior of the concrete slab. After B/S, slab structural models such as the Westergaard model or finite element models are not applicable. The two most important factors that affect the performance of such pavements are (i) the extent of breaking and (ii) the sizes and patterns of the broken slabs. Traditionally, pavements with asphalt concrete overlays on broken and seated concrete slabs are categorized as flexible pavements, and an equivalent modulus characterizing the B/S layer is used for mechanistic modeling. To investigate the validity of this practice, a comparative analysis of a large quantity of Dynaflect deflection data on flexible, composite, and B/S pavements in Ohio is presented. The original pavement in all composite and B/S sections studied was jointed reinforced concrete. Based on maximum deflection, spreadability, and the W_1/W_5 ratio, the observed performance of asphalt overlays on B/S pavements with 0.152- to 0.762-m fragments closely resembles those of composite pavements rather than those of flexible pavements.

The proper categorization of pavements is an essential step toward developing techniques for their design and evaluation. Historically, pavements are divided into two broad categories, namely, flexible and rigid. The characteristics of the materials used in the construction of these pavements have a major influence on their categorization. Accordingly, several design and evaluation procedures have been developed for new as well as in-service flexible and rigid pavements. When an in-service flexible pavement receives a rehabilitation treatment in the form of an asphalt concrete (AC) overlay, the pavement is still classified as a flexible pavement. When a rigid pavement is in need of rehabilitation, a widely used action is, again, to provide an AC overlay. Such pavements have come to be known as composite pavements.

The performance of composite pavements is largely governed by the underlying concrete layer. Thermal movements of the concrete slabs at the joints and at working cracks exert excessive strains in the AC layer that result in the development of reflection cracking (Figure 1). The cracks form at the bottom of the asphalt layer, above a joint or a crack, and propagate vertically to the surface. Such cracks cause early deterioration of the overlay, increase life-cycle costs, and reduce the useful life of the pavement.

Some of the methods proposed for the control of reflection cracking in AC overlays include (a) providing a thick overlay; (b) changing the viscosity of the asphalt; (c) using admixtures in the AC mix; (d) treating the existing, cracked pavement before overlay by means of breaking, stabilizing, and crack sealing; (e) using stress-relieving interlayers (e.g., asphalt rubber, fabrics, and membranes); and (f) sawing and sealing the joints in the overlay directly above the joint in the concrete (*1*). A recent comprehensive survey by the National Asphalt Pavement Association (*2*) showed the widespread use of the cracking and the breaking and seating (B/S) procedure for rehabilitating portland cement concrete (PCC) pavements.

Rehabilitation of a composite pavement by (B/S) PCC slabs involves milling the existing AC layer, breaking the PCC slabs, and seating the slab fragments with a heavy roller. In doing so composite pavements are transformed into B/S pavements, and with the addition of AC overlays, they are categorized as flexible pavements. However, the operation of breaking induces many variables in the pavement, as shown in Figure 2.

The two most important factors that affect the performance of such pavements are (a) the extent of breaking and (b) the size and pattern of the broken slabs. Slabs have been broken into sizes ranging from 0.152 to 0.762 m. A considerable discrepancy in establishing the crack pattern has been noticed among states. Cracking is normally achieved in both the transverse and the longitudinal directions. Some states require cracking in only a transverse pattern. Also, certain agencies do not break the steel reinforcement. Other factors such as the moisture condition of the subgrade soil also have a significant effect on the extent of breaking achieved.

No specific studies have been carried out to ascertain the effects of these variables on the performance of asphalt overlays. There is a need to establish the effect of the extent of breaking and the cracked slab size in classifying AC overlays on B/S PCC pavements.

CONSEQUENCES OF BREAKING

Crack initiation in PCC pavements is generally believed to be caused by the vertical and horizontal movements of the slabs. Horizontal movements may be due to temperature variations that induce

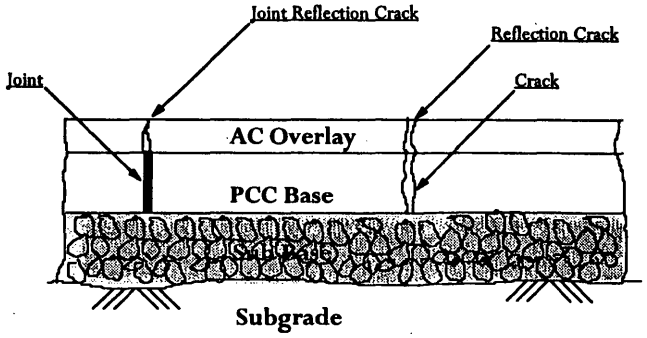

FIGURE 1 Reflection cracking on composite pavements.

Department of Civil and Environmental Engineering, University of Cincinnati, P.O. Box 210071, Cincinnati, Ohio 45221–0071.

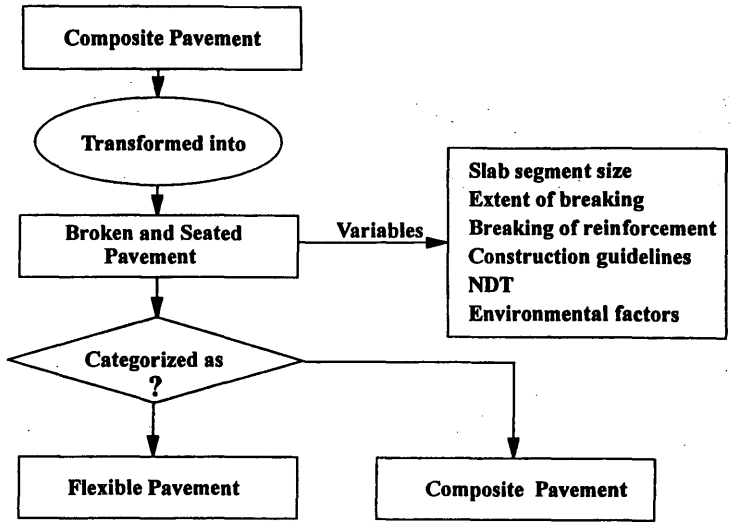

FIGURE 2 Categorization of broken and seated pavements.

contraction and expansion in the slabs. Studies show that such movements are directly proportional to the length of the slab (*3*). This implies that with a shorter length there is a better chance of reducing crack development and in turn reflection cracking. However, breaking PCC slabs into smaller pieces results in a reduction of the flexural strength and an increase in surface deflection and subgrade stress. The optimum size of the cracked pieces for retaining structural integrity and at the same time minimizing thermal movements is yet to be established. The AASHTO (*4*) specifications suggest breaking the slab into nominal pieces of 0.610 to 1.067 m in size.

OBJECTIVES

The Ohio Department of Transportation (ODOT) has built several lane miles of experimental sections with AC overlays on B/S PCC pavements. These sections along with the road network in the state are routinely monitored by ODOT as part of its maintenance and management program. A vast quantity of Dynaflect deflection data has been recorded for all pavements since 1985. By using this information the present study attempts to accomplish the following objectives:

1. Develop a data base of Dynaflect deflections for various classes of pavements,
2. Analyze the deflection data to examine the structural effectiveness of pavements,
3. Investigate the effect of cracked slab size on the structural effectiveness of AC overlays on B/S pavements,
4. Statistically compare the deflection characteristics of various pavements, and
5. Find the validity of treating B/S pavements as flexible pavements.

DATA GATHERING

Since 1984 ODOT has used Dynaflect deflection measurements to design AC overlays on all four-lane pavements programmed for rehabilitation. Slight variations in measured deflections on rigid pavements resulted in substantial differences in overlay thicknesses when they were calculated by a two-layer elastic procedure. After observing the deflection data it seemed that a dynamic load larger than 4.448 kN (that is used in Dynaflect equipment) would result in a better design of overlay thicknesses on rigid and composite pavements. Thus, research was initiated to compare the results obtained from Dynaflect and a falling weight deflectometer (FWD). The results presented in an ODOT report by Edwards et al. (*5*) indicated that although differences occurred from pavement to pavement, the deflections obtained with Dynaflect on the average correlated quite well with FWD measurements. Pavement nonlinearity was not significant. Based on the results of the study, it was concluded that ODOT will continue to use Dynaflect deflection measurements to design overlays.

All available Dynaflect deflection data due to a 4.448-kN load on flexible, rigid [continuously reinforced concrete pavement (CRCP), jointed reinforced concrete pavement (JRCP)], composite, and B/S pavements were retrieved from the ODOT mainframe computer. Table 1 presents the number of pavement sections, number of deflection tests on each section, and other available details for each class of pavement. On each section 30 to 100 Dynaflect measurements were made, depending on the total section length. Other available data included air and pavement surface temperature at the time of deflection measurements and the thickness of the AC surface and PCC layers. For composite pavements data such as the year of construction, jointing arrangement, the use of load transfer devices, and reinforcement details were not available. For some sections, however, the condition of the pavement in terms of the presence of cracks, rutting, or faulting was available at the points where deflection measurements were made. Since this information was not available for all sections, the condition data were not used in the analysis and are not presented here.

Seven in-service composite pavement sections were rehabilitated with AC after removing the existing AC surface layer and then breaking and seating the underlying PCC pavements. These PCC pavements consisted of jointed reinforced concrete slabs on a 0.152-m granular subbase. Breaking was achieved by using either a guillotine or a pile hammer. An attempt was made to get uniform breakage in each section; however, most of the pavements broken with the guillotine hammer had a problem where drops overlapped,

TABLE 1 Dynaflect Deflection Measurements

Pavement Type	# of Pavement Sections	# of Deflection Tests	AC Thickness Range (m)	PCC Thickness (m)		Pavement Surface Temperature (°C)	W_1 (mm)	W_5 (mm)	Spreadability (%)	W_1/W_5
Flexible	108	3711	0.165 -0. 311		Average	13	0.014	0.005	66.71	2.88
					Deviation	18	0.30	0.09	8	1.11
Composite	188	17956	0.076 -0. 216	0.228	Average	15	0.011	0.006	75.19	1.96
					Deviation	14	0.19	0.08	7.87	0.4
CRCP	29	556		0.228	Average	10	0.012	0.007	75.96	1.84
					Deviation	21	0.08	0.06	3.98	0.28
JRCP	134	8258		0.228	Average	13	0.012	0.007	75.86	1.93
					Deviation	19	0.17	0.11	5.65	0.35
Break and Seat (0.152 m fragments)	3	54	0.076 -0. 216	0.228	Average	14	0.012	0.005	79.9	1.86
					Deviation	9	0.20	0.07	4.58	0.32
Break and Seat (0.457 m fragments)	7	246	0.076 -0. 216	0.228	Average	10	0.011	0.005	73.44	2.36
					Deviation	14	0.14	0.08	12.75	0.56
Break and Seat (0.762 m fragments)	3	54	0.076 -0. 216	0.228	Average	16	0.010	0.005	82.28	1.7
					Deviation	11	0.10	0.08	2.5	0.16

Note: 1m = 39.37 in.
1 mm = 0.039 in.
°F = 1.8 *(°C) + 32

usually in the middle of the lane. This area was cracked much more than the other parts. Breaking resulted in thorough slab cracking, and no additional effort was made to break the reinforcement. All of the data collected were entered into a data base and were sorted by type of pavement. A separate data base was established for each type of pavement.

DATA PROCESSING

The thickness of the PCC layer in composite and B/S pavements was constant and was equal to 0.229 m (Table 1). However, the thickness of the AC layer and the surface temperature at the time of deflection measurements varied with each project. Although subgrade soil characteristics varied, no laboratory data on soil properties were available for analysis. The broken and seated pavements received thick overlays, either 0.165 or 0.216 m. Initially, an attempt was made to normalize deflection values to a standard temperature by using a model developed at the University of Toledo (*6*). This model requires data on site-specific conditions such as solar radiation, wind, air temperature, cloud cover, and other factors to calculate the temperature profile within an AC layer at a given time. Since such data were not available for all sections, the analysis was simplified by normalizing deflections to a standard temperature of 21°C by the Asphalt Institute method (*7*). This method relies only on surface temperature, which was measured at the time of the Dynaflect tests.

The Dynaflect data from each group of pavements were analyzed for three structural parameters, namely W_1, W_1/W_5 ratio, and spreadability. The results are provided in Table 1. The numbers of flexible and composite pavement sections were significantly higher than the numbers of B/S sections (Table 1). The scatter of the average maximum deflections (W_1), the W_1/W_5 ratios, and spreadability are plotted (see Figures 4, 5, and 6). For a better visualization of the data section averages were plotted for composite and flexible pavements and individual points were plotted for B/S pavements. This was necessary because only a few sections were available for B/S pavements.

SIGNIFICANCE OF W_1/W_5 RATIO

The measurement of the deflection basin on the pavement surface is used to evaluate its structural capacity. Figure 3 shows the stress distribution in a typical pavement structure subjected to a load (*4*). The stress due to the load gets distributed over a wide area through the upper layers of the pavement before reaching the subgrade level. The deflection values measured at or beyond a_{3e} are indicative of subgrade characteristics. The measured surface deflection at this radial offset value must logically be influenced by the subgrade layer. It is generally believed that the deflection value W_5 obtained from Dynaflect measurements indicates subgrade soil properties. A ratio of W_1 and W_5 can be a good indicator of the load-spreading characteristics of pavement layers, which is a function of pavement type. If two pavements have nearly equal W_5 measurements, the values of the maximum deflections (W_1) would indicate the relative strengths of the two pavements, with the weaker pavement exhibiting a higher maximum deflection. The ratio of W_1/W_5 for the weaker pavement would be higher than that for the other pavement. This means that with a higher W_1/W_5 ratio the load-spreading ability of the pavement is lower. By this rationale rigid and composite pavements would exhibit lower W_1/W_5 values than flexible pavements.

The primary use of W_5 is in the calculation of the subgrade modulus, which is in turn used for stress computations. In the present study an attempt was made to investigate the possible relation between pavement type and W_1 and W_5 values. Table 1 presents the average W_1, W_5, and W_1/W_5 values for various classes of pavements obtained from the Dynaflect measurements. Flexible pavements

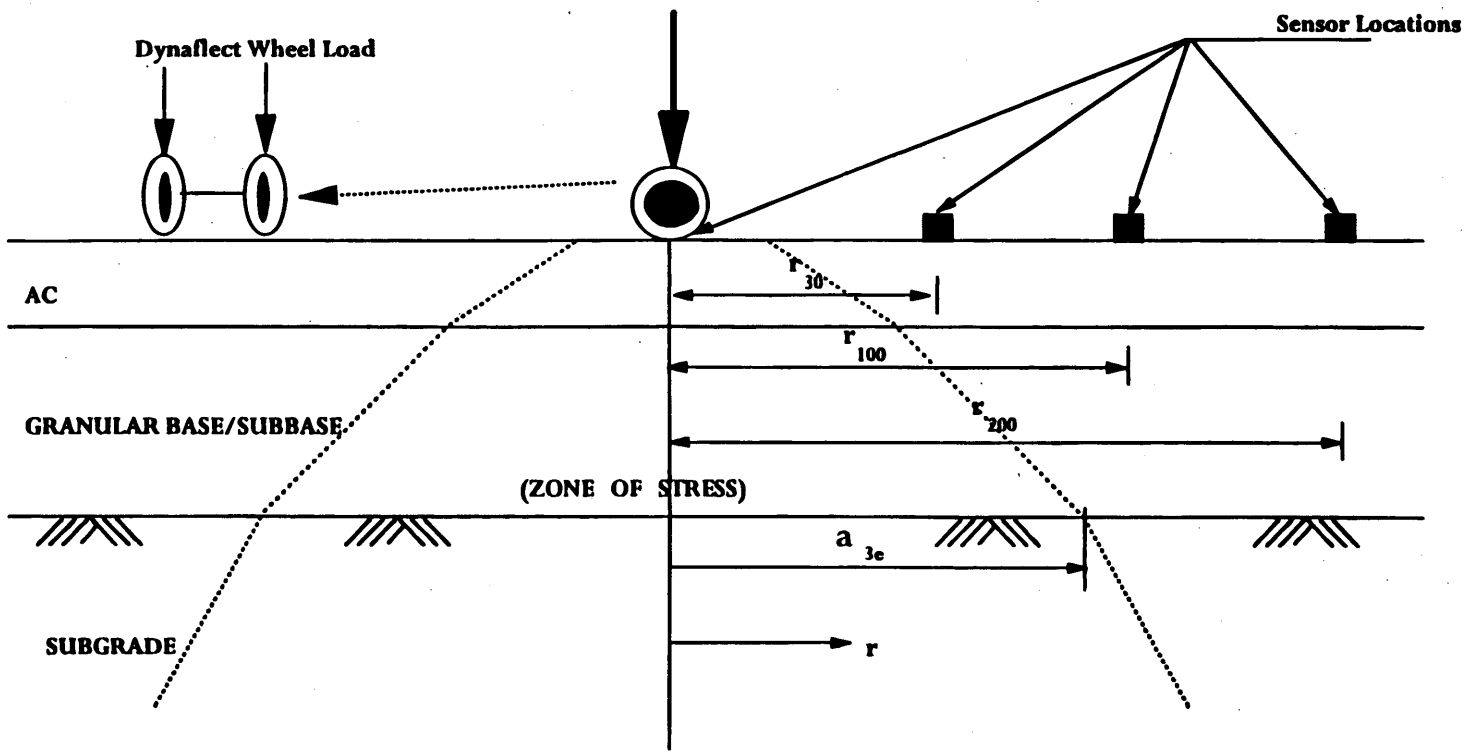

FIGURE 3 Stress zone within pavement structure.

have an average W_1/W_5 ratio of 2.88. For rigid pavements (CRCP and JRCP) this average is 1.89, and for composite pavements it is 1.96. Thus, it can be concluded that the W_1/W_5 ratio is a good indicator of pavement type. In addition to other parameters, this paper attempts to use this ratio to categorize the B/S pavements.

COMPARING STRUCTURAL CHARACTERISTICS OF PAVEMENTS

Structural Parameters

In an area of the pavement containing no joints or cracks, the structural condition of a pavement, when using Dynaflect measurements, is determined from W_1, W_5, and spreadability values. W_1 is the reading of the sensor closest to the load that measures maximum deflection and, thereby, determines the overall pavement integrity. W_5 is the sensor farthest from the load and is indicative of subgrade strength. Spreadability is a measure of the volume of the deflection bowl and indicates the load-spreading characteristics of the pavement layers. Spreadability is calculated by the following equation:

$$\text{Percent Spreadability} = \frac{\Sigma\,(W_1 + W_2 + W_3 + W_4 + W_5)}{5W_1} \times 100$$

Backcalculated moduli or structural numbers, or both, could also be used to characterize the behaviors of these pavements. Such an approach was not possible in the present study because of the lack of information on the subbase.

Evaluation Based on Maximum Deflection

From Table 1 the average maximum deflection values for B/S pavements with 0.152-, 0.457-, and 0.762-m fragments and composite pavements were nearly equal, with a range of between 0.010 and 0.012 mm. The average maximum deflection on flexible pavements was higher and was equal to 0.014 mm.

The scatter of maximum deflections is plotted in Figure 4. Flexible pavements and B/S pavements with 0.152-m fragments have a wide scatter. Composite pavements also have a wide scatter, but most of the points lie in a narrow band between 0.005 and 0.018 mm. B/S pavements with 0.457- and 0.762-m fragments have less scatter, with most of the points lying in a band between 0.005 and 0.015 mm, which indicates a behavior similar to that of composite pavements.

Based on maximum deflection measurements, the structural responses of all B/S pavements closely resemble those of composite pavements.

Evaluation Based on Spreadability

Spreadability is a direct function of the load distribution characteristics of the materials used in the pavement layers. Materials with higher moduli of elasticity distribute the load over a wider area. The spreadability of concrete pavements is higher than that of flexible pavements (*5*) owing to the better load dispersion characteristics of concrete. Composite pavements with a concrete base should have spreadability values greater than those of flexible pavements but nearly equal to those of concrete pavements. As seen in Table 1, the average spreadability of composite pavements is 75.19 percent compared with 66.71 percent for flexible pavements. The spreadability values for all B/S pavements in general were higher than those for both flexible and composite pavements: 79.90 percent for 0.152-m fragments, 73.44 percent for 0.457-m fragments, and 82.28 percent for 0.762-m fragments. Again, the B/S sections behaved the same irrespective of the size of the fragments.

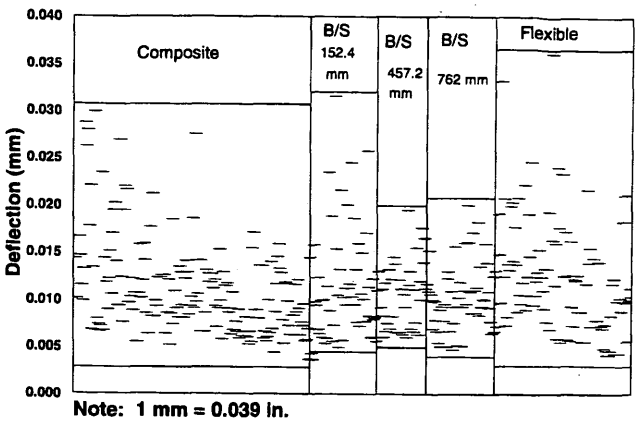

FIGURE 4 Scatter of maximum deflections (Dynaflect deflection measurements).

As seen in Figure 5, the spreadability values for flexible pavements exhibit a wide scatter, whereas most of the points for composite and B/S pavements fall within a range of 70 to 85 percent.

Therefore, on the basis of spreadability values, it is observed that the behavior of B/S pavements is similar to that of composite pavements.

Evaluation Based on the W_1/W_5 Ratio

The W_1/W_5 values for all types of pavements studied are presented in Table 1. As stated earlier W_1/W_5 values for flexible pavements are about 2.9 and those for rigid and composite pavements are about 2.0.

Figure 6 shows the scatter of W_1/W_5 values for different types of pavements. Most of the values for composite and all B/S pavements lie within a narrow range of 1.3 to 2.2, whereas the values for flexible pavements exhibit a wide scatter.

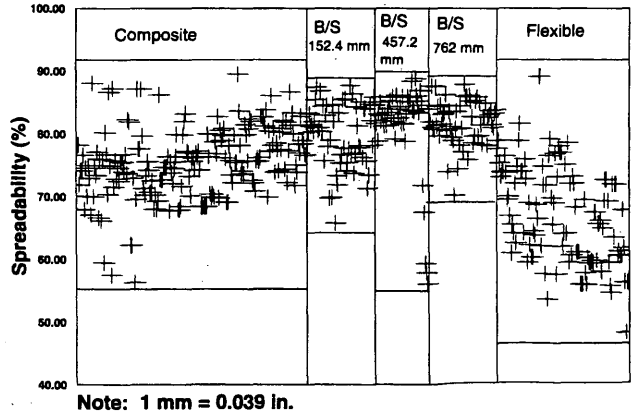

FIGURE 5 Scatter of spreadability (Dynaflect deflection measurements).

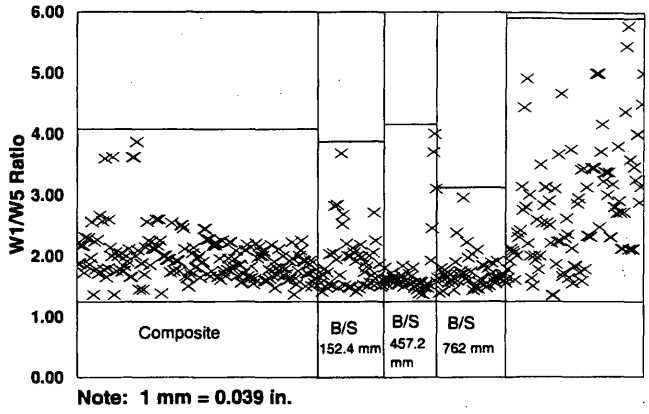

FIGURE 6 Scatter of W_1/W_5 ratio (Dynaflect deflection measurements).

It can thus be seen that on the basis of the computed W_1/W_5 values all B/S sections can better be identified as composite pavements.

STATISTICAL ANALYSIS

Based on the structural response parameters, B/S pavements behave in a manner similar to composite pavements, irrespective of the size of the cracked slab. A statistical analysis was performed to check the validity of this conclusion.

When comparing two measurements it is desirable to know if the mean values for the two groups are different. If the mean values of measurements are significantly different, then the variable under question is said to have a pronounced effect on the measurement. In the present study the means of the maximum deflections, spreadability, and W_1/W_5 ratios for each section were compared. The results of the statistical analyses are presented in Table 2. The null hypothesis (H_0) tested was the difference in means equal to 0 at a level of significance of α equal to 0.05.

The differences in the mean values of the average maximum deflection, spreadability, and the W_1/W_5 ratio for composite and all B/S pavement sections were statistically insignificant (Table 2). However, this result may have been influenced by unequal sample sizes. A better comparison may have resulted if the two sample sizes had been equal or approximately equal. Therefore, to minimize the effect of unequal sample sizes on the outcome of hypothesis testing, it was decided to generate smaller samples from the composite pavement data. To ensure that a sample is representative of the population from which it is obtained, statistical procedures recommend the use of random sampling techniques. There are several ways of ensuring the selection of a sample that is at least approximately random. For example, if a population has 500 elements and one wishes to select a random sample of size 10, one can use standard random digit tables to obtain 10 different three-digit numbers less than or equal to 500, which will then serve as the serial numbers of those elements to be included in the sample (*8*).

In the present study all of the data from composite pavements were serially numbered from 1 to 188 for each of the structural parameters investigated. By the random sampling technique, a random sample of size 10 was selected. A hypothesis test as described before was performed with this randomly generated sample in place of the previously used large sample size (sample size of 188). This procedure was repeated 10 times for each structural parameter, which resulted in a total of 90 tests. A summary of the results of these tests is presented in Table 3. Of the 90 tests performed, 87 showed that the differences between the structural responses of composite and B/S pavements are insignificant.

TABLE 2 Statistical Analysis of Pavement Structural Parameters

Structural Parameters	Pavements compared	Sample Size	Average	Significant difference between averages	Level of Significance (Probability of error)
Maximum Deflection (mm)	Composite Vs. B/S (0.152 m fragments)	188 3	0.011 0.012	No	0.85
	Composite Vs. B/S (0.457 m fragments)	188 7	0.012 0.009	No	0.21
	Composite Vs. B/S (0.762 m fragments)	188 3	0.011 0.010	No	0.77
Spreadability (%)	Composite Vs. B/S (0.152 m fragments)	188 3	75.19 79.90	No	0.30
	Composite Vs. B/S (0.457 m fragments)	188 7	75.19 73.55	No	0.37
	Composite Vs. B/S (0.762 m fragments)	188 3	75.19 82.28	No	0.12
W_1 / W_5	Composite Vs. B/S (0.152 m fragments)	188 3	1.96 1.86	No	0.67
	Composite Vs. B/S (0.457 m fragments)	188 7	1.96 2.05	No	0.61
	Composite Vs. B/S (0.762 m fragments)	188 3	1.96 1.70	No	0.25

Note: 1m = 39.37 in.
1 mm = 0.039 in.

TABLE 3 Statistical Analysis of Pavement Structural Parameters Using Random Samples from Composite Pavements

Structural Parameters	Pavements compared	Sample Size	# of Tests performed	Significant difference between averages		Range of Level of Significance (Probability of error) for each test.
				# of 'Yes'	# of 'No'	
Maximum Deflection (mm)	CompositeVs. B/S (0.152 m fragments)	10 (random) 3	10	0	10	0.173 - 0.934
	CompositeVs. B/S (0.457 m fragments)	10 (random) 7	10	0	10	0.066 - 0.873
	CompositeVs. B/S (0.762 m fragments)	10 (random) 3	10	0	10	0.328 - 0.946
Spreadability (%)	CompositeVs. B/S (0.152 m fragments)	10 (random) 3	10	0	10	0.036 - 0.906
	CompositeVs. B/S (0.457 m fragments)	10 (random) 7	10	0	10	0.202 - 0.994
	CompositeVs. B/S (0.762 m fragments)	10 (random) 3	10	3	7	0.008 - 0.339
W_1 / W_5	CompositeVs. B/S (0.152 m fragments)	10 (random) 3	10	0	10	0.426 - 0.995
	CompositeVs. B/S (0.457 m fragments)	10 (random) 7	10	0	10	0.415 - 0.977
	CompositeVs. B/S (0.762 m fragments)	10 (random) 3	10	0	10	0.065 - 0.605

Note: 1m = 39.37 in.
1 mm = 0.039 in.

This analysis further reinforces the previous conclusions that all B/S pavements behave as composite pavements.

SUMMARY AND CONCLUSIONS

1. Based on maximum deflection, spreadability, and W_1/W_5 ratios, the performances of asphalt overlays on B/S pavements with 0.152-, 0.457-, and 0.762-m fragments closely resemble those of composite pavements. The original pavement in all composite and B/S sections studied was jointed reinforced concrete. This finding will help engineers identify the appropriate theories to use in the design of the maintenance and rehabilitation needs of such pavements.
2. The ratio W_1/W_5 is a good indicator of pavement type. A value of 2.88 represents flexible pavements and a value of 2.00 and below represents composite and rigid pavements types.
3. The findings of the present study may be improved upon by selecting a large number of B/S sections and grouping all of the pavement sections on the basis of AC layer thicknesses, the ages of the pavements, environmental characteristics, and soil characteristics before comparing them.
4. To better understand the performances of B/S pavements and to compare their behaviors with those of other pavements a study has been initiated by ODOT in which test pavements have been constructed to investigate the effects of several variables. The validity of the current findings would be verified by such a study, and the results will be presented when they become available.

ACKNOWLEDGMENTS

The authors gratefully acknowledge the assistance of William F. Edwards, Engineer of Research and Development, and Roger Green, Physical Research Engineer, ODOT, for providing data to conduct the study. The authors express their sincere appreciation to Ali A. Houshmand, Assistant Professor, University of Cincinnati, for suggestions in statistical analyses.

REFERENCES

1. Thompson, M. R. *NCHRP Synthesis of Highway Practice* 144: *Breaking/Cracking and Seating Concrete Pavements*, TRB, National Research Council, Washington, D.C., March 1989.
2. *Guidelines and Methodologies for the Rehabilitation of Rigid Highway Pavements Using Asphalt Concrete Overlays.* Pavement Consultancy Services, A Division of Law Engineering, Inc., Beltsville, Md., June 1991.
3. Minkarah, I. A., A. Bodocsi, R. Miller, and R. Arudi. *Final Evaluation of the Field Performance of ROS 23 Experimental Concrete Pavement.* Final Report to the State of Ohio Department of Transportation and FHWA, Dec. 1993.
4. *AASHTO Guide for Design of Pavement Structures.* AASHTO, Washington, D.C., 1986.
5. Edwards, W. F., R. L. Green, and J. Gilfert. *Implementation of a Dynamic Deflection System for Rigid and Flexible Pavements in Ohio.* FHWA, U.S. Department of Transportation, and Ohio Department of Transportation, Aug. 1989.
6. Wolfe, R. K., and B. W. Randolph. *Temperature Adjustment of Dynamic Deflection Measurements on Asphalt Concrete Pavements.* Final Report to the State of Ohio Department of Transportation and FHWA, April 1993.
7. Kingham, R. I. *Development of the Asphalt Institute Method for Designing Asphalt Concrete Overlays for Asphalt Pavement.* Research Report 69-3. The Asphalt Institute, June 1969.
8. Miller, I., and J. E. Freund. *Probability and Statistics for Engineers.* Prentice-Hall, Inc., Englewood Cliffs, N.J., 1965.

Publication of this paper sponsored by Committee on Pavement Rehabilitation.

Overlays on Faulted Rigid Pavements

DAN MCAULIFFE, LUIS JULIAN BENDAÑA, HONG-JER CHEN, AND RICK MORGAN

Steel dowels for load transfer at joints were replaced with two-component, malleable iron devices in New York State's rigid pavements from 1960 to 1973. Unfortunately, this joint system proved to be less effective, losing load transfer capability much sooner than the steel dowel joint system it had replaced. The performance of bituminous overlays on nine faulted rigid pavements containing load transfer devices over periods of 6 to 9 years is summarized. The study investigated (a) the trend toward fault return and its relation to other variables, (b) the relation between fault return and underlying slab movement, (c) the overall performance of overlays on faulted pavements, and (d) the effects of overlays on temperatures and stresses within the underlying rigid pavements. The results show that return of faulting through the overlay is minimal (60 percent of the joints had no or little fault return, and with thinner overlays the fault return was faster) and that the use of overlays should be considered only when surface distress is substantial. Although differential vertical joint movement generally increased with time, no exact relation was found between such movement and fault return. Thicker overlays were found to reduce daily and seasonal temperature changes in the underlying rigid pavements, which in turn reduced curling and compressive stresses as well as the potential for fatigue cracking and blowups.

Many pavements in New York State fail prematurely because of severe joint deterioration. The major problem is corrosion of load transfer devices (LTDs), which, combined with water infiltration and vertical deflections, creates ideal conditions for pumping, loss of support, and subsequent faulting and slab cracking. The study reported here was specifically designed to investigate long-term solutions to faulting problems by using various bituminous overlay thicknesses on rigid pavements constructed from 1960 to 1973 with two-component malleable iron LTDs (MILTDs) (*1–3*). Unfortunately, these MILTDs proved to be less effective than the steel dowels that they replaced, losing load transfer capability much sooner. During that period MILTDs were installed in about 1,800 lane km of jointed concrete pavement. As more of these pavements require rehabilitation, it has become necessary to determine the most effective rehabilitation procedure for fault removal. In New York State two long-term rehabilitation techniques have been used on faulted pavements: load transfer retrofit and bituminous overlay. The study reported here considers how initial faulting and overlay thickness affect fault return and will shortly be reported in greater detail (*4*).

INVESTIGATION

Bituminous overlays are a standard rehabilitation procedure in New York State, but no hard data on the performance of various overlay thicknesses on faulted pavements existed. To find a more rational method for selecting overlay thickness for faulted rigid pavements with LTDs, the following three questions had to be answered: (a) what effect does initial faulting have on overlay performance, (b) what factors (including other rehabilitation procedures) affect the continuation of faulting, and (c) what effects do overlays have on thermal gradients and critical stresses within overlaid slabs. The other rehabilitation procedures considered were sawing and sealing, installation of underdrains, installation of stress relief joints, and use of truing-and-leveling (T&L) and/or shim courses. Rigid pavements with MILTDs were chosen as a worst case; few rigid pavements in New York State have no LTDs. Subsealing was not included because no subsealed overlay site could be found. Grinding was not evaluated because it is not used as a preparation for overlays in New York State.

RESULTS AND DISCUSSION OF RESULTS

Faulting

Initial faulting (*4*) before overlay and fault return after overlay were measured at 18 sites on nine highways. Figure 1 indicates the absence or continuation of joint faulting reflected through the overlay. Faults were measured with a device called a fault meter, which was developed by the Transportation Research and Development Bureau in New York in the 1970s (Figure 2). It is placed 150 to 230 mm from the original shoulder-pavement joint and measures in millimeters.

When the study began in 1984 it was decided to select some test roads that were already overlaid but that had exhibited faulting recurrence in the overlay to obtain immediate results concerning the factors that affected fault return. These sites are called older overlay sites here. It was also necessary to include faulted concrete pavements scheduled to receive overlays as test sites, so that preoverlay pavement conditions could be measured, and they are termed newer overlay sites.

For seven older overlay sites the amounts of faulting before overlay were determined by coring at the joint. Before filling the core holes the overlay thickness on each side of the joint was measured. The amount of faulting before the overlay was calculated by subtracting the overlay thickness on the approach slab from that on the leave slab (Figure 3). For the 11 newer overlay sites, preoverlay faults were measured directly on the concrete slabs by using the fault meter.

Faulting was measured annually for 7 years. Measurement began 4 years after overlay for the older overlay sites, 1 year after overlay for 10 of the 11 newer overlay sites, and 2 years after overlay for the last site. The amount of faulting at each joint is shown in Figure 1. All pavements had 230-mm rigid slabs. Table 1 summarizes slab lengths, joint types, the year each pavement was built, the year it was overlaid, annual average daily traffic (AADT), percent trucks, and preoverlay treatments.

Transportation Research and Development Bureau, New York State Department of Transportation, State Campus, Albany, N.Y. 12232-0869.

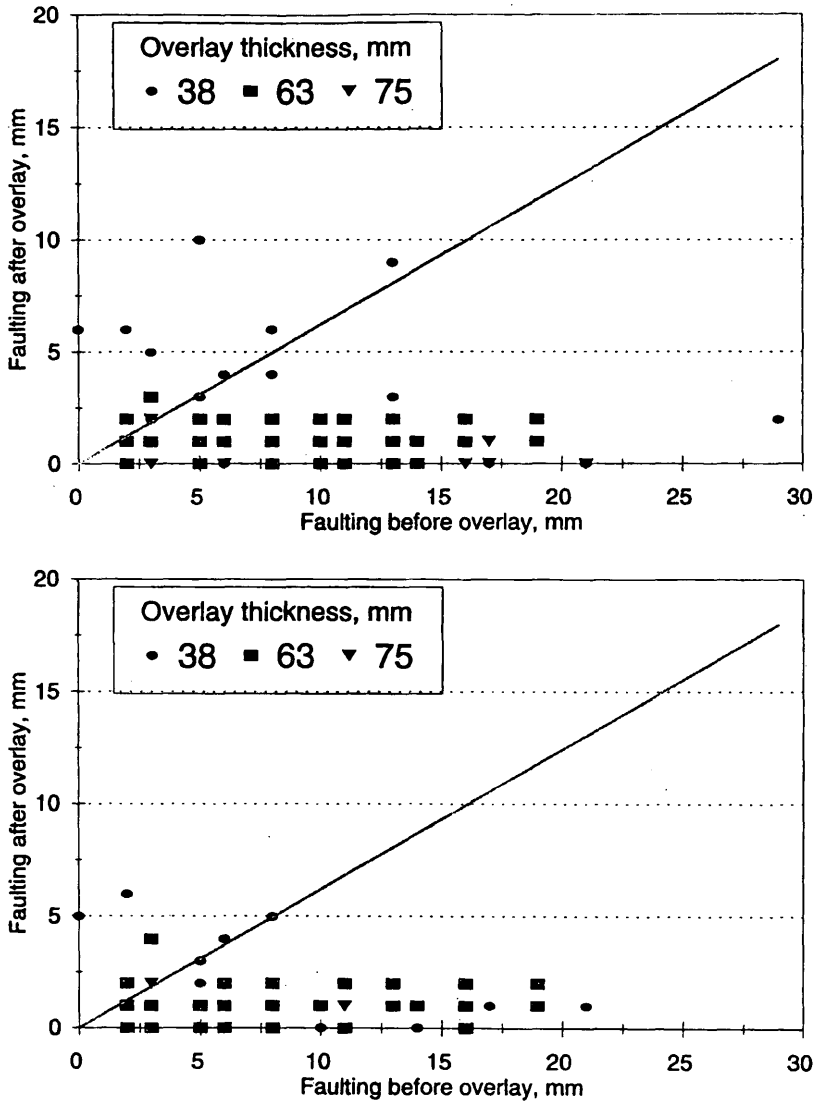

FIGURE 1 Faulting at all sites: (*a*) 4 years after overlay; (*b*) 6 years after overlay.

The first finding that should be noted is that there are fewer joint readings for the sixth year than for the fourth year. This was because some joints were no longer being monitored because either the site containing that joint had been rehabilitated or joint distress made accurate readings impossible. Nearly all of the joints omitted were in the 38-mm overlays. Next, it should be noted that with regard to overlay thickness, the 63- and 75-mm overlays performed well for up to 6 years, with all readings being in the mild faulting range, and that only a few sites had as much or more faulting as they did before overlay. Joints beneath the 38-mm overlays, however, generally showed more faulting after 4 years than they did before overlay.

The effects of the following factors were assessed: (a) joint type, (b) overlay thickness, (c) use of sawed-and-sealed joints, (d) use of underdrains, (e) use of pressure relief joints, (f) use of a shim course, (g) use of T&L course, (h) rigid pavement slab length, and (i) AADT. The program used to assess the effects of these factors was PROC GLM in SAS (*5*), which permits examination of the effect of each factor on the response variable. Those factors contributing a significant amount of variation were judged to be influential. After the first computer run, joint type was eliminated because it was shown to have the least effect on fault return. Of the factors examined, only two, overlay thickness and slab length, were found to influence fault return at the 95 percent significance level. Table 2 gives the results of these analyses. The last column indicates the probability that a given factor does not influence fault return. A relationship between fault return and slab length was found through this analysis, but closer examination of overlay thickness and slab length revealed that slab length and overlay thickness were not inde-

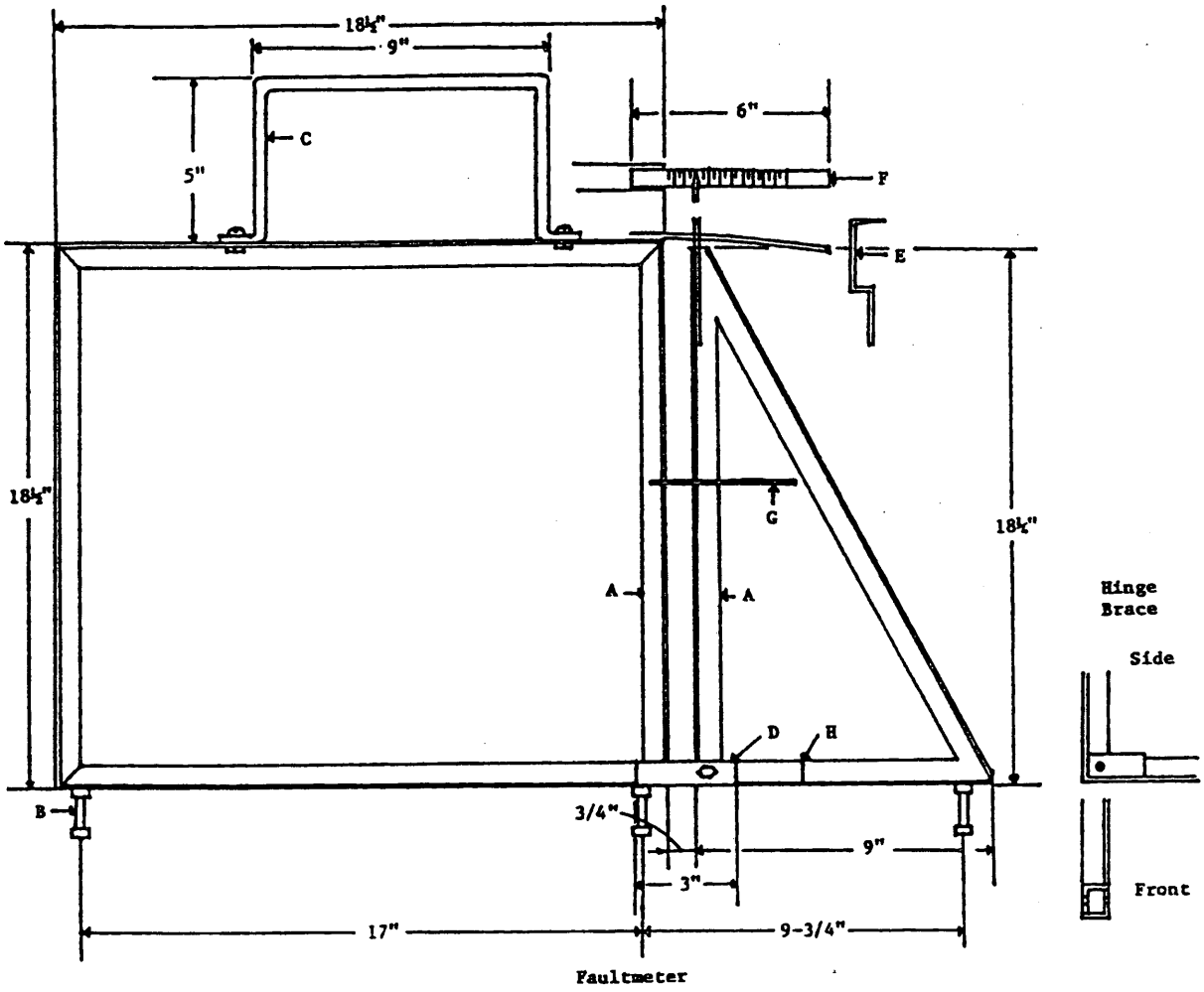

FIGURE 2 Fault meter.

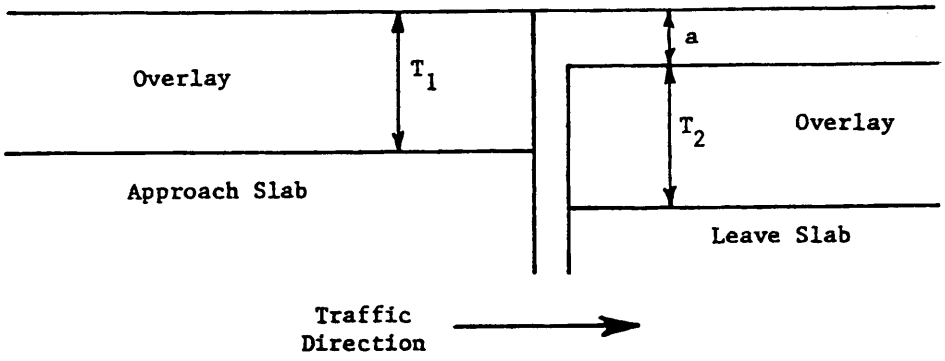

a = fault measurement 4 yr after overlay

T_1 = overlay thickness on approach slab

T_2 = overlay thickness on leave slab, and

$(T_1 - T_2)$ = fault before overlay

FIGURE 3 Asphalt density measurements.

TABLE 1 Characteristics of Test Sites

Highway	Test Site	Slab Length, ft	Joints		Year Built	Year Overlaid	AADT	Percent Trucks	Preoverlay Treatment*
			Expansion	Contraction					
A. OLDER OVERLAYS									
38 mm Thickness									
Rte 110	110-TS1	12	9	--	1954	1981	38,500	10	T&L
Rte 146	146-TS1	29	10	--	1947	1981	8,000	4	--
63 mm Thickness									
I-495	495-TS1	18.5	10	--	1962	1981	92,400	10	T&L
I-390	390-TS1	18.5	--	10	1968	1981	9,400	31	Shim, S&S, UD
	390-TS2	18.5	--	9	1968	1981	9,400	31	Shim, UD
	390-TS3	18.5	--	10	1968	1981	9,400	31	Shim
B. NEWER OVERLAYS									
63 mm Thickness									
I-81	81-TS1	18.5	--	5	1964	1986	17,700	26	Shim, T&L, S&S, UD
	81-TS2	18.5	--	9	1964	1986	17,700	26	Shim, T&L, S&S
Rte 5S	5S-TS1	27.5	15	--	1959	1983	4,300	9	T&L
Rte 236	236-TS1	29	15	--	1947	1985	5,600	7	T&L, S&S
75 mm Thickness									
Rte 17	17-TS1	18.5	--	15	1961	1985	9,400	8	T&L, S&S
	17-TS2	18.5	--	17	1961	1986	9,400	8	T&L, S&S
I-87	87-TS1	18.5	--	5	1959	1985	44,200	11	Shim, T&L, S&S
	87-TS2	18.5	--	5	1959	1985	38,600	9	Shim, T&L, S&S
	87-TS3	18.5	--	11	1959	1985	38,600	9	Shim, T&L, S&S, PR
	87-TS4	18.5	--	11	1959	1985	43,400	9	Shim, T&L, S&S, PR
	87-TS5	18.5	--	5	1960	1985	22,800	10	Shim, T&L, S&S
C. TEMPERATURE SITES									
38 mm Thickness									
Rte 29	29-TS1	27.5	5	--	1940	1982	5,200	1	--
75 mm Thickness									
I-87	87-TS5	18.5	--	5	1960	1985	22,800	10	Shim, T&L, S&S
Control (no overlay)									
Rte 29	29-TS2	27.5	6	--	1940	1982	5,200	1	--
I-87	87-TS6	18.5	--	5	1960	1985	22,800	10	Shim, T&L, S&S

* Shim = shim course, T&L = truing and leveling course, S&S = sawing and sealing over underlying rigid pavement joints, UD = underdrain, PR = pressure-relief joint.

pendent and that the determining factor was overlay thickness, not slab length. Slab length could affect faulting because there would be less load transfer between slabs at lower temperatures. Joints between longer slabs open more than those between shorter slabs, reducing aggregate interlock more between longer slabs. This relationship could lead to greater faulting between longer slabs. However, the present study found greater faulting between shorter slabs, and because this statistical result could not be logically supported, slab length was removed from the analysis, and thus no conclusions could be drawn concerning slab length.

It was also desired to determine if rigid pavements continue to fault under overlays without this being apparent on the surface. Initially, cores were taken from 12 joints (6 joints at each of two test sites), and if evidence of faulting had been found, cores from more joints would have been taken. Two cores were taken at each joint (one on the approach slab and one on the leave slab), and overlay thickness was measured at both locations. If the difference in the two overlay thicknesses at a given joint was greater than the original overlay faulting, this would indicate that faulting had continued under the overlay without being detectable on the surface. Table 3 summarizes the initial faulting and measured overlay thicknesses in 1991 after 6 years of service. Of the 12 joints examined, only 1 was found to have greater faulting than before overlay, showing that joint faulting did not continue under overlays without this being detectable on the surface.

Some variation in fault recurrence may be attributed to the decreasing number of joints being measured and to problems with the overlay surface that became increasingly obvious. Unlike rigid slabs with two level surfaces on which to measure faulting, the overlay surface was not necessarily flat. The problem was twofold: (a) bumps and depressions at or near the joint resulting from shoving and/or (b) the presence of cracks in the overlay due to aging and reflective cracking. Also, a bituminous surface is more susceptible to temperature change than a rigid pavement surface, resulting in seasonal variations in the surface profile. This problem first became apparent when selecting the older overlay sites and became more noticeable as the overlays aged. These profile irregularities were most severe in 38-mm overlays. The depressions and bumps affected faulting measurements and made many of the faulting measurements on 38-mm overlays questionable after the fourth year.

Differential Vertical Joint Movement

Differential vertical joint movement (DVJMs) are measurements of the differences in the vertical movements of adjoining slabs at the transverse joint during loading, which indicate the amount of load transfer that has been lost. They were measured with another device developed by New York reseachers in the 1970s (Figure 4); this

TABLE 2 Analysis of Variance

	Factor	DF	F Value	P Value
Test 1:	Joint Type	1	0.10	0.7581
	OL Thickness	2	7.80	0.0006
	Saw & Seal Jt.	1	0.10	0.7569
	Underdrain	1	0.53	0.4659
	Pressure Relief Jt.	1	1.09	0.2979
	Shim Course	1	0.90	0.3445
	T & L Course	1	2.14	0.1458
	Slab Length	2	5.87	0.0035
Test 2:	AADT	2	0.73	0.4820
	OL Thickness	2	3.21	0.0429
	Saw & Seal Jt.	1	0.10	0.7566
	Underdrain	1	0.54	0.4654
	Pressure Relief Jt.	1	0.12	0.7295
	Shim Course	1	0.03	0.8573
	T & L Course	1	0.02	0.8975
	Slab Length	2	5.94	0.0007

General Linear Models Procedure

Dependent Variable Source	Total DF	Sum of Squares	Mean Square	F Value
Model:	12	15.808	1.317	19.66
Error:	160	10.722	0.067	P Value
Corrected Total:	172	26.530		0.0001
R Square	C. V.	Root MSE	Total Mean	
0.596	159.205	0.259	0.163	

TABLE 3 Average Faulting by Site

Site	Total Joints	Year Overlaid	Overlay Thickness, mm	Initial Fault, mm	Year after overlay								Annual Rate of Faulting, mm/yr
					2nd	3rd	4th	5th	6th	7th	8th	9th	
110-TS1	9	1981	38	3.2	--	--	4.1	4.0	3.5	3.2	--	--	0.46
146-TS1	10	1981	38	6.7	0.1	0.7	0.1	0.4	0.5	0.5	--	--	0.08
5S-TS1	15	1984	38	3.3	0.5	0.8	0.7	0.7	0.6	--	--	--	0.10
236-TS1	15	1985	63	7.8	0.3	0.3	0.3	--	--	--	--	--	0.08
81I-TS2	9	1985	63	6.5	--	--	1.4	1.1	1.4	2.1	1.8	1.6	0.18
390I-TS1	10	1981	63	5.8	--	--	1.3	0.5	--	--	--	--	0.10
390I-TS2	9	1981	63	7.6	--	--	1.4	0.5	1.2	1.5	1.2	2.2	0.25
390I-TS3	10	1981	63	6.5	--	--	1.4	1.1	1.4	2.1	1.8	1.6	0.18
495I-TS1	10	1981	63	6.2	0.4	0.2	0.3	--	--	--	--	--	0.08
17-TS1	15	1985	75	6.1	0.3	0.2	0.3	0.4	--	--	--	--	0.09
17-TS2	17	1986	75	6.2	0.4	0.2	0.3	--	--	--	--	--	0.08
87I-TS1	5	1985	75	2.0	0.4	--	0.2	0.4	0.6	--	--	--	0.10
87I-TS2	5	1985	75	5.2	0.6	0.2	0.4	0.2	0.4	--	--	--	0.07
87I-TS3	12	1985	75	2.6	0.3	0.3	0.4	0.4	0.5	--	--	--	0.08
87I-TS4	12	1985	75	4.3	0.3	0.3	0.3	0.5	0.5	--	--	--	0.08
87I-TS5	5	1985	75	2.6	0.4	0.4	0.8	1.0	0.8	--	--	--	0.13
81I-TS1	5	1985	75	6.0	0.0	0.0	0.4	--	--	--	--	--	0.10

Average Annual Rate of Faulting, mm/yr	38 mm Overlays	63 mm Overlays	75 mm Overlays
	0.21	0.14	0.09

device spans the joint while a truck with a 100-kN single rear axle is driven across it. DVJM is the maximum deflection reading of the approach slab (usually occurring near the joint) subtracted from the maximum deflection reading of the leave slab (also usually near the joint). DVJMs were measured annually at about the same time as faulting measurements.

DVJMs were measured to determine the amount of load transfer across transverse joints. No definite relationship appeared between load transfer efficiency and faulting. Table 4 gives average DVJM measurements for selected overlay sites. These readings show that the greatest vertical movement of concrete slabs occurred when temperatures were below 6°C. For the three highest annual average DVJMs for these sites, 13 of 18 readings occurred under such conditions. Between freezing and 6°C the effect of aggregate interlock is reduced or eliminated, and the not-yet-frozen subgrades do not provide any additional support, so that load transfer occurs almost exclusively through the LTDs.

Temperature Study

Pavement and ambient air temperature data were recorded for 20 months on I-87 and for 25 months on Route 29. The overlay thickness of each section is given in Table 1. Pavement temperatures at each depth were recorded as the average reading at that depth for five locations at each site (Figure 5). For reporting purposes average monthly temperatures were classified in three categories: hot,

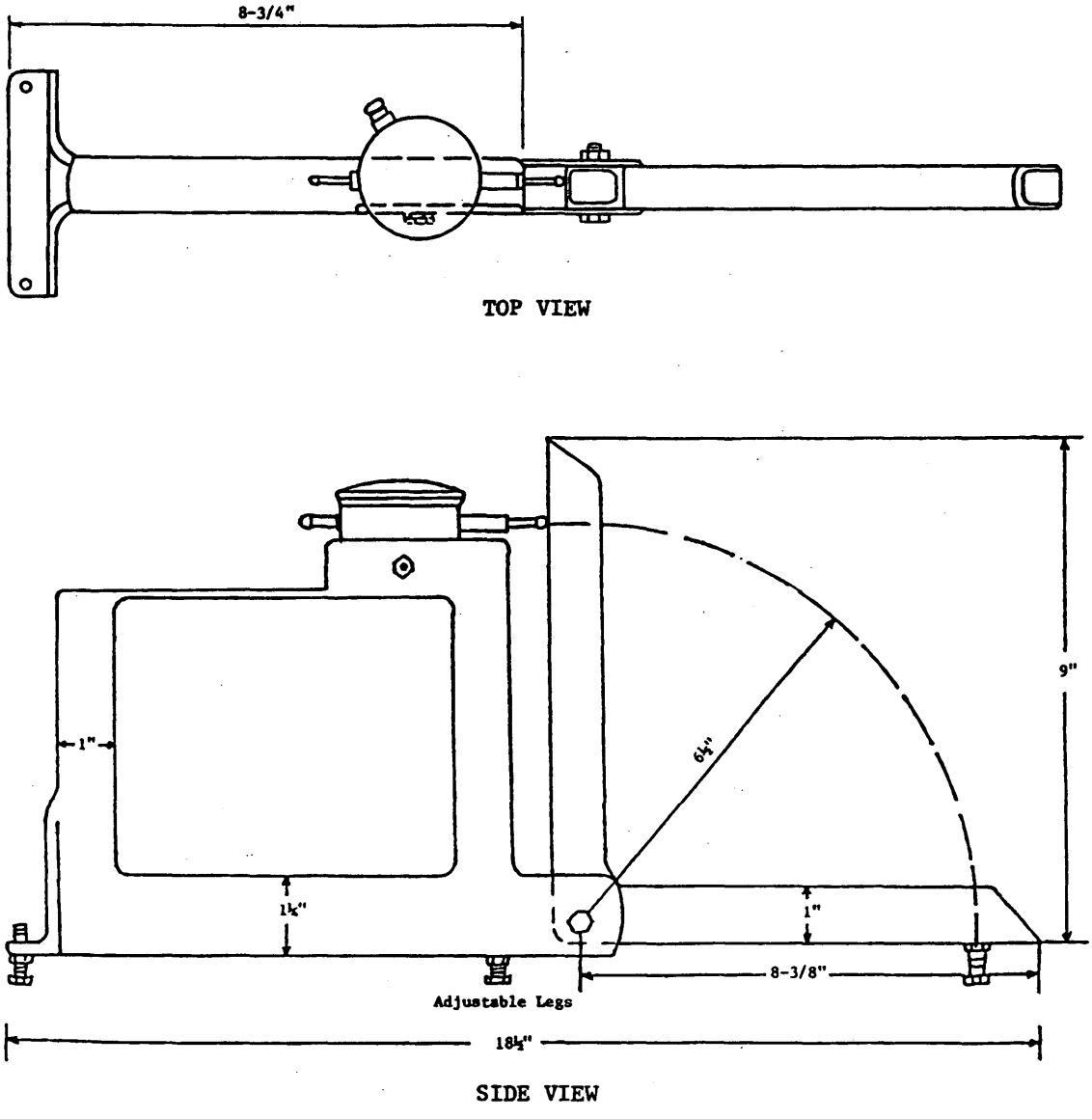

FIGURE 4 NYSDOT meter for measuring DVJM.

TABLE 4 Summary of DVJMs*

Site	Total Joints	Before Overlay	Year After Overlay 1st	2nd	3rd	4th	5th	6th	7th
5S-TS1	15	0.11	--	--	0.25	0.19	0.41	0.27	0.35
		None	--	--	20.0/18.9	13.3/17.2	3.3/5.6	6.7/11.1	5.0/7.8
236-TS1	15	0.93	0.33	0.33	0.44	--	0.48	--	--
		8.9/11.1	7.2/8.9	11.1/14.4	12.2/15.0	--	11.7/15.6	--	--
17-TS1	15	0.07	0.11	0.21	0.29	0.33	0.38	--	--
		13.3/18.9	-2.2/2.8	11.7/15.6	3.9/8.3	2.8/5.0	-2.8/2.8	--	--
17-TS2	17	0.30	0.03	0.07	0.12	0.23	--	--	--
		13.3/18.9	11.7/15.6	3.9/8.3	2.8/5.0	-2.8/2.8	--	--	--
I-87 ALL	37	0.05	0.09	0.14	0.11	--	0.23	--	--
		13.3/21.7	13.3/21.7	16.7/16.1	7.2/10.0	--	9.4/12.2	--	--
I-81 ALL	14	0.13	0.13	0.13	0.23	0.20	--	--	--
		16.1/25.6	13.3/18.3	2.2/6.7	10.0/4.4	8.9/5.6	--	--	--

*Upper value is average DVJM, mm;lower value is average air/pavement surface temperature, deg C

Range of DVJMs, mm	DVJM Severity
0 to 0.25	Low
0.25 to 0.50	Moderate
>0.50	High

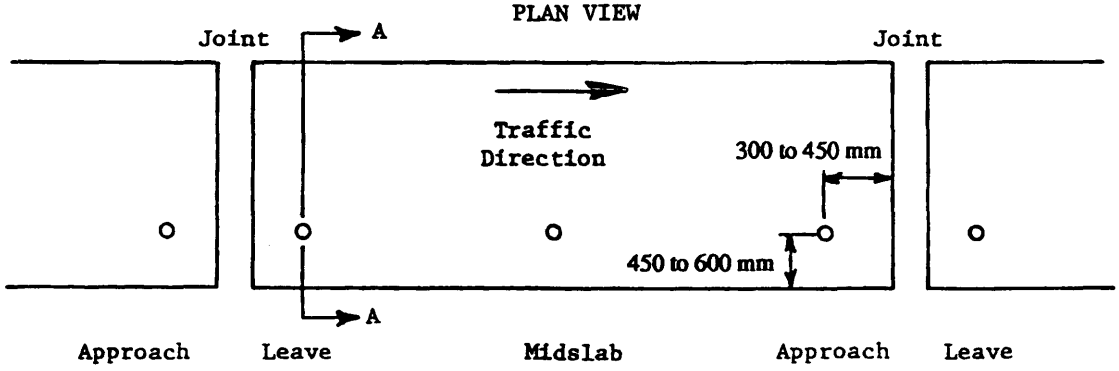

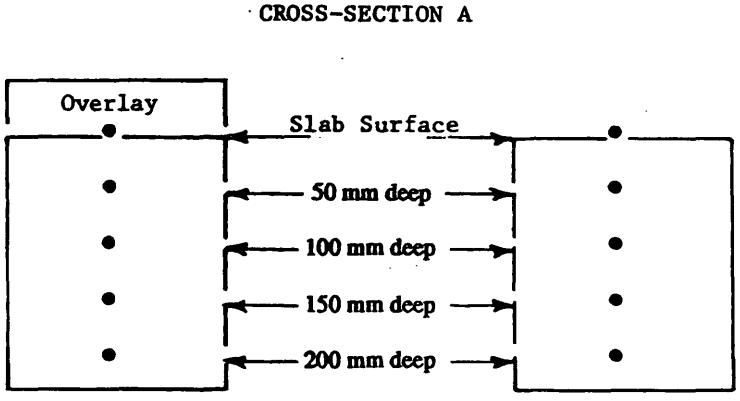

FIGURE 5 Thermocouple locations.

mild, and cold. Hot months were those when the average daily air temperature was over 15.5°C, mild months were those when the average daily air temperature was between 1.5 and 15.5°C, and cold months were those when the average daily air temperature was below 1.5°C. Note that monthly averages were based on from 2 to 4 days of data, not entire months. Control sections were pavements without overlays on the same route.

Figure 6 shows typical temperature variations within a slab during a hot day on I-87, with air temperature plotted as a reference. It shows that at a given depth, daily temperature variation (i.e., variation between maximum and minimum temperatures) is less for test sections than for control sections.

Load Transfer Retrofit

From 1982 to 1985 on the New York State portion of I-84, 289 joints were retrofitted with I-beam LTDs or a double-V device (*1,2*). The objective was to establish the criteria for when load transfer restoration and various procedures for fault removal might be effective. Figure 7 shows faulting (in millimeters) versus the number of years in service for three or four double-V devices (LTDs) per joint and four or eight I-beams per joint. Comparing the three and four double-V devices, the former performed better, with an annual fault return of less than 0.8 mm. Paradoxically, the four double-V devices per joint performed worse, with an annual fault return of 2 mm.

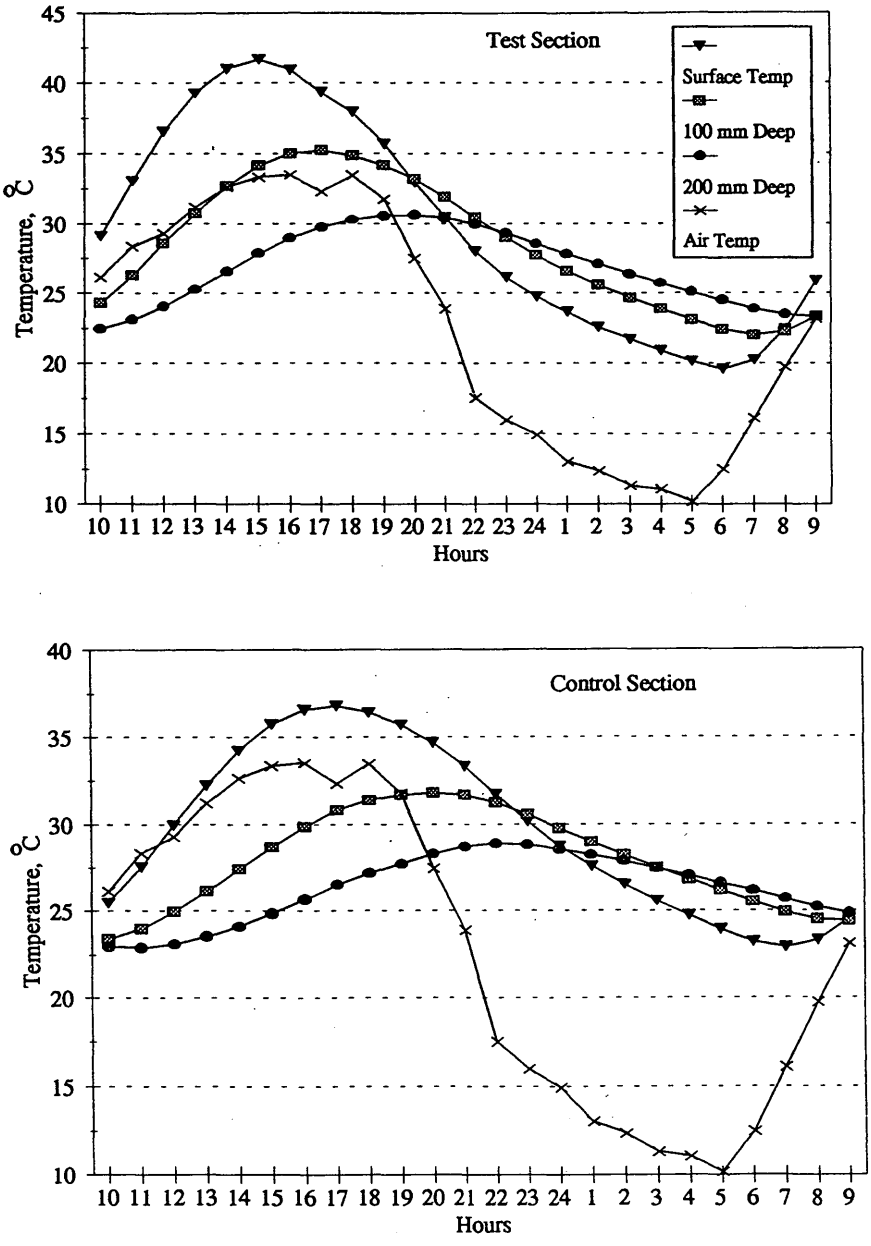

FIGURE 6 Hourly temperature at various depths.

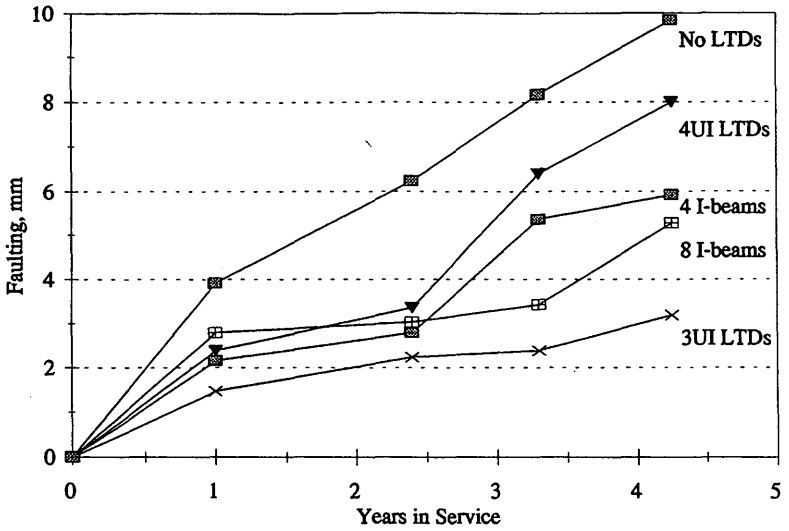

FIGURE 7 Faulting with and without LTDs.

Inadequate compaction of polymer concrete within the retrofitted joint and improper aggregate gradation of this concrete were two construction and material problems that resulted in the poor performance of joints containing four double-V devices.

Recently, with the availability of equipment capable of cutting multiple slots simultaneously, a patching material more thermally compatible with existing concrete, and better specifications and recommendations concerning the appropriate use of this technique, the New York State Department of Transportation (NYSDOT) is again considering the use of retrofitting. This rehabilitation technique is more cost-effective than other fault removal methods (slab jacking, etc.) when it is used for preventive maintenance to rehabilitate rigid pavements before serious surface deterioration problems are present.

CONCLUSIONS

Faulting

Figure 1 shows faulting in relation to overlay thickness, and Figure 8 shows annual faulting progression. These figures indicate that the return of faulting through overlays is slight: 60 percent of the joints had little or no faulting. Figure 9 shows average fault return for three overlay thicknesses. Other distresses (shoving, raveling, and cracking) make it impossible to accurately measure faulting on many 38-mm overlays. These problems were less severe on the 75- and 63-mm overlays. The 63-mm overlay showed only slightly more faulting than the 75-mm overlay, suggesting that minimum overlay thickness on a faulted rigid pavement should be 63 mm.

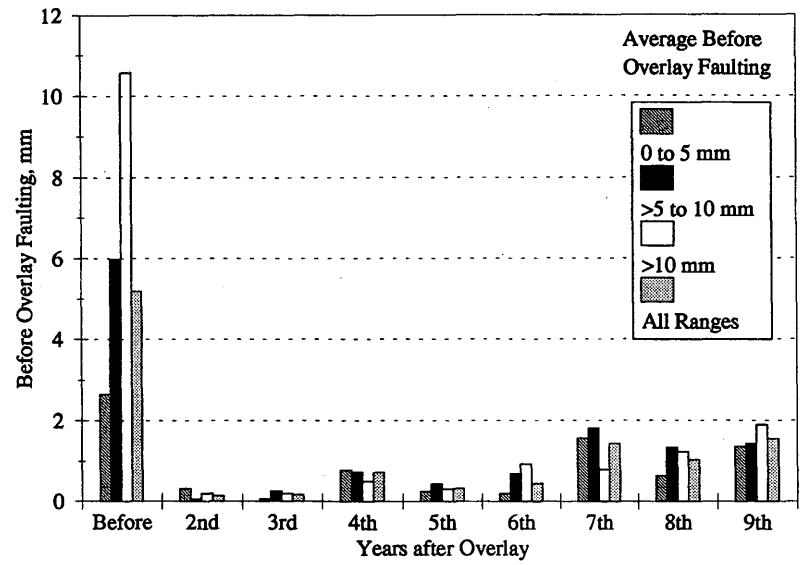

FIGURE 8 Annual faulting progression versus faulting before overlay.

Initial faulting and truck traffic were also examined. Figure 10 also shows the relation between initial faulting and fault return in the sixth year for 75-mm overlays. Although increased fault return might be expected, no noticeable relation was found. Figure 11 shows the percentage of fault return after 6 years versus AADT for the 75-mm overlay. Daily truck traffic was then grouped into two categories: one with about 300 and the other with about 3,000 trucks per day. Average fault return was found to be higher for the heavily traveled group than for the lightly traveled group: 25 percent and no average initial fault return, respectively. However, with only two truck volume groups it was not possible to determine an exact relationship between AADT and fault return.

DVJMs

The initial effect of overlays on DVJMs was inconsistent. In some cases differential movements were reduced after overlay placement, but in others they increased or stayed the same The only consistent trend was that regardless of the initial affect, DVJMs continued to increase with time.

Temperature Study

Thermal gradient is the temperature differential per unit length along the slab's depth. Figure 12 shows typical variations of temperature gradients over a 24-hr period, indicating positive gradients during daylight and negative gradients at night. The greatest thermal gradients occurred at about the same time of day, regardless of the month, with maximums for test sections occurring slightly later than those for control sections. However, the time for pavement to reach the minimum gradient varied with the season. Reduction of stresses due to thermal gradients is important, because stresses due to positive thermal gradients act to increase fatigue damage, and thus a reduction in thermal gradient results in less fatigue damage caused by each axle loading. In addition, it was found that thicker overlays reduced maximum and minimum rigid pavement temperatures and delayed the temperature cycle (the times to reach maximum and minimum temperatures were later for test sections than for control sections). The average time lag for all depths and temperature categories was 2 hr.

Retrofitted LTDs

Although the NYSDOT experience with retrofitting was not completely successful, several lessons learned from the results can help others to improve this technique: (a) retrofitting is effective when slabs are in good to excellent condition and distress is mostly due to LTD deficiencies, (b) retrofitting is essential for retarding fault recurrence when load transfer efficiency is low and the pavement is subjected to heavy truck traffic, and (c) good workmanship, sound concrete slabs, adequate LTDs, and good-quality patching material are critical for achieving satisfactory long-term performance.

RECOMMENDATIONS

The use of overlays 63 mm or thicker can be an effective rehabilitation procedure for faulted rigid pavements, but their use is recommended only when there is severe pavement surface distress. In cases in which faulting is the primary problem, retrofit LTDs are the preferred rehabilitation procedure. Finally, in any area where subsurface drainage is problematic, the use of retrofit underdrains should be considered.

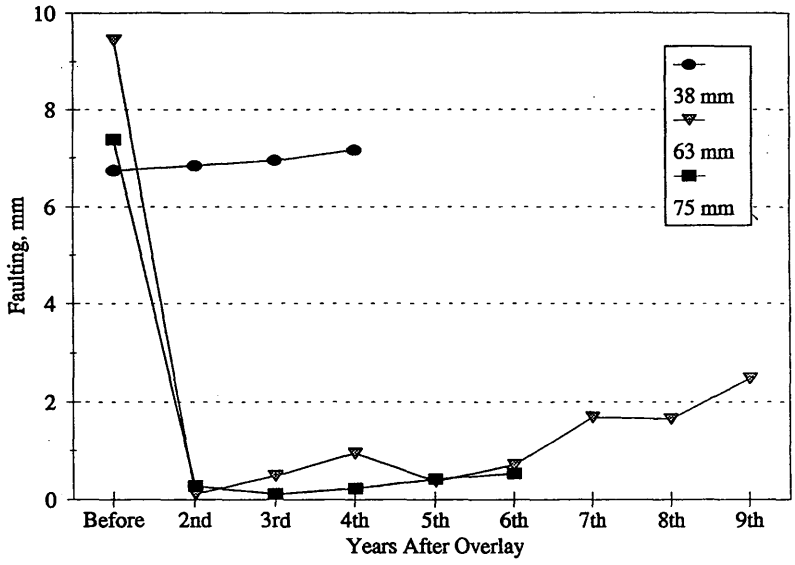

FIGURE 9 Faulting versus overlay thickness.

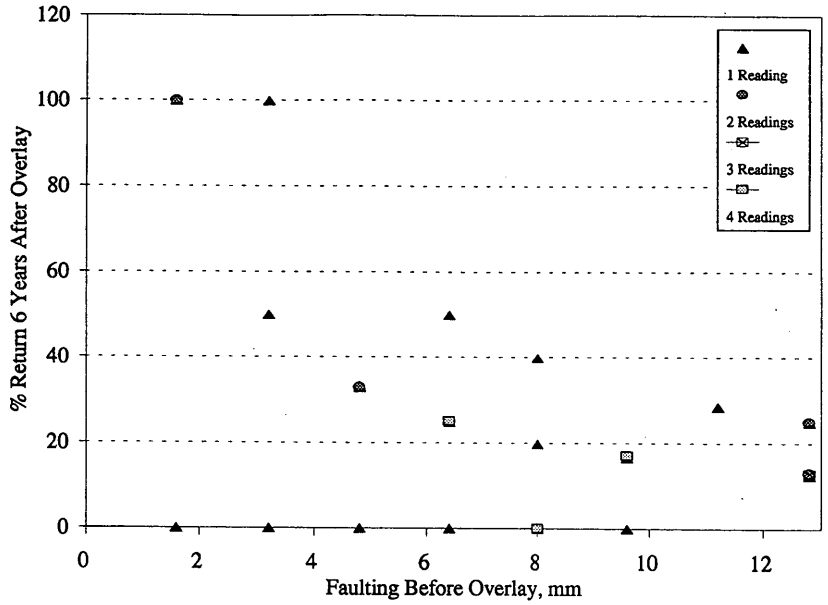

FIGURE 10 Fault return versus initial faulting (78-mm overlays).

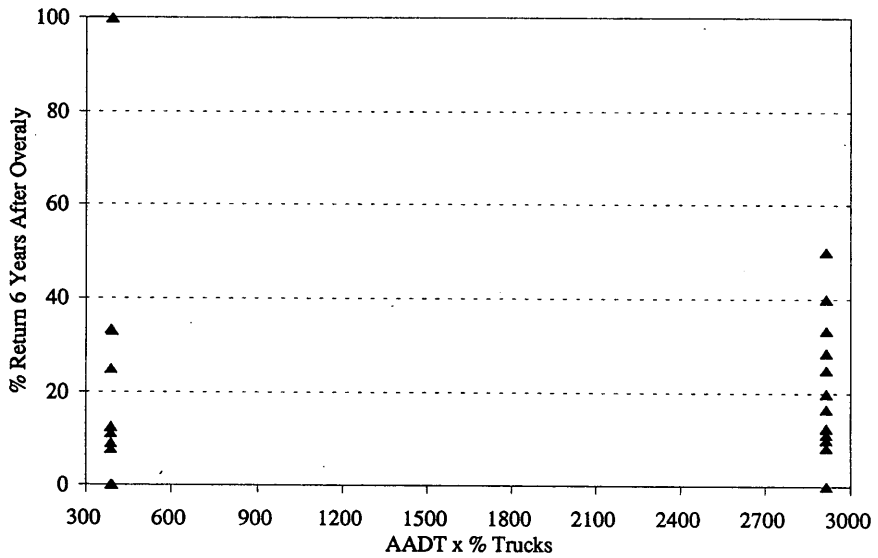

FIGURE 11 Fault return versus truck traffic (78-mm overlays).

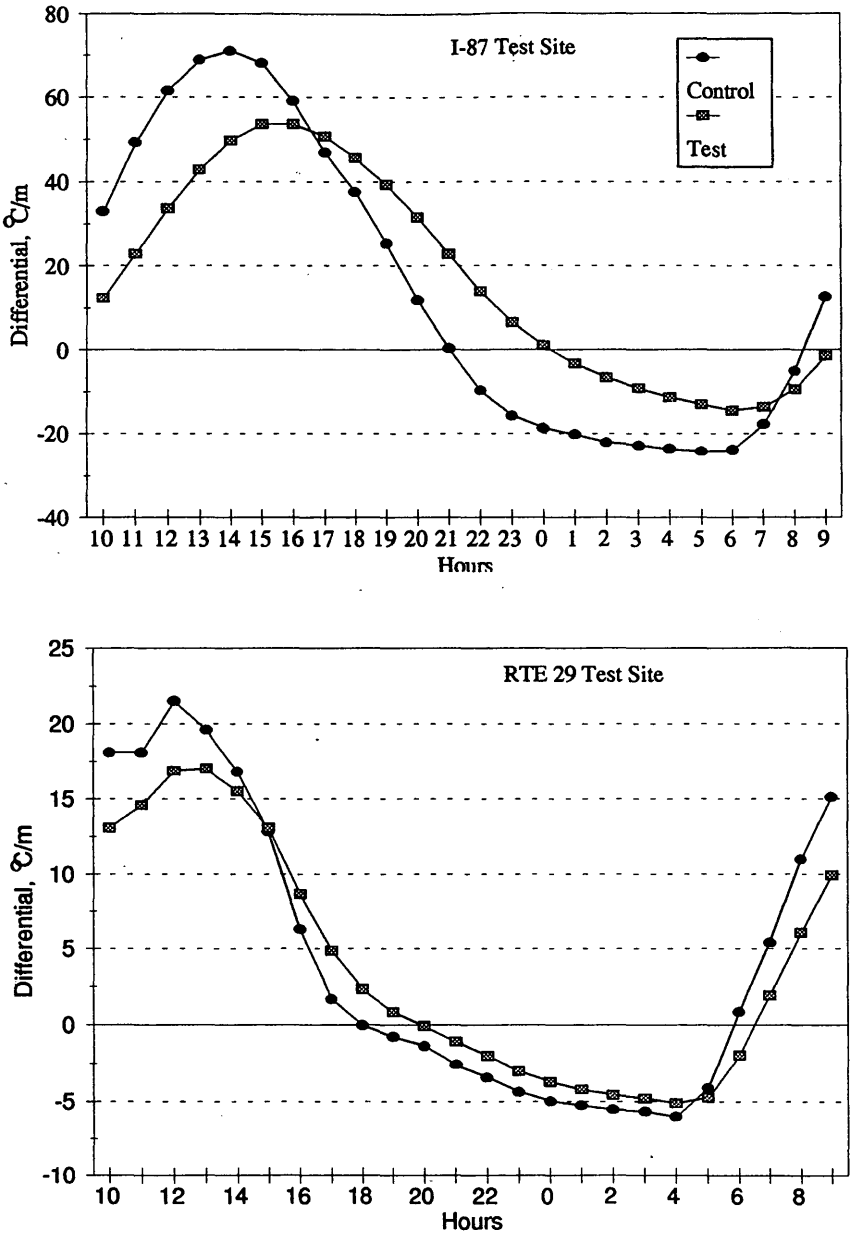

FIGURE 12 Typical daily variations in temperature differentials.

REFERENCES

1. Vyce, J. M. *Fault Removal Techniques for Rigid Pavement Joints.* Research Report 121. Engineering Research and Development Bureau, New York State Department of Transportation, April 1985.
2. Vyce, J. M. *Performance of Load-Transfer Devices.* Research Report 140. Engineering Research and Developing Bureau, New York State Department of Transportation, July 1987.
3. Bendaña, L. J., and W. S. Yang. *Rehabilitation Procedures for Faulted Rigid Pavement.* Research Report 158. Engineering Research and Development Bureau, New York State Department of Transportation, Nov. 1992.
4. Morgan, R. L., H. J. Chen, and D. E. McAuliffe. *Overlays on Faulted Concrete Pavements.* Final Report on Research Project 188. Engineering Research and Development Bureau, New York State Department of Transportation, in preparation.
5. *SAS/STAT User's Guide,* Version 6, Vol. 2, 4th ed. SAS Institute Inc., Cary, N.C., 1989.

Publication of this paper sponsored by Committee on Pavement Rehabilitation.